E.O. Paton Electric Welding Institute
of the National Academy of Sciences of Ukraine

Laser Technology Research Institute
of the National Technical University of Ukraine
«Kyiv Polytechnic Institute»

International Association «Welding»
Local Charity Foundation «Welding Community»

# Laser Technologies in Welding and Materials Processing

## Proceedings of the Fourth International Conference

*26 May – 29 May, 2009, Katsiveli, Crimea, Ukraine*

Edited by
Prof. B.E. Paton and Prof. V.S. Kovalenko

E.O. Paton Electric Welding Institute, NASU
Kyiv 2009

(2009) **Laser Technologies in Welding and Materials Processing.** Kyiv: E.O. Paton Electric Welding Institute, NASU, 90 pp.

The book contains papers presented at the Fourth International Conference «Laser Technologies in Welding and Materials Processing», covering the latest achievements in the field of laser welding, cutting, surfacing and other advanced processes of laser machining of materials. Prospects of application of laser technologies are considered. Authors of the papers are the known specialists from many countries all over the world.

Information Support:
«Avtomaticheskaya Svarka»
«The Paton Welding Journal»

Compiled by *V.S. Kovalenko, I.V. Krivtsun*

Publishing Project *A.T. Zelnichenko*

CRC Preparation *T.Yu. Snegiryova, A.I. Sulima*

Design *D.I. Sereda*

Editor *N.A. Dmitrieva*

Illustrations in cover page one — by courtesy of A.N. Grezev
(CJSC «Laser Complexes», Shatura, Moscow oblast, Russia)

State Registration Certificate DK 166 of 06.09.2000

ISBN 966-8872-12-9



Sent to press on 14.12.2009. 60×84/8 form. Offset paper. Offset print. Ukr. Pet. Font. 22,0 cond. print. sheets. 16,2 publ. print. sheets.
Camera-ready copy was prepared at E.O. Paton Electric Welding Institute. 11, Bozhenko st., Kyiv, 03680.
Published by «Esse». 34/1, Vernadsky Ave., Kiev, 03142.

# Contents

Participants of the Fourth International Conference «Laser Technologies in Welding and Materials Processing»,
May 26-29, 2009, vil. Katsively, Crimea, Ukraine

# *PREFACE*

*This year we were quite lucky to manage to organize our International Conference for the fourth time. Usually to conduct the international conference means to overcome a lot of problems for organizers and especially in post Soviet country nowadays. But to do this in the conditions of global crisis was a tremendous problem... More so the very distressing additional factor in this respect was the swine flue spreading this year all around the world. Many international conferences in different countries couldn't overcome the problems and had been postponed or even cancelled. But in spite of all those extraordinary circumstances WE HAVE DONE THIS!*

*Thanks to the great efforts of all participants and the Organizing Committee the planned event indeed took place and around 80 participants from 7 countries has arrived to Katsiveli, Crimea, to discuss the current problems and further prospects of laser technology development. Congratulations to all of us, congratulations to the whole laser community!*

*In the majority of cases those who have come have done that at their own expense and I am especially thankful to those participants — professors, researchers and students who couldn't get the financial support from their universities or from some other sponsors and have done their best to gather at the Conference.*

*In the Conference Proceedings which we have the honor to present to you we tried to publish all the materials discussed at the Conference meetings but to our great regret not every participant was able to send to us the complete texts of their presentations.*

*Keeping in mind that in times of global crisis the increase in efficiency of manufacturing plays the most important role in economics of any country, in presented papers the accent had been placed on high technologies, innovations implementations and technology improvements. Considering as well the increasing lack of different natural resources in the world — energy, material, labor etc. — the new paradigm in industrial development is coming ahead — «Competitive Sustainable Manufacturing».*

*Alongside analysis of global economic and industrial problems we see in presented papers the new data on development of hybrid laser technologies, on the use of high power laser in material welding and cutting, on development of advanced laser technologies for sheet metal forming, on further improvements of widely spreading now processes of laser surface hardening, surface cladding, alloying and coating. The new results are demonstrated in laser micro and nanomachining, in manufacturing new types of medical stents for cardio surgery etc. The importance of relying on new modern types of highly efficient lasers — diode lasers, diode-pumped solid-state lasers, fiber lasers, etc. in implementation of new advanced technologies in industry is constantly underlined in every presentation.*

*From presented papers we may conclude that laser technology is still dynamically developing further and prospects for future are quite bright.*

***Prof. Volodymyr S. KOVALENKO***
*Co-Chairman of the Conference*
*Director of the Laser Technology Research Institute of the NTUU «KPI»*

# MODERN TRENDS IN PRODUCTION ENGINEERING HIGH TECHNOLOGIES DEVELOPMENT

V. KOVALENKO
Laser Technology Research Institute, NTUU «Kyiv Polytechnic Institute», Kyiv, Ukraine

Paper is demonstrating some new solutions in modernization of classic technologies in components manufacturing, today approaches in improvements of different products assembling and disassembling processes, new moves in decreasing the dimensions of machines, modern trends in products miniaturization, achievements in micro manufacturing, the latest results in development and application of nanotechnologies, etc. Special attention is paid to development of new types of highly efficient lasers – diode-pumped solid-state, diode, fiber lasers and different new technologies based on the use of these lasers. Some consequences of the global crisis are considered which may positively influence the further development of new technologies and their implementation into industry.

There are no countries in the world now, which had not been affected by the global economic crisis. Too many factors have caused this situation but it is obvious now that those industries had suffered mostly which didn't pay the proper attention to implementation of new ideas and different innovations in their production process, neglected the demands of further energy and material economy, the general trends to productivity increase and production cost decrease. Even the highly developed industrial countries of the world had suffered the heavy losses. Such advanced industries like automotive and electronics have appeared at the edge of bankruptcy at their enterprises – GMC, Ford, Chrysler (USA), Citroen, Renault (France), Sony (Japan), to say nothing about metallurgy plants in China, Russia, the USA, Ukraine and others.

At the same time the companies with active innovation policy in spite of economic difficulties are managing still to be afloat – these are for example some German and Japanese automotive enterprises which are reacting very fast on market changes. In very strong competition fights such companies are developing the new means of improving products quality, modernizing the design of manufactured machines and devices, implementing the advanced materials and manufacturing technologies, widely using the advanced laser technologies, reducing the cost of final products manufacturing and assembling. And all this has to be done in conditions of severe economy of natural resources excluding the extensive economy growth.

*Evolution of manufacturing*. Industrial revolution has brought to life the enormous development of the world economy. Industrialization has spread in the past two centuries from Europe to USA, to East Asia, to other continents and is still moving [1]. Until recently the leading paradigm of society development was the economic growth without any concerns about environmental problems. But extensive development has caused the catastrophic decrease of available energy, natural resources, global pollution etc. So the «Club of Rome» in 1970s had opened the way to sustainable development, promoting the study «The limits to growth» [2].

With time the situation in the world was deteriorating. The key challenges became very critical especially at the end of 1990s and at the first decade of this century: climate change, ageing population, public health, ecological-environmental problems, lack of energy and mineral resources, poverty and social problems etc. In this context it is worth to mention the sad facts that only 1 % of the world population is able to use the running water and to cover the mankind demand in nutrition the norm in 1.8 global hectares of biological capacity per capita is needed (at existing level of population today). It goes without saying that there is not such amount of fertile land on the globe to provide the whole population with high quality food. The situation with non-renewable resources is much worse.

So at this stage of mankind development the new paradigm is appearing on the horizon – the competitive sustainable manufacturing (CSM). Actually this is the incoming global technological and industrial revolution.

*CSM*. CSM high added value is knowledge-based. CSM depends on and affects, firstly, manufacturing industry, i.e. products and services, processes, business models, and, secondly, the related education, research and technological development, innovation system. CSM generates wealth, sustains jobs, directly and through related services, manages human and physical resources, from materials to energy. This has to enhance human living standards not at the expense of extensive use of natural resources and the neglecting of environmental problems.

To develop the sustainable society one of the main features has to be persuaded – minimal manufacturing and maximum servicing.

*Innovations – means to improve the quality and to decrease the cost of the product*. To follow the strategy of CSM the accent has to be made on wider use of innovations in any field of economy and especially in manufacturing. In many cases many new

ideas are mistakenly considered as innovation. But the main features of innovation are as follows:

- innovation – something new, which after implementing will add the value to the product by the quality improvement, increase of productivity at manufacturing and decrease of cost;
- innovations will bring the victory in fight with competitors;
- innovations may be a stimulus for further advancement in high technologies.

The main strategy in managing enterprise must be the stimulation of innovation developments and spreading them in the every field of manufacturing process.

*Manufacturing technologies improvements*. Among many others there are three main directions of manufacturing technologies improvements, namely: modernization of classic technologies, non-conventional technologies development, and hybrid technologies.

Modernization of classic technologies is permanent process which is characterized usually by moderate changes in manufacturing directed to achieving positive results at minimal cost. They are as a rule quite trivial and thus are not considered here.

Non-conventional technologies are based on the use of electro-physical and electro-chemical effects to intensify the material processing. They have many advantages in comparison with traditional (classic) technologies. The mostly developed and widespread are the following:

- EDM – electro-discharge machining, using the energy of electrical discharge between electrode–tool and electrode–component for material erosion;
- ECM – electro-chemical machining, based on the use of electro-chemical dissolution of material for its processing;
- USM – ultra-sonic machining, based on the use of the tool vibrating with ultra-sonic frequency (18–22 kHz) in abrasive media;

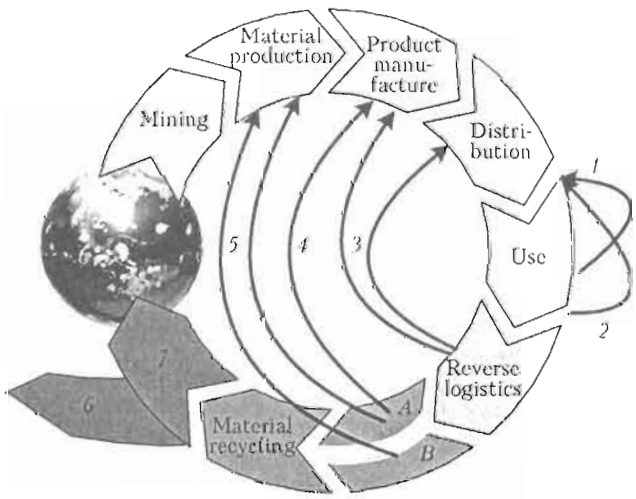


**Figure 1.** Product of life cycle with most important end of life scenarios (*1* – maintenance; *2* – repair; *3* – product reuse; *4* – upgrading, downgrading, remanufacturing, component reuse; *5* – material recycling; *6* – incineration; *7* – landfill) and related processes (disassembly (*A*), shredding (*B*), and other processes (sorting, cleaning, inspection))

- Irradiation technologies, using different types of beam irradiation for material processing: LBM – laser beam machining, EBM – electron beam machining, and IBM – ion beam machining.

Hybrid technologies are usually representing the combinations of different physical processes in one process. The result of such combination is the increase in productivity, quality improvement and/or gaining some additional special properties by processed material (component). Considering that laser itself is electrically low efficient system the straight additional use of electric discharge or plasma makes the processing more efficient. Among different hybrid technologies there are known the following few combinations: electro-laser hole piercing; laser + EDM; laser + plasma; laser + ECM; laser + USM; laser + liquid jet; machining + laser; laser hardening (cladding) + mechanical rolling; laser surface alloying + electro-magnetic field, etc.

*Modernization of assembling and disassembling processes*. Considering the necessity to limit the consumption of material, energy, labor at every stage of product life cycle there must be the careful monitoring of the processes to find the new reserves of increasing the efficiency of product manufacturing and use.

Keeping this in mind it is important to evaluate various life cycle aspects of products and to optimize their value and benefits including engineering, assembly, servicing, maintenance and end of life (EoL) phases [3].An important opportunity in this context is the possible recovery of products, components, parts or materials at the end of completed use phase. The main EoL recovery strategies are direct reuse, reuse small repairs (refurbishment), remanufacturing and material recycling (Figure 1).

In product life cycle the share of disassembling used to be considered as not significantly important. At the same time the disassembling is a very time and energy consuming process. Up to recently the disassembling productivity was almost impossible to increase, to say nothing about its automation.

Efforts are taken to implement automation into disassembling procedure using different design peculiarities. These are usually specially embedded elements – innovative fasteners which enable self disassembling procedure without any heavy loading on the joining parts (Figure 2). These fasteners may be triggered by different means – mechanically, thermally, chemically, electro-magnetically, and electrically. The unlimited number of connections can be unfastened with the same disassembly action as soon as the trigger signal is switched on.

*Further development of laser technologies*. In modern economy the role of advanced laser technologies is increasing with every new day. It is really impossible to name all fields of human activity where lasers are successfully used. This is becoming possible thanks to the new types of laser which has been developed recently – diode lasers, solid-state lasers with diode laser pumping, high power $CO_2$-lasers,

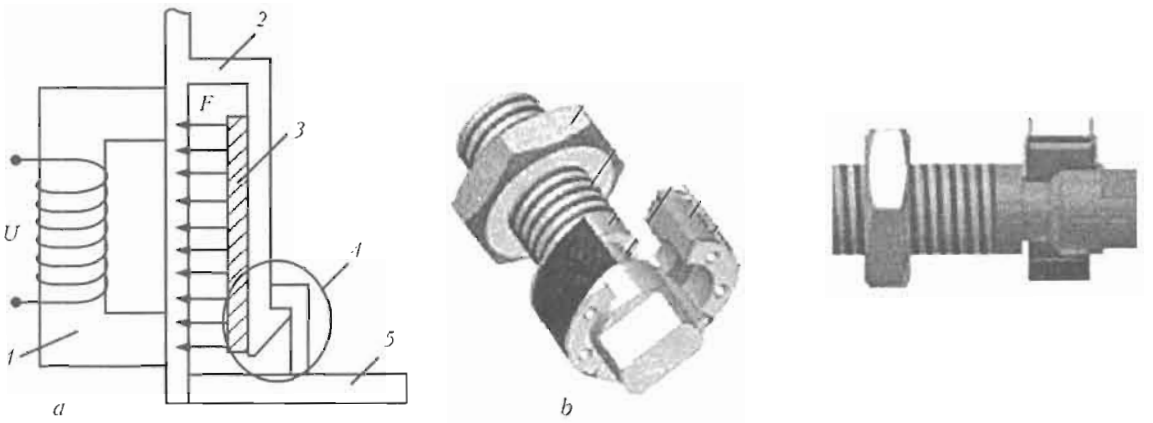


Figure 2. Disassembly embedded fit, triggered by electromagnetic field (*1* – electromagnet; *2* – part to remove; *3* – magnet anchor; *4* – connection element; *5* – basis), and disassembly embedded nut and bolt, triggered by electric current

CO-lasers, excimer lasers and, finally, fiber lasers. The main advantage of these new lasers is their high efficiency and, hence, the decrease in dimensions, shortage of maintenance cost, ability to integrate them quite easily into robotized system, possibility to improve the reliability and the precision of the performed processing. It is known already about high power 10 kW fiber laser developed by IPJ Company for industrial application in Canada.

Industrial application is considered now the most widespread use of lasers. Very popular in industry became laser welding, sheet material shearing, cutting, hole piercing, surface hardening, alloying, cladding, rapid prototyping, and marking.

*Micro- and nanotechnologies development*. The need in micro- and nanofabrication is dictated not only by the development of sophisticated devices and structures with new properties and abilities but because of far going trends of decreasing the size, material, as well as energy consumption of such products considering the global lack of natural resources, the catastrophic pollution of the earth and many other rapidly rising global problems of society. Rejecting the paradigm of extensive growth of economy in further development of mankind [4, 5] the society has to develop more intellectually efficient manufacturing technologies, based on the latest achievements of science. In this respect the very logic steps were first to achieve the mentioned results through the development and wide implementation of microtechnologies and different microdevices and than based on gained experience to start the new move in advancing further «deep into the nature» [6–8].

Laser radiation is a unique instrument which may perform a lot of different functions in realization of nanomanufacturing – manufacturing of nanoparticles (powders, tubes, wires, etc.), material machining at nanolevels, production of nanoproducts, devices, systems, surface super finishing with roughness at nanolevel etc. [9–13].

3D rapid prototyping is quite well-known and wide spread process. There are plenty of different versions of this process. Among them the laser stereo lithography is considered as very reliable and precise.

The further development of this technology is two photon polymerization (2PP) [11, 12]. For 2PP technology the special photosensitive materials are used. They may be the negative resists (solid or liquid), based on epoxy or acrylate, or positive resists. In Figure 3 the samples of products manufactured by using the laser 2PP technologies are demonstrated.

Speaking about nanotechnology in biomedical application the following factors have to be taken into consideration [12]:

- due to the presence of numerous nanostructures (i.e. proteins) in the body, cells are accustomed to interact with nano-sized materials;
- today, synthetic materials used in tissue engineering possess conventional surface feature only;
- it is believed that one reason why current orthopedic implants only have a 15 year lifetime is due to non-biologically inspired surface roughness.

*Human factor in further development of high tech*. In spite of heavy losses the economic crisis apart from negative moral influence on individuals has some positive effect in mobilizing their opportunities to find the unused reserves and to start «the new life». The current crisis has given the chance for society to reconsider its attitude to manufacturing industry.

Attitude reconsideration to the manufacturing industry:

- in the past it was usually associated with bad working conditions, dirt, noise, even high level of danger for life;
- but for young generation of the XXI century well acquainted with PC and information technologies such situation is considered as entirely impossible!

Andrea Gentili, EU's coordinator for the Manufuture project (Manufuture Conference-2008 in Saint-Etienne, France: «The factory of the future will no longer be a hostile, dirty and nosy place, but rather a super-technology site. It is for us to convince young Europeans, who are now discovering the limitations of the world of finance, that there are other ways of creating wealth.»

The youthful minds has to be inspired by highly intellectual machines and technologies in combination with innovation ideas and strong believe in great op-

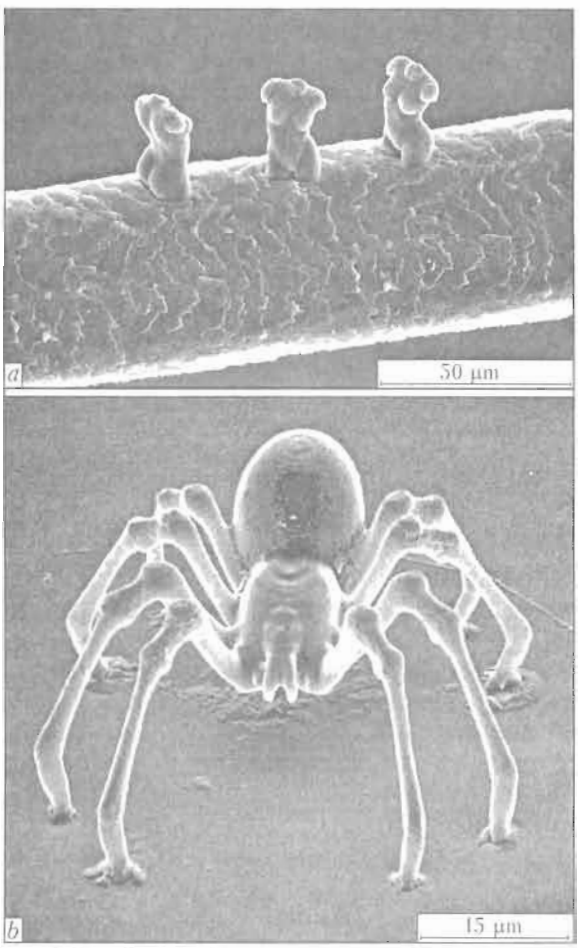


**Figure 3.** Samples of products manufactured by laser 2PP: *a* – 3D nanostructuring Venus stature on the top of human hair; *b* – nanospider 3D body

portunities and prospects of modern science and technique.

*Some first steps in the global crisis recovering.* Countries which made the accent on modernization of industry and implementing new technologies has started the gradual process of recovering from economic recession. They have mobilized all resources, introduced the regime of total economy, decreased substantially the import of foreign products and paid the special attention to growth of manufacturing fields.

Based on this policy China was the first country in the world which managed even to increase the GNP at the beginning of this year up to 8 % and the prospect for the next year is even brighter! Based on the manufuture technological Platform, initiated by EU the industry of European countries has reached some success as well. Manufuture is a pan-European initiative to develop new manufacturing technologies and integrate them rapidly into European industrial processes [14]. Its role in fostering innovation and regional collaboration is becoming increasingly important as companies seek new ways to survive, rethink, and regenerate their businesses in the economic crisis.

For Ukraine we have developed the national manufuture technological platform, which will allow concentrating the efforts and resources on manufacturing the advanced products [15].

## CONCLUSIONS

- The main goal of modern economy development (and especially of industrial field) should be the permanent harmonization of human activity with the limited natural resources of the globe.
- Efforts have to be done to promote competitive sustainable manufacturing (CSM).
- Innovations implementation – one of the main means to create the highly efficient manufacturing.
- Non-conventional technologies bring the latest achievements of science into manufacturing industry thus improving the quality of manufactured products.
- Hybrid technologies open the new horizons in manufacturing by increasing the efficiency of processing.
- Modernization of assembling and disassembling save the energy and material resources and is raising the manufacturing culture.
- Laser technologies are becoming the leading in manufacturing and have tremendous prospects for future development.
- Young generation may be attracted to manufacturing field only by promoting the highly intellectual technologies and equipment.

1. Tseng, M. (2007) Global manufacturing, the Eastern perspective. In: *Proc. of Conf. on Manufuture* (2–4 Dec. 2007, Porto, Portugal).
2. Meadows, D., Randers, J., Behrens W. (1972) *The limits to growth*: Universe Book.
3. Duflou, J.R., Seliger, G., Kara, S. et al. (2008) Efficiency and feasibility of product disassembling: A case based study. *Annals of the CIRP*, 57(2).
4. Jovane, E., Yoshikawa, H., Alting, L. et al. (2008) The incoming global technological and industrial revolution towards competitive sustainable manufacturing. *Ibid*.
5. Westkamper, E. (2007) Sustainable manufacturing. In: *Proc. of Conf. on Manufuture* (2–4 Dec. 2007, Porto, Portugal).
6. Kovalenko, V. (2006) Laser micro and nano processing. *Int. J. Nanomanufacturing*, 1(2), 173–180.
7. Kovalenko, V., Meijer, J., Anyakin, M. et al. (2008) Some results of studying laser micromachining at medical stents manufacturing. In: *Proc. of 6th Int. Symp. on Nanomanufacturing* (Athens, Greece, Nov. 2008).
8. Meijer, J., Gilner, A., Kovalenko, V. et al. (2002) Laser machining by short and ultrashort pulses: State of the art. *Annals of the CIRP*, 51(2).
9. Burges, D.S. (2001) Laser ablation generates nanoparticles. *Photonics Spectra*, 1 July, 26–29.
10. Sipavicius, C., Mazeika, K., Vaitiekunas, P. et al. (2009) Laser method for generation of micro- and nano-particles and their selection in gas flow. In: *Abst. of papers and program of 4th Int. LTWMP Conf.* (Katsiveli, Ukraine, May, 2009). Kiev: PWI, 41–42.
11. Kawata, T. et al. (2001) Two photon polymerization. *Nature*, 412, 697.
12. Chichkov, B.N. (2008) 3D-laser based nanofabrication for application in photonics and biomedicine. In: *Proc. of 6th Int. Symp. on Nanomanufacturing* (Athens, Greece, Nov. 2008).
13. Namba, Y., He, Y. An investigation of a unit-machined shape for the three-dimensional micromachining of silicon surfaces with a pulsed ultraviolet laser. *Int. J. Japan Society of Precision Engineering*, 32 (1), 13–18.
14. Jovane, F., Westkamper, F., Williams, D. *The manufuture road towards competitive and sustainable high-adding value manufacturing*.
15. Kovalenko, V.S. (2007) Manufuture – European future of Ukraine. *Metalloobrabotka – Oborudovanie i Instrument*, 6, 14–16.

# CALCULATION OF SIZES OF THE WELD AND HAZ IN WELDING OF TITANIUM WITH A SCANNING CONCENTRATED HEAT SOURCE

S.V. AKHONIN, V.Yu. BELOUS and A.F. MUZHYCHENKO
E.O. Paton Electric Welding Institute, NASU, Kyiv, Ukraine

Application of the controlling magnetic field in welding of titanium allows widening of technological capabilities of traditional argon-arc welding. Owing to application of the external magnetic field generated by electromagnet, the developed welding technology makes it possible to provide redistribution of thermal energy of the arc in surface-arc welding and portioned heat input of the arc into the lower wall of the groove, vertical side edges and molten pool in narrow-gap welding. This ensures reliable fusion of the vertical side walls of the groove to the weld in narrow-gap welding, change in the weld shape, change in the weld pool and HAZ shape, and decrease in the base metal penetration depth. The 3D mathematical model of thermal processes occurring in titanium during welding using the scanning heat source, based on the differential thermal conductivity equation, was developed to calculate the effect of parameters of the magnetic field and welding process on the weld formation. Modelling made it possible to investigate the effect on the weld and HAZ shapes by such parameters as the value of displacement of the anode spot from the weld centre, frequency of displacement of the anode spot, duration of the transition process, speed of displacement of the anode spot, and value of the heat input.

Development of new combined welding methods, which are a combination of the welding arc and laser beam, is currently an active area of R&D efforts. But, in our opinion, potential of the conventional welding arc is far from being exhausted. Tungsten-electrode arc welding in the atmosphere of inert gases, i.e. argon and helium (TIG), is still the most common, relatively simple and versatile method for fabrication of structures from titanium alloys. With this method, welding can be performed in different spatial positions, and welding equipment can be easily readjusted if necessary to change type of the welded joint and thickness of the metal welded. Application of the controlling magnetic field makes it possible to substantially widen technological capabilities of the process in narrow-gap TIG welding of thick pieces and in welding deposition operations. This is particularly important for welding of titanium and titanium-base alloys. Arc welding of titanium is most often performed by using tungsten electrodes, which is attributable to intensive spattering of filler metal and violation of shielding in the case of using metal electrodes. When necessary to deposit a wide bead (in repair of worn-out parts), the deposition process is performed in two, three or more passes. In this case the base metal is penetrated to a large depth, and the process itself is characterised by a low productivity.

As shown by the studies performed at the E.O. Paton Electric Welding Institute, application of the controlling magnetic field holds high promise for improving the quality of deposition. This makes it possible to control redistribution of thermal energy of the arc on the lower wall within the preset ranges, thus ensuring reliable fusion of the weld to base metal and minimal size of the HAZ. Flow diagram of the process of deposition of titanium parts with magnetic control is shown in Figure 1, *a*.

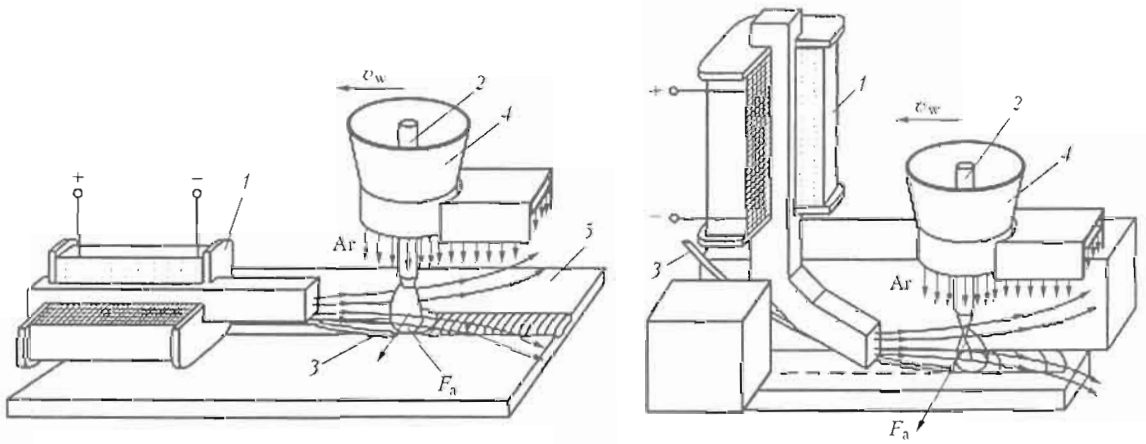


**Figure 1.** Flow diagram of welding with external controlling magnetic field: *a* — deposition process diagram; *b* — flow diagram of narrow-gap welding with magnetic control: *1* — electromagnet; *2* — tungsten electrode; *3* — filler wire; *4* — shielding nozzle; *5* — workpiece; $v_w$ — welding speed; $F_a$ — Lorentz force

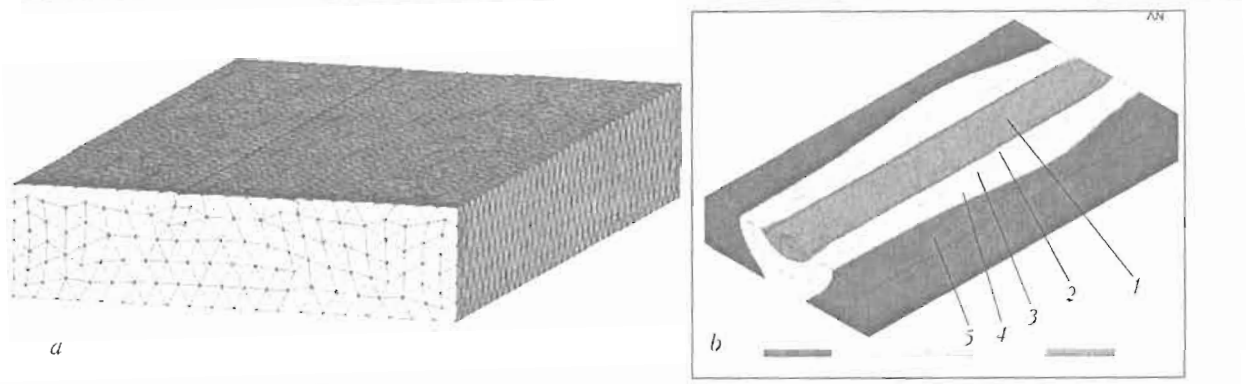


Figure 2. Finite-element model used for calculations (*a*) and result of calculations of penetration zone (*b*): heating temperature of 3533–1941 (*1*), 1941–1233 (*2*), 1233–1073 (*3*), 1073–293 (*4*) and < 293 (*5*) K

TIG welding is performed with the tungsten electrode located at the groove centre. Filler wire is fed normal to the electrode into a leading portion of the weld pool, and electromagnet with a core induces the magnetic field. Interaction of the magnetic field with the arc current generates the Lorentz force, which diverts the arc and causes displacement of the anode spot in a direction of action of this force. Special device was developed to induce the controlling magnetic field. This device provides the magnetic field with a value of the transverse component of magnetic induction in the arc zone at a level of up to 12 mT and reversing frequency of up to 80 Hz.

Experimental study of the principles of the weld formation in welding with the arc controlled by the external transverse magnetic field is time-consuming because of a large number of parameters of the welding process. Therefore, the authors also carried out analytical investigations of the welding process with the controlling magnetic field by using mathematical modelling of narrow-gap welding with a moving heat source.

Modelling made it possible to study the effect on the base metal penetration shape and HAZ shape by such process parameters as the value of displacement of the anode spot from the groove centre, frequency of movement of the anode spot, time of the transition process, speed of movement of the anode spot, etc.

Mathematical model based on a differential thermal conductivity equation in the 3D Cartesian coordinate system was used to calculate thermal conditions that accompany the process of fusion of the groove walls and metal surface.

The source moves on the perimeter of the groove under the effect of the external controlling magnetic field. The law of variations of magnetic induction in the arc zone is set by the value of the magnetisation current flowing through the electromagnet.

The 3D finite-element model of thermal processes occurring in square-groove welding deposition on titanium plates using a moving heat source is shown in Figure 2, *a*. Temperature fields (Figure 2, *b*) in a workpiece were calculated by using software module ANSYS, allowing for the above initial and boundary conditions. There are zones where the metal was heated above the melting points (*1*), and zones where the metal was heated above the polymorphic transformation point (*2*). The calculation results were used to plot the isothermal lines of maximal temperatures, from which geometry and sizes of the penetration zone, HAZ and polymorphic transformation zone were determined (Figure 3).

Also, welding with the controlling magnetic field is efficient for joining thick (up to 500 mm) pieces. The method of narrow-gap welding has currently received wide acceptance for fabrication of such structures. It is advantageous over U-groove welding in reduction of the amount of the deposited metal (up to 30 %), lower labour intensity in preparation of grooves of the pieces joined, and substantial increase in the process productivity.

Main difficulties lie in ensuring reliable melting of the vertical side walls and fusion of the weld metal to side walls. In the case of welding without movement of the welding arc or oscillations of tungsten electrode, the major part of thermal energy of the burning arc is spent for excessive melting of the lower wall in a narrow groove, or for repeated penetration of the previous-pass weld metal. To achieve reliable melting of the vertical wall in the narrow groove, it is necessary to redistribute heat input into a welded joint.

The work performed by the E.O. Paton Electric Welding Institute proved a high potential of application of the alternating magnetic field for assurance of the quality of thick (up to 100 mm) welded joints [1]. This allows redistribution of thermal energy of the arc between the lower groove wall, vertical side edges and molten pool to be controlled over wide ranges, thus providing reliable fusion between the weld and base metal. Flow diagram of narrow-gap welding with magnetic control is shown in Figure 1, *b*. Welding is performed with tungsten electrode immersed into the groove. In this case, the shielding


Figure 3. Effect of the value of amplitude of displacement of the heat source (anode spot) on penetration of base metal at $\omega$ = 10 Hz, $x$ = 3 (*a*), 5 (*b*) and 7 (*c*) mm

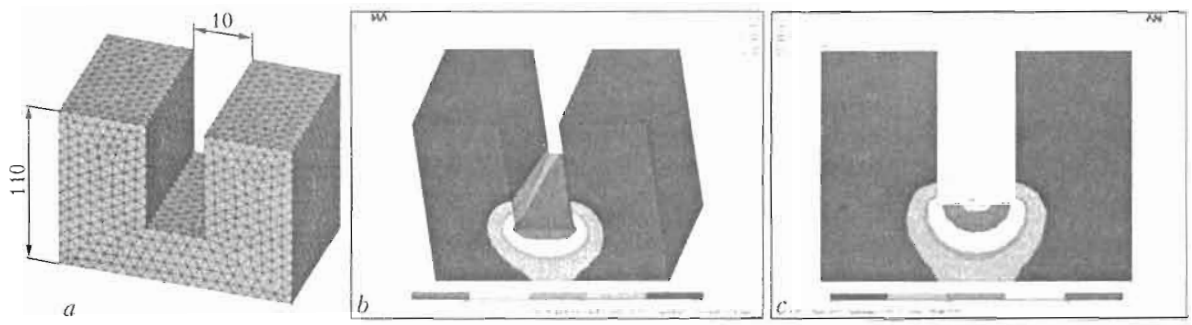


**Figure 4.** Finite-element model used for calculations (*a*), result of calculations of penetration zone (*b*), and weld shape without deviation of welding arc (*c*)

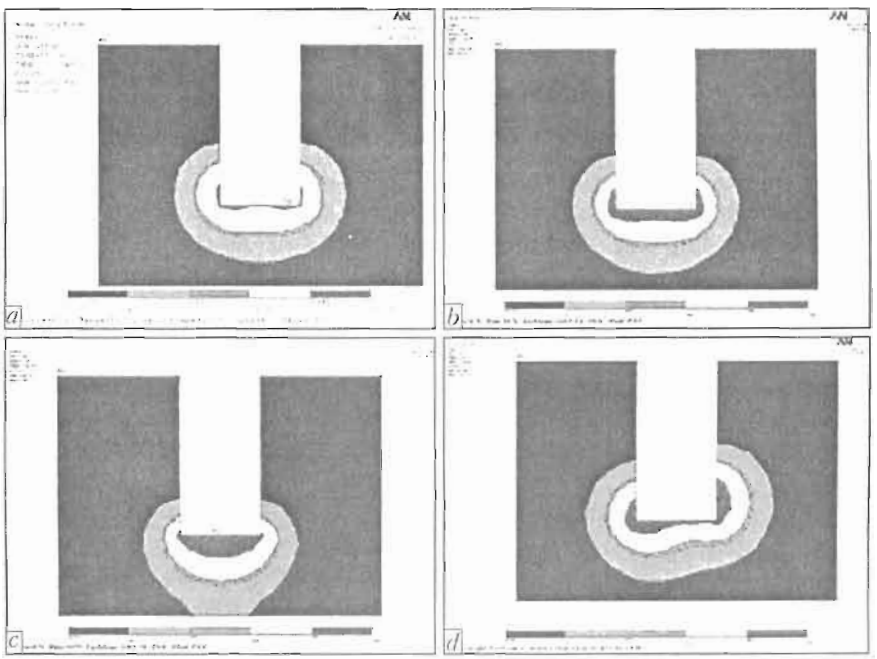


**Figure 5.** Effect of movement height of the heat source centre (anode spot) on penetration of base metal (*a–c*) and of 1 mm displacement of tungsten electrode from the joint centre on penetration of base metal (*d*) at $\omega$ = 2.5 Hz, $x$ = 0.7 ($\Delta l$ = 5.5 mm) (*a*), 0.5 ($\Delta l$ = = 4.5 mm) (*b*, *d*) and 0.3 mm ($\Delta l$ = 3.5 mm) (*c*)

nozzle is placed over the wed edges, this making it possible to considerably reduce the weld width. Filler wire is fed to the leading portion of the weld pool. The magnetic field is generated by the electromagnet with a special shape of the core, placed into the groove (see Figure 1, *b*). Interaction of the magnetic field with the arc current induces the Lorentz force, which deviates the arc and leads to displacement of the anode spot to the side wall.

Application of mathematical modelling with experimental studies [2] in this case also made it possible to investigate the effect on the penetration shape of the base metal and shape of HAZ by the main parameters of the welding process. The 3D finite-element model of thermal processes occurring in square-groove welding of titanium plates with a heat source moving on the perimeter of a slot is shown in Figure 4, *a*. Results of the calculations of zones of the welded joint in 3D form are shown in Figure 4, *b*.

As shown by the calculation results, height of melting of the vertical walls increases with increase in deviation of the welding arc (Figure 5). It is significant that increase in deviation of the welding arc leads not only to increase in height of melting of the vertical walls, but also to decrease in volume of the molten metal due to a greater dissipation of heat of the welding arc. An intensive heat removal takes place in a location of intersection of the vertical walls with the previous pass surface. Position of the tungsten electrode in the central plane of the groove also affects melting of the groove walls.

## CONCLUSION

Mathematical modelling methods allowed establishing the main principles of weld formation in welding with the external controlling magnetic field. The controlling magnetic field substantially widens the technological potentialities of TIG welding.

1. Paton, B.E., Zamkov, V.N., Prilutsky, V.P. (1996) Narrow-groove welding proves its worth on thick titanium. *Welding J.*, **4**, 37–41.
2. Belous, V.Yu., Akhonin, S.V. (2007) Influence of controlling magnetic field parameters on weld formation in narrow-gap argon-arc welding of titanium alloys. *The Paton Welding J.*, **4**, 2–5.

# NUMERICAL ANALYSIS OF HEATING, MELTING AND CONNECTIVE EVAPORATION OF METALS IN PULSED LASER PROCESSING

V.F. DEMCHENKO[1], I.V. KRIVTSUN[1], I.L. SEMENOV[1] and G.A. TURICHIN[2]
[1]E.O. Paton Electric Welding Institute, NASU, Kyiv, Ukraine
[2]St. Petersburg State Technical University, St. Petersburg, Russian Federation

Self-consistent mathematical model of gas-dynamic and heat transfer processes at pulsed laser processing of metallic materials is proposed. This model enables to study processes of metal heating, melting and evaporation together with gas-dynamic process in metal vapor flow. The detailed numerical analysis of these processes is carried out on the basis of suggested model. The radiation of pulsed Nd:YAG laser is assumed. The duration of the pulse was 1 ms, and the intensity of laser radiation varied within the limits of $10^5$–$10^6$ W/cm$^2$. As an example of the metal being processed a low-carbon steel is considered. One-dimensional and two-dimensional (axisymmetric) cases of the gas-dynamic flow of vapor are investigated. The scope of applicability of the proposed self-consistent mathematical model is established. The obtained results demonstrate that proposed model can be used for numerical simulation of physical processes taking place during laser processing of metals which involves pulsed and pulsed-periodic laser.

Studying the physical processes that occur during the interaction of high intensity laser radiation with the matter plays a prominent part in developing new technologies of laser welding and processing of various (primarily metallic) materials [1–4]. The research into the interaction of metals with focused radiation of the pulsed and pulsed-periodic lasers [5–8] is of particular interest for developing such technologies as microwelding, engraving, drilling etc. The processes referred to in this paper include absorption of laser radiation in metal; heating, melting and subsequent evaporation (in convective regime) of metal into the external gas. Most commonly, while analyzing the convective evaporation of metals, the model proposed by Knight [9] is put to use for evaluating the quantitative characteristics of evaporation process (density, temperature and vapor expansion rate). This model includes a premise that the vapor flux is one-dimensional and stationary. However, at a high rate of metal heating by the focused radiation of a pulsed laser both of the assumptions prove to be wrong, since above the boiling temperature $T_b$ the surface temperature of the melt at the center of the spot keeps raising up to the temperature, much exceeding $T_b$, while the vapor flux flowing from the heating spot undergoes a side unloading, which disrupts the one-dimensional flow assumption taken in [9]. The current work deals with analysis of applicability of various models of convective metal evaporation to the case of metal sheet heating by the focused radiation of a pulsed laser (without regard for vapor ionization and laser plasma generation).

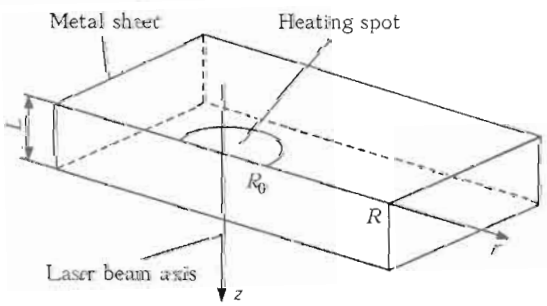


**Figure 1.** Layout of the metal sheet heating by laser beam

Let us consider the metal sheet heating by a single pulse of the focused laser radiation. Assuming the spatial distribution of radiation intensity to be symmetric relative to the beam axis, the mathematical model of metal sheet heating, as an axially symmetric problem, can be formulated as follows. The coordinate system is chosen to be cylindrical (Figure 1). The radiation intensity $I_0$ is taken to be uniformly distributed across the heating spot of radius $R_0$ and constant during the pulse. The radiation intensity $I_0$ is defined by the full pulse energy $W$, its duration $\tau$ and beam cross-section $S = \pi R_0^2$ on a sheet surface, i.e. $I_0 = W/(\tau S)$.

For the majority of metals the volumetric nature of laser radiation absorption may be neglected. Thus the heating effect of the laser beam on a metallic specimen can be stated as a surface heat source distributed over the sheet surface of density $q(r)$:

$$q(r) = \begin{cases} A(T_s)I_0 \text{ at } r \le R_0, \\ 0 \text{ at } r > R_0, \end{cases} \qquad (1)$$

where $A(T_s)$ is the laser radiation absorption coefficient depending on the metal surface temperature $T_s(r)$.

The heat conduction in the specimen is determined by the following equation:

$$C(T)\rho(T)\frac{\partial T}{\partial t} = \frac{1}{r}\frac{\partial}{\partial r}\left(r\lambda(T)\frac{\partial T}{\partial r}\right) + \frac{\partial}{\partial z}\left(\lambda(T)\frac{\partial T}{\partial z}\right), \qquad (2)$$
$$0 < r R,\ 0 < z < L,\ t > 0,$$

where $C(T)$, $\rho(T)$ and $\lambda(T)$ are respectively the effective heat capacity of metal (allowing for the latent heat of melting), density and heat conduction coefficient. The boundary conditions to the equation (2) are written below:

$$\left.\frac{\partial T}{\partial r}\right|_{r=0} = 0;\ T(r, L, t) = T(R, z, t) = T_0;$$
$$-\lambda(T_s)\left.\frac{\partial T}{\partial z}\right|_{z=0} = q - q_{rc} - q_e. \tag{3}$$

Here $q_{rc}(T_s) = \varepsilon\sigma(T_s^4 - T_0^4) + \alpha(T_s - T_0)$ is the heat loss due to radiation and heat exchange of the surface with an atmosphere; $\varepsilon$ is the emissivity of metal; $\sigma$ is the Stefan–Boltzmann constant; $\alpha$ is the heat conduction coefficient; $T_0$ is the temperature of the environment; $q_e(T_s) = \kappa q_m(T_s)$ is the specific flux of heat removed from the melt surface; $\kappa$ is the specific heat of evaporation; $q_m(T_s) = \bar{\rho}\bar{u}$ is the specific mass flux of vapor; $\bar{\rho}$, $\bar{u}$ is the density and the velocity of metal vapor near the evaporating surface, respectively.

To complete the problem (2)–(3) the model of convective metal evaporation should be adopted to calculate the velocity $\bar{u}$ and the density $\bar{\rho}$. Within the frame of evaporation model by Knight, the structure of one-dimensional subsonic vapor flow can be depicted as shown in Figure 2, namely the shock wave propagates through the external gas, followed by the contact discontinuity, comprised as the contact area of external gas and expanding metal vapor.

Near the evaporating surface the Knudsen layer extends over the several mean paths, beyond which (in the gas-dynamic flow region) there establishes equilibrium over translational degrees of freedom of vapor particles. In [9] the following expressions were proposed, which bind the density $\bar{\rho}$ and the vapor temperature $\bar{T}$ at the Knudsen layer boundary with saturated vapor density $\rho_s$ and evaporating surface temperature $T_s$:

$$\frac{\bar{T}}{T_s} = \left[\sqrt{1 + \pi\left(\frac{\gamma-1}{\gamma+1}\frac{m}{2}\right)^2} - \sqrt{\pi}\,\frac{\gamma-1}{\gamma+1}\frac{m}{2}\right]^2, \tag{4}$$

$$\frac{\bar{\rho}}{\rho_s} = \sqrt{\frac{T_s}{\bar{T}}}\left[\left(m^2 + \frac{1}{2}\right)e^{m^2}erfc(m) - \frac{m}{\sqrt{\pi}}\right] + \frac{1}{2}\frac{T_s}{\bar{T}}\left[1 - \sqrt{\pi}me^{m^2}erfc(m)\right]. \tag{5}$$

Here $m = \bar{u}/\sqrt{2\Re\bar{T}} = \sqrt{\gamma/2}M$; $\Re$ is the gas constant; $\gamma = 5/3$ is the heat capacity ratio of vapor which is assumed to be an ideal monoatomic gas; $M$ is the Mach number at the Knudsen layer boundary. The pressure of saturated vapor is determined by the Clausius–Clapeyron equation, while the density is defined by the ideal gas law $\bar{p} = \bar{\rho}\Re T$. The velocity $\bar{u}$ and the pressure $\bar{p}$ are bound with the density $\rho_0$ and the pressure $p_0$ in the external gas by the relation for the shock wave [9]:

$$\bar{u} = \frac{\bar{p} - p_0}{\sqrt{\frac{\rho_0}{2}(\bar{p}(\gamma+1) + p_0(\gamma-1))}}. \tag{6}$$

The expressions (4)–(6) yield a single nonlinear equation for obtaining the velocity $\bar{u}$. In this regard it is worth mentioning that applicability of the conjugate model (2)–(6) is not restricted to the Knight's assumption for the stationary nature of vapor flow.

The non-stationary problem of metal vapor gas-dynamics, dealt with hereafter, will be approached by adhering to the previously formulated assumption of one-dimensional flow pattern. Let $OZ'$ be an axis in cylindrical coordinate system, perpendicular to the sheet surface along the vapor phase flow direction. At a high Reynolds number (vapor expansion rate being of the order of 500 to 700 m/s) the Euler equations can be used to describe the gas-dynamics of vapor mixture:

$$\frac{\partial\vec{U}}{\partial t} + \frac{\partial\vec{F}}{\partial z'} = 0, \quad z' \in [0, H]. \tag{7}$$

Here $\vec{U} = (\rho_m, \rho, \rho u, E)$; $\vec{F} = (\rho_m u, \rho u, \rho u^2 + p, (E + p)u)$; $\rho$, $u$, $p$ are respectively the density, velocity and mixture pressure; $\rho_m$ is the density of metal vapor; $E = \rho e + \rho u^2/2$ is the energy of mixture; $e = p/\rho(\gamma - 1)$ is the internal energy. Equations (7) are integrated under the following boundary and initial conditions:

$$\left.\frac{\partial\vec{U}}{\partial z'}\right|_{z'=H} = 0, \quad t > 0, \tag{8}$$

$$u(0, t) = u_{0+} + \frac{p(0, t) - p_{0+}}{\frac{\sqrt{\rho_{0+}}}{2}\left[p(0, t)(\gamma+1) + p_{0+}(\gamma-1)\right]}, \tag{9}$$

$$\rho_m(0, t) = \rho(0, t), \quad p(0) = \rho(0, t)RT, \quad t \geq 0,$$
$$p(z', 0) = p_0, \quad u(z', 0) = 0, \quad \rho(z', 0) = \rho_0, \tag{10}$$
$$\rho_m(z', 0) = 0, \quad 0 < z' < H,$$

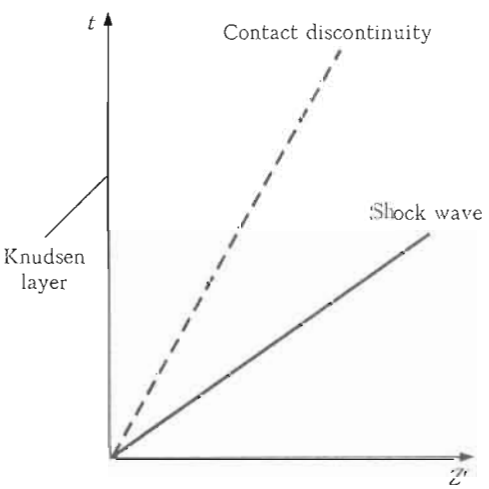


Figure 2. Diagram of one-dimensional vapor expansion [9]

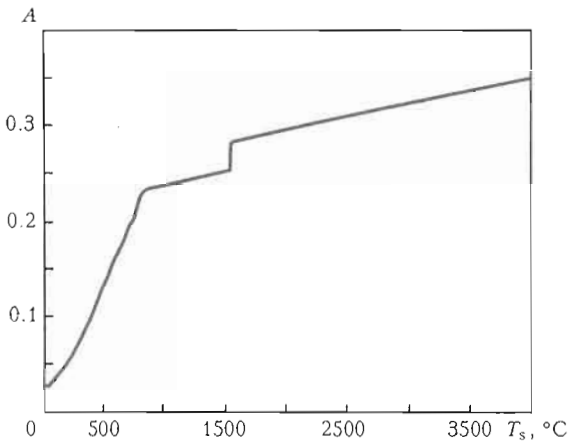


Figure 3. Temperature dependence of absorption coefficient of Nd:YAG laser radiation for low-carbon steel

where $p_{0+} = p(+0, t)$; $\rho_{+0} = \rho(+0, t)$; $u_{+0} = u(+0, t)$, while the density ρ and the temperature $T$ are defined by conditions (4) and (5), setting $\overline{\rho} = \rho$, $\overline{T} = T$, $\overline{u} = u(0, t)$.

The solution of the problem (2)–(3) was numerically solved using the Peaceman–Rackford [10] method with local iterations over nonlinearity in the finite difference analogue for the local energy balance on the sheet surface. The non-stationary gas-dynamics problem (7)–(10) was solved by using the second order Godunov method [11].

The heating of the low-carbon steel sheet by the single pulse of the focused laser radiation is considered with the following parameters: $I_0 = 5 \cdot 10^6$ W/cm$^2$, $\tau = 1$ ms, $R_0 = 0.1$ mm, corresponding, for example, to the characteristic operating conditions of the pulse Nd:YAG laser which is a constituent of the welding, cutting and deep engraving facilities [12].

The sheet thickness and the radius of an operating area were set to $L = 1$ mm and $R = 2$ mm (see Figure 1). The heat transfer properties of low-carbon steel were borrowed from [13], and the relevant temperature dependence of the absorption coefficient was calculated using the data from [14–16] (Figure 3).

Iron was chosen as an evaporating material, an air at normal conditions being an atmospheric gas.

Let us conduct a comparative analysis of the self-consistent problem of the metal heating (1)–(3) and convective metal evaporation for the two models of vapor gas-dynamics, i.e. stationary [9] and non-stationary (4), (5), (7)–(10) ones as applied to the sheet heating by pulse laser radiation. The computation results are presented in Figures 4 and 5 (time in Figures 4, *b* and 5 is marked since the commencement of evaporation). At the specified laser pulse parameters the temperature at the center of the heating spot reaches the boiling point in 7 μs (Figure 4, *a*), and within about 80 μs it continues to grow up to 3800 °C, followed by its essentially constant value until the pulse end. In stabilization mode of the metal sheet surface temperature the heat flux, by virtue of laser heating, is compensated for by the heat losses due to evaporation and partially to irradiative heat exchange with the environment.

By the moment (relative to commencement of evaporation) when the metal sheet surface temperature ceases to vary in time, the shock wave moves over the distance, much exceeding the characteristic dimension of the solution space of the gas-dynamic problem (for example, the heating spot diameter), and does not affect the process kinetics of the metal evaporation from the melt surface.

If the time of attaining the stationary value of liquid metal surface temperature tends to zero (at an infinitely large heating rate), then the gas-dynamic flow characteristics (velocity, pressure) are consistent with the Knight model. Despite the fact that in non-stationary model of convective evaporation these characteristics differ from Knight's idealized flow pattern (see Figure 5), the specific vapor mass flux values obtained using both stationary and non-stationary models agree very closely (see Figure 4, *b*). This accounts for the reason that the time of attaining the stationary value of the surface temperature (see Figure 4, *a*) is much less than the characteristic time

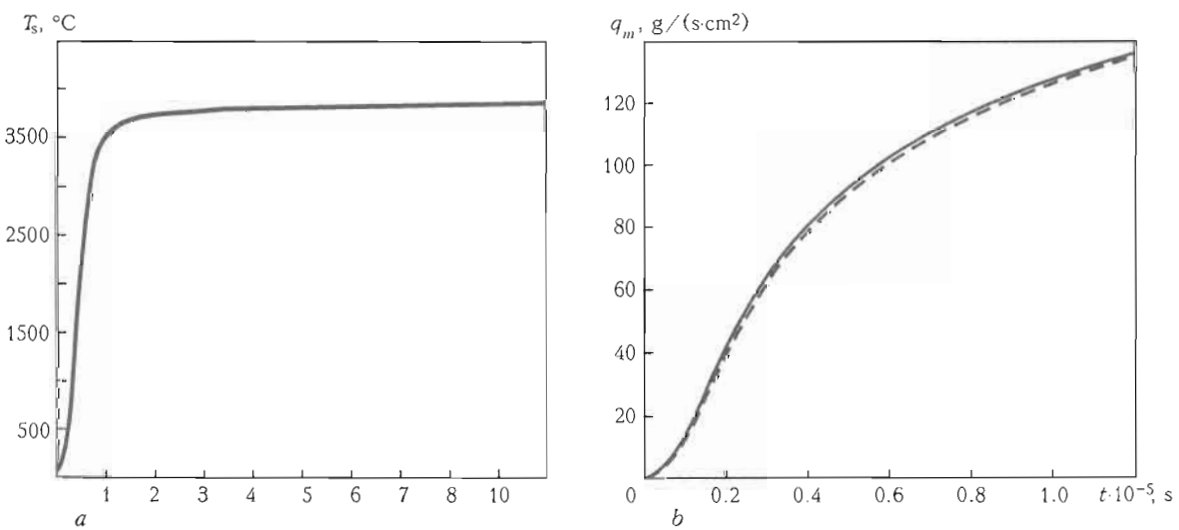


Figure 4. Variation of vapor mass flux from the melt surface (*a*) and metal temperature at the center of a laser heating spot (*b*): solid lines — non-stationary model; dashed — stationary one

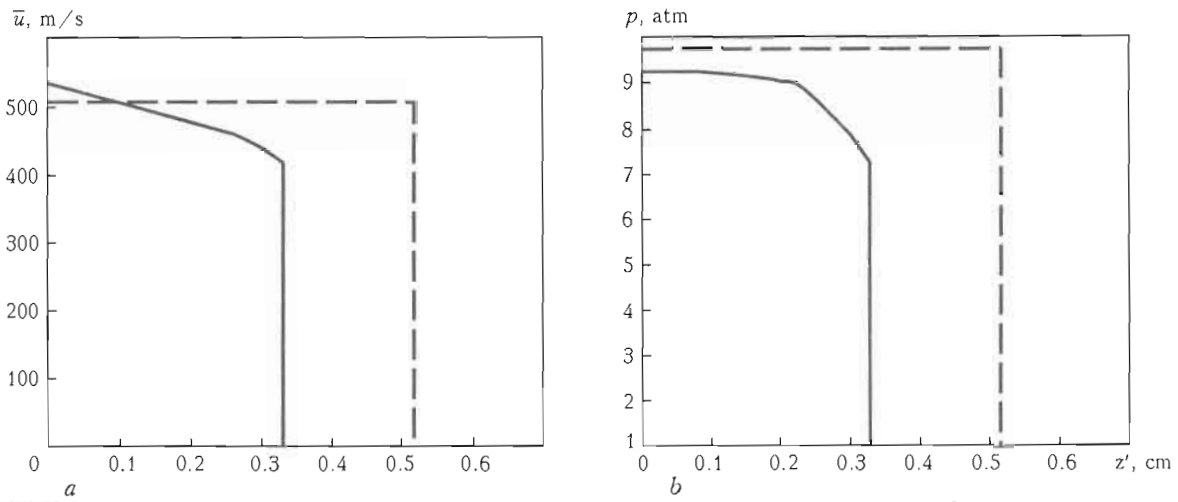


**Figure 5.** Distribution of vapor velocity (*a*) and gas-dynamic pressure (*b*) in vapor phase at $t = 6.7 \cdot 10^{-6}$ s: solid and dashed lines — non-stationary and stationary model, respectively

of establishing the gas-dynamic processes. Hence it is expectable that with the decreasing heating rate, more drastic difference in flow pattern and, accordingly, in amount of specific mass flux $q_m(t)$, can be observed.

To illustrate the above statement let us consider the sheet heating by the laser radiation with lesser intensity $I_0 = 7 \cdot 10^5$ W/cm$^2$. In contrast to the heating conditions mentioned earlier, at a low heating rate the difference between stationary and non-stationary evaporation models with respect to the solution of the heat problem becomes more evident (Figure 6).

The non-stationary nature of gas-dynamic process needs thus be taken into account at a lower heating rate.

The models considered above are valid for metal evaporation from the developed liquid surface (rigorously speaking, from the unbounded flat surface). For evaporation from the spot surface of small diameter, as it is the case for the focused laser radiation impact on metal, the assumption of the one-dimensional pattern of gas-dynamic flow is no longer feasible.

To study an influence of the side vapor expansion, the 2D gas-dynamics problem will be considered for gas-vapor mixture in axisymmetric formulation.

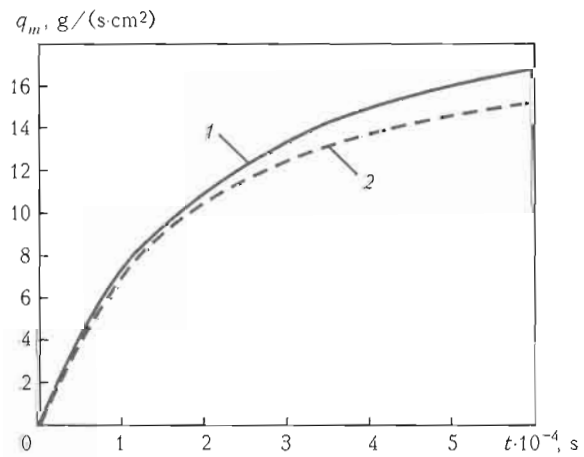


**Figure 6.** Variation of the vapor mass flux in time at $I_0 = 7 \cdot 10^5$ W/cm$^2$

The Euler equations in cylindrical coordinate system $(r, z')$ appear as

$$\frac{\partial \vec{U}}{\partial t} + \frac{\partial \vec{F}}{\partial r} + \frac{\partial \vec{G}}{\partial z'} = -\frac{\vec{f}}{r}. \qquad (11)$$

Here $\vec{U} = (\rho_1, \rho, \rho u, \rho v, E)$; $\vec{f} = (\rho_1 u, \rho u, \rho u^2, (E + p)u)$; $\vec{F} = (\rho_m u, \rho u, \rho u^2 + p, \rho uv, (E + p)u)$; $\vec{G} = (\rho_m v, \rho v, \rho u \rho v, \rho v^2 + p, (E + p)v)$; $\rho_m$ is the density of metal vapor; $\rho$, $p$ are relatively the pressure and the density of mixture; $u$ and $v$ are the the axial and radial components of velocity vector, respectively; $E = \rho e + (\rho u^2 + \rho v^2)/2$ is the energy of mixture; $e = p/\rho(\gamma - 1)$. Equations (11) are integrated over the region shown in Figure 7.

The boundaries $\Gamma_4$, $\Gamma_5$ are external relative to the flow region boundaries, the boundary $\Gamma_3$ is the symmetry axis, $\Gamma_6$ is the metal surface beyond the evaporating spot. The Knudsen layer on the surface of liquid metal pool is modeled as a rectangular projection with the boundaries $\Gamma_1$, $\Gamma_2$. At the boundary $\Gamma_1$ a condition, similar to (9), is set. A tangent component of velocity vector at this boundary is redefined from the flow region by the characteristic correlations. On a metal surface the boundary non-percolation condition is set, at the flow axis the symmetry condition is laid down, while at the external boundaries $\Gamma_4$ and $\Gamma_5$ non-reflection boundary conditions are established.

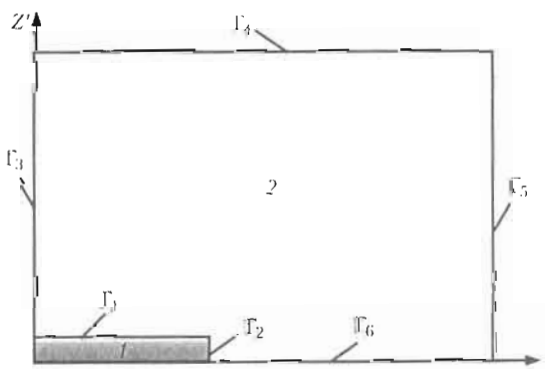


**Figure 7.** Computation region for solution of 2D equations of gas-dynamics: *1* — Knudsen layer; *2* — gas-dynamic region; for designations see the text

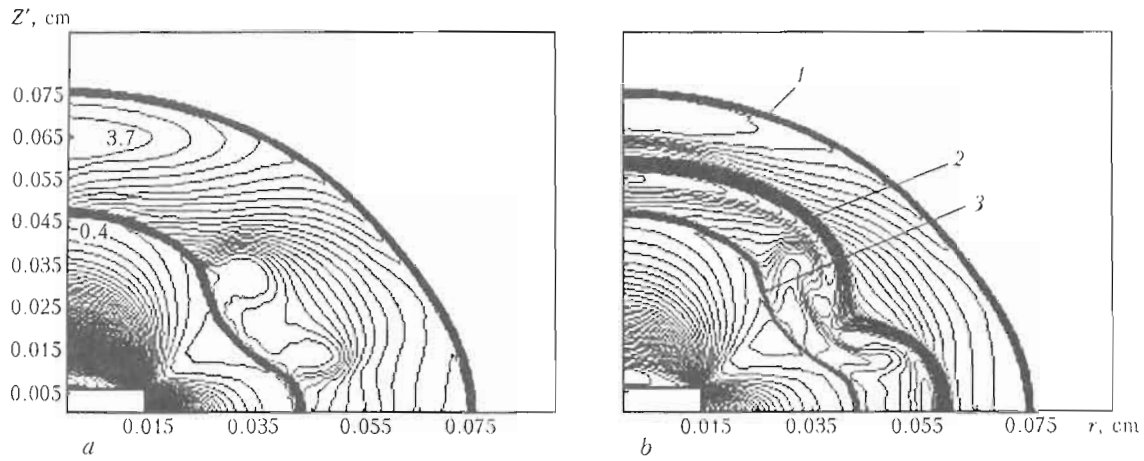


**Figure 8.** Pressure contours $p/p_0$ (*a*) and density contours (*b*) at $t = 4 \cdot 10^{-7}$ s: *1* — shock wave; *2* — contact discontinuity; *3* — compression shock

Initial conditions are given by $p = p_0$, $u = 0$, $v = 0$, $\rho = \rho_0$, $\rho_1 = 0$, where $p_0$ and $\rho_0$ are relatively pressure and density of atmospheric gas. The formulated problem of two-dimensional gas-dynamics was solved by the second order Godunov method (TVD scheme). The dimensions of the calculation region are determined by the boundary $\Gamma_1$ with the length $L_0 = 0.015$ cm and the Knudsen layer $\Gamma_2$ with the thickness being equal to $0.4L_0$ (taking into account the mean free path in atmospheric gas and in metal vapor straight above the melt). The dimensions of external boundaries of the calculation region $\Gamma_5$, $\Gamma_6$ are equal to $6L_0$. Air at normal conditions is taken as an external gas. The temperature of evaporating metal surface is assumed to be constant and amounting to 4000 °C.

The calculation results are charted in Figures 8 and 9. Given the side unloading of vapor flux, the qualitatively different flow pattern comes to emerge. The velocity at the Knudsen layer boundary does not reach the stationary point (as it does in one-dimensional case), but instead grows monotonously until the Mach number becomes equal to unity (see Figure 9, *b*). Thereupon, in the vapor flow region the stationary compression shock occurs, followed by a contact discontinuity at a steady propagation rate. The compression shock originates from the fact that pressure in the region between the Knudsen layer boundary and external gas decreases to below atmospheric (see the low pressure region in Figure 9, *a*).

The shock wave at the current moment is 0.075 cm away from the Knudsen layer boundary, while the low pressure region and compression shock are at a distance of 0.05 cm. The similar flow pattern was experimentally observed in [5] when studying the impact of pulsed laser radiation on metal. It is worth mentioning that the analogous flow structure can also be evidenced in supersonic gas flow from a nozzle in underexpansion mode.

We now turn our attention to the conditions of non-stationary regime of metal heating by laser radiation. It should be noted that the time of attaining the stationary value of the surface temperature is about three orders longer than that which takes for Mach number at the Knudsen layer boundary to become equal to unity.

Therefore, with the side unloading in action, the problem of metal heating by laser radiation can be fairly well approximated by putting Mach number at the Knudsen layer boundary to unity. In such a setting the mass flux can be found from expressions (4) and (5) without solving the gas-dynamics problem. The performed numerical study of metal heating and con-

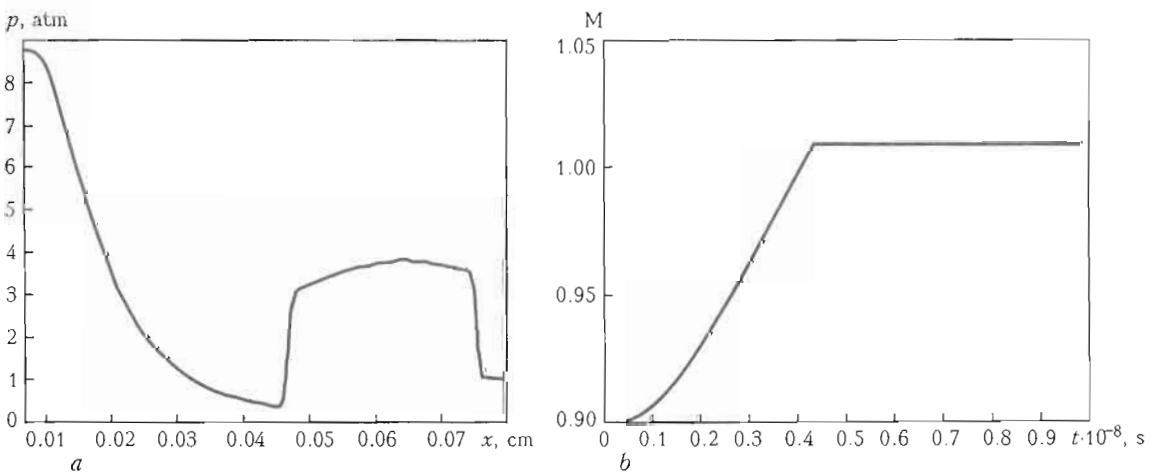


**Figure 9.** Pressure distribution along the symmetry axis at $t = 4 \cdot 10^{-7}$ s (*a*) and peak Mach number value at the Knudsen layer boundary over the time $t$ (*b*)

vective evaporation induced by pulsed laser radiation effect reveals the fact that such important (from a technological standpoint) characteristics as the thermal state of metal, the density of metal vapor mass flux, its expansion rate, heat losses due to evaporation and the pressure of vapor recoil reaction, are determined not only by metal heating conditions but also by gas-dynamic processes that occur in a vapor phase. Generally, for modeling the case under consideration it is necessary to utilize the self-consistent model describing the heating processes in a metal volume, the processes of heat and mass transfer in the Knudsen layer, as well as gas-dynamic processes in a vapor flux.

***Acknowledgments.*** *This work was supported by the National Academy of Sciences of Ukraine and the Russian Foundation for Basic Research.*

1. Arutyunyan, R.V., Baranov, V.Yu., Bolshov, L.A. et al. (1989) *Effect of laser radiation on metals.* Moscow: Nauka.
2. Vedenov, A.A., Gladush, G.G. (1985) *Physical processes in laser treatment of materials.* Moscow: Energoatomizdat.
3. Duley, W.W. (1983) *Laser processing and analysis of materials.* New York: Plenum Press.
4. Anisimov, S.I., Imas, Ya.A., Romanov, G.S. et al. (1970) *Impact of high power radiation on metals.* Moscow: Nauka.
5. Batarov, B.A., Bunkin, F.V., Prokhorov, A.M. et al. (1970) Static shock wave generated during stationary metal evaporation under laser radiation. *Pisma v Zhurnal Tekhn. Fiziki*, **11**, 113–118.
6. Gusarov, A.V., Gnedovets, A.G., Smurov, I. (2000) Gas dynamics of laser ablation: Influence of ambient atmosphere. *J. Appl. Phys.*, **88**, 4352–4364.
7. Afanasiev, Yu.V., Belenov, E.M., Krokhin, O.N. et al. (1969) Ionization processes in laser plasma. *Pisma v Zhurnal Tekhn. Fiziki*, **10**, 553–557.
8. Vorobiov, V.S. (1993) Plasma generated during the interaction of laser radiation with solid targets. *Uspekhi Fizich. Nauk*, **163(12)**, 51–82.
9. Knight, C.J. (1979) Theoretical modeling of rapid surface vaporization with back pressure. *AIAA J.*, 17(**5**), 519–523.
10. Peacemen, D.W., Rackford, H.H. (1955) The numerical solution of parabolic and elliptic differential equations. *J. Soc. Ind. Appl. Math.*, **3**, 28–41.
11. Kulikovsky, A.G., Pogorelov, N.V., Semyonov, A.Yu. (2001) *Mathematical issues of numerical solution of hyperbolic systems of equations.* Moscow: Fizmatlit.
12. Kirichenko, V., Gryaznov, N., Krivtsun, I. (2008) Experimental facility for research on pulsed laser-microplasma welding. *The Paton Welding J.*, **8**, 26–29.
13. Hu, J., Tsai, H.L. (2007) *Heat and mass transfer in gas metal arc welding.* Pt 1: The arc. *Int. J. Heat and Mass Transfer*, **50**, 833–846.
14. Kikuo, U. (1972) Reflectivity of metals at high temperatures. *J. Appl. Phys.*, 43(**5**), 2376–2383.
15. Ordal, M.A., Long, L.L., Bell, R.J. et al. (1983) Optical properties of the metals Al, Co, Cu, Au, Fe, Pb, Ni, Pd, Pt, Ag, Ti, and W in the infrared and far infrared. *Appl. Optics*, 22(**7**), 1099–1119.
16. Miller, J. (1969) Optical properties of liquid metals at high temperatures. *Phil. Mag.*, 20(**12**), 1115–1132.

# LASER TREATMENT OF SILICON AND ITO THIN LAYERS

V.P. GARASHCHUK, A.G. LUKASHENKO and V.M. SYDORETS
E.O. Paton Electric Welding Institute, NASU, Kyiv, Ukraine

Solar batteries are renewable energy sources and nowadays they are more and more used in life. Their structure is a sequence of sprayed layers of silicon as a semiconductive material, and tin doped indium oxide as electroconductive material. The last one is identified in technical literature as ITO. In engineering and in life a value of electric voltage should amount to around several thousands of volts. It poses a problem in the face of manufacturers to joint in series separated solar elements in a battery. For this purpose conductive and semiconductive layers should have electric contact. As soon as their thickness makes up not more than 1 μm, this problem is technologically complicated, especially if the batteries have large area. It is necessary, therefore, to have such technological process which will allow removing of sprayed layer in certain places without damaging lower one. It is obvious that mechanical techniques are not possible for this purpose. In the present work modes of laser evaporation of the sprayed layers of silicon and ITO of the thickness less than 1 μm are investigated and the laser with the necessary wavelength is selected.

*Selection of laser beam wavelength.* During interaction with the solid surface, one part of electromagnetic radiation is reflected from it, and other one is penetrated and is absorbed by it. In metals the light quanta are absorbed by conductivity electrons, which transfer absorbed energy to thermal oscillations of a lattice approximately for $10^{-11}$–$10^{-10}$ s. This time is called a time of relaxation and is marked as $\tau_{rel}$. This process occurs in the layer $\delta \sim 10^{-6}$ cm thick, which corresponds to the depth of light penetration in metal [1].

For metal films of $h > \delta$ thickness a light wave, reflected from the boundary with substrate, can be ignored and considered that intensity of light flux reduces on a depth according to Lambert–Burger–Bert law (LBB law), where $I(x)$ and $I(0)$ is the light intensity on depth $x$ and $x = 0$ from illuminated surface; $A$ is the absorbing capacity; and $\alpha_1$ is the film material absorption factor. However, a depth of calorification area differs from depth of light absorption area. Length $l$ of free path of electron in the film material makes up several units by $10^{-6}$ cm. Taking into account that electron returns its excess energy as a result of approximately 100 impacts, i.e. on distance of about $100l >> \delta$, it is assumed that in metal thickness $h > 100l$ heat evolution is uniformly. Such an approximation is acceptable for most metals if their thickness is less than 5 μm, as $l \approx 0.05$ μm. If film thickness exceeds certain values then it is necessary to take into account inhomogeneity of heat evolution on thickness.

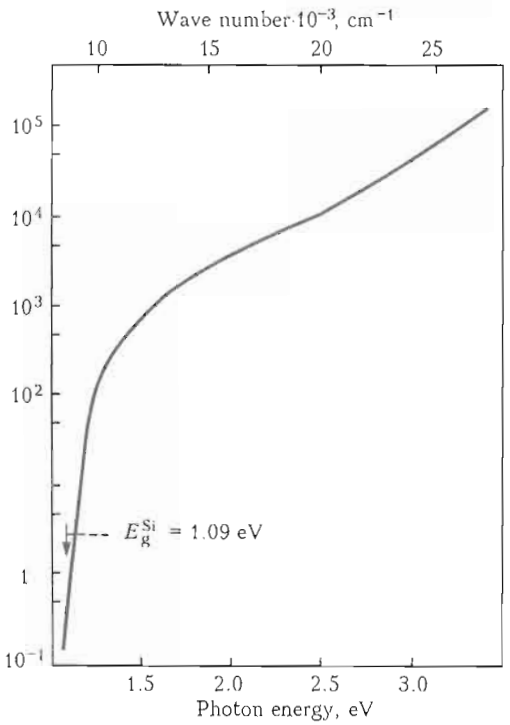


**Figure 1.** Dependence of absorption factor on photon energy for silicon at $T = 300$ K

Heat from layers, directly heated by light, is transfered to the depth by heat conduction, and the main heat conduction in metal films is an electron one.

*Evaporation of thin silicon layers.* Amount of free electrons in a band of conduction is small in semiconductors at room temperature. Therefore, for wavelengths, for which energy of light quantum is less than the thickness of band gap, absorption factor is small and light penetrates to relatively high depths. For example, for silicon that is for $\lambda > 1.137$ μm. For light with the wavelength shorter than $\lambda = 1.137$ μm, absorption takes place with the transfer of electron from valence into conduction band. This is so called a proper absorption of semiconductors. Absorption factor grows with the increase in light quantum energy, i.e. with shortening of the length of its wave (Figure 1) [2].

LBB law will be used for calculation of the part of beam intensity not absorbed by material of $a$ thickness. Light beam $AI(0)$ enters in illuminated surface and after passing thickness a beam intensity reduces up to $I(a) = AI(0)e^{-\alpha_1 a}$. Part of absorbed intensity will be

$$\beta = 1 - e^{-\alpha h}. \qquad (1)$$

Non-absorbed part of beam intensity comes deeper into material or to a sublayer. In the last case at high intensity of the beam, which reached the sublayer, the last one can be destroyed. It is necessary, therefore, to select such lengths of laser beam, for which

absorption factor $\alpha_1$ is so high that light does not reach the sublayer. Criterion of such mode of processing is being introduced. As in our technological problem there is a necessity to evaporate material, then, as it is known from practice, for most of the material a density of laser beam power of $10^7$–$10^8$ W/cm$^2$ should be created in a processing region. It is assumed that at power density of $10^3$–$10^4$ W/cm$^2$ the sublayer will not change its characteristics (i.e. will not be destroyed). Thus, beam attenuation should be not less than $10^4$ times. Then at thickness $a$ = = $10^{-4}$ cm (1 μm) of silicon layer, which should be evaporated, $\alpha_1 \geq 10^5$ cm$^{-1}$ will be received, using formula (1). It is seen from Figure 1 that silicon has such a factor of absorption for quanta with energy more than 3 eV, i.e. $\lambda \leq 0.4$ μm. For light quanta with energy of about 1 eV (≈ 1 μm ) factor of absorption makes up from several units to several tens cm$^{-1}$. At such $\alpha_1$ values several tens of percents of initial beam intensity come into the sublayer. Consequently, the first harmonic of beams of neodymium laser ($\lambda$ = = 1.06 μm) is not suitable for this problem. The second harmonic, in which energy of quantum makes up 2.35 eV ($\lambda$ = 0.53 μm), also is not appropriate. Among well-known lasers, nitrogen laser ($\lambda$ = 0.3371 μm) and excimer lasers on the basis of XeCl ($\lambda$ = 0.308 μm) and XeF ($\lambda$ = 0.352 μm) meet the requirements best of all. Nitrogen and excimer laser generates pulses of about 10 and 30 ns duration, respectively. Nitrogen laser is of a little use. This laser is based on self-restricted transitions and, therefore, its beams are low-coherent and quality of light beam is low. Moreover, duration of its pulse is small. Thus, in the case of necessity to monitor its duration some restrictions can occur. Therefore, in future in order to evaluate necessary laser beam power the orientation will be made, in particular, on parameters of excimer lasers.

*Evaluation of necessary power of laser beam.* Minimum necessary power of laser beam can be determined by a heat-balance equation. It is proposed that area $s$ of thickness $h$ sprayed layer is illuminated. It is assumed that sprayed layer is heated adiabatically, i.e. heat transfer to lower-situated layers is ignored, as their heat conductivity is unknown. Besides, heating takes place for a small amount of time so that big quantity of heat will not come into lower layers. However, the attention is paid to the fact that minimum necessary power is calculated. Density of power in focused beam at illuminated surface is $q$ (W/cm$^2$). For the time $t$ of illumination the layer will absorb energy $Q = Aqst$.

In order to evaporate sprayed layer, it should be heated up to the melting temperature, introducing energy counting on unit of mass $C_p(T_m - T_0)$, and melted, i.e. introduce of energy into the layer equals to latent melting heat $L_m$, then heated up to temperature of sublimation or boiling $C_p(T_{evap} - T_m)$, and at the end introduce of energy in it equals to latent evaporation heat $L_{evap}$. Taking into account all these stages, the following equation is written:

$$Aqst = \rho sh[C_p(T_m - T_0) + L_m + C_p(T_{evap} - T_m) + L_{evap}], \quad (2)$$

where ρ is the density of sprayed layer. So, minimum necessary density of power in area of illumination $q$, mean power in pulse $qs$, pulse energy $qst$, mean energy of laser generation $qsf$ (where $f$ is the pulsing frequency) can be determined for silicon using the following values of its thermal-physical quantities [1]: ρ = 2.33 g/cm$^3$; $C_p$ = 1.05 J/(g·K); $L_m$ = = $1.81 \cdot 10^3$ J/g; $L_{evap}$ = $13.7 \cdot 10^3$ J/g; $T_0$ = 293 K; $T_m$ = 1688 K; $T_{evap}$ = 2623 K.

Heat capacity of silicon depends on temperature, and its analytic expressions are represented in [3]. However, in order to simplify calculations the mean value is taken. Error does not exceed 15 %. Since in this work all calculations are estimating, then such accuracy is completely satisfactory.

Absorption capacity of any material is equal to $A = 1 - R$, where $R$ is the reflection coefficient. The last is determined by the following relationship [4]:

$$R = \frac{(n-1)^2 + \kappa^2}{(n+1)^2 + \kappa^2}, \quad (3)$$

where $n$ and κ are the indices of refraction and absorption of sprayed layer material. Index of silicon refraction has value [5], for example, for wavelength $\lambda$ = 0.53 μm in amorphous state of $n$ = 4.7 and in crystalline state of $n$ = 4.1. Sprayed layer is rather amorphous than crystalline. Index of absorption can be determined if coefficient of absorption, shown in Figure 1, is known, using relationship [4]

$$\kappa = \frac{c\alpha}{4\pi\omega} \equiv \frac{\lambda\alpha}{4\pi}, \quad (4)$$

where $\lambda$ and $\alpha$ is the wavelength and the absorption factor of sprayed material, respectively. For photon energy 3 eV (wavelength $\lambda$ = 0.4132 μm) the factor of absorption is $\alpha = 5 \cdot 104$ cm$^{-1}$; inserting it in (4) κ = 0.16 will be received. From relationship (3) the value $R$ = 0.45 for amorphous silicon is received. Using this $R$ value, quantity of absorption capacity $A$ = 0.55 is obtained.

In order to evaluate density of power, pulse power and mean laser power, the geometrics of focused laser beam are the following: length of focused beam of 1 cm, width of 0.1 cm, i.e. area of light spot $s$ = = 0.1 cm$^2$. Using (2) and data on thermal-physical properties of silicon above mentioned, the following will be obtained:

- necessary density of power at pulse duration $\tau$ = = $30 \cdot 10^{-9}$ s is $2.8 \cdot 10^8$ W/cm$^2$;
- power in pulse is $2.8 \cdot 10^7$ W;
- mean power of laser generation at pulsing frequency $f$ = 100 Hz is 85 W.

Other approach is also possible. In 1970–1980 laser technology was developed for receiving layout of microelectronic circuit, adjustment of parameters of resistances, inductances, laser burning off $p$–$n$ transitions, etc., and investigations of physical processes which occur at that. In works [1, 6] obtained that speed of evaporation of thin layer can be described by formula

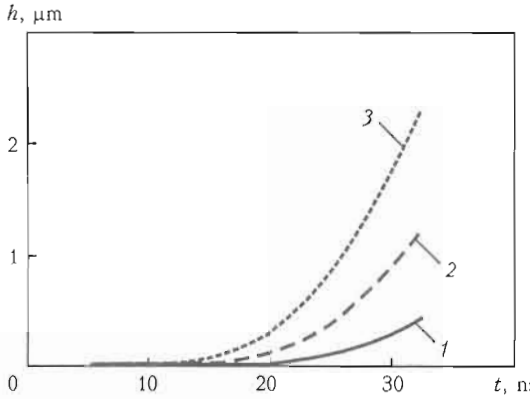


Figure 2. Change of evaporated layer thickness in time (in $10^{-9}$ s) at $q = 3{\cdot}10^8$ (*1*), $5{\cdot}10^8$ (*2*) and $4{\cdot}10^8$ (*3*) W/cm$^2$

$$V_{evap} = \frac{P}{\rho}\sqrt{\frac{\mu}{2\pi R_g T}},$$

where $P$, $R_g$, $\mu$ is the pressure of saturated vapor, gas constant, molecular weight of the evaporated thin layer, respectively. If assumed that evaporation takes place at any temperature, then thickness of evaporated layer $h$ for time $t$ is

$$h = \int_0^t V_{evap} dt = \int_0^t \frac{P(t)}{\rho}\sqrt{\frac{\mu}{2\pi R_g T(t)}}\, dt. \qquad (5)$$

In this relationship it is estimated that temperature increases with time of illumination and pressure of saturated vapor depends on temperature, and in other words on time. It is well-known that dependence of saturated vapor pressure on temperature is described by relationship $P(T) \equiv P(t) = 10^{\alpha - \frac{\beta}{T(t)}}$, where $\alpha$ and $\beta$ are the constants. In works [3, 7, 8] data on measurement of pressure of saturated silicon vapor in dependence on temperature are represented. During performance of this work, using data indicated above, the following dependence has been built:

$$\lg P(T) = \alpha - \frac{\beta}{T}.$$

Dependence was linear from $\frac{1}{T}$. Its approximation by linear function with the MathCAD means after log-to-linearization is described by expression

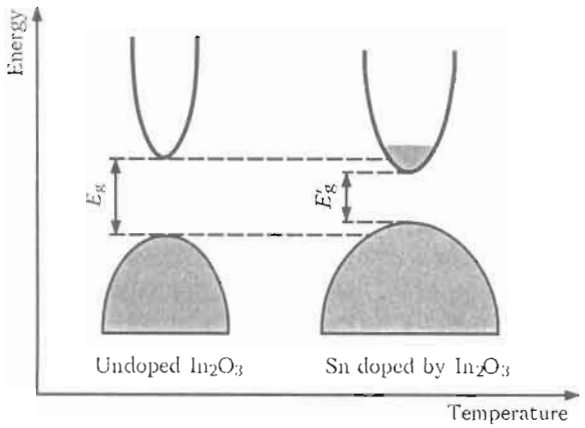


Figure 3. Scheme of energy areas in indium oxide and ITO

$$P(T) = 10^{11.538 - \frac{18360}{T}}. \qquad (6)$$

If latent melting heats and evaporations are ignored, then from (2) similar equitation temperature of illuminated layer is

$$T(t) = T_0 + \frac{Aq}{\rho C_p h}\, t. \qquad (7)$$

Inserting (6) and (7) in (5) and also using indicated above values of thermal-physical values, relationships of change of evaporated layer thickness in dependence on illumination time $h(t)$ were obtained with MathCAD means for layer thickness $h_1 = 1$ μm.

Results are shown in Figure 2. In the first and third cases (see curves *1* and *3*), thickness of evaporated layer does not reach 1 μm, in the second (see curve *2*) exceed virtually in 2 times. This is evidence of high sensitivity of this technological process to power of density in the area of illumination. Obtained values are less than 2 times higher than the corresponding ones received from heat-balance equation. Obtained dependences in this case should be evaluated only as qualitative illustration of growth of evaporated layer thickness in illumination time because of the fact that they were calculated at very rough assumptions. Here latent heats were ignored which in silicon significantly exceeds heat content at heating up to the evaporation temperature. These dependences indicate that almost half of the pulse duration comes for metal heating up to the temperature at which considerable evaporation takes place.

*Evaporation of thin ITO layers.* ITO is an abbreviation of English term «Indium Tin Oxide», i.e. it is the indium oxide, doped by tin. ITO includes 90 % $In_2O_3$ and 10 % $SnO_2$. Indium oxide has very wide band gap. Band gap of tin oxide equals to 2.5–3.0 eV. Tin doped by indium oxide provides creation of a donor level due to which ITO becomes conductive (Figure 3) [9]. Width of ITO band gap makes up 3.75 eV. Therefore, in visible region this layer is transparent as well as conductive at the same time. Width of band gap is $E_g = 3.75$ eV.

Unfortunately, thermal and physical characteristics of these combinations do not enough studied. Search for in Internet gave the following results for indium oxide: $\rho = 7.14$ g/cm$^3$, $T_m = 1800$–$2000$ K, and $\rho = 6.3$ g/cm$^3$, $T_m = 1353$ K for tin oxide. According to the data of Fire Protection Department of USA, the last one decomposes without reaching boiling temperature $T_b$. As for the other characteristics it is indicated that they are unknown. Insufficient data on thermal and physical characteristics of ITO components do not allow making for them the same evaluation as it has been done for silicon.

Data on ITO pass band and absorption factor represented in [9]. These dependences are shown in Figures 4 and 5. Analyzing two above mentioned illustrations it is seen that beams of neodymium laser are not suitable for ITO layers evaporation, since its transparence in the area 1.06, 0.53 and 0.353 μm is significant (wavelength 0.353 μm corresponds to quantum energy of 3.51 eV). For this reason excimer XeF laser with the wavelength of 0.351 μm is also not suitable.

Data on excimer lasers of LAMBDA PHYSICS Company

| LAMBDA SX | 315C | 300C | 200C | 100C |
|---|---|---|---|---|
| Wavelength, nm | 308 | | | |
| Stabilized energy range, mJ | 800–1050 | 800–1000 | 550–670 | 800–1000<br>800–900 |
| Maximum stabilized average power, W | 315 | 300 | 200 | 90 |
| Maximum repetition rate, Hz | 300 | 300 | 300 | 50 / 100 |
| Energy stability (rms), % | <1 | <2 | <1 | <2 |
| Pulse duration (FWHM, typ.), ns | 29 | 29 | 29 | 29 |
| Beam dimensions $w \times h$ (FWHM, typ.), mm | 35 × 13 | 35 × 13 | 35 × 12 | 35 × 13 |
| Divergence $w \times h$ (FWHM, typ.), mrad | <4.5 × 1.5 | | | |
| Electrical, kVA | 26 | 26 | 18 | 18 |
| Dynamic gas lifetime at maximum stabilized energy, mio. pulses | >40 | >40 | >40 | >20 |
| 3-phase | 400 VAC, 50 or 60 Hz, 190–480 VAC2 | | | |
| Weight without transformer, kg | 1400 | 1400 | 1370 | 1300 |
| Cabinet size $l \times w \times h$, mm | 2500 × 850 × 1925 | | | |

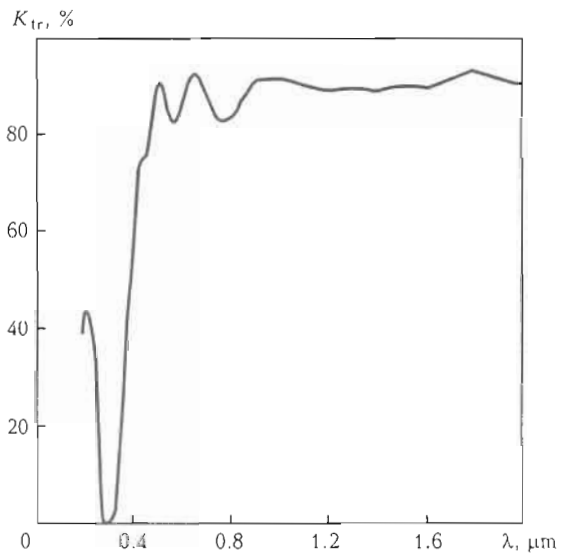


Figure 4. ITO layer transmission factor versus wavelength

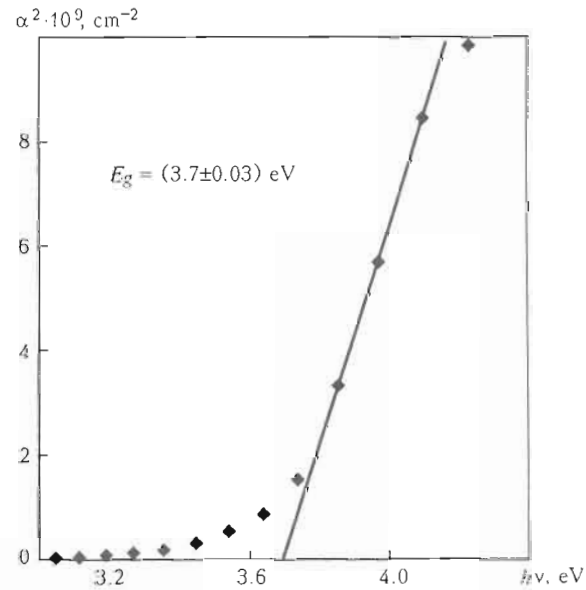


Figure 5. Dependence of square of ITO layer absorption factor on photon energy

From technical data of excimer lasers of LAMBDA PHYSICS Company (Table) it is seen that almost all their characteristics meet the requirements for evaporation of ITO and silicon sprayed layers. Mean powers of these lasers exceed 2–3 times calculated values, accuracy of which is not high. The requirements on laser beam dispersion are also fulfilled. Shape of the beam, which goes out from resonator, is rectangular (35 × 13 mm). If the resonator in laser is stable, then the beam dispersion of 4.5 mrad will be in the direction of the side of 35 mm length and 1.5 mrad – of 13 mm. Such beam can be easily focused in a line of 1 mm width by cylindrical lens with focal length of several tens of millimeters. However, a problem with materials for optical parts is appearing: all the parts should be made of quartz glass.

## CONCLUSIONS

1. Excimer XeCl lasers should be used for treatment of thin silicon and ITO layers.

2. Laser should work in following pulse mode: pulse duration of about 30–40 ns, power in pulse of $10^7$–$10^8$ W, pulsing frequency of 100–300 Hz.

3. Quartz glass should be used as a material for optical parts.


1. Anisimov, S.I., Imas, Ya.A., Romanov, G.S. et al. (1970) *Influence of illumination of high power on metals*. Moscow: Nauka.
2. Vavilov, V.S. (1963) *Influence of illumination on semiconductors*. Moscow: Fizmatgiz.
3. *Tables of physical values*: Refer. book. Ed. by I.K. Kikoin. Moscow: Atomizdat.
4. Landsberg, G.S. (1967) *Optics*. Moscow: Nauka.
5. Lietoila, A., Gibbons, J.F. (1982) Computer modeling of the temperature rise and carrier concentration induced in silicon by nanosecond laser pulses. *J. Appl. Phys.*, 53(4), 3207–3213.
6. Vejko, V.P. (1986) *Laser treatment of film elements*. Leningrad: Mashinostroenie.
7. (1962) Silicon. In: *Physical encyclopedia*. Moscow: Sov. Entsiklopediya.
8. (1976) *Properties of elements*: Refer. book. Pt 1: Physical properties. Moscow: Metallurgiya.
9. Shabbir, A.B. (1998) *Study of indium tin oxide (ITO) for novel optoelectronics devices*. London: University of London.

# SPATIAL REDUCTION SIMULATION STRATEGY FOR INCREMENTAL THERMAL FORMING PROCESS

M. GRDEN and F. VOLLERTSEN
BIAS – Bremer Institut fuer angewandte Strahltechnik GmbH, Bremen, Germany

A straight forward FEM simulation of multiple pass thermal sheet forming usually results in an extraordinarily time-consuming computation. In this paper an approach allowing much faster thermal-mechanical calculation is presented. The main idea for calculation time reduction is based on spatial partitioning of the sheet in several irradiated and non-irradiated sections. Each of the irradiated sections is simulated separately using initially set-up boundary conditions. In order to obtain the boundary conditions on heat flux and mechanical force very few simulated irradiation cycles are needed, in which the complete sheet metal is considered. Based on the output data of the first irradiation cycles the boundary conditions for subsequent cycles are estimated. In one last step the simulated sheet sections are rejoined. The result of the presented simulation strategy is finally compared to experimental results.

The utilization of heat sources in sheet metal forming provides a flexible metal forming method. This process does not require specialized mechanical tools or big external forces. The use of laser for thermal bending has been investigated by several authors [1, 2]. Alternative to lasers, a plasma jet can be used for thermal forming. The use of both heat sources is based on same bending principles, which are the local creation of thermal stresses beyond the yield strength and plastic-elastic deformations. The main difficulty in thermal bending lies in the prediction of correct process parameters like required heat source power, velocity or number of irradiations. In order to avoid high experimental effort, attempts have been made to simulate the bending by a finite element analysis [3, 4]. The standard approach for this may even require weeks of computations on powerful workstations. In order to make iterative thermal forming more attractive to industrial applications more efficient planning methods have to be found. In an earlier work [5] a reduced model strategy for straight irradiation paths has been discussed. In this paper, more sophisticated approach is presented where also curved paths can be handled. By the modified method further calculation time shortening and accuracy improvement can be obtained. The sheet region being irradiated is simulated partition wise with boundary conditions referring to stress and heat flux. These explicit boundary conditions are based on trend functions obtained by automatic analysis of output data resulting from a straight forward FEM simulation set up for 3 cycles.

For validation purposes thermal forming experiments have been performed for straight and curved irradiation paths.

**Experimental setup.** The thermal forming experiments done for the aim of the work discussed in this paper have been performed utilizing a non-transferring plasma jet as the underlying heat source. However the presented optimization to the simulation strategy is not limited to plasma beam, even more it is suitable for any energy distribution provided by an energy beam. The nominal power of the used plasma current source is 6 kW. The mean absorbance behavior is 16 ± 3 % at 18 mm distance of the nozzle to the sheet metal. The effective energy spot has a diameter of 14 mm with a nearly Gaussian energy distribution. The velocity at irradiation is 3400 mm/min. The processed material is the austenitic steel alloy 1.4301. This type of material has been chosen to achieve a high temperature gradient over the sheet thickness and also to avoid effects resulting from phase transformations due to high temperatures and cooling rates. The used specimens are of 2 mm thickness. For the purpose of verification several geometry variants have been considered, which include straight and curved irradiation paths. The clamping of the sheets has been realized by one point fixing, which does not affect the thermal bending result. The following variant models are considered (Figure 1):

• quarter-circle path: specimen 125 × 125 × 2 mm, 95 mm path radius (Figure 1, *a*);

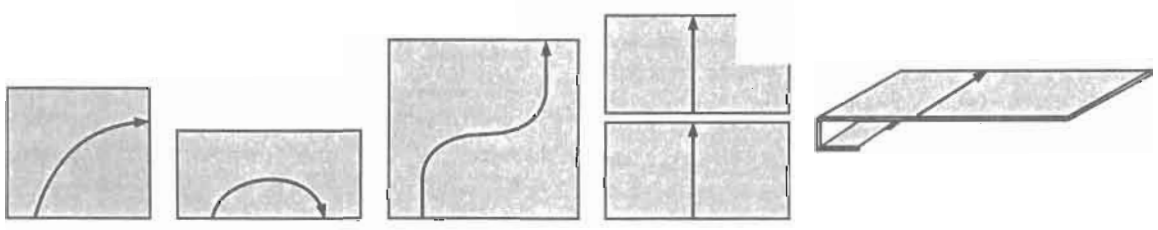


**Figure 1.** Geometry of specimens to be processed

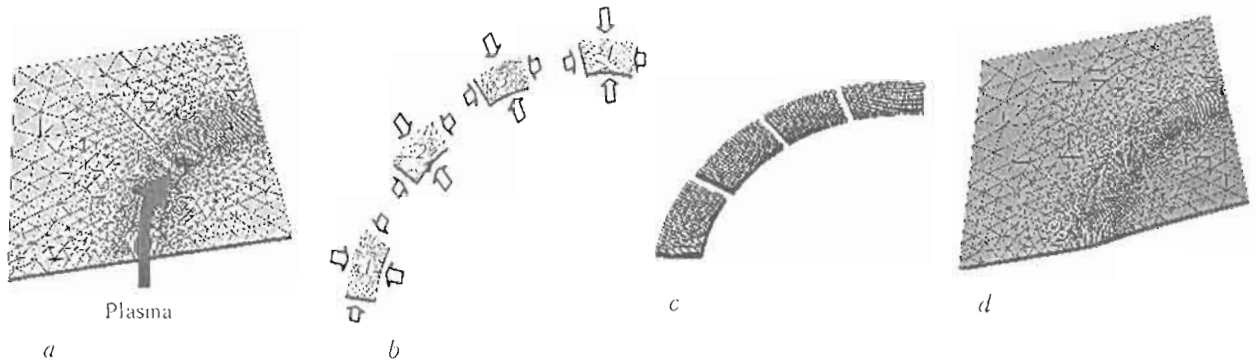


**Figure 2.** 4-steps schema of the optimized simulation approach: *a* – 3-cycles standardt simulation; *b* – creation of boundary conditions; *c* – decomposed simulation; *d* – reintegration

• half-circle path: specimen 150 × 75 × 2 mm, 39 mm path radius (Figure 1, *b*);

• S-path: specimen 150 × 75 × 2 mm (Figure 1, *c*)

• sheet with and without cut-out: specimen 125 × × 125 × 2 mm (Figure 1, *d*)

• one side stiffened sheet: specimen 125 × 70 × × 2 mm (Figure 1, *e*)

**Optimized FEM simulation method.** *General strategy.* The optimized simulation strategy is based on model decomposition combined with an application of time- and position-dependent boundary conditions. It can be applied to straight as well as to curved irradiation paths. Also complex sheet geometries can be dealt with. The main course of this strategy has been sketchily described in [6]. However, that publication did not include specific results because of not fully developed detail solutions, which are presented here. Four main steps of the approach are recapitulated in brief (Figure 2):

• simulation of the first 3 irradiation cycles using a straight forward non-decomposed FEM modeling;

• automated output data processing and extraction of 4 structure partitions from the irradiated sheet region, as well as automated creation of extrapolated boundary conditions for decomposed partitions simulation of remaining irradiation cycles;

• simulation of another $n$ process cycles for each of the 4 partitions in a successive way or in parallel on different CPUs/computers (purely elastic loaded sections are not simulated);

• reintegration of the simulated section results into the removed purely elastic loaded regions into the initial sheet geometry according to the balance of forces condition.

The mechanical and thermal boundary conditions are defined individually for every element adjacent to each boundary side of an extracted model partition. A representative example is provided by Figure 3, where an individual pressure/tension function *PRESS* and heat flux function *HFL* is applied perpendicularly to one side of an element *el*.

*Extrapolation of boundary conditions.* The specification of the boundary functions *PRESS* and *HFL* is based on observed differences between the calculated values for the 3 simulated cycles. A trend function calculating the values for higher cycle numbers $k$ is set up for every element *el* and point of time $t$ within one cycle $c$. The currently implemented approach is based on the behavior of a geometrical series, but has been adjusted according to the exponent of the multiplying factor $q$. The provided equations are a result of functional behavior matching to averaged incremental stress and heat flux development observed within a standard non-decomposed FEM simulation. For the extrapolation an asymptotic behavior has been assumed. The boundary function *PRESS* is defined by the following equations (*HFL*-function formulation is analogous):

$$k \in \{1, 2, 3\}: PRESS\ (t, el, k) = \text{const}_{t, el, k};$$

$$k > 3: PRESS\ (t, el, k) = PRESS\ (t, el, 3) + \\ + \sum_{i=4}^{n} (\Delta\sigma_m q^{(1-2)^{1.5}}),$$

where

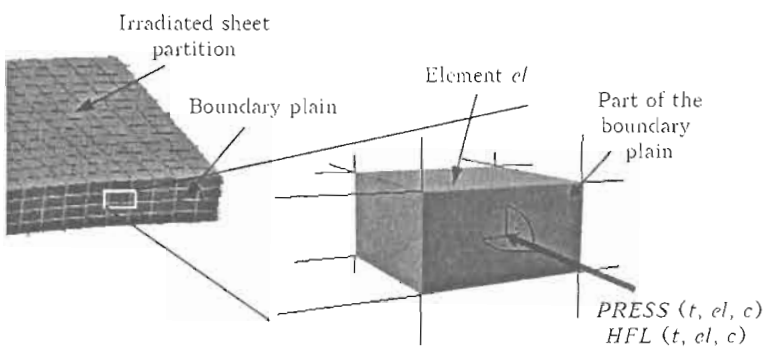


**Figure 3.** Distributive mechanical and thermal load application as boundary condition (for designations see the text)

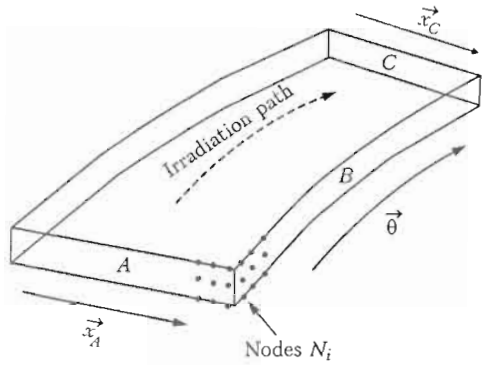


$$\sum_{i=1}^{|A|} U_{N_i,\overrightarrow{x_A}} = \sum_{i=1}^{|A|} U_{N_i,\vec{z}} = 0 \text{ with } N_i \in A; \quad (1)$$

$$\sum_{i=1}^{|B|} U_{N_i,\vec{\theta}} = \sum_{i=1}^{|B|} U_{N_i,\vec{z}} = 0 \text{ with } N_i \in B; \quad (2)$$

$$\sum_{i=1}^{|C|} U_{N_i,\overrightarrow{x_C}} = \sum_{i=1}^{|C|} U_{N_i,\vec{z}} = 0 \text{ with } N_i \in C. \quad (3)$$

**Figure 4.** Virtual clamping of a decomposed sheet section using displacement constraints

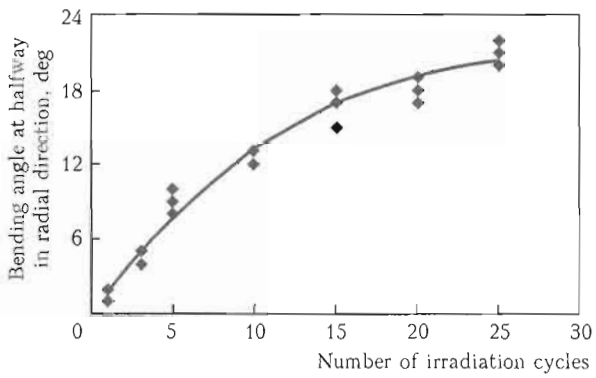


**Figure 5.** Quarter-circle ($r$ = 95 mm), experimental result including trendline

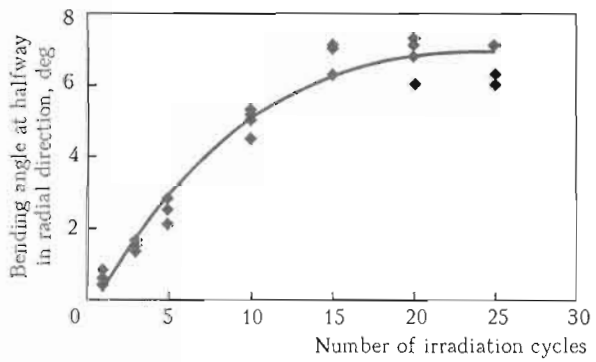


**Figure 6.** Half-circle ($r$ = 39 mm), experimental result including trendline

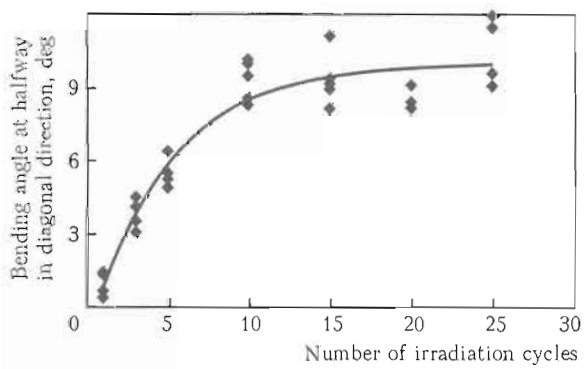


**Figure 7.** S-path, experimental result including trendline

$$\Delta\sigma_m = \frac{\sigma_3 - \sigma_1 + \sigma_2 - \sigma_1}{2 \cdot 1.5}; \; q = \frac{\min\left(|\Delta\sigma_m|, \left|\frac{\sigma_2 - \sigma_1}{2}\right|\right)}{\max\left(|\Delta\sigma_m|, \left|\frac{\sigma_2 - \sigma_1}{2}\right|\right)}.$$

Extrapolated values obtained by the given boundary function are in good agreement with respect to the ones resulting from simulations considering the complete structure model.

*Virtual clamping of decomposed partitions.* Another task requiring a non-trivial solution is given by the aspect considering the separately performed simulation of the component part decomposed sections. Since the boundary planes of these sections experience an external distributed mechanical load there may occur a translation and/or rotation of these substructures. Because these effects do not serve the purpose of local pressure increase/decrease they need to be counteracted by a suitable virtual clamping. The main requirements to such a clamping are the avoidance of an overall section translation/rotation in/around the $x$-, $y$- and $z$-axis, no large increase of computational complexity as well as low clamping force at individual nodes. To meet these requirements a set of mathematical propositions on nodes displacement behavior has been constructed. Three equations are used

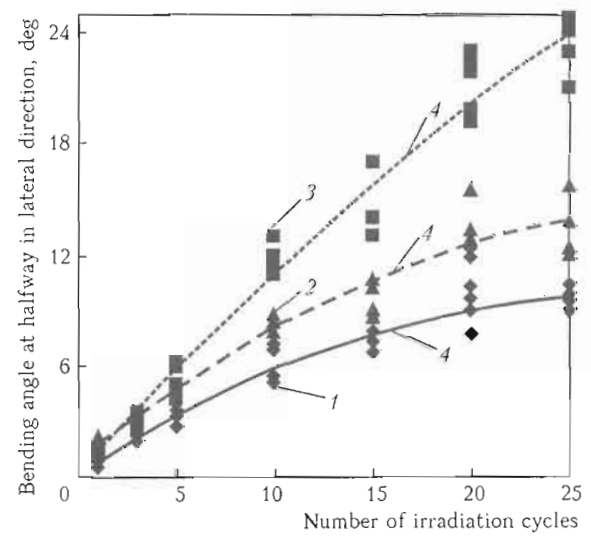


**Figure 8.** Straight path on different plate geometries: *1* — rectangular plate; *2* — plate with cut-out; *3* — edged plate; *4* — trendline

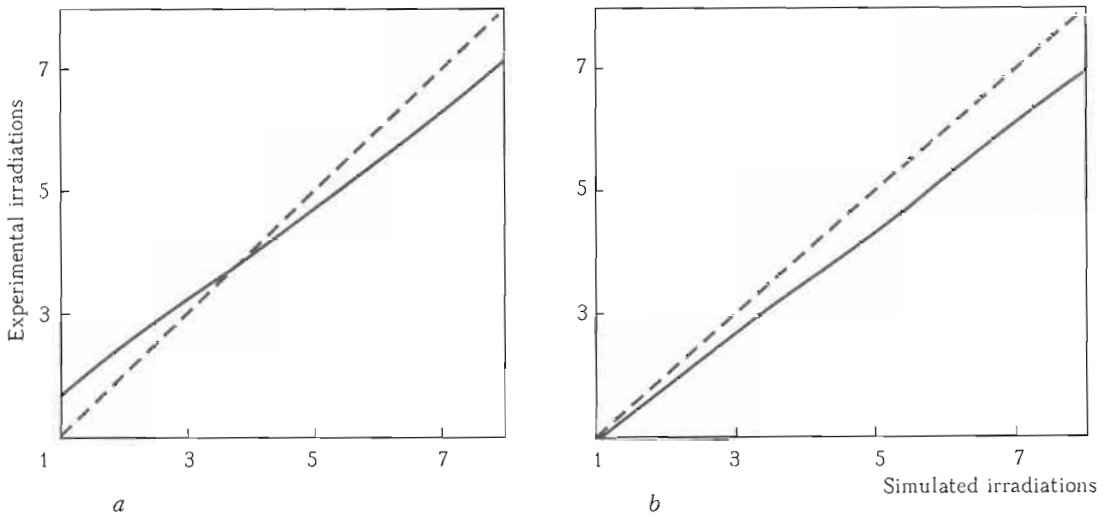


**Figure 9.** Experiment and simulation bending angle matching: *a* — quarter-circle ($r$ = 95 mm); *b* — half-circle ($r$ = 39 mm)

thereby to constrain the average displacement of nodes belonging to selected planes along convenient directions. Figure 4 provides these equations.

**Experimental and simulation results.** In Figures 5–8 the results of thermal forming experiments for different shapes of irradiation paths and component part geometries are shown up to 25 irradiation passes.

So far the discussed simulation strategy has been tested with the quarter- and half-circle in the partial range of the first 8 irradiation cycles. Figure 9 shows the matching degree of experimental bending angles (trendlines) and the simulated ones with respect to the irradiation number. The dashed diagonal line marks the best possible matching. In the depicted range the deviation in the reference bending angle lie within 18 %. The optimized quarter-circle simulation provides an 8 times shortening of the time effort per pass than using a standard FEM approach including a non-decomposed model. The half-circle simulation was simulated 9 times faster. This holds for utilizing, on one hand, 4 CPUs to calculate one irradiation cycle with the complete element mesh and, on the other hand, having each of the 4 CPUs simulating one irradiated partition. The obtained time advantage is in a good agreement to the following corresponding efficiency estimation:

assuming simulation computational complexity to be $O(n^{1.5})$, a model including 14784 elements, 4 irradiated partitions and 1652 elements each, the time shortening coefficient amounts $\frac{4(1652)^{1.5}}{(14784)^{1.5}} \approx \frac{1}{7}$. Hence, a larger time advantage is to be expected for larger models.

## CONCLUSION

The presented simulation strategy for the incremental thermal forming is able to handle straight and curved irradiation paths, as well as complex and large sheet geometries. It takes advantage of the nonlinear complexity of thermal-mechanical FEM simulations. According to provided results and estimation it provides a time advantage of more than 8 times regarding non-decompositive simulation strategy. For larger or more complex sheet geometries an even higher advantage is expected. Results gained so far possess a high accuracy with a deviation below 18 % for a limited range of irradiation cycles.

***Acknowledgment.*** *We acknowledge the DFG (Deutsche Forschungsgemeinschaft) for the financial support of the project VO 530/8-3 in SPP1146.*

1. Namba, Y. (1986) Laser forming in space. In: *Proc. of Int. Conf. on Lasers* (1985), 403–407.
2. Vollertsen, F. (1994) Mechanisms and models for laser forming. In: *Laser assisted net shape engineering.* Bamberg: Meisenbach, 345–360.
3. Komlodi, A., Otto, A., Geiger, M. (2004) On the way to real-time simulation of incremental laser beam bending. In: *Laser assisted net shape engineering 4.* Erlangen, 1059–1070.
4. Vollertsen, F., Geiger, M. (1993) FDM and FEM simulation of laser forming: A comparative study. In: *Proc. of 4th Int. Conf. on Advanced Technology of Plasticity,* 1793–1798.
5. Grden, M., Pretorius, T., Woitschig, J. et al. (2007) Fast simulation method of sheet forming by plasma jet usage. In: *Proc. of 2nd ICNFT.* Bremen: BIAS, 305–313.
6. Grden, M., Vollertsen, F. (2008) Fast simulation method of thermal bending along curved irradiation paths. In: *Proc. of IWOTE.* Bremen: BIAS, 289–296.

# TWO-DIMENSIONAL MODELING OF THERMAL ROCK SPALLATION WITH LASER RADIATION

S. HOSHOVSKIY, Yu. ROGANOV, P. SYROTENKO and Yu. VOYTENKO
Ukrainian State Geological Research Institute, Kyiv, Ukraine

Thermal spallation is one of the untraditional rock destruction methods. Its application in oil-and-gas industry opens new technological possibilities in improving quality and performance of perforation and drilling of oil and gas wells. However, required efficiency of drilling will be achieved only in case of creation of precise models of laser destruction process, which should take into consideration all basic internal and external factors. Modeling is based on iterative in time finite-difference calculation of heat propagation with using heat conduction equation on Crank–Nicolson's scheme and application of a finite-difference scheme at staggered-grid in order to form stresses in a dynamic task of thermoelasticity. The boundary conditions of model are updated synchronically with propagation of extreme stresses.

The first mention of application of high power lasers for destruction of rocks is dated to the end of 1970s of the last century. Application of lasers for drilling is possible in two ways: with fusion and with evaporation of rocks. Such mechanism of rock destruction is more power consuming than traditional mechanical technique of rotary drilling. It requires up to 120 times more energy than traditional mechanical techniques. At the same time, methods of drilling wells with the help of thermal spallation with utilization of fire-jet principle have emerged [1]. This method of thermal destruction of rock is the most advanced for drilling shallow wells in field conditions. However, it has a number of essential technical limitations connected with work safety measures and complexity of supplying with reagents (components), which took place in creating flame jet [2].

Much later it is appeared laser method of spallation of rocks during their destruction, when the efforts were made towards development of laser method of drilling in the US [2–4]. At that time laser technology was focused on the problem of investigation of physical basement of processes of rocks mooring off and diminishing energy needed for this process support.

Advantage of laser breakdown of rocks when drilling of wells and their perforation is indisputable fact. Fast control over radiation stream of light energy of laser allows reaching necessary heating and mechanical stresses for rock destruction within the area of action of laser radiation. There are three methods of rock destruction: spallation, melting, and evaporation. These regimes are reached only on correct conditions of necessary laser radiation of rock in time and space. Such task may be solved only on condition of precise construction of rock destruction simulation. Laser system of rocks destruction must be adaptive to changes of conditions during its functioning. For adaptation realization it is necessary to carry out monitoring over the process rock destruction and define heat and physical characteristics of rocks in situ.

It should be noticed that at present it was made some success in laser rock destruction modeling of rock with the number of organizations in USA [3–5] (Argonne National Laboratory; Parker Geosciences, LLC; Department of Petroleum Engineering, Colorado School of Mines), Japan [5] (Now with Kyushu University) and Ukraine (Laser Technology Research Institute of NTUU «Kiev Polytechnic Institute»). Now it is early to declare that the problem of modeling rock laser destruction was solved fully on the base of conduction investigations of early mentioned organizations.

Actuality of utilization of laser technology for rock destruction is rising nowadays lifting up today because of world tendency of enlarging the depth of oil-and-gas wells. In particularly, already it takes place gas wells boring at depth of 6 km within the Dniper-Donetsk Depression on the territory of Ukraine at present. In such cases accomplishment of mathematical modeling is much more simple than to conduct experimental investigations on rock destruction with mimicking conditions in the bore at great depths or conduct the experiment directly in the well. In addition, the created high-effective mathematical model of laser process for rock destruction must take into account practically all important external and internal factors, which essentially influence the process of rock laser destruction. Also the mathematical modeling of process rock destruction with the help of laser presents the ability of its optimization upon chosen criteria for various rocks and conditions of their imbedding in the Earth.

*Mathematical model of a spalling process with the influence of laser radiation.* Under the influence of laser radiation absorption of heat energy on the surface of the rock and considerable local warming up of rock lead up to volume dilating takes place. As a result additional deformation and stress appears. In the area where stress exceeds permissible limit, it takes place destruction of substance. As the additional thermal shifts are not significant, and the process of destruction is not of those enlarging in time quickly, therefore it is possible to use decoupled dynamic model of thermoelasticity for its describing [6]. All the non-

linearity, which is connected with the process of destruction of rock for such model, is taken into account with the help of dynamic changing boundary conditions.

In accordance with decoupled dynamic model of thermoelasticity thermal field $T(x, t)$, where $x \in \Omega$, is independent of deformation and stress, which appear during the process of heating. It is estimated fully with heat source, coefficient of thermal conduction of medium and thermal conditions on the boundary $\Gamma = \overline{\Omega}$ of the area of calculation $\Omega$. Practically heat exchanging is not taking place between this and exterior area at the boundary $\Gamma$, which is far from the source. Hence, the lines of temperature gradients are parallel to $\Gamma$. Therefore it had to fulfill Neumann convention about mutual perpendicularity of normal vector $\mathbf{n} = (n_1, n_2, n_3)$ to the surface $\Gamma$ and vector $\nabla T = \left(\frac{\partial T}{\partial x_1}, \frac{\partial T}{\partial x_2}, \frac{\partial T}{\partial x_3}\right)$:

$$\frac{\partial T}{\partial n} = n_1 \frac{\partial T}{\partial x_1} + n_2 \frac{\partial T}{\partial x_2} + n_3 \frac{\partial T}{\partial x_3} = 0. \qquad (1)$$

Within the area of source (laser) action, if it is switched on, it emits energy $q$ (density of heat flow) onto the unity surface at unit of time, which is proportional to the power of the laser radiation $P$, the coefficient of absorption of material $A$, and inversely proportional to area of cross-section of the laser beam $S = \pi r^2$:

$$q = \frac{PA}{\pi r^2}.$$

This energy is proportional to velocity of temperature changing along the corresponding normal to a surface:

$$q = -\lambda_{ij} \frac{\partial T}{\partial n} = -\lambda_{ij} \left( n_1 \frac{\partial T}{\partial x_1} + n_2 \frac{\partial T}{\partial x_2} + n_3 \frac{\partial T}{\partial x_3} \right), \qquad (2)$$

where $\lambda_{ij}$ is the coefficient of heat conduction, W/(m·K), and $q$ is the density of heat flow, W/m$^2$.

Temperature $T(x_1, x_2, x_3, t)$ inside the body satisfies heat conduction equation

$$\frac{1}{\chi} \frac{\partial T}{\partial t} = \frac{\partial^2 T}{\partial x_1^2} + \frac{\partial^2 T}{\partial x_2^2} + \frac{\partial^2 T}{\partial x_3^2}, \qquad (3)$$

where $c$ is the specific heat capacity, J/(kg·K); $\rho$ is the density, kg/m$^3$; $\chi = \frac{\lambda_{ij}}{c\rho}$ is the thermal diffusion coefficient. Initial temperature conditions contain in itself designed temperature field for $t = 0$: $T(x_1, x_2, x_3, 0) = T_0(x_1, x_2, x_3)$. Conditions (1)–(3) define field of temperature uniquely for all times $t > 0$ inside the area $\Omega$.

In the presence of various meanings of temperature inside the media, additional stresses appear. In that case the law of Duhamel–Neumann [7] is fair, as to which of stress tensor $\delta_{ij}$ is connected with strain tensor $\varepsilon_{ij} = \frac{1}{2}\left(\frac{\partial u_i}{\partial x_j} + \frac{\partial u_j}{\partial x_i}\right)$ and temperature field $T(x_1, x_2, x_3, t)$ with relationship

$$\sigma_{ij} = 2\mu\varepsilon_{ij} + [\lambda\varepsilon_{kk} - (3\lambda + 2\mu)\alpha\Delta T]\delta_{ij}, \qquad (4)$$

where $\alpha$ is the coefficient of thermal linear expansion, K$^{-1}$; $\delta_{ij}$ is the Kronecker symbol; $T_0$ is the temperature of environment; $\Delta T = T - T_0$; $\varepsilon_{kk} = \varepsilon_{11} + \varepsilon_{22} + \varepsilon_{33} = \operatorname{div} u$ is the change of unit volume during deformation $\varepsilon_{ij}$.

Stresses $\sigma_{ij}$ are coupled with the outside forces $f_i$ and components of acceleration in accordance to formula

$$\rho \frac{\partial^2 u_i}{\partial t^2} = \frac{\partial \sigma_{i1}}{\partial x_1} + \frac{\partial \sigma_{i2}}{\partial x_2} + \frac{\partial \sigma_{i3}}{\partial x_3} + f_i, \qquad (5)$$

where $i = 1, 2, 3$.

On the surface $\Gamma$, it is fulfilled either condition of absence of displacement, and then

$$u_i = 0, \qquad (6)$$

where $i = 1, 2, 3$, or absence of stresses at the planes, which are tangent to the surface $\Gamma$, and then

$$\sigma_{i1}n_1 + \sigma_{i2}n_2 + \sigma_{i3}n_3 = 0, \qquad (7)$$

where $i = 1, 2, 3$.

Initial conditions for dynamic problem of elasticity are of designed stresses $\sigma_{ij}(x_1, x_2, x_3)$, $(ij = 1, 2, 3)$ at $t = 0$, which may be different from 0 because of radiation of the medium with laser during the previous stages and action of the exterior gravitational field.

So, the mathematical task consists of defining temperature field $T(x_1, x_2, x_3, t + \Delta t)$ for the not great stretch of time $\Delta t$ proceed from boundary problem (1)–(3), and thereafter finding field of shift-stresses proceed from boundary problem (4)–(7).

The area of the points $M(x_1, x_2, x_3)$ is found at next stage, in these points maximum stress exceeds boundary stresses to compression $\sigma_c$ and tension $\sigma_p$ for designed rock. The last is fulfilled with transformation of tensor $\sigma_{ij}$ to its main axis and finding eigenvalues $\sigma_1 > \sigma_2 > \sigma_3$ of matrix $\sigma_{ij}$. Then the condition (8) is tested according with Mohr's criterion

$$\sigma_1 - (\sigma_p/\sigma_c)\sigma_3 \geq \sigma_p, \qquad (8)$$

and $\sigma_c = (8–10)\sigma_p$ for brittle rocks. Therefore, in such case condition (8) may be changed with more simple one $\sigma_1 \geq \sigma_p$.

Under the execution relationship (8), points $M$ are being removed from the area $\Omega$, and boundary $\Gamma$ is moving inside the area $\Omega$. It smoothing out, and the problem is started again with already found fields of temperature and shift-stresses. Change of position

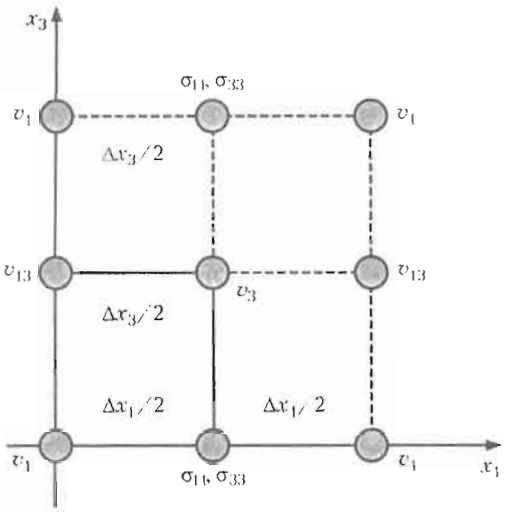


**Figure 1.** Allocation of variables $\sigma_{ij}$ and $v_{i,j}$ on the staggered grid

of laser and its impulse regime are taking into account in analogous way.

Let us consider 2D problem of thermoelasticity. For this, we shall use velocities of displacements $v_i = \frac{\partial u_i}{\partial t}$ in equations instead of displacements $u_i$.

Using the same notations the system of equations (4), (5) may be represented for 2D media as

$$\rho \frac{\partial v_1}{\partial t} = \frac{\partial \sigma_{11}}{\partial x_1} + \frac{\partial \sigma_{13}}{\partial x_3} + f_1;$$

$$\rho \frac{\partial v_3}{\partial t} = \frac{\partial \sigma_{13}}{\partial x_1} + \frac{\partial \sigma_{33}}{\partial x_3} + f_3;$$

$$\frac{\partial \sigma_{11}}{\partial t} = (\lambda + 2\mu)\frac{\partial v_1}{\partial x_1} + \lambda \frac{\partial v_3}{\partial x_3} - (3\lambda + 2\mu)\alpha \frac{\partial (\Delta T)}{\partial t}; \quad (9)$$

$$\frac{\partial \sigma_{33}}{\partial t} = \lambda \frac{\partial v_1}{\partial x_1} + (\lambda + 2\mu)\frac{\partial v_3}{\partial x_3} - (3\lambda + 2\mu)\alpha \frac{\partial (\Delta T)}{\partial t};$$

$$\frac{\partial \sigma_{13}}{\partial t} = \mu \left( \frac{\partial v_1}{\partial x_3} + \frac{\partial v_3}{\partial x_1} \right).$$

*Finite-difference realization of 2D mathematical model.* As area $\Omega$ is not itself complex geometrical figure, and its boundary $\Gamma$ moving inside $\Omega$ in time on the influence of laser radiation and spallation, then it is desirable to use uniform simple grid of calculation where meshes are equal. The most suitable is ordinary rectangular grid and finite-difference algorithms for parabolic boundary problem of heat conductivity and dynamic problem of elastic waves propagation.

In the practice it is used non-explicit schemes of alternation directions of Crank–Nicolson [8], Douglas [9], Peaceman–Rachford [10] and others for finite-difference solving of equation of heat conductivity. In this work absolutely convergent scheme is used, which reduces to three-diagonal set of equations, which may be solved with the sweep method:

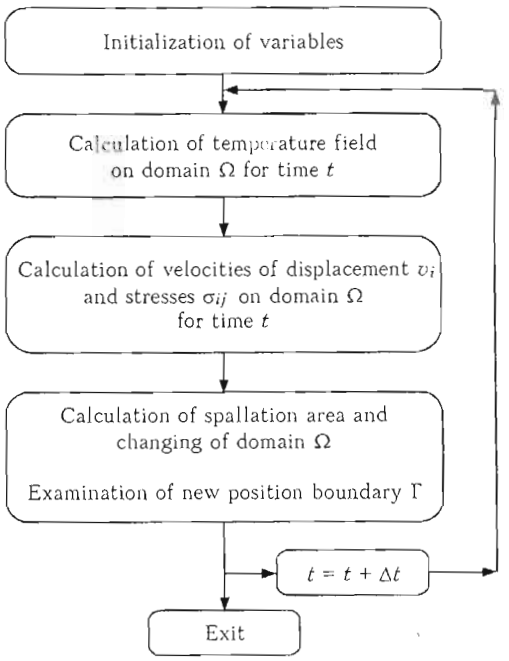


**Figure 2.** Flow chart of calculation process

$$\frac{T^{k+1/2}_{i+1/2,j} - T^{k}_{i+1/2,j}}{\Delta t/2} = \chi \frac{\delta^2 T^{k+1/2}_{i+1/2,j}}{\delta x_1^2} + \chi \frac{\delta T^{k}_{i+1/2,j}}{\delta x_3^2};$$

$$\frac{T^{k+1}_{i+1/2,j} - T^{k+1/2}_{i+1/2,j}}{\Delta t/2} = \chi \frac{\delta^2 T^{k+1/2}_{i+1/2,j}}{\delta x_1^2} + \chi \frac{\delta^2 T^{k+1}_{i+1/2,j}}{\delta x_3^2}. \quad (10)$$

Here $T^k_{i,j}$ is the temperature field in the point of the medium $M(i\Delta x_1, j\Delta x_3)$ at time moment $t = k\Delta t$; $\frac{\delta^2 T^{k+1/2}_{i+1/2,j}}{\delta x_1^2} = \frac{T^{k+1/2}_{i+3/2,j} - 2T^{k+1/2}_{i+1/2,j} + T^{k+1/2}_{i-1/2,j}}{\Delta x_1^2}$; and $\frac{\delta^2 T^{k+1/2}_{i+1/2,j}}{\delta x_3^2}$ is defined in analogous way. Temperature field for the problem of thermoelasticity is calculated with the shift along variables $x_1$ and $t$ at the half of steps of grids, that is $T^{k+1/2}_{i+1/2,j}$ meanings are used.

Finite-difference scheme for system of equations (9) is fulfilled within the staggered grid [11], that is the different components of stress tensor, and vector of velocities of displacements are placed into different meshes (Figure 1). Such distribution of values allows us construct the simple central finite-difference scheme of the second order precision on all variables:

$$(v_1)^{k+1/2}_{i,j} = (v_1)^{k-1/2}_{i,j} + \rho^{-1}_{i,j} \frac{\Delta t}{\Delta x_1} ((\sigma_{11})^k_{i+1/2,j} - (\sigma_{11})^k_{i-1/2,j}) + \rho^{-1}_{i,j} \frac{\Delta t}{\Delta x_3} ((\sigma_{13})^k_{i,j+1/2} - (\sigma_{13})^k_{i,j-1/2}) + \rho^{-1}_{i,j} f_1;$$

$$(v_3)^{k+1/2}_{i+1/2,\,j+1/2} = (v_3)^{k-1/2}_{i+1/2,\,j+1/2} +$$

$$+ \rho^{-1}_{i+1/2,\,j+1/2}\frac{\Delta t}{\Delta x_1}((\sigma_{13})^{k}_{i+1,\,j+1/2} - (\sigma_{13})^{k}_{i,\,j+1/2}) +$$

$$+ \rho^{-1}_{i+1/2,\,j+1/2}\frac{\Delta t}{\Delta x_3}((\sigma_{33})^{k}_{i+1/2,\,j+1} - (\sigma_{33})^{k}_{i+1/2,\,j}) + \rho^{-1}_{i,\,j} f_3;$$

$$(\sigma_{11})^{k+1}_{i+1/2,\,j} = (\sigma_{11})^{k}_{i+1/2,\,j} + (\lambda + 2\mu)_{i+1/2,\,j}\frac{\Delta t}{\Delta x_1}\times$$

$$\times((v_1)^{k+1/2}_{i+1,\,j} - (v_1)^{k+1/2}_{i,\,j}) + (\lambda)_{i+1/2,\,j}\frac{\Delta t}{\Delta x_3}\times$$

$$\times((v_3)^{k+1/2}_{i+1/2,\,j+1/2} - (v_3)^{k+1/2}_{i+1/2,\,j-1/2}) -$$

$$- (3\lambda + 2\mu)_{i+1/2,\,j}\alpha(T^{k+1/2}_{i+1/2,\,j} - T^{k-1/2}_{i+1/2,\,j});$$

$$(\sigma_{33})^{k+1}_{i+1/2,\,j} = (\sigma_{33})^{k}_{i+1/2,\,j} + (\lambda)_{i+1/2,\,j}\frac{\Delta t}{\Delta x_1}\times$$

$$\times((v_1)^{k+1/2}_{i+1,\,j} - (v_1)^{k+1/2}_{i,\,j}) + (\lambda + 2\mu)_{i+1/2,\,j}\frac{\Delta t}{\Delta x_3}\times \qquad (11)$$

$$\times((v_3)^{k+1/2}_{i+1/2,\,j+1/2} - (v_3)^{k+1/2}_{i+1/2,\,j-1/2}) -$$

$$- (3\lambda + 2\mu)_{i+1/2,\,j}\alpha(T^{k+1/2}_{i+1/2,\,j} - T^{k-1/2}_{i+1/2,\,j});$$

$$(\sigma_{13})^{k+1}_{i,\,j+1/2} = (\sigma_{13})^{k}_{i,\,j+1/2} + (\mu)_{i,\,j+1/2}\frac{\Delta t}{\Delta x_1}\times$$

$$\times((v_1)^{k+1/2}_{i,\,j+1} - (v_1)^{k+1/2}_{i,\,j})\frac{\Delta t}{\Delta x_3}\times$$

$$\times((v_3)^{k+1/2}_{i+1/2,\,j+1/2} - (v_3)^{k+1/2}_{i-1/2,\,j+1/2}).$$

Except free surface, it is satisfied the attribute of energy absorption at boundaries of calculation, that is their transparency [12]. Flow chart of calculation process is presented in Figure 2.

## CONCLUSION

2D mathematical model of process of spallation of rocks under the influence of laser radiation has been developed. Calculation scheme has been built at the base of finite-difference approximations of boundary problem of heat conductivity and dynamic problem of thermoelasticity. While numerical modeling, all used basic parameters, which influence developing of physical process of investigation, are taken into account. Modeling may be used for forecasting of destruction of rocks, that depends on selected regime of laser energy radiation.


1. (1994) *Drilling and excavation technologies for the future.* Washington: National Academy Press.
2. Pierce, K.G., Livesay, B.J., Finger, J.T. (1996) *Advanced drilling systems study*: SAND 95-0331. Unlimited Release Printed, June 1996.
3. Parker, R., Xu, Z., Reed, C.B. et al. (2003) Drilling large diameter holes in rocks using multiple laser beams. In: *Proc. of 22nd Int. Congress on Applications of Laser & Electro-Optics* (October 13–16, 2003, Jacksonville, Florida, USA).
4. Xu, Z., Reed, C.B., Parker, R. et al. (2004) Laser spallation of rocks for oil well drilling. In: *Proc. of 23rd Int. Congress on Applications of Laser & Electro-Optics* (October 4–7, 2004, San Francisco, USA).
5. Xu, Z., Yamashita, Yu., Reed, C.B. (2005) *Two-dimensional modeling of laser spallation drilling of rocks.* http://www.ne.anl.gov
6. Kovalenko, A.D. (1970) *Thermoelasticity principles.* Kiev: Naukova Dumka.
7. Boley, B.A., Weiner, J.H. (1960) *Theory of thermal stresses.* New York; London.
8. Crank, J., Nicolson, P. (1947) A practical method for numerical evaluation of solutions of partial differential equations of the heat conduction type. *Proc. of Cambridge Phil. Soc.*, 43 (50), 50–67.
9. Douglas, J. (1962) On the numerical solution of heat conduction problems in two and three space variables. *Transact. of Amer. Math. Soc.*, 82, 421–439.
10. Peaceman, D.W., Rachford, H.H. (1955) The numerical solution of parabolic and elliptic differential equations. *J. Soc. Indust. Appl. Math.*, 3 (1), 28–41.
11. Virieux, J. (1986) P-SV wave propagation in heterogeneous media: Velocity-stress finite-difference method. *Geophysics*, 51, 889–901.
12. Clayton, R., Engquist, B. (1977) Absorbing boundary conditions for acoustic and elastic wave equations. *Bull. of Seis. Soc. Amer.*, 67, 1529–1540.

# LASERS AND BEAM DELIVERY FOR PERFORATION AND DRILLING OIL-AND-GAS WELLS

S. HOSHOVSKIY, P. SYROTENKO and Yu. VOYTENKO
Ukrainian State Geological Research Institute, Kyiv, Ukraine

The results of the research of possibility of transfer high-intensive optical energy using fiber optical cables and conventional optical systems are analyzed in this report. The perspective of application of such methods for beam delivery in laser drilling and perforation systems is estimated. It is recommended to divide tasks into creation of laser perforation system and creation of laser drilling system as far as there is a possibility of using high-power laser diode arrays directly in a well in laser perforation systems. The analysis of the reasons and factors that complicate transfer of optical energy for large distance in such systems are provided.

Now one of the most important and difficult tasks of creation of laser systems for perforation and drilling oil-and-gas wells is the transmission of optical energy on the large distance into the well. The first proposals on utilization of lasers for rock destruction appeared in the 1970s. However, there were no fundamental investigations on ability to light energy transfer on large distances at that time. Now it is possible to mark three types of transmission of light energy which are suitable for utilization in the well, namely: traditional, waveguide, and fiber optical systems. Traditional and waveguide systems have appeared so complex in realization in oil-and-gas wells that they were finished at the level of technical proposals. At the same time developers of lasers systems have had a wrong opinion, which had been borrowed from communication and electric technology that the optical fiber lines can transfer the light energy to significant distances. However, further basic research on light energy transmission from high power lasers on the long distances with utilization of optical fiber cables have confirmed the existence of many problems. Therefore, the task of maintenance of light energy transmission in laser systems for perforation and drilling oil-and-gas wells is very important. In addition, it was established that not all of existed types of lasers are capable to transmit the radiation via optical fiber cable, and therefore their correct choice of losses is necessary for their utilization in laser systems.

*Modern lasers of high power for utilization in oil-and-gas industry.* During selecting high power lasers for perforation and drilling oil-and-gas well, it is necessary to take into account not only their efficiency on rock destruction, but also their ability to transmit light energy on large distances. Recently research have been conducted in the USA and Russia with the purpose to estimate efficiency of rock destruction with the help of various types of lasers. Crystalline solid-state, semiconductor diode, fiber, gas, chemical and dye lasers have been investigated.

According to results of the investigations, the most perspective lasers for perforation and drilling of oil-and-gas wells are given in the Table. Certainly, diode and fibre lasers would be the most suitable for creation systems for perforation and drilling oil-and-gas wells. Thus, diode lasers because of their small size may be placed into oil-and-gas wells with transmission electric power to them from the ground surface. Fiber lasers will find their utilization at a surface arrangement with transition of light energy from them to the place of destruction of rocks in oil-and-gas wells. Characteristics of lasers given in the Table allow estimating efficiency of their perforation and drilling process in oil-and-gas wells. It is necessary to note that $CO_2$- and diode lasers have the least price, as the price of 1 W of their emitted power equals approximately $50 US on the average.

Now practically all developed countries are taking part in creation and development of laser diode arrays of high power. The leading role belongs to the USA, Germany, Great Britain, and France. It is necessary to emphasize three main ways of utilization of high power laser diode arrays, namely: pumping solid-state lasers; input of radiation of diode matrix into core of fiber for subsequent transmission to object of processing, and utilization laser diode arrays for creation phased diode matrix. The second and third trends are of the most interest for oil-and-gas industry. Thus the losses of laser radiation at the stage of its input into core of fiber reach are of about 20–30 %, that forces to work on their decreasing actively. Also the actual problem for today is creation phased diode matrixes. The output radiation of such laser represents a set of narrow-directed interference peaks of tight direction (one peak in a special case) with small divergence that will allow energy transmission to be supplied on large distances.

*System of delivery of laser beam.* The standard configuration of usual system of delivery of laser beam assumes the presence of beam expander, set of filling mirrors, and focusing lens system. Optics of all listed components is quite simple, as all of them work in weakly divergent beams. Dimension of laser beam in usual systems of delivery is usually essentially smaller than the linear sizes of optical elements that simplifies the process of adjustment. Besides, internal points of

Main characteristics of lasers considered

| Parameter | For drilling and perforating oil-and-gas wells required | $CO_2$-laser | Nd:YAG laser with lamp pumping | Nd:YAG laser with diode pumping | Diode laser | Fiber laser |
|---|---|---|---|---|---|---|
| Output power, kW | Up to 5 | 1–30 | 1–5 | 1–4 | 1–4 | 1–30 |
| Wavelength, μm | Infrared range | 10.6 | 1.064 | 1.064 or 1.03 | 0.80–0.98 | 1.07 |
| Efficiency coefficient, % | > 20 | 8–10 | 2–3 | 4–6 | 25–30 | 20–25 |
| Radiation delivery range with fiber, m | Up to 1500 (6000 in the long term) | – | 20–40 | 20–40 | 10–50 | 10–300 |
| Stability of output power | As much as possible | Low | Low | Low | High | Very high |
| Sensitivity to reflection | As low as possible | High | High | High | Low | Low |
| Dimension | As low as possible | Very large | Large | Medium | Very small | Small |
| Technical resource, h | As much as possible | – | 300–500 | 2000–5000 | 2000–5000 | > 50000 |

focus control over a beam is absent in ordinary delivery systems that allows a problem of beam strength to be reduced to a minimum. However, such system of delivery has not found its utilization in deep oil-and-gas wells. The basic cause of this is the complexity of technical realization of such a system of delivery, and difficulties in maintenance of transparent environment for propagation of laser beam, and also surface condition of cleanness components of delivery system in operation [1].

Proposals to use waveguides for transmission laser energy into oil-and-gas wells have not found their utilization also because of engineering complications. In addition it is very difficult to guarantee high stability and accuracy of waveguide dimensions while its deployment. Utilization of cooled-tubing system with appropriate overcoat of internal side of tube with silver as a delivery system for a waveguide simplifies a little designing of system for delivery of laser beam. Nevertheless, the problems on delivery laser energy into the well were not solved because of great energy losses.

Standard fiber system for delivering laser beam is the most perspective one for utilization in oil-and-gas wells [2–5]. Such system includes in itself system of beam input into optical fiber, optical fiber of required length, and fiber-adaptive lens system (Figure 1). The last one operates in conditions of divergent beam (the amount of divergence is characterized by numerical aperture of the fiber). It brings to essential complication of optical system of lenses. Also laser beam input into the fiber assumes adjustment, and complicate, and expensive system of laser beam input into the fiber. Besides, the problems, connected with beam input, and output reliability of fiber may occur while derivation of focusing laser beam of high power on the end surfaces of the fiber.

Encouraging information about successful introduction continuous radiation (CW) into fiber with core diameter of 560 μm and power of 2000 W (US Lasers Corp.) appeared in 1996, as early as five years later of about 4500 W CW Nd:YAG laser was declared in [6] that was fixed on the output end surface of fiber with core diameter of 300, 400 and 600 μm while numerical aperture was equal to 0.1.

Now the next stage of modernization of beam delivering with laser system will be support as much as possible remoteness of transmission light energy of high power. For this purpose let us carry out an analysis on energy losses in the fiber.

The losses of light energy in the fiber are connected with absorption and dispersion. Possible propagation of laser beams in a fiber is shown in Figure 2. Absorption is taking place because of presence of core (silica) in material, along which the light is propagating, doping agents, various inclusions such as metal ions and water, and structural defects in fiber texture. The last two mechanisms of absorption were eliminated completely by high quality modern industry production.

Beam *A*, within acceptance angle, propagated internal reflection. Beam *B*, outside acceptance angle, escapes into cladding (see Figure 2). Another source of losses of energy in a fiber is Rayleigh dispersion, which is proportional to $1/\lambda^4$, where $\lambda$ is the length of the wave. Mechanisms of absorption in silica and Rayleigh dispersion are the main ones, and their elimination is an impossible task. Absorption in the fiber with low maintenance of OH silica is demonstrated

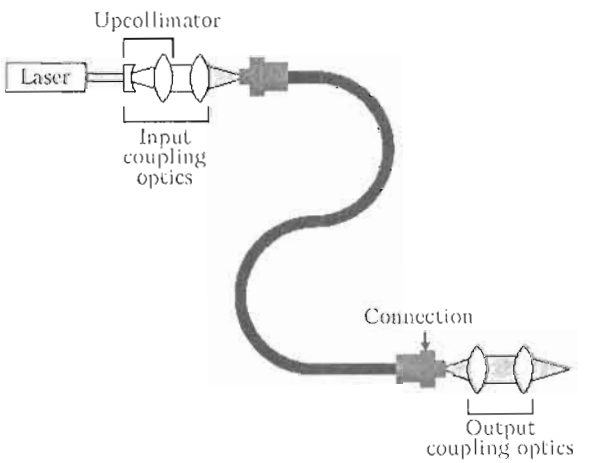


**Figure 1.** System of laser beam delivery by an optical fiber (US Lasers Corp.)

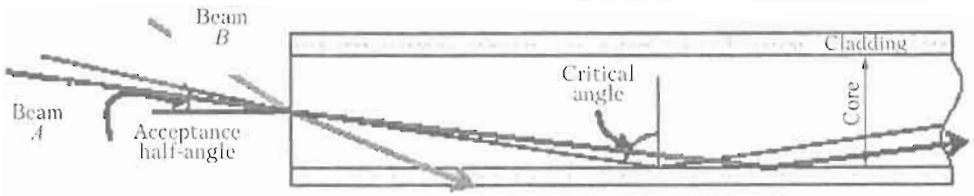


**Figure 2.** Possible distribution of laser beams in a fiber (US Lasers Corp.)

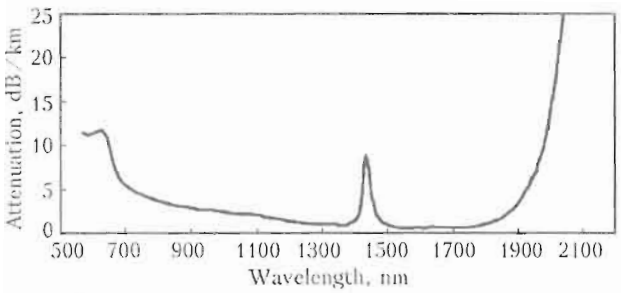


**Figure 3.** Attenuation of a low OH silica fiber manufactured by Polymicro Technologies

in Figure 3. Today the least absorption is reached in such a fiber with wavelength of 1.55 mm at the level of 0.16 dB/km [1]. It becomes obvious in Figure 3, why it is impossible to utilize fiber systems for beam delivery for $CO_2$-laser. The fiber systems of laser beam delivery have very strong absorption of frequencies within the near infrared range of spectrum.

There are additional losses except ones mentioned above in fiber channel in the process of light energy transmission, namely: losses in cable bends and connections or during fiber cable binding, and on the end surfaces losses during input and output of light energy. The level of these losses can be controlled by developer and producer. The level of such losses is very large and approximately equal 10 dB for the light energy transmission along the channel with length of several kilometers. As a result today high capacity fiber laser energy transmission at a distance up to 300 m is guaranteed on NTO «IRE-PLUS» data. Multimode fibers are in use for high power laser beam transmission along a fiber only, which have larger diameter than single-mode fiber.

Thus, it is prematurely to speak about high power laser light energy transmission at a large distance (of several kilometers), and the task was put to reach light energy transmission up to 6 km along the fiber.

*Modern beam control system of high power lasers.* Laser systems of perforation and drilling oil-and-gas wells possess on advantage that they are controlled by laser radiation which can not be reached in traditional systems. With the help of laser system it is possible to construct the large holes with the help of utilization a multi of beams of small diameter. In such case the beams had to be moved at the surface in more complicate systems, beam focusing is controlled automatically for deep penetration into rocks.

Effective interaction of laser beam with rock is possible if it moves according to established law for achievement of the next regimes: spallation, melting, and vaporization. Spallation of rock requires the most dynamics of moving of laser beam. Facilities with electromechanical driving gears (galvanometers) are of greatest propagation among the ones controlling space position of laser beam. They ensure scanning of laser beam according to arbitrary law with high resolution and precision. 2D ($x$, $y$) and 3D ($x$, $y$, $z$) scanning systems exist. Critical dimension of scanners is great achievement together with ability to radiate laser beam of high power among the problems, which necessary to solve while creating laser system of perforation and drilling of oil-and-gas wells. Therefore 2D scanners have preference for installation.

## CONCLUSION

Laser diode arrays of high power are the most perspective among considered lasers for utilization in laser system of perforation and drilling oil-and-gas wells. Among advantages of such lasers are density, small external dimensions and weight, absence of high electric voltages in feed system, rigidity to vibration, and overload. Minimum coefficient of absorption of water at wavelength in a range 0.6–0.9 μm, in which diode lasers can operate, is very important for utilization high power diode lasers in laser system of perforation and drilling oil-and-gas wells. Despite of significant improvement of parameters of fiber channels light energy transmission from lasers of high power, the required parameters for laser systems of perforation and drilling oil-and-gas wells are not reached for today. But the perspective exists, as the main losses while transmission of light energy take place in joint components and assembly units of input and output of light energy that can be diminished with correct designing and adjustment of system. The modern industrial systems of control for radiation of high power lasers can be applied appreciably for utilization in laser system of perforation and drilling oil-and-gas wells in case of their modernization for utilization in conditions of oil-and-gas-wells while processing materials with of 2D and 3D scanners.

1. Leong, K.H., Xu, Z., Reed, C.B. et al. (2003) *Lasers and beam delivery for rock drilling*: ANL/TD/TM03-01.
2. Hunter, B.V., Leong, K.N., Miller, C.B. et al. (1996) Selecting a high-power fiber-optic laser beam delivery system. In: *Proc. of ICALEO* (1996), Vol. 81T, 173–182.
3. Setchell, R.E. (2000) Laser in ejection optics for high-intensity transmission in multimode fibers. In: *Proc. of SPIE* (2000), 74.
4. Hunter, B.V., Leong, K.H., Miller, C.B. et al. (1996) Understanding high-power fiber-optic laser beam delivery. *J. Laser Appl.*, 8, 307–316.
5. Mitchell, J.N. (2000) *Limits of electrical power generation by transmission of light through optical fibers.*
6. Hoffman, D., Bonati, G., Kays, P.F. et al. (2001) Modular fiber coupled DPSSl with up to 5 kW average output power. In: *Proc. on Advanced Solid-State Lasers.* Seattle.

# PERFORATING AND DRILLING WELLS WITH LASER RADIATION IS A PERSPECTIVE TECHNOLOGY FOR OIL-AND-GAS INDUSTRY

S. HOSHOVSKIY, P. SYROTENKO and Yu. VOYTENKO
Ukrainian State Geological Research Institute, Kyiv, Ukraine

The concept of construction of the laser system for perforating and drilling oil-and-gas wells is proposed. The estimation of advantages and disadvantages of different laser perforating systems has been done. The comparison laser technique with traditional technique of rotator-mechanical drilling is provided. Three types of rock destruction (spallation, melting and evaporation) are described withe the estimation of their efficiency.

The intensive investigations in laser technique of rock destruction have started since 1970s in the USA and USSR [1–4]. Today activity of investigations is not decreasing, that is called by appearance of modern powerful fiber and diode lasers, and extension of industry tasks as well, which may be solved with the help of laser technique only. The tasks of state energy insurance are going on the foreground nowadays. They require more complete usage of an energy potential of the Earth. World resources of oil and gas within the shallow depth, and geothermal energy resources are exhausted, that makes it necessary to drill exploratory and development wells on more large depths. For example, today in Ukraine it is necessary to drill gas wells up to 6 km within the most perspective Dnipro-Donetsk oil-and-gas basin, that complicates conditions and process of drilling considerably [5]. Though a lot of things are made for development of modern high hardness materials for drill bits, but sometimes their technical characteristics can not be improved anymore, and that leads to increasing of expenditures during drilling deep wells. Also it is complicate to provide perforation of high efficiency of gas-and-oil wells with traditional methods, that has influence on intensity of inflow of hydrocarbons in the well. It is possible to solve this problem with the help of utilization of controlled laser perforation for oil-and-gas wells, which guarantees large depth perforation of rock mass, and permeability, and porosity as well. Therefore development of new unconventional effective techniques is an actual task for geology and oil-and-gas industry.

*Modern industrial powerful lasers and estimation of an opportunity of their usage for drilling and perforating oil-and-gas wells.* The primal ideas on laser power utilization for rock destruction were based on using of super powerful lasers with power up to megawatt. However, the investigations, which nave been conducted in the USA and Russia, have shown that such power isn't required if radiated laser power is correctly controlled, and necessary density of power of laser radiation is provided while affecting on the rocks [5, 6]. There are three types of heat destruction of rocks, namely: spallation, melting, and evaporation. The specific energy consumption while traditional rotary drilling, and early mentioned three types heat destruction of rock in the average are equal with rotary bit to 100 J/cm$^3$, high pressure jets – 1000 J/cm$^3$, thermal spalling – 1500 J/cm$^3$, melting – 5000 J/cm$^3$, and vaporization – 12500 J/cm$^3$ [1]. Hence, among three types of heat destruction of rock the thermal spalling is the least power consuming one, at the same time it refers to as ones which is most complicate to realize, as it requires construction and realization adaptive model of heat destruction of rocks. However, to reach such a mode of rock destruction it is necessary to know precisely and trace change of thermal-physical and mechanical attributes of rocks in time while destruction of rocks. Such a model of rock destruction is based on utilization of heat stresses which occur in rock, that is the reason of appearance of cracks and rock spallation.

More simple methods of realization of rock destruction are melting and vaporization. In such case it is necessary to define required power of laser radiation according to the following equations:

$$P_m = \left[\rho(\pi r_h^2)\frac{ds}{dt}\right][k_h(T_f - T_a) + k_f], \qquad (1)$$

$$P_v = \left[\rho(\pi r_h^2)\frac{ds}{dt}\right][k_h(T_v - T_f) + k_v] + P_m, \qquad (2)$$

where $\rho$ is the rock density; $r_h$ is the hole radius of well or beam; $ds/dt$ is the penetration rate; $k_h$ is the specific heat capacity; $k_f$ is the heat of fusion; $k_v$ is the heat of vaporization; $T_f$ is the fusion temperature; $T_v$ is the vaporization temperature; $T_a$ is the ambient rock temperature; $P_m$ is the power required to heat the rock to the fusion temperature and convert it to liquid; $P_v$ is the power required to heat the rock to the vaporization temperature and convert it to liquid and gas.

Basing on equations (1) and (2), the necessary capacity $P_m$ and $P_v$ for melting and vaporization of rock can be defined approximately. The following thermal-physical parameters can be used for reservoirs

(sandstones and limestones): $k_h = 0.85$ J/(g·K); $k_v = 400$ J/g; $k_f = 200$ J/g; $\rho = 2.7$ g/cm$^3$; $T_a = 50$ °C; $T_f = 1500$ °C; $T_v = 3000$ °C; $ds/dt = 0.1$ cm/s; $r_b = 0.5$, 1 and 4 cm.

Then, in accordance with equation (1), we shall receipt power of laser radiation, which is needed for rock melting, namely: 0.55, 2.2 and 35.2 kW for $r_b = 0.5$, 1 and 4 cm, respectively. Power of laser radiation to get vaporization of rock will be 2 times higher than that for melting rock with the laser in accordance to (1) and (2).

Thus, the conducted analysis demonstrates that industry lasers with radiation power up to 5 kW are quite enough for rock destruction provided that diameter of laser beam is 1–3 cm, and boring hole of great diameter in rocks is conducted using of a multiple laser beams that was proposed in the work [6]. This assertion is approved with specified expenditures of power for heat destruction of rocks mentioned above.

*Support of arranging and utilization both laser and auxiliary equipment in limited free space and severity conditions of wells.* Invention of powerful laser diode arrays with several kilowatts power has opened the ability to place them directly in the oil-and-gas wells. However, many difficulties arise which are connected with their utilization, particularly, protection of laser radiation from the influence of drilling mud, where the great part of laser energy can be absorbed. This problem can be solved with design methods [5].

System of laser radiation control and technical vision are related to auxiliary equipment of laser complex for perforation and oil-and-gas well drilling. It is possible to state that today high temperature electronics has been developed in the US and Norway for oil-and-gas utilization, and it can be operate at temperatures up to 180 °C (or 225 °C) [5].

Mentioned electronics includes in itself not only the simple electronic components, but microprocessor facilities for quick processing, and its transmission to the land surface. Also it is designed high temperature microprocessor for the spectrum analysis of rocks, that will enlarge essentially functionalities of control system of laser radiation and computer vision. Now it will be possible not only to detect the temperature in the well directly, but a rock composition as well.

The existed large problem of cooling of powerful diode lasers and power electronics now can be solved technically, as cooled-tubing systems are exist to feed liquid and gas into the well for their cooling. It is forecasted utilization of liquid for cooling in modern construction of powerful laser diode arrays, that is simplifying its cooling in the well, however, it is necessary to keep high standard of liquid quality. It is possible to provide supplementary cooling to diode laser with the help of thermo-electric technique in condition of undercooling. Thermo-electric technique finds usage in modern down-hole equipment. Although liquid cooling of lasers in the well is considered as the best today, combination of various method of cooling is considered as a solution for the abnormal requirements. In addition, we are anticipating for the appearance of technology of thermo-acoustic cooling of powerful electronics in the long term, which is in active development for space research today.

*Concept of constructing laser complex for perforation and drilling oil-and-gas wells.* For today the next two variants of constructing laser complex perforation and drilling oil-and-gas well are most close to the success:

- with surface allocation of power fiber laser and light energy transmission by fiber line to optical system which controls laser beam (scanning);
- with high power laser diode allocation in the well, which is designed as a powerful laser diode arrays up to some kilowatts with optical laser beam controlling (scanning), and electrical energy delivering by standard geophysical seven-cord cable.

The first variant of concept of constructing of a laser complex for perforation and boring oil-and-gas wells has some problems which are connected with transmission of light energy of high power by fiber line. Today the works on diminishing transmission losses are conducted actively, and they reached 0.2 dB/km. However, fiber line has many connections, which are the sources of large losses of light energy. The information about trials in laboratory conditions of laser for boring hydro-geological wells on depths from 100 up to 300 m recently has appeared [2].

The second variant has advantage especially in a case of its utilization for perforation task only. As it follows from short process of perforator working in the well, less laser energy required for perforation in comparison with drilling, and the ability to high up the quality of perforation as contrasted to traditional perforation with shaped charges.

The important task of laser complexes for perforation and drilling oil-and-gas wells is a control over borehole preservation and process of rock destruction. Today technical means for the control over pressure borehole preservation are exist. These means control drilling course and cavity formation in the borehole while drilling. Undoubtedly, it is necessary to save traditional casing string in any kind of drilling appearance. The ability to get casing string with utilization of rock melting may be looked at only as an additional facility for organizing casing along individual intervals of the well. Undoubtedly, laser complexes for perforation and drilling oil-and-gas wells require of utilization of cooled-tubing system for liquid and gas supplying to the bottom of the well to clean out the last one of drilling sludge, which was gotten during the laser destruction of rocks. At present the construction of cooled-tubing systems are mastered full-scale in some countries.

## CONCLUSION

The held analysis of world-wide state of investigations of laser technology for perforation and drilling oil-

and-gas wells, and principles of complex constructing for perforation and drilling oil-and-gas wells demonstrate that today preproduction model of laser perforation of oil-and-gas wells has the greatest perspective for development, construction and testing. The most perspective method of laser rock destruction while drilling and perforation of oil-and-gas wells is spallation, as the last one consumes the least energy among other methods of heat rock destruction. Development of small-sized laser diode arrays with power up to some kilowatts allow their allocation inside oil-and-gas wells, and in perspective they are considered like a main variant for constructing laser complex for perforation and drilling oil-and-gas wells, and their reliability would be proved.

Advantages of laser methods of perforation and boring oil-and-gas well are as follows:

- higher velocity of rock destruction in comparison with mechanical methods;
- functional capabilities of laser complex for perforation and drilling oil-and-gas well, which are unattainable in traditional complexes of rock destruction;
- ability to increase and save permeability and porosity of rock mass at perforation is a prospect for laser method for oil-and-gas wells.


1. (1994) *Drilling and excavation technologies for the future.* Washington: National Academy Press.
2. Pierce, K.G., Livesay, B.J., Finger, J.T. (1996) *Advanced drilling systems study*: SAND 95-0331. Unlimited Release Printed, June 1996.
3. Emelin, M.A., Morozov, V.N., Novikov, N.P. et al. (1990) *New methods of rock failure.* Moscow: Nedra.
4. Poluyansky, S.A., Galyas, A.A., Larkina, A.P. (1971) *Optical generators and their application in mining.* Kiev: Naukova Dumka.
5. Hoshovskiy, S., Sirotenko, P. (2007) Laser drilling and perforating oil and gas wells becoming the reality. In: *Proc. of 3rd Int. Conf. on Laser Technologies in Welding and Materials Processing* (29 May–1 June, 2007, Katsiveli, Crimea, Ukraine), 67–70.
6. Parker, R., Xu, Z., Reed, C.B. et al. (2003) Drilling large diameter holes in rocks using multiple laser beams. In: *Proc. of 22nd Int. Congress on Application of Laser & Electro-Optics* (October 13–16, 2003, Jackonville, Florida, USA).

# OPTIMIZING TECHNOLOGICAL FABRICATION TECHNIQUES FOR LASER CUTTING OF STENTS

ILNAZ VAHDATINIA, V.P. KOTLYAROV, MOHAMMAD ALI ALIVERDI and HAMIDREZA HAJI MOLLABASHI
Laser Technology and Materials Science Department of the NTUU «Kyiv Polytechnic Institute», Kyiv, Ukraine

According to the results of research based on typical stent production methods such as varying the pulses duration, achieve various cut quality (kerf width and surface quality on the sidewall and bottom surface quality), productivity, maintenance, need for post-processing and technological treatment (choosing mode and equipment), and also considering cost value, for optimizing the cut millisecond laser pulses is recommended.

High quality, productivity, and cost of coronary stents are determined by improvements and utilized optimal technological applications and methods that are using in stent manufacturing processes. The ultimate result depends on related application equipments, procedures for manufacturing the workpiece (tube), its perforation, and finishing methods.

The limitations in laser cutting of stent (such as instability of cut width, roughness, and waviness of sidewalls surfaces, presence of burrs and dross on contour lines) caused by nonoptimal organization of this process that would increased the intensity and cost of finishing methods and post treatments. Hence, to optimally organize the production process, the following problems should be considered:

- technological scheme should have maximum productivity as well as enhanced structural quality;
- operating mode (CW or pulsed one by various modifications) should be in proportion to different mechanisms of destruction for the particular workpiece material;
- laser beam parameters (energy, time and spatial character) and levels of radiation during operation (pulse range, beam transmission and workpiece manipulation) should be carefully tailored to fulfill all requirements for the high precision production of stents on industrial scales for economical comparisons.

According to these instructions, the laser selectively removed the material from the tube by ablation so that the pattern cut into the tube. Despite how to position the tubing (vertically or horizontally) it has longitudinally and rotating movements relative to the laser during the cut. Due to the thin-wall and the small geometry of the stent pattern, it is necessary to have a very precise control on the laser power level, and also precise positioning of the laser cutting path, to prevent overheating and warping of the stent structure and less heat build-up at critical locations (bends and turns) during the manufacturing process, so that the material would not be damaged.

The majority of industrial laser cutting of stents systems are using pulsed processing for generation mode of a laser; however manufacturers prefer various types, such as milliseconds pulses [1] or microseconds durations [2] when others used nanoseconds wavelength duration [3] or even femtoseconds. Increasing pulse duration, enhanced efficiency of operation meanwhile the cost value decreases relatively using cheaper lasers. Shorten pulse duration in free-running mode (FRM) from $\tau$ = 0.3–0.5 ms to 50–100 μs at a constant power lasing output conduces to more intensity of spikes ($I_{ps} \geq 10^8$ W/cm$^2$), therefore, decelerates heating process in cutting front that accelerates vaporization and restricts the HAZ width. Increasing pressure of vaporized material in the cut zone promotes self-expel molten material that enhanced cut quality (stability of cut width, reduce surface roughness and suppress solidifying of drops on the underside (dross) or burrs on the distal surface). One such approach (at $\tau$ = 0.3–0.5 ms and $I_{ps} = 10^7$ W/cm$^2$) to evacuate molten material, it is necessary to employ additional equipment such as a stream of gas (air). The HAZ thickness (which is proportional to the radiation period $Z \sim (a\tau)^{1/2}$ ) would be slightly increased. Maximum cutting speed (that is proportional to the material and geometry of stent) approaches to 250 mm/min for both operating modes, while the identical pulse duration frequency $f$ got less than 200 Hz for pulse mode and the spot size on the workpiece surface $d_0 \approx FQ$ (where $F$ is the focal length of the lens, and Q is the beam divergence). As well as practically using similar laser technological equipments (LTE), there would be a slight difference between these operations in their production costs. Further reduction of pulse duration results in restricts of liquid amount in molten part and decrease the HAZ depth, but as $\tau < 1$ ps (femtosecond pulses) it would practically extinguished. However, as intensity grows up to $10^{10}$ W/cm$^2$ and cut width of $b < 40$ μm, the pulse energy would not be sufficient to pierce the material by one single pulse, so the formation of kerfs cut would be different (Figure 1).

Consequently, cut edge roughness is determined by the overlap factor of adjacent holes $k_{overlap} = S/d$ (where $S = V_f$ is the striation spacing, and $f$ is the pulse duration frequency), while for fixed values of $f$ and the default value for surface roughness $R_z$ restricts the linear cutting speed $v$:

$$v \le fd\left[1-\left(1-\frac{R_z}{d}\right)^2\right]^{1/2}. \qquad (1)$$

If a tube with a wall thickness $d$ pierced by $N$ pulses (Figure 2), then $d = N\Delta$ ($\Delta$ is the raise of depth width in one pulse), so to decrease the striation spacing to the value of $S_i = S/N$, cutting speed is relatively reduced, while the pulse duration frequency is fixed $v_i = S_i f$.

Cutting with high beam intensity would cause the ionization of the ejected metal vapor in form of high temperature plasma, consequently would cause instabilities in the beam–material interaction zone, and may screen the beam, which is unacceptable. Therefore, the pause between pulse duration frequency should be settled properly so that the ejection of destruction products would be occurred, and it should not be less than $(T - t) \ge Z/v_e$ (where $T = 1/f$, and $v_e$ is the ejection velocity of destruction products of about $10^5$ cm/s). This model causes a substantial loss of productivity of cutting operations down to about 2.5 times for picoseconds pulses and more than 10 times for ultrashort femtoseconds. In addition, a rise in cost value would be happened, not just because of above problem but also due to the significant appreciation of laser equipment needed for such implementation. Additionally, in piercing by super positioning pulses (see Figure 2) formation of continuous contour lines got more complicated in comparison with a single pulse piercing (see Figure 1), it also complicates selection of surface roughness level that is relative to the operating mode.

Studies on stent manufacturing at one of the leading manufacturers of laser equipments Lasag AG demonstrated that a gas-laser with pulse duration of 0.1–0.3 ms and intensity of no more than $10^7$ W/cm$^2$ may be efficient to completely remove molten material from the cut kerfs. Such pulse duration produces an incident power density at the tubular workpiece surface that is sufficient for perforation (see Figure 1).

In this case, edge roughness across the cut decreased due to «healing» of defects (micro-indents) by moving melt portions, while longitudinal roughness would be minimized by appropriate $K$ factor of the overlap ratio ($k_{overlap}$). Consequently, plasma formation suppressed, therefore beam caustic region would be saved during perforation. Although the HAZ width increased but these consequences can readily removed by heat treatment, which is usually performed as post treatment in stent manufacturing, that also enhanced resistance and flexibility of stent. Obviously, further treatments after such cutting have much more quality with a lower cost value. Thus, in comparison with other conventional cutting methods for stent, using a gas-laser with millisecond pulse duration excelled in productivity, high quality and a simplified finishing operation.

To provide a restrict mode for laser treatment using free-running pulses, cutting speed (repetition rate and peak power of pulses) should be balanced with the gas flow rate in order to succeed ejecting molten material from the cut zone. Considering these as well as the multilateral technological procedure, utilizing enhanced laser technological application equipments and processing mechanisms, should be set to one of the methods of experimental optimization [4], which is a long and complicated procedure.

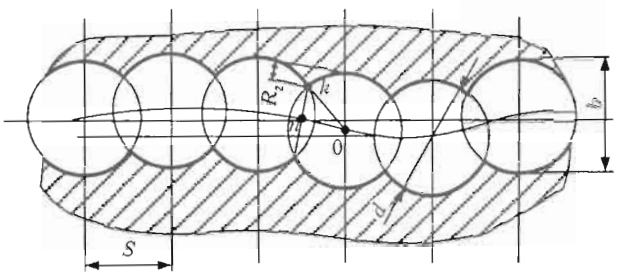


**Figure 1.** Scheme of edge roughness $R_z$ formation

In assessment, the method developed by J. Steffen [5] can be used, which as experienced results of its implementation under certain conditions had given an impressive prerequisite result. These conditions are as follows:

- cutting parameters $4d/d_0 >> 1$;
- workpiece material — metal $\frac{L_v\rho}{T_v c} \approx 5$ with melting point of $T_m \approx 0.5T_v$, where $L_v$ is the volumetric latent heat; $\rho$ is the density; $T_v$ is the evaporation point (K); and $c$ is the specific heat;
- pulse duration by $\tau << 4.5d_0^2/a$, where $a$ is the thermal conductivity of the material.

Under sufficient depth of focus $2z_f$, $Z_{f\infty} = \pm\frac{4\lambda F^2}{\pi D_l^2}$ for $TEM_{00}$ and $Z_{fmn} = \pm 5.56\left(\frac{\lambda F^2}{2\pi D_l^2}\right)$ for $TEM_{mn}$, that is greater than the tube wall thickness $d$, and the following scheme for formation of the through channel cut can be adopted (Figure 3), using a single pulse, which assumes a linear increase in the through channel cut equal to the tube thickness in the duration of one pulse radiation $t$.

In this case, processing mode can then defined as

$$\tau_e = 0.33\frac{b^2}{a};\quad I_e = 1.65\frac{\delta L_v\rho}{A\tau_r};$$

$$E = 0.5\delta\rho L_v b^2/A;$$

$$f \le (t+\tau)^{-1} = (0.05b^2/a + \tau)^{-1};$$

$$P_a = \pi b^2 I\tau f/4;\quad d_0 = 0.6b$$

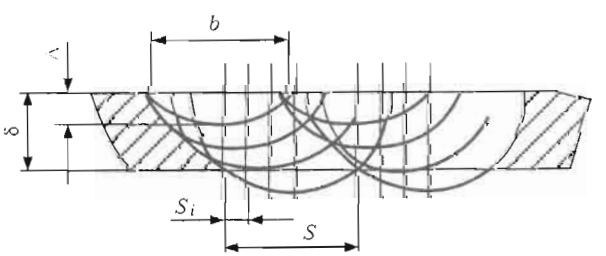


**Figure 2.** Scheme of cutting formation by super positioning long-pulses

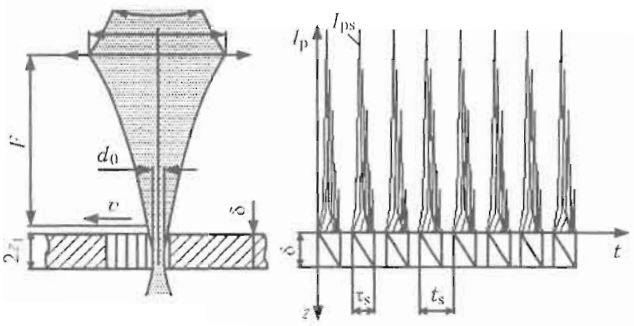


Figure 3. Scheme of through channel formation using single pulses

(here $\tau_e$ is the estimate value of pulse duration; $I_e$ is the beam intensity; $E$ is the pulse energy; $f$ is the pulse repetition frequency; $P_a$ is the average power; and $d_0$ is the beam spot size on the workpiece surface);

• cutting speed is proportional to the longitudinal roughness of workpiece (1);

• divergence of the beam is determined by the focal length of the lens $F/Q \approx d_0/F$, and if it is necessary to adjusted, optical components would be implemented to the beam path.

Generating pulse energy power can be extended in various lasers by means of either a pulse pumping or a Q-switching with continuous excitation source. In optical pumping using, alternating current mode refers to frequencies in the range up to the several hundreds of kilohertz, which gives a sufficient productivity as well as high quality in cutting edges. However, chaotic character of peak structure in FRM pulses causes instability in dimensional results, and overextended it up to $0.25\tau$, would substantially increased the proportion of viscous liquid fraction in the kerfs width or the HAZ depth. So to eject material sufficiently, gas pressure up to 1.5 MPa and water jet under 0.5 MPa would be required to prevent abnormal molten regions and formation of dross.

In addition, pumping lamps under pulse repetition mode of operation reduces the lamp lifetime. Structure of pulses could be stabilized by placing additional Q-switches resonators, which splits them into series of high peak power intensity $I_{ps} = 10^8$ W/cm$^2$, that results in evaporation mechanism for micro-indents discussed above. The same mode would be achieved at continuous train of peaks emitted from Q-switching with continuous excitation source, which has the same shortcomings and imperfections. Other Q-switch type modulators placed in resonator, such as acousto-optical and electro-optical modulators, may only ensure 100 % depth of modulation in single radiation, which limits their energy capabilities. Ultrasonic Q-switch

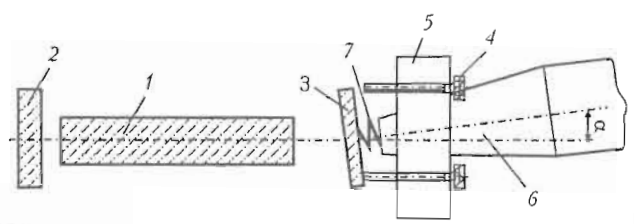


Figure 4. Swinging mirror modulator (for designations see the text)

modulators based on Doppler effect [6] successfully utilized in emitters with low excitable active medium ($Al_2O_3:Cr^{+3}$) in which the accessible linear speed would be achieved by changes in resonator length, to be sufficient for the drift of oscillation frequency beyond the limits of bandwidth of the excited host center ($Cr^{+3}$) as the wave grows up. In order to strongly amplified active medium (garnet doped with neodymium ions $Nd^{+3}$) by such mode of excitation, trains of peaks [7] with a manageable total duration and an average intensity would be achieved that are suitable to use in gas-laser cutting without rear sections. However, such modulators are not widely commercial because of the complexity of reciprocating motion of mirror by means of piston (without any twisting).

A more efficient and a simplified way in practical implementing modulators based on a periodic exciting of active medium to just above a threshold level [8] would be achieved with a trivial misalignment in optical cavity *2* by periodic actuation of mirror *3* from normal position within a small angle (up to 10 min) (Figure 4) [9]. Fully reflecting mirror *3* fixed via the elastic coupling *7* to the end of the ultrasonic head *6*, as it set out in the body *5* at a certain angle α to the resonator axis. While the ultrasonic head is standing, mirror *3* pressed to the ends of the adjusting screw *4* by means of the elastic element *7*, which constructed the lowest level of gain energy. This leads to a higher threshold by detuning resonator mirror from the normal position due to a sharp increase in diffraction loss of resonator.

During this period, pumped energy would be stored in the active medium, contributes to raise pulse power, which formed at the frequency of ultrasonic head during mirror set back to its normal position. Changes in frequency and amplitude of oscillation affect the pulse duration as well as pulse power.

Q-factor in spherical mirrors (in this case an unstable optical cavity) can also periodically change from a high value to a low value due to the increase of diffraction losses and hence change the CW radiation into the pulse radiation [10]. Once such thing occurs, fully reflecting mirror *1* may periodically changed surface curvature, which eliminates possibility of formation of standing wave between the quiescent states of the mirror (Figure 5).

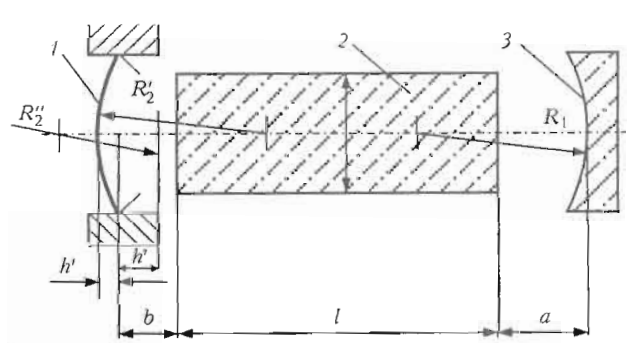


Figure 5. Scheme of mirror-membrane resonator (for designations see the text)

At the concave state, mirror *1* has radius curvature $R_2' > R_1 - (a + b + nl)$, where $a$, $b$ and $l$ are the linear dimensions of resonator, and $n$ is the index refraction of active medium *2*. At the convex state, mirror *1* should have radius curvature $|R_2''| < R_1 - (a + b + nl)$.

Under 50 % curvature of mirror *3* $R_1 > a + b + nl$ and the concave state of mirror *1* (stable optical cavity), it would be capable for forming of standing wave, hence beam radiation would be happened. At the convex state of mirror *1* (unstable optical cavity), energy would be stored to excite active medium *2*. Hence, curvature periodic changes of reflecting surface lead to storing energy for excitation and transition of this power into radiation pulse at a fixed position of the mirror in concave state. Engineering design of such mirror characterized by its simplicity.

Both schemes of modulators with continued excitation of active medium have no restrictions on the motion speed of mirrors, thus it is possible to control the frequency and energy parameters of radiation over a wide range.

## CONCLUSION

In the technology of laser cutting of stents it is not necessary to use expensive and often exotic laser systems operated with ultrashort pulses or high harmonics of infrared or visible radiation. It would be enough highly organized mode of composition and carefully changes to optical beam transition so that by the simplest mode of generation with the use of special processing techniques to obtain results comparable to those received by more expensive means.

***Acknowledgments.*** *Thanks to Dr. Ronald Holtz (Senior Applications Engineer at LASAG AG) for private informal conversation.*

1. Vejko, V.P. (2005) *Laser microprocessing.* St. Petersburg: ITMO.
2. Flanagan, A. *Laser stent cutting.* Pat. 6,696,667 USA. Int. Cl. B26/38.
3. Schuessler, A., Strobel, M. (2003) Stent materials and manufacturing: Requirements and possibilities. In: *Proc. of Conf. on Opportunities of ASM Materials and Processes for Medical Devices* (8–10 Sept. 2003, Anaheim).
4. Kotlyarov, V.P., Leleka, C.V., Nedal, Z. (1999) Optimization process of gas-laser cutting. *Exspress Novyny, Series Science, Technique, Production,* **15**, 20–23.
5. Steffen, J. (1987) Prozessoptimierung bei materialabtragenden Bearbeitungs problemen mit Laserstrahlung. *Feinwerktechn. und Messtechnik,* 8(7), 309–320.
6. Sokolov, B.M., Varks, E.D. et al. (1971) Ultrasound sync ruby laser radiation. *EF& ECHMO,* **10**, 8–12.
7. Belova, G.N. (1979) Neodymium glass laser with controlled intensity of ultrasound radiation. *Kvant. Elektronika,* 6(**8**), 1740–1745.
8. Jones, S., Kleine, K., Whitney, B. *Pulsed fiber laser cutting system for medical implants.* Pat. 6,521,865 USA. Int. Cl. B23K 26/38.
9. Kotlyarov, V.P., Shtoma, I.I. *Laser emitters for technological installations.* USSR author's cert. 1610707. Publ. 1990.
10. Kotlyarov, V.P., Kovalenko, V.S., Aniyakin, N.I. Optical quantum generation for laser processing plans. In: *Electrochemical and electrophysical methods of processing materials.* Tula: TPI, 31–35.

# RESEARCH ON LASER REMANUFACTURING OF STEAM TURBINE BLADES

JIANHUA YAO[1, 2], CHUNYAN YU[1, 2], QUNLI ZHANG[1, 2], XIAODONG HU[1, 2], CHENGHUA LOU[1, 2] and V.S. KOVALENKO[3]

[1]MOE Key Laboratory of Mechanic Manufacture and Automation, Zhejiang University of Technology, China
[2]Research Center of Laser Processing Technology and Engineering, Zhejiang University of Technology, China
[3]Laser Technology Research Institute, NTUU «Kyiv Polytechnic Institute», Kyiv, Ukraine

Electric power industry is the basic industry of national economy. About 75 % of power all over the world comes from boiler-steam turbine-electric generator of heat-engine plant and reactor-steam turbine-electric generator of nuclear power station. Turbine blade is the key component of steam turbine, which operational life span directly influences the overhaul life of turbine generating units. Using $CO_2$-laser as the heat resource, this research introduced laser cladding technique for recovering the failure dimension and laser alloying technique to strengthen the repaired layer, and thus to perform the laser remanufacturing of turbine blade. This paper the method of laser remanufacturing for the stainless 2Cr13 steel blade is described with analyzing the microstructure, wear and cavitation resistance. The results showed that through laser remanufacturing technique the microstructure of treated blade was significantly changed, and the hardness of laser treated layer was changed tremendously from surface to core material, which in the range of *HV*0.2 737–250, while the hardness of matrix is *HV*0.2 200–250. The wear and cavitation resistance of the treated blade were increased to at least twice compare to that of the untreated ones after performances testing. Therefore, the laser remanufacturing technique may be applied more extensively in the failure turbine blades with its high flexibility, strongly controllable performance and free of pollution.

Along with the rapid economic development, questions about power shortage become highlighted. Steam turbine equipment plays more and more important role in some main fields such as petroleum, chemical, light and heavy industries. Turbine blade is the heart of steam turbine, which operational life span directly influences the overhaul life of turbine generating units [1–4], and it works in high temperature with high speed. Due to high-speed impact of the steam and water droplets, the leading edge of steam turbine blades is often prone to cavitations [5, 6]. This makes blade loss its value and has to be abandoned. Generally, there are two solutions to the failure leaves: one is replacement and the other is repairing. The traditional repair methods, such as surfacing, spraying and mosaic ceramic lining, are difficult to meet its working conditions. So it is urgent to find a new remanufacturing method to meet its requirements.

Since the development of applications of high power laser in the 1970s, laser cladding technology has been developing rapidly. Using high-energy and high-speed laser beam as the heat resource, it can form a metal coating of dense, homogenous, high performance with high heating and cooling rates and adjustable metal powder material composition [7–9]. With the growing maturity of laser cladding technique, it was considered a particularly effective means of remanufacturing technology [10]. The paper introduced laser cladding technique for recovering the failure dimension and laser alloying technique to strengthen the repaired layer, and thus to perform the laser remanufacturing of turbine blade. Based on steam turbine blades of 2Cr13 martensitic stainless steel, this paper mainly analyzed the microstructure, microhardness, wear resistance and cavitation resistance.

**Experiments.** In this paper, both laser cladding (Figure 1, *a*) and laser alloying (Figure 1, *b*) were

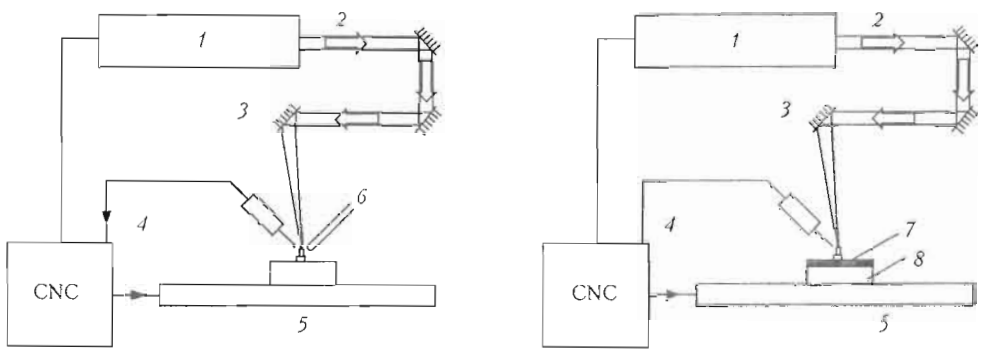


**Figure 1.** Schematic diagram of laser cladding (*a*) and laser alloying (*b*): *1* — laser processing system; *2* — laser beam; *3* — focusing system; *4* — temperature detection system; *5* — working table; *6* — selected powder; *7* — alloying layer; *8* — cladding layer

used on turbine blade to realize the remanufacturing. First of all, laser cladding was carried out for 3D restoration through multi-cladding with special alloy powder. In this process, the interaction time between the laser beam and powder material plays a crucial role for the desired successful cladding. Cladding was accomplished by delivering the selected powder through the FS-1 powder feeder with a feeding rate of 3.04 g/min. The main cladding parameters were scanning speed $v = 0.3$ m/min and power density $q = 222$ W/mm$^2$. Secondly, laser alloying method was used to enhance the properties of the surface of cladding layer, and thus to perform the entire laser remanufacturing. The main laser alloying parameters were scanning speed $v = 0.35$ m/min and power density $q = 44$ W/mm$^2$. Two processes were carried out in a laser system consisting of a 7 kW CW $CO_2$-laser and a CNC controlled working table. The Sonser Therm MI16 temperature detection system was used to measure the temperature of both laser cladding and laser alloying on line. Argon was used as shielding gas during laser irradiation.

Before remanufacturing, the substrate and selected powder should be pretreated, so as to meet the demands of laser cladding and laser alloying. At first, specific mechanical polishing was performed to remove the surface oxides and improve the wetting property. Secondly, alcohol or acetone was used to clean the surface oils. The chemistry was as follows, wt.%: 2Cr13 substrate — 0.16–0.21 C, 12–14 Cr, ≤0.8 Mn, ≤0.6 Si, Fe — balance; powder for laser cladding — 20.1 C, 13 Cr, 1.16 Si, 0.77 Ni, Fe — balance; powder for laser alloying — 76.47 Co, 6.67 W, 6.58 Ni, 5.72 Cr, Fe — balance. The powders should be preheated to 110 °C for 2 h and cooled in the oven to approximately 50 °C.

**Results and discussion.** *Microhardness and microstructure of laser-remanufactured layer.* Surface microhardness was tested by HXD-1000 digital hardness tester. The load was 200 g and the action time is 15 s. The distribution of the cross-section microhardness after laser remanufacturing is shown in Figure 2. The test result showed that the surface hardness of remanufacturing section increased obviously to *HV*0.2 800–650, in average being *HV*0.2 737.

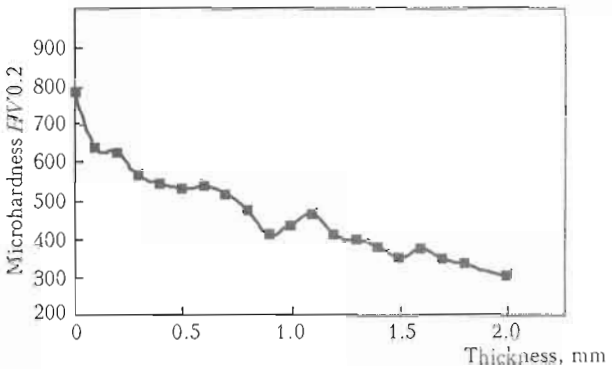


**Figure 2.** Cross-section microhardness after laser remanufacturing

Compared to the microhardness of substrate *HV*0.2 200–250, that of laser-remanufactured layer was 2 times harder. In the experiment, the thickness of laser remanufacturing layer was controlled in 0.7 mm through controlling the thickness of laser cladding. Microhardness from laser remanufacturing layer to the substrate declined uniformly from *HV*0.2 800–250.

The sample after laser remanufacturing was cut along the scanning direction vertically, inlayed, marked, polished, burnished and displayed according to the standard of metallographical sample. The $FeCl_3$ was chosen as the corrosive. After eroding, the metallographical structure was observed using HXD-1000 digital microhardness apparatus. The cross-section is divided into four regions (Figure 3, *a*): remanufacturing layer, integration layer, HAZ and substrate, where no pores or cracks were observed. Compared with substrate (Figure 3, *b*), the surface microstructure of remanufacturing layer was much finer and there is a metallurgical bond between the remanufacturing layer and substrate. The remanufacturing layer was composed of laser cladding layer and alloying layer.

In order to further research the microstructure of laser-remanufactured layer, the samples were observed under the FEI SIRION-100 scanning electron microscope. Figure 4, *a* and *b* showed that the selected power for cladding fed to the molten pool of the substrate occurred some physical and chemical reactions. Some of the primary crystal of high temperature melting point first separated out in fir-tree crystal

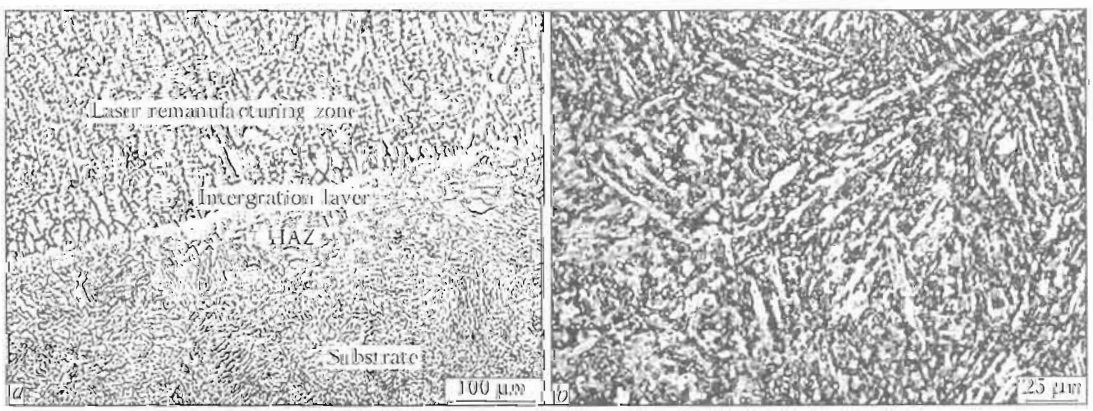


**Figure 3.** Cross-section structure of laser remanufacturing (*a*) and metallography of substrate structure (*b*)

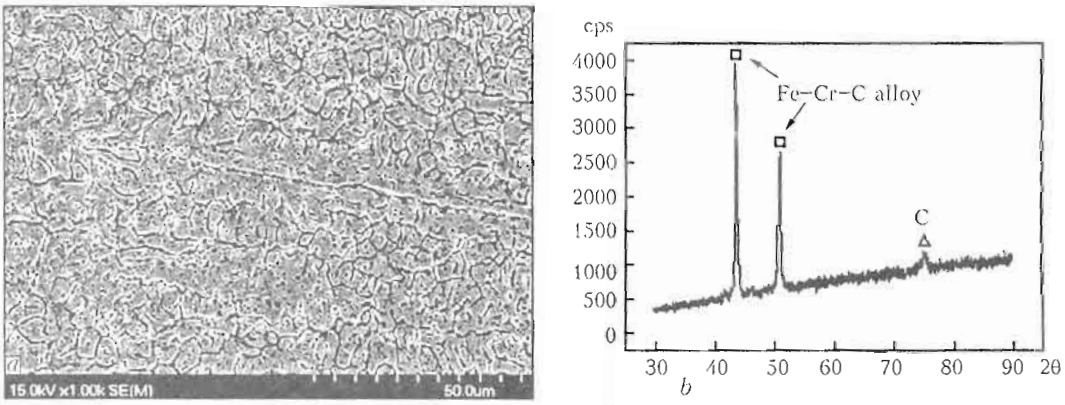


Figure 4. Results of SEM (*a*) and XRD analysis (*b*) of laser cladding layer

from the molten pool. With the temperature reduced, the others solidified between the fir-tree crystals and then formed multi-eutectic microstructures with non-equilibrium crystal characteristics. Figure 5 showed that the physical and chemical reaction of laser alloying were more complex than that of laser cladding. The main changes in alloying process included:

• the surface was melted because of the laser irradiating, formed a molten pool, infiltrated the alloying elements (W, Cr, Ni etc.) instantly and carried some chemical reactions. Tungsten and carbon formed WC ceramic particles distributing in the surface of the substrate dispersedly, increasing the hardness of the alloyed layer effectively; chromium and carbon formed $Cr_7C_3$ particles, contributing to the hardness, and nickel enlarged the austenite section and prevented from forming the second-phase particles, increasing the performance of corrosion resistant;

• a few of the austenite could not transform duly due to the heating quickly and cooling quickly of laser irradiation. This layer possessed of high hardness and plasticity because the residual austenite existed in the surface. Both laser alloying and cladding layer formed the laser-remanufactured layer and the alloying layer outside made the laser remanufacturing possess of excellent wear resistance and corrosion resistance because of its fine microstructure and high microhardness.

*Wear resistance analysis*. For some steam turbines of bad sealing, the blades of turbine could be worn inevitably because of some impurity in cylinder. In order to analyze the wear resistance, the WM-2002 frictional wear equipment was used. The samples were cut into disks 8 mm in diameter, the load was 150 g, and the standard reference sample was $Si_3N_4$ ceramic ball. After 2 h testing, the samples were weighted by BS-224S electronic balance made in Germany. The testing results obtained for substrate and laser-remanufactured layer were respectively as follows: mass loss of 0.68 and 0.31 mg, coefficient $\mu$ = 0.260 and 0.209. Observed the whole process of wear test, the wear process between laser-remanufactured layer and standard reference sample was greatly stable. Coefficient of friction was reduced by about 20 % and the relatively wear performance $\varepsilon$ = 0.456, which indicated that the wear resistance of laser-remanufactured layer was one time higher than that of substrate, then prolonged the operational life span of steam turbine.

After 2 h dry friction, the substrate and remanufacturing layer were observed under SEM for researching the wear pattern (Figure 6). The wear of laser-remanufactured layer and substrate were mainly abrasive particle wear, but the wear pattern was different. Figure 6, *a* showed that after wear test the scratch of the surface of substrate was the same direction and the width of furrows was not uniform. Some adhesive objects were found on the surface with different size and different shape. Following the trace of flake-off, the area of the adhesive objects was also different. Figure 6, *b* showed the distribution of fur-

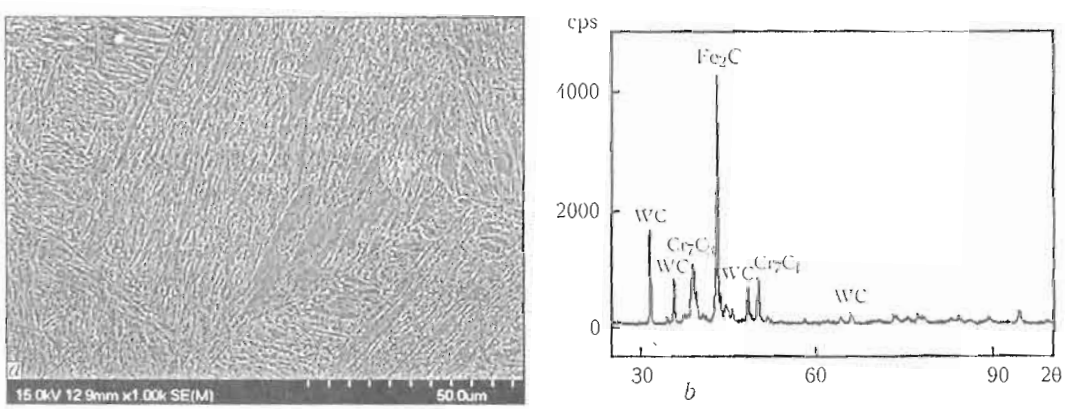


Figure 5. Results of SEM (*a*) and XRD analysis (*b*) of laser alloying layer

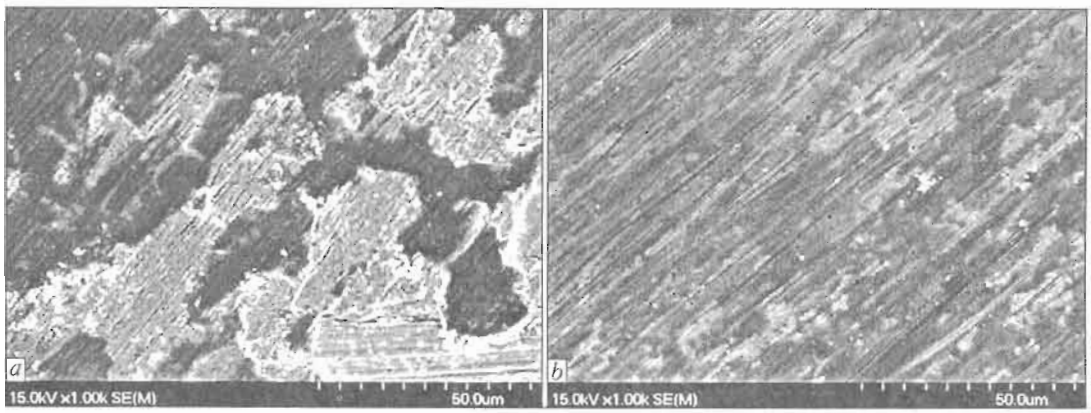


Figure 6. Wear morphology of substrate (*a*) and laser-remanufactured layer (*b*)

rows of laser-remanufactured layer was uniform relatively and found no adhesive objects. The furrows were a bit shallow and narrow, which reduced the contact area of $Si_3N_4$ ceramic ball, so the wear coefficient and mass loss were lower than those of substrate. Some white disperse distribution spots were found on the wear surface. As EDS analysis showed these spots were hard WC- and $Cr_7C_3$-phases, which improved the surface hardness and wear resistance effectively. The surface of laser-remanufactured layer owned uniform microstructure, fine grains and high microhardness of *HV*0.2 737. This makes a great help to improve the wear resistance.

*Cavitation resistance analysis*. The JY96-II ultrasonic wave cell breaking machine was rebuilt a ultrasonic wave shock cavitation instrument, which included ultrasonic wave generator, energy conversion device and an taper amplitude pole on energy conversion device. The surface of the sample was abraded by metallographical abrasive, polished by buffing machine, then the sample was cleaned for 10 min and weighted by the BS-224S electronic balance. The experimental solution was 3 % NaCl, test time was 10.5 h, every 90 min the sample was weighted and cleaned and NaCl solution was changed. The mass loss–time curve is shown in Figure 7. After cavitation experiment, surface shape of the substrate and laser-alloyed layer were observed by SEM SIRION-100.

The mechanism of cavitation has not been identified by a uniform knowledge until now. The main

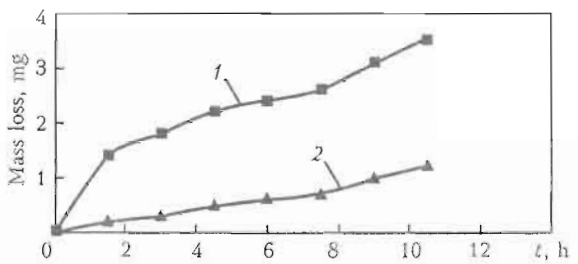


Figure 7. Mass loss–time curve for substrate (*1*) and laser remanufacturing zone (*2*)

viewpoint is that the cavitation is HF blast wave coursed by collapsing cavity, which is equivalent to hundreds or one thousand atmospheric pressure acting on the material surface. Under the continuous alternating stress, the surface of material was mechanically damaged, which resulted in the fatigue flake. After SEM researching the cavitation surface, cavitation pits were found, which were deep, uniform and massive, formed by flaking metal of surface. Figure 8 showed that in the same cavitation condition, the cavitation pits of laser-alloyed zone were a bit shallow and uniform relatively. No any crack was found on cavitation surface and none-cavitation surface because of the effect of quick heating and quick cooling of laser beam. The surface hardness was increased and the microstructure was fined. A mass of diffused carbide hard phase restricted the expansion of cracks, the flaking of surface metal and then reduced the

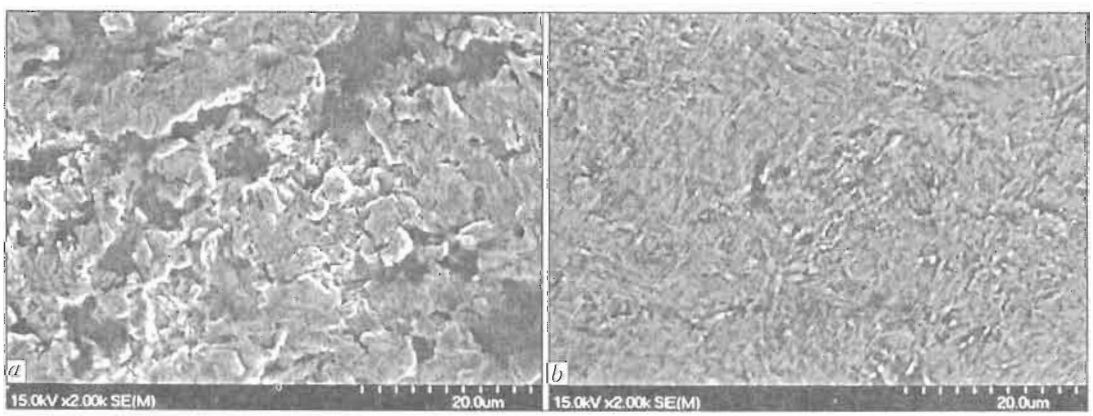


Figure 8. Cavitations morphology of substrate (*a*) and laser-remanufactured layer (*b*)

erosion rate, which resulted in increasing the cavitation resistance one time higher than that of substrate.

## CONCLUSION

Turbine blade was successfully remanufactured by laser cladding and laser alloying. Laser cladding technique was used to recover the failure dimension and laser alloying – to strengthen the repaired layer. The surface structure of remanufacturing layer was much finer. There is a firm metallurgical bond between the remanufacturing layer and substrate. After laser remanufacturing on 2Cr13 steel matrix, it was found that the remanufacturing layer was different from the substrate obviously through adding new alloying elements and high power laser beam, obtained finer grains, formed diffused carbide hard phase and chemical compound, increased surface hardness 2 times higher than that of substrate. Microhardness and microstructure of laser-remanufactured layer were changed obviously, which resulted in its better wear resistance and cavitation resistance than those of substrate. Laser remanufacturing is an easy processing with high efficiency and low cost, which has expansive application on increasing the wear resistance, cavitation resistance and enlarging the life span of steam turbine blades.

***Acknowledgements.*** *The authors would like to appreciate financial support from the Key International Science & Technology Cooperation Project of Zhejiang Province, P.R. China (2005C14009), the Scientific Research Fund of Zhejiang Provincial Education Department, P.R. China (20051394).*

1. Zhu, X.Y., Wang, Y.H. (2000) Development and actuality of fatigue life and failure diagnostics. *Information on Electric Power*, **2**, 12–15.
2. Qiu, J.L. (1998) Fracture accident of heavy steam turbine. *Electric Power*, **4**, 8–11.
3. Sun, J.X., Zhang, Z.W., Sheng, M. (2001) Steam turbine fixing technology. *Shanghai Electric Power*, **5**, 42–43.
4. Lewis, B.L. (1982) Unfield approach to turbine blade life predication. *SAE Technology Paper Series*, 821439.
5. Li, Y.G. (1994) Study on the cavitation erosion resistance of bead layer welded on nickel-based alloy. *J. Xi'an Highway University*, **14**, 77–80.
6. Zhao, M.H. (1999) Study on cavitation resistance of a new type precipitation hardening stainless steel. *Materials Sci. and Eng.*, 7(**4**), 60–63.
7. Wu, W., Wang, M.C. (2001) Advanced laser cladding and welding process for GT. *Gas Turbine Technology*, **4**, 25–30.
8. Ju, Y., Guo, S.Y., Li, Z.Q. (2002) Status and development of laser alloying and laser cladding in China. *Materials Sci. and Eng.*, 20(**1**), 143–145.
9. Kathuria, Y.P. (2000) Some aspects of laser surface cladding in the turbine industry. *Surface & Coatings Techn.*, **132**, 262–269.
10. Yang, X.C., Li, H.S., Wang, Y.S. (2003) Laser refabricating technology for repairing expensive and important equipments. *Laser & Optronics Progress*, 40(**10**), 53–57.

# HYBRID LASER-PLASMA AND LASER-ARC WELDING OF VARIOUS ALUMINUM ALLOYS

I.V. KRIVTSUN, V.D. SHELYAGIN, V.Yu. KHASKIN, V.S. MASHIN and A.S. ZATSERKOVNY
E.O. Paton Electric Welding Institute, NASU, Kyiv, Ukraine

The authors investigated the technological features of hybrid welding of butt joints of 0.8–6.0 mm Al–Mn, Al–Mg (AMg5, AMg6), Al–Zn–Mg (1915), Al–Cu–Mg (D16) and Al–Mg–Li (1420) on aluminum alloys, and there have been defined the working ranges of laser radiation welding modes using the pulse arc, consumable electrode or using heteropolar pulses of direct action plasma. The mechanisms of joint formation depending on laser power (up to 4 kW), arc current (up to 210 A) or plasma source current (100 A) were established. The influence of alloying elements on the pecularities of joint formation and the possibility of additional alloying of joints with filler wires (AMg6 and AK5) was studied. It has been shown that in hybrid welding in heat conduction mode of penetration the main mechanism of laser radiation influence on arc plasma behavior is evaporation of metal under the focused laser beam and use an electric arc in laser welding can reduce the temperature of transition from heat conduction mode to more effective mode of deep penetration. The optimum correspondence between time and current of direct and returning pulses at hybrid welding speed of up to 300 m/h has been also established.

In modern industry it is often necessary to manufacture thin-walled structures made of aluminum alloys. These structures include the bodies of cars and various kinds of devices, shape tubes, the aviation and space technology products etc. The traditionally used arc (including plasma) technologies may bring about the residual deformation and internal stresses in welded structures. Moreover, such technologies do not always provide the required strength characteristics of the joints. This fact has stimulated the use of electron beam and laser welding [1].

Recently there has been a substantial advancement in the study of the hybrid welding processes, including those combining laser and arc power sources [2]. The use of hybrid welding allows reducing up to 50 % of the running meter cost of the welded joint, and improving the process performance by 50 % for account of partial replacement of laser power by arc power [3]. The combination of laser radiation with a plasma arc is designed to permit preserving most of the advantages of laser welding and to make the welding process more attractive to the consumer.

The aim of this work is creation of basic methods of obtaining the aluminum alloy joints, based on a study of physical and technological peculiarities of hybrid welding using laser radiation of different wavelengths. To achieve this goal the mathematical modeling of geometrical parameters of the laser-plasma penetration was carried out, thus providing a possibility to determine an approximate range of welding mode parameters; the experimental studies on welding of aluminum alloys, enabling the mode parameters adjustment, were accomplished; the metallographic and mechanical tests were conducted which facilitated identification of typical defects and means for their elimination, and helped establish the scope of the welding process application.

The data obtained from literature [4–7] made it possible to determine characteristic change in shape of laser-plasma penetration depending on such parameters as radiation power $P$, process rate $v$ and arc current $I$.

This allowed a mathematical model to be developed describing dependence of depth $h$ and width $b$ of penetration in aluminum alloys on the following parameters:

$$h(P, v, I) = a_0 + a_1 P + a_2 v + a_3 I + a_4 P^2 + a_5 v^2 + a_6 \sqrt{I} + a_7 \frac{PI}{v}; \quad (1)$$

$$b(P, v, I) = c_0 + c_1 P + c_2 v + c_3 I + c_4 P^2 + c_5 v^2 + c_6 \sqrt{I} + c_7 \frac{PI}{v}, \quad (2)$$

where $a$ and $c$ denote the coefficients of depth and width of penetration, respectively. The coefficients corresponding to Al–Mn alloy were as follows:

| | |
|---|---|
| $a_0 = 0.578$ mm | $c_0 = 2.369$ mm |
| $a_1 = 0.719$ mm/kW | $c_1 = 0.899$ mm/kW |
| $a_2 = -0.023$ mm·h/m | $c_2 = -0.021$ mm·h/m |
| $a_3 = -0.019$ mm/A | $c_3 = -0.010$ mm/A |
| $a_4 = -0.110$ mm/kW$^2$ | $c_4 = -0.291$ mm/kW$^2$ |
| $a_5 = 1.258 \cdot 10^{-4}$ mm·h$^2$/m$^2$ | $c_5 = -2.396 \cdot 10^{-5}$ mm·h$^2$/m$^2$ |
| $a_6 = 0.272$ mm/A$^{1/2}$ | $c_6 = 0.328$ mm/A$^{1/2}$ |
| $a_7 = 0.371$ mm·m/(h·A·kW) | $c_7 = 0.095$ mm·m/(h·A·kW) |

Since the welding of aluminum alloys is performed using heteropolar pulses, in (1) and (2) the arc current is assumed as its average value over the time and determined as follows:

$$I = \frac{I_d t_d + I_{rev} t_{rev}}{t_d + t_{rev}}, \quad (3)$$

where $I_d$, $I_{rev}$, $t_d$ and $t_{rev}$ are the currents and the duration of direct and reverse polarity, respectively.

The calculation of dependences (1)–(3) revealed that at laser radiation power $P = 2$ kW and the ratio of direct and reverse polarity currents $I_d/I_{rev} = 100/50$ A ($t_d/t_{rev} = 0.8/0.8$ s) the hybrid welding

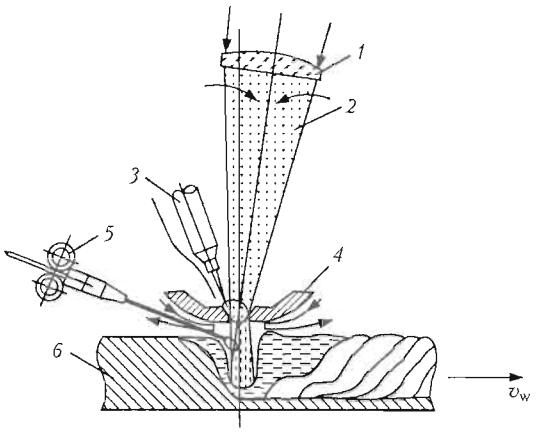


**Figure 1.** Scheme of the experiments on hybrid welding using the integrated direct action plasma torch: *1* — focusing lens; *2* — laser radiation; *3* — cathode; *4* — nozzle; *5* — filler wire; *6* — anode

at a speed of 70 m/h provides the penetration depth of up to 2 mm with about twice a width. The main mechanism of welding with these penetration parameters is of a conduction character [1]. The main mechanism of laser radiation impact on behavior of arc plasma in this mode of hybrid welding is the evaporation of metal under the focused laser radiation [6, 7].

The use of external ionizer (electric arc) in laser welding allows reducing the boundary temperature of the metal surface, at which the transition from heat conduction mode to more effective mode of deep penetration takes place. Furthermore, such parameters of hybrid welding as the radiation wavelength and polarization influence the process efficiency [8]. To increase the efficiency of laser and hybrid welding it is appropriate to use laser beams with linear polarization of radiation in the direction of welding.

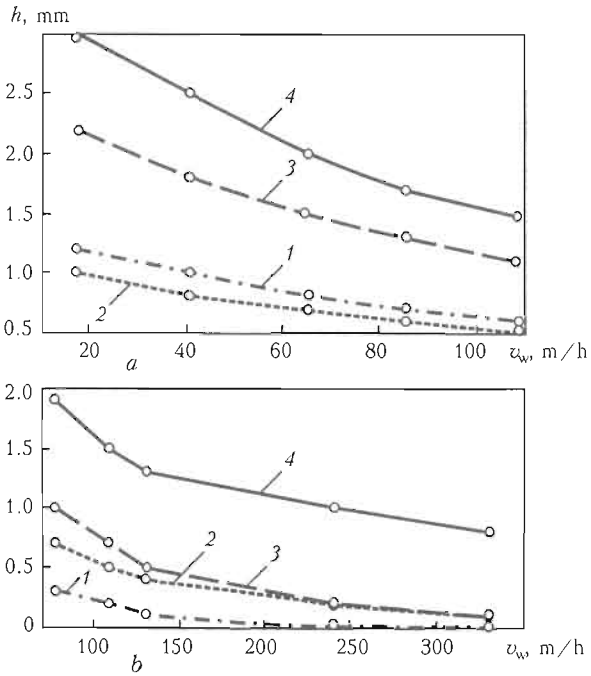


**Figure 2.** Dependences of penetration depth $h$ on speed of the laser-plasma welding $v_w$ of AMg3, AMg5M AMg6 and 1915 alloys at $P$ = 1.2 kW, $I_d/I_{rev}$ = 50/50 A and $U$ = 18 V: *a* — diode laser radiation; *b* — $CO_2$-laser radiation; *1* — laser welding; *2* — plasma welding; *3* — aggregate value in laser and plasma-arc welding; *4* — hybrid welding

Experiments on laser-plasma welding were carried out according to the scheme in Figure 1, using the samples of aluminum alloy AMn, AMg3, AMg5M, AMn6 and 1915 of small thickness ($\delta$ = 0.6–3.0 mm). The hybrid direct action plasma torch similar to the one described in [7] was used in the experiments, with focused radiation of diode (wavelength $\lambda$ = = 0.808/0.940 μm) and $CO_2$-lasers ($\lambda$ = 10.6 μm) at power of up to 2 kW. The thermal effect of the plasma arc and laser welding on the weld pool was analyzed by studying the patterns of the joints, as well as the burnout rate of magnesium and manganese.

According to the results of the experiments the corresponding dependences were plotted in Figure 2. From this Figure it can be noticed that the sum of the depths of the laser (curve *1*) and plasma (curve *2*) penetration (curve *3*) is less than the depth of the hybrid penetration (curve *4*). Thus, non-additivity of the sum of the penetration depths with the use of the heat sources that are included in hybrid process, and the depth that is yielded by hybrid penetration, takes place. The distance between curves *3* and *4* proves the existence of hybrid (synergetic) effect and shows its intensity.

A comparison of the results of experiments with the use of $CO_2$- and diode lasers revealed that the presence of synergy, linking of the plasma arc to the area of the laser beam and the stability of high-speed hybrid welding is more related to the power density of laser radiation than its wavelength.

It was experimentally established that in the investigated range of parameters the optimal welding speed corresponds to the minimum reinforcing bead generation at maximum power of the laser and plasma sources. This mode permits to obviate the use of the filler wire for obtaining the thin-sheet butt joints.

Selection of optimal durations ($t_d$ and $t_{rev}$) and currents ($I_d$ and $I_{rev}$) of direct and reverse pulses with high-speed (up to 300 m/h) hybrid welding has shown that both ratios tend to 1:1. The optimization criterion was ensuring the high-quality cathode surface cleaning of the oxide film by pulses of reverse polarity. Such kind of surface refining facilitates preparing of parts for welding and makes the laser-plasma process more efficient for industrial use than laser welding.

The mechanical tests of the samples, welded by laser radiation, plasma and laser-plasma method, showed that

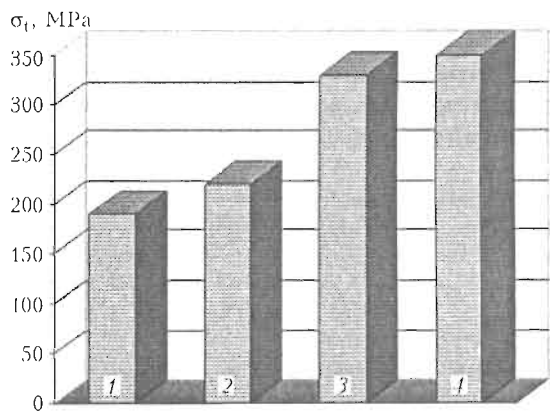


**Figure 3.** Tensile strength tests of hybrid-welded AMg3 and AMg6 alloy: *1* — AMg3 welded joint; *2* — AMg3 base metal; *3* — AMg6 welded joint; *4* — AMg6 base metal

the strength of the hybrid welded joints reaches 90 % of the base metal strength (Figure 3). This allows recommending the laser-plasma welding solutions for solving practical problems associated with the welding of thin-walled structures of Al–Mg–Mn alloys.

To determine the availability of the interior pores the welded samples of AMg3 and AMg6 alloys ($\delta$ = = 0.8–3.0 mm) were exposed to the X-ray analysis. In some cases, these pores have been recorded. More detailed studies revealed that the cause of their occurrence is a high content of hydrogen, as well as partial burnout of magnesium and manganese in the welded joints. Introduction of additives (AMg6 1.2 mm wire) helped completely eliminate the pores. Metallographic studies have shown that the structure of aluminum alloy compounds, obtained in hybrid welding, bears a closer resemblance to the structures that are characteristic of the laser process than of plasma one. In the case of utilizing a filler wire the opposite situation holds true – the structure of hybrid joints are much closer to the structures obtained in plasma welding (Figure 4). This is due to intensive overheating of metal through the melting of filler metal in the weld pool.

A comparison with laser welding showed that in hybrid welding the power of contracted arc partially replaces the power of laser radiation. For thin-sheet aluminum alloys, this effect can be roughly estimated as a replacement for 1 kW of laser power with 1 kW of plasma power. Thus, the economic effect of replacing the laser welding with its hybrid analog is the significant reduction in the cost of laser equipment. It is indeed reasonable, since the cost of plasma is usually much lower.

Welding AMn alloy ($\delta$ = 0.3 mm) shaped tubes utilized as a constituent part of the glass packets provides the example of an industrial application of the developed technology. In the course of experiments conducted at the $CO_2$-laser radiation power of 1.5 kW and the welding current $I_d/I_{rev}$ = 100/50 A, the high-quality joint of this alloy was obtained at the welding speed of more than 1000 m/h. It should be noticed that in the case of $CO_2$-laser welding about 3–5 kW would be required to reach a similar speed.

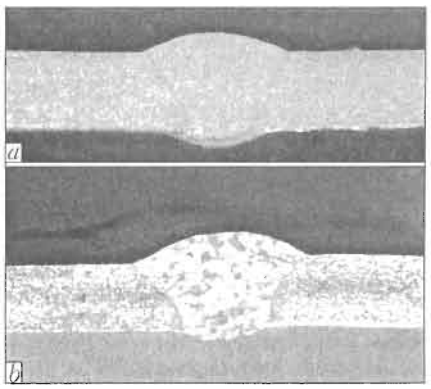


**Figure 4.** Structures of the AMg5M ($\delta$ = 3 mm) alloy butt joints obtained using the $CO_2$-laser radiation and AMg6 1.2 mm filler wire: *a* – laser welding ($P$ = 2 kW, $v$ = 30 m/h); *b* – hybrid welding ($P$ = 2 kW, $v$ = 120 m/h, $I_d/I_{rev}$ = 100/50 A, $U$ = 20 V)

## CONCLUSIONS

1. In the range of parameters under consideration the optimal welding modes correspond to welding speed at which the minimum reinforcing bead generation at the maximum power occurs. In most cases such modes permit to obviate using the filler material in virtue of the volume expansion of the penetrated metal.

2. In hybrid welding with the use of diode laser radiation the ratio of laser and plasma powers should approach 1:1 or vary in the direction of increase in laser power. This is due to improvement in the stabilization process of welding in proportion to metal evaporation enhancement under the laser radiation.

3. In laser-plasma welding of aluminum alloys with heteropolar pulses the reverse polarity pulses ensure the cathode cleaning of oxide film on the sample surface. In high-speed hybrid welding in order to achieve high-quality cathode cleaning the pulse duration ratio of direct and reverse polarity should approach 1:1. The reverse polarity pulse current should amount up to 70–100 % of the direct polarity pulse current.

4. The investigation of the chemical inhomogeneity of joints revealed the presence of burnout of such elements as magnesium and manganese in the case of hybrid welding without additives. This effect leads to the pore formation in the cast metal joints. Moreover, the high content of hydrogen in the welded joints affects the presence of pores. The use of filler wire allowed controlling the process of joint alloying and eliminating the effect of pore generation.

5. Application of laser-plasma hybrid welding of aluminum alloys enables a 2 to 4 fold increase in the penetration depth compared to the case of laser welding and similar increase in welding speed, as compared to plasma welding.

6. Comparison of effects of $CO_2$- and diode lasers application revealed that the presence of synergy, linking of the plasma arc to the area of the laser beam action and the stability of high-speed hybrid welding are rather related to the degree of laser radiation focusing than its wavelength.

7. Tensile strength and impact toughness tests of AMg3, AMg5, AMg6 and 1915 aluminum alloy compounds have proved the advantage of a hybrid method to the laser and plasma ones.

8. Future prospects of the work progress concern the use of fiber and Nd:YAG laser radiation taking into account the small wavelength and radiation focus spot, as well as a flexible optical fiber feed.

1. (1974) *Technology of fusion welding of metals and alloys*. Ed. by B.E. Paton. Moscow: Mashinostroenie.
2. Katayama, S. (2008) Advances of hybrid laser-arc welding. *Welding Technology*, 56(2), 51–58.
3. Irving, B. (1994) Automotive engineers plunge into tomorrow's joining problems. *Welding J.*, 73(11), 47–50.
4. Walduck, R.P., Biffin, J. (1994) Plasma arc augmented laser welding. *Welding and Metal Fabr.*, 62(4), 172–176.
5. Dilthey, U., Wieschemann, A. (2000) Prospects by combining and coupling laser beam and arc welding processes. *Rivista Italiana della Saldatura*, 52(6), 749–759.
6. Krivtsun, I.V. (2003) Modelling of hybrid laser-PTA processes and integrated plasma torches for their realization. In: *Proc. of Int. Conf. on Laser Technologies in Welding and Materials Processing* (Katsiveli, Ukraine, 2003), 122–130.
7. Krivtsun, I.V. (2004) Modelling hybrid plasma-laser processes and integrated plasmatrons. *Welding Int.*, 18(4), 268–276.
8. Garashchuk, V.P., Kirsei, V.I., Shinkarev, V.A. (1986) Influence of polarization of $CO_2$-laser radiation on geometric parameters of molten zone in welding of metals. *Kvant. Elektronika*, 16(12), 1660–1662.

# NON-LINEAR MODELLING OF THE DEFECTS GROWTH DYNAMICS IN LASER WELDS

O.V. KUZKO
National Antarctic Scientific Center, Ministry for Education and Science, Kyiv, Ukraine

Phenomenological model of the postweld defects growth dynamics in laser welds is developed in wave equation form of the hyperbolic type to analyze the weld metal strength characteristics. Mathematical modelling gives the opportunity to predict the conditions of the weld mechanical strength loss as a result of the defects volume growth by mechanical and climatic disturbances. This approach is intended to use for development of the automated control system of the functional state of the new welded fuel tank at the Ukrainian Antarctic Station «Akademik Vernadsky» as the complementary measure of the Antarctica environment protection.

It is well known [1–6] that to develop the laser welding technology and materials processing, in particular, such matters have great importance during the welding:

- defect formation mechanisms in welds, in particular, internal pores, cavities, and cracks;
- morphology of the welds, micro- and macrostructure of defects.

This article is devoted to the mathematical modelling of the welds defects growth after the welding that results in loss of the weld mechanical strength. For simplification we will understand the defects as the elements of the weld metal structure in the form of pores (nucleus) with different diameters which have lower mechanical strength in comparison both with other joint zones and with materials to be welded. We assume that the weld has a constant cross-section area along the entire weld length and is exposed to the mechanical and climatic disturbances which result in the defect volume increase in weld metal and ultimately — in mechanical strength losses.

To analyze the dynamics of the weld defects growth after laser welding, let us consider a continuous distribution of defects on the weld cross-section in an arbitrary time $t$ and define the defect state density $\rho(x, t)$ as the defect amount on the weld cross-section with the diameter $x$ per unit of measurement of the defects diameters or as the defects distribution on the weld cross-section depending on their diameters [defect amount/unit of the defect diameter measurement]. In addition we define the change of the defect state $q(x, t)$ as the defects amount in the weld cross-section in an arbitrary time $t$ which change the size $x$ per an unit time [defects amount/unit of time]. Then in the proposed terms the rate of the weld defect state change in time can be defined as $V(x, t) = q/\rho$ [unit of the defect diameter measurement/unit of time]. Let us assume that the defect total amount in the weld metal has been retaining and under the exposure of the mechanical and climatic disturbances their sizes have been increasing. Then the rate of the defect total amount change with sizes $x_1 > x > x_2$ is equal to the difference of the change defect states $q(x_2, t)$ and $q(x_1, t)$:

$$d/dt\int_{x_2}^{x_1} \rho(x, t)dx = q(x_2, t) - q(x_1, t). \qquad (1)$$

Supposing that $\rho(x, t)$ has continuous derivatives and going on to the limit $x_1 \to x_2$ we obtain the conservation law in the form of the hyperbolic type equation:

$$\frac{\partial \rho}{\partial t} + \frac{\partial q}{\partial x} = 0. \qquad (2)$$

From empirical considerations one can assume that the functional relationship exists between $q$ and $\rho$ in the form shown in Figure 1.

Here it is assumed that when the defect state density is $\rho = 0$ the corresponding change of the defect state $q$ is also equal 0. In another extreme case when $\rho$ has the value approaching to value of $\rho_{max}$, i.e. to value of the weld cross-section «saturation» when the defects occupy practically the entire weld cross-section, the value of $q$ also is tended to the «saturation» maximized value $q_{max}$.

If this functional relationship is written as

$$q = Q(\rho), \qquad (3)$$

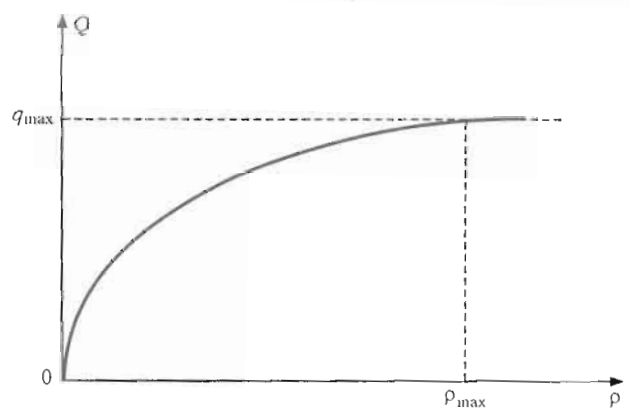


**Figure 1.** Functional relationship of the defect state change $q$ and defect state density $\rho$

then equations (2) and (3) form the closed system which leads to the equation of the hyperbolic type solved by the characteristics method [7]:

$$\frac{1}{V(\rho)}\frac{\partial \rho}{\partial t}+\frac{\partial \rho}{\partial x}=0, \qquad (4)$$

where $v(\rho)=\dfrac{\delta Q}{\partial \rho}$.

Let us take the initial condition of the defect state distribution in the form of Gaussian distribution (Figure 2) at time $t = 0$ which supposes the primary defects sizes near $x_0$. Solutions of equation (4) in subsequent moments of time $0 < t_1 < t_2$ demonstrate the defect size growth with the shock wave effect in the weld defect structure. That is the defect state distribution changes its shape because the defects with different sizes increase its volume with the different rate. It can be assumed that the noted dynamics of the defects growth determines the dynamics of the mechanical strength loss in welded joints when the structure of defect sizes and total defect volume in the weld metal attain the proper critical values.

The shock wave formation on the right front of the defect density distribution is stipulated by the increasing behaviour of dependence $q = Q(\rho)$ (see Figure 1). Continuing the wave approach to the analysis of the defects growth dynamics in the welds we consider now qualitatively the case of the elastic mechanical oscillations exposure which affect the weld metal. Assume that the elastic mechanical oscillations lead both to an increase in defect sizes in the weld and to nucleation of new defects along of the entire weld length. The new defects occurrence on the entire weld length can be taken into account by the introduction of the corresponding term in the right side of the equation (3):

$$\frac{1}{v(\rho)}\frac{\partial \rho}{\partial t}+\frac{\partial \rho}{\partial x}=G(x)\exp(i\omega t), \qquad (5)$$

where $\omega$ is the elastic mechanical oscillation frequency; $G(x)$ is the mechanical oscillation amplitude. It should be noted that the new defect nucleation leads to the changes in the shock wave structure (see dashed lines in Figure 2).

For the simplification we will assume that we work on the linear rising part of $q = Q(\rho)$ and $v(\rho)$ is equal to the constant rate of the state change of weld defect density $V_{gr}$. We will also assume that under the exposure of the elastic mechanical oscillations the defect state density also will be varied with the frequency $\omega$:

$$\rho(x, t)=\rho(x)\exp(i\omega t). \qquad (6)$$

Taking into account the made simplifications we rewrite the equation (5) for the convenience in the integral form by $\rho(0) = 0$:

$$\rho(x)=\frac{1}{V_{gr}}\exp\left(-\frac{i\omega x}{V_{gr}}\right)\int_0^x G(z)\exp\left(\frac{i\omega z}{V_{gr}}\right)dz, \qquad (7)$$

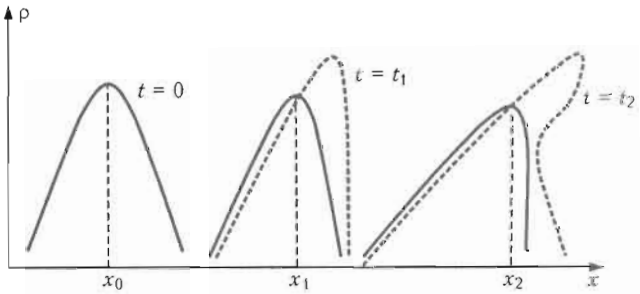


**Figure 2.** Shock wave formation in the structure of the weld defects ($x_0 < x_1 < x_2$): solid lines — effect of shock wave occurrence when the defects amount in weld metal is unchanged and the area under lines is constant; dashed lines — shock wave occurrence when new defects are formed in weld metal

where $z$ is the current integration variable. Now assuming that the exposure is the travelling wave in the weld face direction with the phase velocity $V_{osc}$, constant amplitude $G_0$ and frequency $\omega$, that is

$$G(x, t)=G_0\exp\left(i\omega t-i\omega\frac{x}{V_{osc}}\right), \qquad (8)$$

and integrating (7) we obtain

$$\rho(x, t)=\frac{G(0)}{V_{gr}}\exp(i\omega t-i\omega x/V_{gr})\times$$
$$\times\frac{\exp(i\omega/V_{gr}-i\omega/V_{osc})x-1}{(i\omega/V_{gr}-i\omega/V_{osc})},$$

and by $\omega/V_{gr} \approx \omega/V_{osc}$ the synchronism wave effect occurs consisting in the $\rho(x, t)$ growth along the coordinate $x$:

$$\rho(x, t)=\frac{G(0)}{V_{gr}}=x\exp(i\omega t-i\omega x/V_{gr}). \qquad (9)$$

In this case we have the phenomena both of the predominant growth of certain defect sizes in the weld metal and of the predominant growth of defect amount and sizes in certain weld points which could significantly change the points topology of the weld mechanical strength loss.

In the case of the spread of elastic mechanical oscillation wave perpendicularly weld length, the synchronism wave effect can result in mechanical strength losses simultaneously along the all weld length, but not only in the separate weld points.

In the case when the weld will be exposured simultaneously by a few waves of elastic mechanical oscillations, the conditions of the waves synchronism may be too a few leading to the more complex topology of the weld mechanical strength loss.

Similar wave approach is proposed to use also for modelling of the defect growth in arc-welded joints, in particular, by development of automated control system of functional state of the new fuel tank at the Ukrainian Station «Akademik Vernadsky» for the early warning of a possible fuel leakage from the tank due to the loss of mechanical strength of welds.

In addition, for natural extreme seasonal (long-) and daily (short-periodical) natural disturbances (wind load, temperature, humidity, salt fog, precipi-

tation) at the Station «Akademik Vernadsky» it is proposed to use as the natural testing ground under the open air for mechanical and climatic tests of the welded joints and coated specimens obtained by the different technologies of welding and materials processing. It should be noted that such natural testing ground unlike from the special test chambers does not require the specific energy expenditures, has no limit on the test sample sizes and its quantity, has no restrictions on the test duration, will not require special expenditures for the samples delivery at the Station and back.

## CONCLUSIONS

1. The phenomenological approach is developed in the form of the hyperbolic type wave equation to analyze the dynamics of the postweld defect growth which results in the losses of the weld mechanical strength. It is intended to use this approach for development of automated control system of functional state of the new fuel tank at the Ukrainian Antarctic Station «Akademik Vernadsky» as an additional means for prevention of the fuel leakage from the tank and for the Antarctica environment protection.

2. The possibility of the shock wave effect is pointed in the defects growth dynamics in welds under the exposure of climatic and mechanical disturbances and the corresponding shock wave effect on dynamics of the mechanical strength loss of welded joints.

3. The synchronism waves effect is considered qualitatively during the spread of the elastic oscillation wave in welds with the new defects formation. This effect can significantly accelerate the process of the mechanical strength loss in entire cross-section of the different zones along the weld length or throughout its length.

4. It is suggested to use the Ukrainian Antarctic Station «Akademik Vernadsky» as the natural testing ground for climatic and mechanical tests of welds and processed materials instead of the specialized test chambers.


1. Klimpel, A., Lisiecki, A., Janicki, D. et al. (2005) High power diode laser welding of aluminium alloy EN AW-1050 A. In: *Proc. of Int. Conf. on Laser Technologies in Welding and Materials Processing* (Katsiveli, Ukraine). Kiev: PWI, 39–42.
2. Kolodziejczak, P., Kalita, W. (2007) Quality assessment of laser-welded joints of dio-cast magnesium alloys. In: *Proc. of Int. Conf. on Laser Technologies in Welding and Materials Processing* (Katsiveli, Ukraine). Kiev: PWI, 84–88.
3. Grezev, A.N. (2007) Mechanism of cavity and weld pool formation in laser welding. In: *Ibid.*, 55–57.
4. Krivtsun, I.V., Shelygin, V.D., Khaskin, V.Yu. et al. (2007) Investigation of hybrid laser-plasma processes of welding of aluminium alloys and stainless steels. In: *Ibid.*, 92–94.
5. Haferkamp, H. et al. (2007) Hot cracks in pulsed laser beam welds of Cr–Ni-alloyed steels: detection methods and prevention by using predeposited plasma spray layers. In: *Ibid.*, 58–63.
6. Plochikhine, V., Prikhodovsky, A., Zoch, H.-W. (2003) Modern approach to modelling of solidification cracking in welds. In: *Proc. of Int. Conf. on Laser Technologies in Welding and Materials Processing* (Katsiveli, Ukraine). Kiev: PWI, 137–141.
7. Whitham, G.B. (1974) *Linear and nonlinear waves*. New York; London; Sydney; Toronto: John Wiley & Sons, 24–31, 72–98.

# EFFICIENCY IN ADOPTING HYBRID LASER-ARC WELDING

A.V. LOPOTA[1], O.V. VELICHKO[1], A.A. AFANASIEVA[1] and G.A. TURICHIN[2]
[1]Laser Technology Center, St. Petersburg, Russian Federation
[2] Institute of Laser and Welding Technology, St. Petersburg, Russian Federation

The results of economical analysis of efficiency of laser hybrid welding of large-diameter pipes are presented. On the base of costs and profits calculations the time of recoupmen is determined for the usage of hybrid welding installation on the pipe welding plant. The number of organizational actions, which are necessary for successful implementation of hybrid technology, are also discussed.

Finding ways and mechanisms to improve the efficiency of production of goods and services is an important task of every leader. At the present stage of development in a market economy, taking into account the peculiarities of the functioning of the Russian market (subjective interests of the parties to the developed market, highly competitive manufacturers of goods-analogues, imperfect regulatory and legal base, etc.), it is difficult to overestimate the importance of the choice of development strategy for production and its optimization. A well-reasoned conclusion about the appropriateness of applying new techniques and technology to replace existing ones can be done only on the basis of comparative economic analysis, which should take into account both quantitative and qualitative factors of the production process.

The development of modern production facilities (pipe, machine-building, machine-tool building, shipbuilding, etc.) is accompanied by a steady increase in all kinds of welding technology, equipment and tools, the rational use of which is the most important condition for the efficient functioning of an enterprise as a whole. Today, in the beginning of the XXI century, the global welding market, which is increasing in proportion to the growth of steel consumption, is not less than $40 bln, about 70 % of which are welding consumables and about 30 % are welding equipment [1]. More than half of the gross national product of industrialized countries is created by welding and related technologies. Up to two thirds of the world's consumption of rolled steel goes to the production of welded designs and structures [2]. In many cases, welding is the only possible or most effective way of creating all-in-one combinations of structural materials and achievement of resource-saving procurement, geometrically close to the finished part or design, where the choice of an optimal welding method becomes more difficult and requires a clear methodology for assessing the efficiency of the applied technology.

One of the most pressing issues in the field of welding technology is improving efficiency and productivity of welding thick-walled structures especially large-diameter pipes with increased wall thickness. The task of welding thick-walled structures (more than 27 mm) is not new and is solved in different ways through arc and electron beam welding. Each of these methods has disadvantages, from which welding pipes at the plant but more so in the field conditions, do not give the required weld quality and productivity. Thus, the arc welding technology involves multiple-pass process that does not always guarantee the desired properties of weld metal. For example, the root pass does not meet the requirements for impact resistance. The use of electron beam welding involves the use of vacuum chambers, which extremely complicates its use. If electron beam is released into the atmosphere, protection from X-rays is necessary. Besides, the use of electron beam requires a high quality and accuracy in the preparation of edges, which is almost impossible, for example, in the manufacture of large structures, such as large-diameter pipes.

All these make the importance of developing common approaches to the measurement of expenses and results to select the best technology and equipment for a specific production, which transform the calculation of efficiency from a formal process into a vital necessity.

Currently, the world's industrial practice to improve the efficiency of welding metals of large thickness is working on using laser and hybrid technology. In Russia, serial laser welding equipment with the necessary capacity and productivity is supplied mostly by foreign companies, as the domestic firms manufacturing similar equipment is single, or do not meet the needed requirements.

Until recently, the use of laser technology for welding longitudinal seams and erection joints at the plant and field conditions has been unreliable due to low laser systems in complex manufacturing conditions. Only in recent years, when powerful fiber lasers of relatively small dimensions of the desired reliability were developed, the development of hybrid laser technological complexes for welding large-diameter pipes became possible.

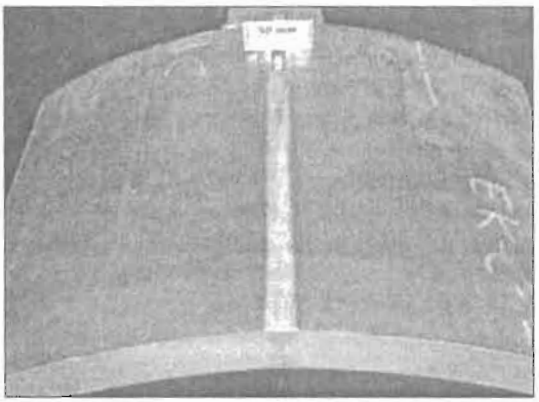

Figure 1. Laser-arc welding of pipe sections

Studies conducted in our country and abroad, have shown the perspectiveness of hybrid welding processes – a combination of laser and arc welding simultaneously. The hybrid laser-arc welding (HLAW) technology makes it possible to automatically achieve the desired quality of welds. On the one hand, such welding processes help to get narrow welds and heat-affected zones, and also to weld at high speeds. On the other hand, it is essential to reduce the demands on the accuracy of the assembly of welded components, which in turn dramatically reduces the cost of production tools and the actual operations of the assembly, and also improves its productivity. In addition, HLAW provides weldability of special steel pipes with an additional electrode wire alloying.

In some European countries, there are already pilot technologies that are used in producing hybrid-welded pipes (Figure 1), ship sections, railway cars and construction structures.

In Russia, the development of technology and creation of equipment for HLAW of large-diameter pipes is carried out by Laser Technology Center Ltd, St. Petersburg. Creating this kind of equipment requires a deep scientific and theoretical work, and so work is carried out jointly with the Institute of Laser and Welding Technology of the St. Petersburg State Polytechnic University (Banks Mud STU). A functioning model for welding of large-diameter pipes, equipped with modern 15 kW capacity fiber laser, arc welding device, systems, guidance and monitoring process (Figure 2). This given complex helps to weld modern steel pipes with a weld root of up to 15 mm thickness and at speeds up to 3 m/s for a single pass. The remaining cutting can be filled by means of welding under a layer of flux, or welding in shielding gases.

The most perspective area of the technology of HLAW of large-thickness metals is straight-line-weld on large-diameter pipes. Currently, automatic gas metal-arc welding (for technological pass) and submerged-arc welding (for the filling passes), which are labour intensive operations that require highly qualified personnel are used in the manufacture of pipes in pipe factories.

Besides, conventional technologies for arc welding of domestic grade K65 steel and above grades do not achieve the necessary values of impact strength of the weld metal. This hinders the transition of pipe-welding factories to the production of high quality steels.

Preliminary analysis showed that the adoption of HLAW technology in the production process of welding large-diameter pipes, for example, in the Chelyabinsk Pipe Rolling Plant, will reduce the cost of producing a unit of product, and significantly improve the mechanical properties of the welded joint that determines the final operating characteristics of the product, and as a result, lower production costs of finished product by more than 30 %, for example, changing the form of cutting will reduce the consumption of fillers by 2–4 times, and the transition from multi-arc to HLAW, on a preliminary estimate, would reduce the cost of working gas by 15 mln rubles per year, with an average productivity of about 320 pipes a day.

The use of HLAW of large-thickness metals, according to experts, will help achieve the following socio-economic effects:

- increase in productivity by 7 %;
- reduction in energy and material consumption by 11 %;
- increase in the level of automation of production processes by 9.6 %;
- increase in the flexibility of production process;
- improved working conditions.

Comparative analysis of the main technical and economic factors in the adoption of HLAW technology in the example of welding pipe 1016 mm in diameter and with wall thickness of 12.4 mm (Table)

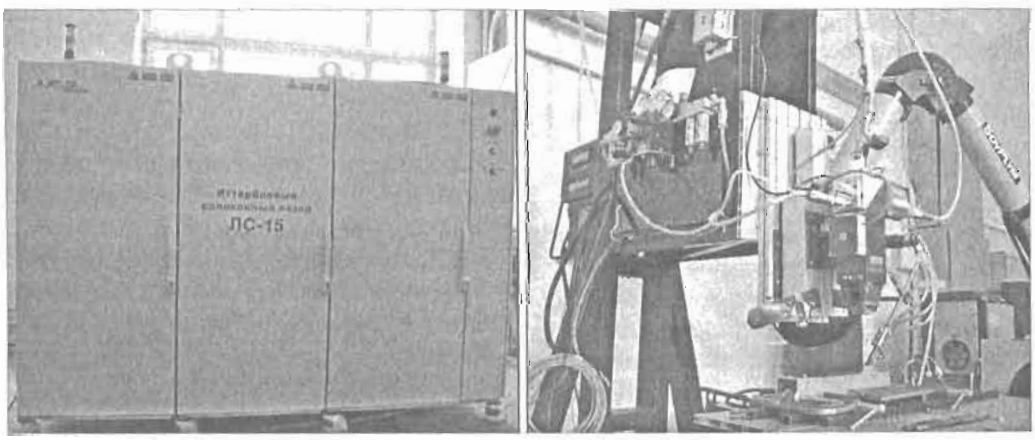


Figure 2. 15 kW fiber laser and experimental facility

shows that despite the higher capital costs on adoption, the efficiency index is significantly higher than that of conventional technologies.

In designing and implementing the new technique and technology in conventional approaches to the subject of managing procedure, determining the economic efficiency consists of at least four main stages. The first stage — determining the necessary expenses for implementing innovative activities, the second stage is the evaluation of the economic impact from the adoption of new techniques and technologies, the third stage consists of the evaluation of the comparative efficacy of the innovation by comparing economic factors, the fourth — identifying the possible sources of funding [3].

Economic efficiency is the ratio of economic effect obtained in the course of a year to the expenses for the adoption of innovation. When comparing the various options for techniques and technology, the general and specific capital investments, the cost price per unit of production and other factors are compared. An option is possible that in the case of innovations, lower expenses may be accompanied not only by inconsistent factors of technical level and quality of innovation, but also by higher specific capital investments. A simple comparison of the technical and economic factors does not help to identify the most rational option. In this case, the adoption and identification of the total comparative efficacy factor based on the comparisons of cost savings on expenses is required. Besides, the identification and taking into account the main risks arising in the transition to the use of new techniques and technologies, especially when considering the latest technologies, is of no small importance. The probabilistic character of adoption results, the amount of operating costs, the need to take into account the timeliness of the transition to new technology, taking into account the competitive position and other qualitative and quantitative factors, significantly complicate the assessment of economic efficiency. This leads to the need for a comprehensive detailed review of possible factors affecting the process of introducing and using new techniques and technologies, as well as a thorough identification of the basic technology and equipment for further comparative analysis.

Calculating the economic impact is carried out in accordance with the methodology for determining the economic efficiency of use in the national economy of the new technology, inventions and rational solutions. Thus, the annual economic impact of the production and use of the new HLAW technology and equipment is defined as follows [4]:

$$E_g = \left[ Z_a \frac{V_n}{V_a} \frac{P_a + E_n}{P_n + E_n} + \frac{(u_a - u_n) - E_n(k_n - k_a)}{P_n + E_n} - Z_n \right] A_n. \quad (1)$$

Here the indices $a$ and $n$ denote the data for the analogue, and the new HLAW technology and equipment respectively; $Z = k + u$ are the expenses on production with the use of analogue and the use of new techniques and technologies; $k$ are the specific capital investments; $u$ are the specific operating costs; $V$ is the productivity or integral factor of quality; $E_n$ is the rate of profitability; $P$ is the deduction on full restoration (renovation) of analogue and new techniques and technologies; $A$ is the annual volume of production.

Economic factors of different welding processes

| Welding method | Cost of welding 1 m of a weld, $ | Time of welding 1 joint, min | Imperfection level, % |
|---|---|---|---|
| Orbital argon-arc welding | 1.32 | 40 | ~ 3–5 |
| Tandem $CO_2$ welding | 0.84 | 20 | ~ 3–5 |
| Resistance welding | 0.84 | 7 | ~ 0.2 |
| Laser-arc welding | 1.25 | 3 | ~ 0.2–0.3 |
| Manual arc welding | 1.53 | 2 h 20 min | ~ 9–15 |

In calculating the annual economic impact of the adoption of new technology as a part of capital investments, all expenses at all the stages of development, adoption and exploitation of new technology are taken into account, namely:

- expenses on scientific research and development activities, *Knr*;
- expenses on acquiring, delivery, mounting (dismantling) of equipment, technical training, adjustment and development of production, *Ktp*;
- expenses on replenishing floating assets of the enterprise with the creation and use of new technology, *Kno*;
- expenses (profit) from the production and implementation of production during the development of production, prior to the current year, *Kosv*.

Then, the total capital investment is calculated using the formula

$$Ksum = Knr + Ktp + Kob + Kosv. \quad (2)$$

In addition to calculating the economic impact of the adoption of new techniques and technologies, the calculation of results from innovation in the form of increased labour productivity, reduction in material and energy consumption, the release of workers, etc. is widely practiced. So, the predicted reduction in the number of staff, $P$, as a result of the adoption of new technology is calculated using the formula

$$P_1 = \frac{Ts_1 N_1}{q_1} - \frac{Ts_t N_t}{q_t}, \quad (3)$$

where $Ts_t$ is the price of a unit of product in $t$-th year, ruble; $q_1$ is the production per worker up to the adoption of new technology; $q_t$ is the production per worker in the $t$-th year; $N_t$ is the production volume in the $t$-th year in physical units.

Besides the important factors of economic efficiency of production and exploitation of innovation, the results of sales volume and business commercial

activity on the implementation of innovations are rather very strong.

Preliminary assessment of the specific operating costs showed that for the conventional technology of welding pipes $u_a \approx 1516.3$ ruble/unit product, and for HLAW technology $u_n \approx 789.3$ ruble/unit product. Significant reduction in operating costs by using the HLAW technology explains the possibility of reducing the number of support staff and, consequently, the payroll. Moreover, the use of HLAW reduces the cost of repairs and consumables, as compared with the use of arc welding technology.

The use of HLAW technology helps to considerably increase the depth of metal penetration, which makes it possible to change the geometry of cutting edges (more than 2 times of decrease in the number of cuts, filled with fillers), and this leads to savings in filler material. At present, the use of arc technology helps in the production of 300 pipes per day, thus $B_a$ = 300 unit product/day. World experience and research results show that the joint effect of the laser and arc (HLAW technology) can improve productivity by more than 7 %, that is $B_n$ = 321 unit product/day.

As already mentioned, when calculating the economic impact in the field of welding technology, it is very important to take into account qualitative factors (strength of the weld, stability of the process, number of defects, level of staff training, environmental compatibility, etc.), taking into account that in monetary terms it is not always possible. For this purpose it is necessary to introduce a complex factor of quality and efficiency $\alpha$. Below is a short list of factors by our assessment, which have the greatest specific weight:

- market demand;
- level of automation;
- manufacturability;
- flexibility of process;
- continuity of processes;
- reliability;
- safety;
- quality of production;
- ergonomics;
- environmental compatibility;
- level of demand;
- timeliness;
- level of accessibility;
- adoption experience;
- competitive positions in the use of technology;
- image factor.

There are a number of risks arising in the adoption and use of the new technologies and equipment, which must be taken into account when evaluating the efficiency of adoption, as the measures taken to minimize them can significantly affect the cost of adopting new technologies and equipment, namely:

- technical risk (non-achievement of planned technical characteristics; qualifications of participants; anticipating the technical level of production and technological capabilities to develop new technology and equipment);
- production risk (equipment failure; violation of the supply chains; exceeding the permissible defect level);
- commercial risk (risk of not making Contracts; mistake in the choice of project objectives; non-achievement of the planned financial factors; change in the terms of payments; violation of the terms of implementation);
- market risk (unanticipated competition; changes in demand; economic crisis).

A comprehensive assessment of the efficiency of the adoption of HLAW technology in the pipe industry in accordance with the given methodology confirmed a high efficiency in comparison with similar welding methods. The estimated cost recovery period is less than 3 years.

The analysis of technical and economic factors and risks of adopting the HLAW technology in the pipe industry, as well as assessment of the socio-economic effects, a detailed analysis of the industry and the factors influencing the efficiency of adopting the technology and equipment help us to talk about the technical requirements and economic feasibility of the adoption of HLAW in firms. The cost of re-equipment for production is paid off by the production quality and reliability of the products. HLAW can provide, in comparison with conventional arc methods, increase in productivity 2–5 times by increasing the welding speed, reduction in the number of passes and decrease in labour costs on support operations.

Compared with domestic and foreign analogues, the range of tasks on the creation of reliable all-in-one bindings is widening. HLAW technology can provide high safety levels and environmental compatibility of welding production processes at low operating costs. High potential capabilities of the laser and arc welding sources, the most manifested in their joint use, as well as the high level of flexibility of the technological process determine long-term preservation of the competitive advantages of this technology.

HLAW technology can be a powerful tool for the modernization of industrial production and a tool for ensuring the competitiveness of domestic goods in domestic and foreign markets. Thus, the introduction of HLAW will enhance productivity and improve working conditions, reduce energy and material consumption, increase flexibility and level of automation of manufacturing processes.

1. Kazakov, V.A. (2008) State and prospects of development of welding production. In: *Proc. of 1st Int. Sci.-Techn. Conf. on Electron Beam Welding Technology and Equipment* (St. Petersburg, May 19–22, 2008).
2. Shalimov, M.P., Panov, V.I. (2006) *Welding yesterday, today, tomorrow*. Ekaterinburg.
3. Safronov, N.A. *Enterprise economy*.
4. Rebrin, Yu.I. (2000) *Fundamentals of economy and production management*.

# ALGORITHM OF LASER WELDING DESIGNING FOR AVERTING THE PORES FORMATION

R.D. SEIDGAZOV
Moscow, Russian Federation

It is shown that verification of melt displacement mechanism, which actual for laser welding, gives the possibility for developing the method of pore formation predicting. This method consists of the determination of welding conditions, which guarantee the minimization of pores of hydrodynamic nature appearance in dependence on welding speed, focusing conditions and metal properties. The verified model gives dependences of pore volume and frequency versus welding speed in a good agreement with experimental data. Algorithm of welding designing has to start with the calculation of value of technological welding speed, which guarantees the absence of pores of hydrodynamic nature.

Three reports at this Conference are presented as a whole cycle of physical investigations, in which the determination of basic hydrodynamic mechanism in deep penetration welding is considered. One report is devoted to verification of hydrodynamic mechanism by systematic analysis of a wide range of experimental data [1]. The proofs of weak intensity of evaporative process in laser welding are represented in this report. The conclusion is drawn that the evaporative hypothesis assuming fusion flow under recoil pressure generated by vapor jet action is not proved by measurements for welding conditions. The thermocapillary model of keyhole formation is proposed in another report, explaining the melt removal from the beam impact zone as being due to tangential thermocapillary forces acting [2]. Estimations of different parameters of the keyhole formation, executed by means of thermocapillary model, correspond to experimental data with high accuracy.

This report, the third of the presented cycle, is devoted to application of the research for preliminary physical designing of welding technology by providing the minimization of latent defects of hydrodynamic nature in a weld. It is known that some of defects of hydrodynamic nature (hamping, undercuts, etc.) may be diagnosed by visual survey that facilitates their elimination procedure. However, if the defects are of latent forming, the process of their elimination is accompanied by high labour and finance consuming with increasing the duration of technology designing. Such defects are pores (voids). They reduce the strength of weld metal, therefore their elimination is important for designing of welding technology for workpieces of responsible appointment. Pores formation associates with hydrodynamic fluctuations inside the keyhole. Researches of these keyhole phenomena are in progress in all technologically developed countries. Many of these technological researches are confidential because of the commercial reasons, and it seems to be the main barrier for progress in physical understanding of the nature of dynamic processes. Because evaporative hypothesis of keyhole formation is not confirmed by experimental data [1] the using of evaporative hypothesis in simulation of hydrodynamic processes in keyhole welding leads not only to wrong prognostications, but also to aberrations in planning of research and in analysis of its results. Such conclusion is deduction of analysis of a number of experimental data.

The model of hydrodynamic processes which has correlation with empirical data has to be used in simulating of keyhole welding including the hydrodynamic fluctuations inside a keyhole.

*Dependence of pores (voids) formation on welding speed*. The dependences of pore volume and their formation frequency in relation of energy input parameters of welding are received in hydrodynamic model. According to these dependences the dynamic fluctuations in keyhole completely disappear at some value of technological speed $v_t$ (Figure 1). The fast growth of the pores volume up to maximum value should be observe with increase of welding speed from $v_w = 0$ up to $v_w = 0.25v_t$. And then with further increasing of welding speed the pores volume should be decrease to zero at the technological speed $v_w = v_t$. This dependence of pores volume on welding speed changes is confirmed by the measurements (see Figure 1). The frequency of pores formation should change somewhat otherwise. It reaches a maximum

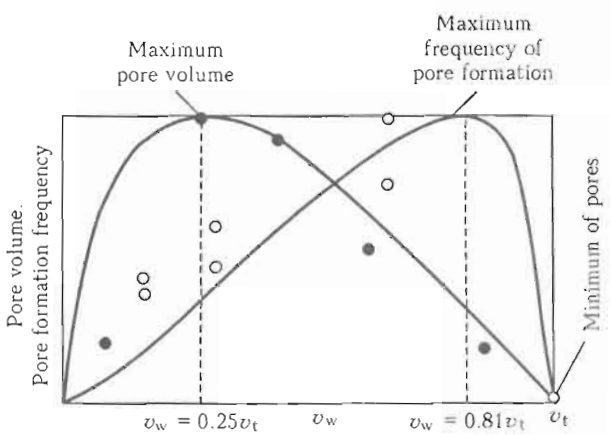


**Figure 1.** Dependence of pore volume (black points) and frequency of their formation (white points) on welding speed (lines – calculations; points – experiments)

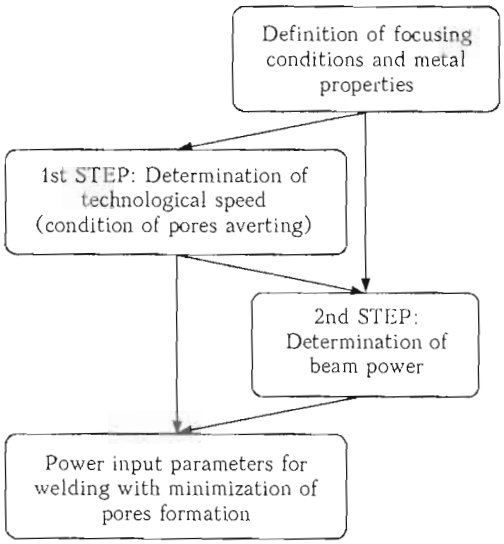


**Figure 2.** Algorithm of preliminary physical express-designing of laser welding technology

at $v_w = 0.81v_t$, and then promptly reduces to zero at $v_w = v_t$. This dependence is also confirmed by the experiment (see Figure 1).

Coincidence of calculated and empirical dependences of volume of pores and also of their formation frequency versus welding speed confirms the hydrodynamic model of keyhole and pores formation. Falling character of both dependences (especially, of frequency) in the range close to technological speed imposes severe constraint on accuracy of definition of its value.

*Algorithm of physical designing of welding technology*. As it follows from the results presented in Figure 1, the welding speed has to be equal to technological speed value to avoid the pores formation completely. In that case, the rigid algorithm of determination of power input parameters for welding could be determined which guarantee the minimum pore formation and even the elimination of these defects. Definition of technological speed using the specified metal properties and conditions of beam focusing is the first step in designing of welding technology. Then, using the received definite decision of the $v_t$ value, the beam power for welding with specified depth should be determined. The complete decision for power input parameters of welding turns out as a result of algorithm performance for specificity of a technological proposition for specified metal with requirements for depth and width of weld. Efficiency of prevention of pores formation by means of offered algorithm depends mainly on accuracy of definition of technological speed, which, in turn, depends on accuracy of definition of all initial parameters. The increasing of method accuracy is the main object of proceeding research.

Welding process includes many various physical phenomena, namely heat conductivity, phase transformation, metallophysical, physicochemical, hydrodynamic, electrodynamic, plasmous, and optical phenomena. It defines the complexity of technology designing, transfers a problem to area of interdisciplinary knowledge where efforts not only technologists, but also physicists and mathematicians are necessary. As a result of interdisciplinary interaction there are three approaches to designing of welding technology, which should be also a three stages for the most effective welding designing:

- preliminary physical designing of welding technology;
- computer modeling by the software for technology designing;
- empirical designing of technology.

The traditional empirical designing is widely used but physical and computer ones are only at the beginning of progress. The maximum reduction of expenses for technology working out is reached by consecutive application of all three approaches to designing of welding technology. The offered algorithm based on predictive definition of technological speed and other parameters of power input in welding should be recommended as the preliminary physical express designing of welding technology (Figure 2).

Application of this algorithm allows sharply reducing the work amount on further stage of empirical designing and the total cost of technology designing. The offered algorithm is formalized for the application in software for designing of laser welding technology as opposed to existing empirical methods of pores reduction which are not capable for such formalization and for application in software, remaining the tool of technological art. The usage of this algorithm in software form reduces a high qualifying barrier for personnel, thus facilitating the spreading of technology.

Besides defects of the hydrodynamic nature there also can be such latent defects of weld metal such as cold and hot cracks. Because the highest resistance of laser-welded joints to cracks formation is obtained at high welding speed, the laser welding with high technological speed is favorable not only for minimization of pores formation, but also for cracks prevention. Therefore, the offered algorithm for preliminary physical express-designing of laser welding technology is of universal technological significance.

1. Seidgazov, R.D. (2009) Verification of the melt displacement mechanism in deep penetration laser welding. In: *Proc. of 4th Int. Conf. on Laser Technologies in Welding and Materials Processing* (26–29 May, 2009, Katsiveli, Ukraine). Kiev: PWI, 62–64.
2. Seidgazov, R.D. (2009) Thermocapillary mechanism of melt displacement during keyhole formation by laser beam. In: *Ibid.*, 59–61.

# THERMOCAPILLARY MECHANISM OF MELT DISPLACEMENT DURING KEYHOLE FORMATION BY LASER BEAM

R.D. SEIDGAZOV
Moscow, Russian Federation

The thermocapillary model of keyhole formation is proposed in this report, explaining the melt removal from the beam impact zone as being due to tangential thermocapillary forces acting. It is shown that estimations of different parameters of the keyhole formation, executed by means of thermocapillary model, correspond to experimental data with high accuracy.

A large amount of empirical data have been accumulated today, but complete understanding of the physical mechanisms involved in formation of the keyhole in deep penetration welding has not been achieved. For example, the hypothesis about the recoil pressure-induced melt displacement is widely used in the simulation of laser welding, despite the existing contradictions with empirical data [1]. It leads to a limitation of the predictive possibilities of simulation.

To resolve these discrepancies, work [2] proposed a hypothesis and theoretical model explaining keyhole formation as being due to tangential thermocapillary forces acting on a non-uniformly heated surface and the melt being removed from the beam impact zone. The Marangony thermocapillary effect is well known and frequently factored in for modelling the vortex flow of fusion during surface fusion of metals by a relatively low intensity laser beam. However, it was noted in [2], a vortex flow with cyclic flow lines is converted into a shear flow with extended flow lines, when $q \approx q_{th}$. Thus, thermocapillary divergent shear flow effectively removes fusion from the beam impact zone and allows a keyhole to be formed.

*Thermocapillary model of keyhole formation.* The flow direction dependence on whether $d\sigma/dT$ is positive or negative. Since the surface tension is always equal to zero at critical temperature and at fusion point $\sigma(T_m) = \sigma_0$, then $d\sigma/dT$ is always negative in a wide temperature interval and tangential thermocapillary stress creates a flow of fusion from the center of beam action to the periphery. The surface force is balanced by the viscous friction with the lower layers. The rotor of velocity will be assigned on the surface

$$\eta \frac{\partial V_x}{\partial y} + \frac{\partial \sigma}{\partial T} \frac{\partial T}{\partial x},$$

where $\eta$ is the dynamic viscosity; $V_x$ is the tangential velocity of flow on the fusion surface; $x$ is the coordinate along the surface of the liquid film; and $y$ is the coordinate perpendicular to the liquid film surface. The motion of viscous fluid is described by the Navier–Stokes equation

$$\frac{\partial V}{\partial t} + (V\nabla)V = -\frac{1}{\rho}\nabla p + \upsilon \nabla V.$$

To find the accurate decision of this equation is very complicate task. Thus for first approximation let us assume that the convective term may be considered small. Therefore the equation is simplified to the linear equation

$$\frac{\partial V}{\partial t} = -\frac{1}{\rho}\nabla p + \upsilon \nabla V.$$

Applying the operation *rot* to both sides of equation and given that $rot\nabla p = 0$ we will obtain

$$\frac{\partial}{\partial t} rotV = \upsilon \Delta rot V.$$

In this form the Navier–Stokes equation is similar to the equation of thermal conductivity. This means that if the characteristic distance of heat propagation in time $t$ is $\sqrt{\chi t}$ (where $\chi$ is the thermal conductivity), the analogous distance of the propagation of viscous forces deep into the melt is $\sqrt{\upsilon t}$. If the thickness of the moving layer of liquid $h$ is small in comparison with beam diameter $d (h << d)$, then after time $t \approx h^2/\upsilon$ the melt displacement will pass into a mode of viscous thermocapillary flow:

$$V_x \cong \frac{1}{\eta}\left|\frac{\partial \sigma}{\partial T}\right| \frac{\partial T}{\partial x} h.$$

Disregarding the convective member in the Navier–Stokes equation means that for metals with Prandtl numbers $Pr = \upsilon/\chi < 1$, nonlinearity (convective heat transfer) in the thermal conductivity equation can also be disregarded. Estimating temperature gradient, it is possible to write approximately

$$V_x \cong \frac{1}{\eta}\left|\frac{\partial \sigma}{\partial T}\right| \frac{qh^2}{\lambda d}. \quad (1)$$

The viscous radial spreading of the thin liquid film from the center to the periphery will lead to a fall in the liquid level on the axis of the beam and a reduction

in thickness of the liquid film, which will in turn cause the motion of the melting front $V_m$ to accelerate. This motion of the melting front simultaneously with a lowering of the molten pool level leads to cavity formation. If we estimate the speed of motion of the melting front deep into the material as $V_m \approx \sqrt{\chi/t}$, then during the viscous spreading of fusion over time interval $t \approx h^2/v$ we may write $V_m \approx \sqrt{\chi v/h}$. According to the condition of flow retention, the rate at which the level of the free surface of the molten pool drops due to viscous thermocapillary spreading can be approximately written as $V_s \approx V_x h/d$. For a steady flow $V_m = V_s$, and then we will obtain

$$\frac{1}{\eta}\left|\frac{\partial\sigma}{\partial T}\right|\frac{qh^3}{\lambda d^2} = \frac{\sqrt{\chi v}}{h}.$$

Hence for evaluating the thickness of the moving layer $h$ we will obtain

$$h = \left[\frac{\lambda\chi^{1/2}\eta^{3/2}d^2}{\rho^{1/2}|\partial\sigma/\partial T|q}\right]^{1/4}. \qquad (2)$$

By substituting (2) into (1), we can obtain quantitative assessments of the flow speed $V_x$. For iron in the intensity range $q$ = 0.5÷3.0 MW/cm$^2$ we will obtain the rate of thermocapillary flow in the interval $V_x \approx$ 3.5÷9.0 m/s and the speed of the motion of the bottom $V_s \approx$ 0.24÷0.38 m/s. The values obtained correspond to the empirical observations $V_x \sim$ 2.0 m/s [3] and $V_s \approx$ 0.12÷0.40 m/s [4].

*Maximum depth of penetration.* We will find for typical laser welding conditions the following characteristic values: $h \sim 10^{-5}$ m, $V_x \sim$ 1÷10 m/s. So, hydrodynamic processes are fairly large Reynolds numbers $\mathrm{Re} = V_x h/v \sim$ 100÷200, when the effect of viscosity can be considered slight. This makes it possible to examine the balance of pressures in the stationary flow of ideal fluid (Bernoulli equation):

$$\frac{\sigma}{r} + \rho g z + \frac{\rho V_x^2}{2} = \text{const}. \qquad (3)$$

For the thermocapillary flow (1) we may write down

$$\frac{\sigma}{r} + \rho g z + \frac{\rho}{2\eta^2}\frac{q^2h^3}{\lambda^2 d^2}\left(\frac{\partial\sigma}{\partial T}\right)^2 = \text{const}. \qquad (4)$$

If we accept the keyhole for a cylinder with radius $R$ and length $L$ and determine boundary conditions for the fusion flow (speed $V_x$ equal to (1) on the bottom of keyhole ($z = 0$) and $V_x = 0$ at the keyhole outlet $z = L$), then we will obtain

$$\frac{\sigma_2(L) - \sigma_1(0)}{R} + \rho g L = \frac{\rho}{2\eta^2}\left(\frac{\partial\sigma}{\partial T}\frac{\partial T}{\partial x}\right)^2 h^2.$$

Let us estimate the value of each term of this equation using empirical data [5]. Armco iron was welded by a 7.2 kW beam. A joint with depth $L$ = = 20 mm and aspect ratio $L/d$ = 8 was obtained, and important measurement was taken of the surface tension of fusion ($\sigma$ = 0.42 J/m$^2$) and pressure inside the keyhole (0.31 kN/m$^2$). So, the hydrostatic pressure was $\rho g L \approx$ 2 kN/m$^2$, the Laplace pressure was $2\sigma/d \approx$ 0.336 kN/m$^2$. The speed of fusion flow reaches $V_x \sim$ 4 m/s [3] but the dynamic pressure — values of $\rho V_x^2/2 \approx$ 64 kN/m$^2$. Thus, the Laplace pressure and pressure inside the keyhole can be disregarded and the pressure balance is determined by the relationship between the hydrostatic and dynamic flow pressures. Given that $\partial T/\partial x \approx qh/\lambda L$ we will obtain

$$L = \left(\frac{1}{2g}\right)^{1/3}\left(\left|\frac{\partial\sigma}{\partial T}\right|\frac{qh^2}{\lambda\eta}\right)^{2/3}. \qquad (5)$$

The estimates of depth $L(P)$ are close to the empirical data [6]. The correlation of the character of dependence (5) and estimates obtained with the results [6] should be seen as confirmation of the principles of the thermocapillary model of keyhole formation in deep penetration welding.

*Threshold of the keyhole formation.* The phenomenon of keyhole formation is accompanied by an increase in penetration depth when the threshold beam intensity $q_{th}$ is reached. For steel $q_{th}$ = 0.5 MW/cm$^2$, and for copper $q_{th}$ = 2 MW/cm$^2$ [7]. When the beam is at sub-threshold intensity, the thermocapillary flow has a vortex flow pattern with the cyclic curves of the flow lines in rotating fluid flow. When the value $q_{th}$ is reached, the structure of thermocapillary flow changes, that is due to the breaking of the flow lines. The flow assumes the character of a shear flow and brings about the more effective removal of fusion from the beam action zone and, therefore, more effective dissipation of the beam power compared with vortex flow.

Let us estimate the value of $q_{th}$ using the ideas of the thermocapillary model of keyhole formation. We will consider that the temperature of the surface of fusion in the centre of the beam spot is close to boiling point $T_b$. The temperature gradient, directed into the depths of the material, can be estimated as $\partial T/\partial x \approx$ $\approx (T_b - T_m)/h$ and the power density as $q_{th} \approx \lambda(T_b - T_m)/h$. If value $h$ is close to (2), we will obtain

$$q_{th} \approx \frac{\lambda(T_b - T_m)^{4/3}}{\eta^{1/2}d^{2/3}}\left(\frac{\partial\sigma}{\partial T}\right)^{1/3}\left(\frac{\rho}{\chi}\right)^{1/6}. \qquad (6)$$

For iron, factoring in a temperature change in properties and the characteristic spot diameter $d \sim$ $\sim (3\div5)\cdot10^{-2}$ cm, we will obtain $q_{th} \approx$ 0.3÷ ÷0.5 MW/cm$^2$, which is close to the empirical data 0.5 MW/cm$^2$ [7]. The threshold of the penetration welding of steel in relation to changes in electron beam diameter and power of the electron beam is empirically determined in [8]. For copper, the calculated interval $q_{th} \approx$ 2.1÷3.0 MW/cm$^2$ is close to the

region of a sharp increase of the penetration depth in copper 1.75÷2.25 MW/cm$^2$ observed in [7].

Correlation of the calculated values (6) with the results of experiment [8] confirms the legitimacy of the underlying principles of the thermocapillary model.

*Intensity interval of thermocapillary keyhole formation.* According to the evaporative model of keyhole formation, at the threshold intensity (for iron $q_{th} \approx 0.5$ MW/cm$^2$) we should expect a perceptible increase in evaporation, which should be manifested by increased mass loss. It has, however, been recorded that at higher intensity $q \approx 3$ MW/cm$^2$ [9]. It is noted that above this intensity the weld quality deteriorates, and the increase in mass losses far beyond the threshold of deep penetration (with $q \approx$ $\approx 3$ MW/cm$^2$) indicates that there is no any casual effect between keyhole phenomenon and evaporation. However, while this position of the region of heightened evaporation appears paradoxical from the point of view of the evaporative hypothesis, it fully conforms with the thermocapillary nature of keyhole formation.

The value of the critical intensity can be obtained from the condition of equality of keyhole growth rates under the action of comparable physical mechanisms of fusion movement. Equating the speed of keyhole growth by thermocapillary melt displacement $V_s \approx$ $\approx V_x h/d$ (where $V_x$ and $h$ are found from (1) and (2)), and the speed of drop in the molten pool level in a splash regime by the vapour recoil pressure [10], we will obtain for iron the value of $q \approx 3$ MW/cm$^2$ [2], which coincides with the intensity of the threshold growth of evaporation [9].

Thus, for iron, the thermocapillary mechanism determines the hydrodynamic processes in the fusion in a beam intensity range of $q \approx 0.5$÷3.0 MW/cm$^2$. Application of the evaporative hypothesis for modelling hydrodynamic processes is possible for a higher intensity $q > 3$ MW/cm$^2$.


1. Seidgazov, R.D. (2009) Verification of the melt displacement mechanism in deep penetration laser welding. In: *Proc. of 4th Int. Conf. on Laser Technologies in Welding and Materials Processing* (May 26–29, 2009, Katsiveli, Ukraine). Kiev: PWI, 62–64.
2. Seidgazov, R.D., Senatorov, Yu.M. (1988) *Kvant. Elektronika*, 15(**3**), 622–624.
3. Grigoriants, A.G. (1989) *Principles of laser treatment of materials*. Moscow: Mashinostroenie.
4. Banishev, A.F., Golubev, V.S., Khramova, O.D. (1993) *Laser Phys.*, 1(**6**), 1198–1202.
5. Verigin, A.M., Erokhin, A.A. et al. (1980) *Fizika i Khimiya Obrab. Materialov*, **2**, 145–146.
6. Banas, C. (1978) High power laser welding. *Optical Eng.*, 17(**3**), 210–216.
7. Garashchuk, V.P., Velichko, O.A., Davydova, V.V. (1971) *Avtomatich. Svarka*, **5**, 31.
8. Pierce, S.W., Burgardt, P., Olson, D.L. (1999) *Welding J.*, Febr., 45–52.
9. Gorny, S.G., Lopota, V.A. et al. (1987) *Zhurnal Tekhnich. Fiziki*, 57(**12**), 2390–2391.
10. Vedenov, A.A., Gladush, G.G. (1985) *Physical processes in laser treatment of materials*. Moscow: Energoatomizdat.

# VERIFICATION OF THE MELT DISPLACEMENT MECHANISM IN DEEP PENETRATION LASER WELDING

R.D. SEIDGAZOV
Moscow, Russian Federation

It is considered that the intensity of evaporation in keyhole welding is slight, the evaporative model of keyhole formation is not confirmed by experiments, and all the empirical data related to keyhole formation have a non-contradictory interpretation under the thermocapillary model of keyhole formation, where the weak process of evaporation can be disregarded.

Accuracy in simulating hydrodynamic processes depends on reliable knowledge about physical mechanism that causes melt removal under a laser beam. However, there are still fundamental problems in understanding this mechanism. Laser-induced melt removal was first reviewed in [1], which put forward the hypothesis of melt displacement by vapor recoil pressure under laser radiation above 10 MW/cm$^2$. Demand for the development of laser technologies spurred the application of this hypothesis for simulating the hydrodynamic processes during laser keyhole welding in the operative intensity range of about 1 MW/cm$^2$ [2]. Since these applications were not substantiated empirically, the evaporative hypothesis was subsequently found to have numerous discrepancies with empirical data in the operative intensity range. To resolve these discrepancies, a thermocapillary hypothesis and model were proposed in [3, 4]. This model explained keyhole formation as melt displacement by tangential thermocapillary forces on its non-uniformly heated surface.

It should be highlighted that the thermocapillary effect is generally considered to be the basic mechanism of melt displacement with a vortex flow structure during the surface melting of metals by low intensity radiation of about 0.1 MW/cm$^2$ [5] or during formation of a weld in the tail section of the weld pool (at a certain distance from the radiation zone) in deep penetration welding [6]. In simulation, the transition to deep penetration mode occurs when the threshold beam intensity $q = q_{th}$ is usually reflected in immediate rejection of the thermocapillary mechanism of melt displacement in favor of another mechanism – its displacement by vapor recoil pressure. When $q < q_{th}$, the simulation of vortex fusion flow is based exclusively on the thermocapillary Marangony effect [5], but when $q \geq q_{th}$, the thermocapillary effect is generally disregarded in favor of recoil-pressure induced melt displacement. The thermocapillary hypothesis, however, proposes a different approach, according to which when $q \geq q_{th}$ the thermocapillary flow changes only in structure, so the active range of the evaporative mechanism should move to a region of higher intensities.



The conflict between the two approaches to simulating hydrodynamic processes in welding can be properly resolved only by experiment. To make a valid choice of hydrodynamic welding model, therefore, a comparative verification must be made of both hypotheses and models based on a systematic analysis of a broad range of empirical data.

*Basic parameters of the evaporative hypothesis.* According to the evaporative model, fusion displacement occurs under the impact of vapor recoil pressure $p = \rho V_2$ (where $\rho$ and $V$ is the vapor density and vapor flux velocity, respectively). If evaporation with a rate of mass loss $m/t$ under the action of a laser beam with focal spot area $S$ causes surface deformation at velocity $V_S$, then we can write down the relationship $V_S \approx m/St\rho_m$ (where $\rho_m$ is the melt density). On the other hand, let us use the condition of mass flux conservation $\rho V = \rho_m V_S$ (where $V_S$ is the rate of liquid level drop due to evaporation, and $\rho$ is the liquid density). The recoil pressure can then be written as

$$p = \rho V^2 = \rho_m V_S V \approx \frac{m}{St} V. \qquad (1)$$

This relationship determines the correlation between the basic evaporation parameters, each of which can be determined experimentally.

The following values were recorded in welding experiments with steel: the rate of mass loss during welding is $m/t \approx 2$–$3$ mg/s [7, 8], and vapor jet velocity during penetration is in the range of 10–30 m/s [9–11]. From relationship (1) we will obtain a recoil pressure in the order of 100–300 N/m$^2$, which corresponds to the experimental measurements [12, 13]. (Indeed, the pressure inside the keyhole during welding of steel by a 7.2 kW electron beam turns out to be 310 N/m$^2$ [12], which corresponds precisely to the measurements of other evaporation parameters and their interdependence according to (1). Pressure inside the keyhole during welding of aluminium alloys by a 1.1–3.85 kW electron beam turns out also to be small: 19–570 N/m$^2$ [13].) This value is paradoxically small compared with the evaporative model prediction of 0.5–1.0 MN/m$^2$. Thus the evaporative

model prediction does not match the empirical data, exceeding the latter by an order of 3 to 4.

In the evaporative model, vapor jet velocity is assumed to be equal to the speed of sound [14, 15]. ($C = \sqrt{\gamma RT/M} \approx 840$ m/s at laser radiation of 2–3 kW and a plasma jet temperature of 3200–3400 K [16].) Here the calculated vapor jet velocity is 1.5–2 times higher than that in empirical data.

According to calculations using the evaporative model, it takes around 30 % of beam power to mechanically maintain the keyhole by vapor recoil pressure [14]. Moreover, during the laser welding of iron by a 2–3 kW beam we should expect the rate of mass loss to be in the order of $m/t = 0.3P/H \approx 100$–150 mg/s (here $H$ is the specific enthalpy of evaporation, J/g). This far exceeds the measurement results (2–3 mg/s). The same conclusions can be drawn when analyzing other experiments. For instance, according to [8, 17], the calculated rate of titanium mass loss is $m/t = 80$ mg/s with power expenditure in the order of 40 % of total beam power, but the measured values also turn out to be 2 orders less (0.7–1.4 mg/s).

It should thus be concluded that all the actual evaporation parameters in relationship (1) are considerably less than those of evaporative model predictions. Despite these huge differences, however, the evaporative model predictions do correspond to (1). A recoil pressure in the order of 0.5–1.0 MN/m$^2$ does indeed correspond to a vapor jet velocity of 840 m/s and mass loss rate of 100–150 mg/s.

The conclusion that pressure inside the keyhole is low was drawn also in [18] after the discovery of shielding gas inside the weld pores during welding with a 25 kW laser beam, which would be impossible if the pressure inside the keyhole was high. Work [19], citing the measurements in [20], also noted low pressure inside the keyhole of about $10^{-3}$ atm.

Thus, the basic evaporation parameters that figure in calculations using the evaporative model differ significantly from the experimental data. This casts doubt on the justification for using the evaporative model to simulate the hydrodynamic processes in laser welding. Just the opposite — the relative weakness of the evaporative process accords with the thermocapillary model [3, 4].

*Deep penetration threshold and intensive evaporation mode.* Laser welding moves into keyhole mode when the threshold radiation intensity is achieved (for steel $q_{th} = 0.5$ MW/cm$^2$ [21]). According to the evaporative hypothesis, the threshold increase in penetration depth and evaporation intensity (rate of mass loss) should occur at the same radiation intensity of $q_{th}$. For steel, therefore, one might expect a surge in mass loss to evaporation when $q_{th} = 0.5$ MW/cm$^2$. However, this surge in mass loss was found at the considerably higher intensity of $q_{vap} = 3$ MW/cm$^2$ [22] (Figure 1). This vast discrepancy between the transition to keyhole mode and the steep increase in evaporation does not blend in with the evaporative

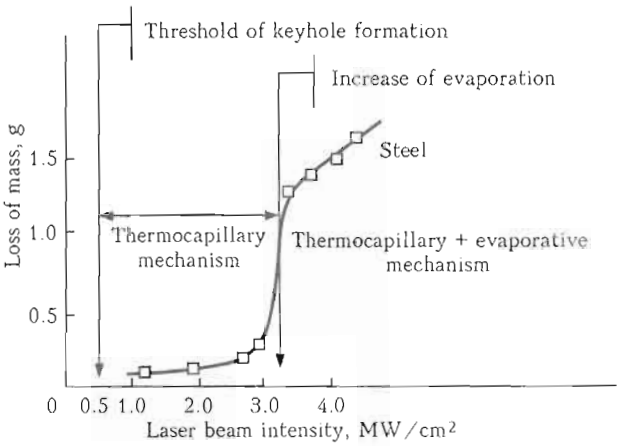


**Figure 1.** Sharp increase in evaporation intensity in steel welding with a 3 MW/cm$^2$ laser beam [22]

hypothesis and indicates the absence of any causal link between the evaporation and the keyhole phenomenon.

We should note that work [3] provides a calculation of the transition boundary of the mechanisms for steel. This figure was obtained based on the condition of equality of melt flow velocities due to both mechanisms action, and corresponds precisely to 3 MW/cm$^2$ [22]. Thus, the range of action of the evaporative mechanism for steel is above $q_{vap} = 3$ MW/cm$^2$. As noted in [22], weld metal quality deteriorates at intensities above $q_{vap} = 3$ MW/cm$^2$ due to melt spatter. This means that the intensity range for quality keyhole welding of steel is $q_{th} < q < q_{vap}$ or $0.5 < q < 3$ MW/cm$^2$, and corresponds to the range of the thermocapillary mechanism. Thus, the measurements [22] should be seen not simply as refuting the evaporative hypothesis regarding welding beam intensity, but as confirming the thermocapillary model of penetration.

*Energy balance in welding.* According to the evaporative model, the calculated power requirement to keep the cavity in a stable state is approximately 30 % of total beam power [14], but measurements of mass loss indicate that only around 0.6 % of beam power is expended on evaporation.

Power absorbed by metal during laser welding is characterized by a net efficiency $\eta_{net} = q/P$ (where $q$ is the effective thermal power absorbed by the workpiece, and $P$ is the laser radiation power). It reaches a value of 0.7 under optimum welding parameters [22]. The net thermal power expenditure on melting is defined as the thermal efficiency $\eta_t = v_w F \rho H_M / q$ (where $v_w$ is the welding speed; $F$ is the cross-sectional area of the penetration zone; and $H_M$ is the specific enthalpy) and reaches $H_M = 0.42$–$0.46$ [23]. Power losses due to thermal conductivity can be accounted for by calculation. In [11] it was proposed that net efficiency and thermal efficiency could be linked by the relationship $\eta_{net} = \eta_T(1 + 2\sqrt{\chi/(d v_w)})$ (where $\chi$ is the thermal diffusivity, and $d$ is the diameter of radiation zone). If the power expenditure on evaporation cannot be disregarded, then we should write $\eta_{net} = \eta_M(1 + 2\sqrt{\chi/(d v_w)}) + m_t H/P$ ( where $H$ is the

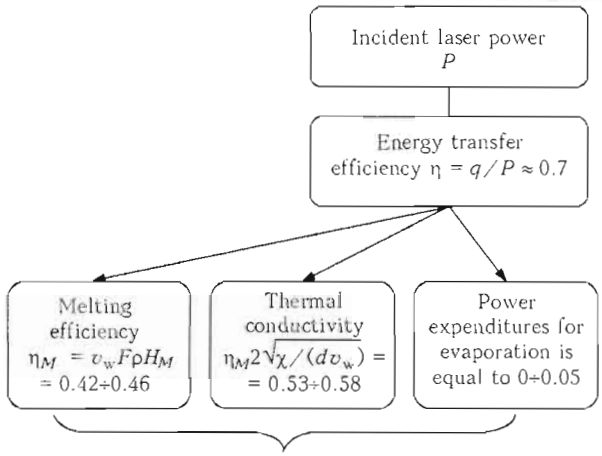


**Figure 2.** Energy balance in laser welding

specific heat of evaporation, and $m_t$ is the rate of mass loss in vapor). This relationship enables us to determine the breakdown of power expenditure on melting, evaporation, and thermal conductivity.

For steel, measurements provide a figure for thermal efficiency of $\eta_T \sim 0.42$–$0.46$ ($\chi = 0.06$ cm$^2$/s, $v_w \approx 2.5$ cm/s, $d \approx 0.06$ cm), and power expenditure on thermal conductivity under these conditions can be calculated as $\eta_T 2\sqrt{\chi/(dv_w)} = 0.53$–$0.58$ (Figure 2). Correspondingly, the sum of the net thermal power expended on melting and thermal conductivity is in the range of 0.95–1 of the power absorbed by the workpiece. Hence, the power expenditure on evaporation cannot be greater than 5 % of the net thermal power or 3.5 % of the incident beam power. Actual power expenditure on evaporation turns out to be far less than the calculated power expenditure on mechanically maintaining the keyhole according to the evaporative model (~30 % [14]). It means that the evaporative model calculations are not confirmed by the actual energy balance. We should note that the actual measured beam expenditure on evaporation (3.5 % of incident beam power) within the range of efficiency measurement error (8–10 %) corresponds to the previously obtained calculation of power expenditure on evaporation using measurements of mass loss rate (~ 0.6 %).

Thus, the energy balance in welding leads to the conclusion that power expenditure on evaporation in laser welding is so small that it conflicts with the evaporative model of penetration, but at the same time accords with the thermocapillary mechanism, which presumes a low power expenditure.

## CONCLUSION

All the above findings mean that the intensity of evaporation in keyhole welding is slight and the evaporative model of keyhole formation is not confirmed by experiments. All the empirical data related to keyhole formation have a non-contradictory interpretation under the thermocapillary model of keyhole formation, where the weak process of evaporation can be disregarded. The range of intensity where the thermocapillary mechanism of fusion transfer is dominant and where the evaporative mechanism can be disregarded lies between the threshold of keyhole formation and the threshold increase in evaporation $q_{th} < q < q_{vap}$ (for steel $0.5 < q < 3.0$ MW/cm$^2$). The evaporative mechanism may become significant at intensities above the intensive evaporation threshold (3 MW/cm$^2$ for steel), but at the same time there is a deterioration in weld quality due to metal spatter.


1. Batanov, V.A., Fedorov, V.B. (1973) *Pisma v Zhurnal Tekhn. Fiziki*, 17(7), 348–351.
2. Andrews, J.G., Atthey, D.R. (1976) *J. Phys. D: Appl. Phys.*, 9(15), 2181–2194.
3. Seidgazov, R.D., Senatorov, Yu.M. (1988) *Kvant. Elektronika*, 15(3), 622–624.
4. Seidgazov, R.D. (2009) Thermocapillary mechanism of melt displacement during keyhole formation by laser beam. In: *Proc. of 4th Int. LTWMP Conf.* (May 26–29, 2009, Katsiveli, Ukraine). Kiev: PWI, 59–61.
5. Anthony, T.R., Cline, H.E. (1977) *J. Appl. Phys.*, 48(9), 3888–3894.
6. Fuhrich, T., Berger, P., Hugel, H. (2001) *J. Laser Appl.*, 13(5), 178–186.
7. Khan, P.A.A., Debroy, T., David, S.A. (1988) *Welding J.*, 67(1), 1–7.
8. Gorny, S.G., Lopota, V.A. et al. (1986) *Avtomatich. Svarka*, 10, 64–65.
9. Vasilchenko, Zh.V. et al. (1994I) *Preprint 694 MAF AN Belarus*.
10. Zaikin, A.E., Levin, A.V., Petrov, A.L. (1995) *Kvant. Elektronika*, 22(2), 145–148.
11. Basov, N.G. et al. (1984) *Izvestiya AN SSSR, Series Physics*, 48(12), 2310–2320.
12. Verigin, A.M., Erochin, A.A. (1980) *Fizika i Khimiya Obrab. Materialov*, 2, 145–146.
13. Bondarev, A.A., Voropaj, N.M. (1974) *Ibid.*, 2, 50–55.
14. Vedenov, A.A., Gladush, G.G. (1985) *Physical processes in laser treatment of materials*. Moscow: Energoatomizdat.
15. Matsunawa, A., Semak, V. (1997) *J. Phys. D: Appl. Phys.*, 30, 798–809.
16. Smirnov, V.S., Tsybulsky, I.A. (1988) *Elektrotekhnika*, 10, 20–22.
17. Gorny, S.G., Lopota, V.A., Smirnov, V.S. (1988) *Avtomatich. Svarka*, 6, 72–73.
18. Grezev, A.N. (2005) *Svarochn. Proizvodstvo*, 5, 20–25.
19. Gatzweiler, W., Maischner, D., Faber, F.J. et al. (1989) In: *Proc. of SPIE*, 1132, 157–165.
20. Myamoto, I., Maruo, H., Arata, Y. (1984) In: *Proc. of ICALEO*, 44, 68.
21. Garashchuk, V.P., Velichko, O.A., Davydova, V.V. (1971) *Avtomatich. Svarka*, 5, 31.
22. Gorny, S.G., Lopota, V.A., Redozubov, V.D. et al. (1987) *Zhurnal Tekhnich. Fiziki*, 57(12), 2390–2391.
23. Grigoriants, A.G. (1989) *Principles of laser treatment of materials*. Moscow: Mashinostrocnie.

# MODELING OF METAL VAPORIZATION AT LASER PROCESSING

I.L. SEMENOV, I.V. KRIVTSUN and V.F. DEMCHENKO
E.O. Paton Electric Welding Institute, NASU, Kyiv, Ukraine

This paper is devoted to the theoretical investigation and mathematical modeling of convective vaporization of metals at laser processing. The most detailed study of the vaporization process can be accomplished on the basis of the Boltzmann kinetic equation which describes evolution of the velocity distribution function of the vapor phase atoms. Since solving this integral-differential equation is a very complicated problem, the model kinetic equation (BGK-model) is used. The BGK equation is simpler than the Boltzmann one, but at the same time retains the kinetic approach main advantages. This equation was solved numerically by a conservative finite-difference method. The characteristics of metal vapor flow inside and outside of the Knudsen layer were calculated for a wide range of the metal surface temperature (above the boiling temperature), covering subsonic and supersonic flow regimes. Comparison of two known models of convective vaporization, proposed by Ch.J. Knight and S.I. Anisimov, with the result obtained was carried out and the bounds of applicability of these models were established. It is shown that the flow pattern, obtained by solving the kinetic equation, can differ from the idealized flow pattern used in the Knight model. In addition, kinetic solution provides detailed information about shock wave and contact discontinuous wave structures. The results of this paper can be used for mathematical modeling of physical processes (heating, melting and convective vaporization of metals) occurring at laser processing, which involves CW lasers as well as pulsed and pulsed-periodic lasers.

Process of convective vaporization exerts essential influence on a thermal state of metal at pulse laser processing. If intensity of laser emission is high enough, the surface of a processed product can heat up to the temperatures exceeding boiling temperature that is accompanied by intensive evaporation of metal. As show estimates [1, 2], loss of heat due to evaporation can be in the order of the energy put in processed metal by laser emission. In addition, a stream of metal vapor, flowing out from a heating spot, qualitatively changes process of interaction of laser emission with metal. At first, metal vapor can absorb emission, shielding the heated up surface. Secondly, vapor can be ionized under effect of emission and, in this case, the absorption of laser emission is governed by characteristics of metal plasma, which essentially depend on vapor flow pattern. Thus, except for definition of heat loss due to evaporation, the research of gas-dynamic flow structure, arising at flowing out of metal vapor in surrounding gas, has also a great sense.

The most detailed description of process of evaporation can be accomplished on the basis of Boltzmann equation or its simplifications. Boltzmann equation describes evolution of the velocity distribution function of the vapor or gas atoms. The statistical approach, based on consideration of distribution function, does not depend on a degree of gas rarefaction unlike classical gas-dynamic approach. The equations of gas dynamics correctly describe behavior of gas only then the condition $l = L$ holds, where $l$ is the average length of particles free path, and $L$ is the characteristic geometrical size of the problem. By virtue of this condition the equations of gas dynamics cannot be used for research of vapor flow characteristics inside Knudsen layer, but also the solution of these equations does not give the information on structure of shock waves and contact discontinuities. Boltzmann equation can be used for research of vapor flow characteristics in all areas and statement of a problem for it does not demand attraction of models of Knudsen layer, such, for example, as the models offered by Anisimov [1] and Knight [2]. At the same time, Boltzmann equation is the complex integral-differential equation which analytical solutions are known only for some simple problems. Generally, for its solution it is necessary to use time-consuming numerical methods. So, recently the approaches, based on the numerical solution of simplified variants of Boltzmann equation, the so-called model kinetic equations, actively develop. Most known of such equations is the BGK equation [3]. In this model equation the integral of collisions is replaced with simplified member, describing a relaxation of distribution function to locally equilibrium Maxwell function. In spite of the fact that BGK equation differs from initial Boltzmann equation, it keeps the basic advantages of the kinetic approach and is successfully applied to study various gas-dynamic flows.

In the present work process of evaporation of metal is analyzed on the basis of the one-dimensional model kinetic BGK equation, which has been written for particles of metal vapor. In case of evaporation in surrounding gas it is necessary to consider two kinetic equations: for particles of metal vapor, and for particles of gas. In the given work for simplicity the model situation, in which metal vapor scatters in an atmosphere consisting of atoms of the same metal, is considered. It allows one kinetic equation instead of two to be considered.

*Statement of the problem and solution method.* Let us consider one-dimensional non-stationary kinetic equation BGK which can be written as follows:

$$\frac{\partial f}{\partial t} + \xi_x \frac{\partial f}{\partial x} = \nu(f_M - f), \qquad (1)$$

where $f(t, x, \xi_x, \xi_y, \xi_z)$ is the velocity distribution function of vapor particles; $f_M$ is the local equilibrium

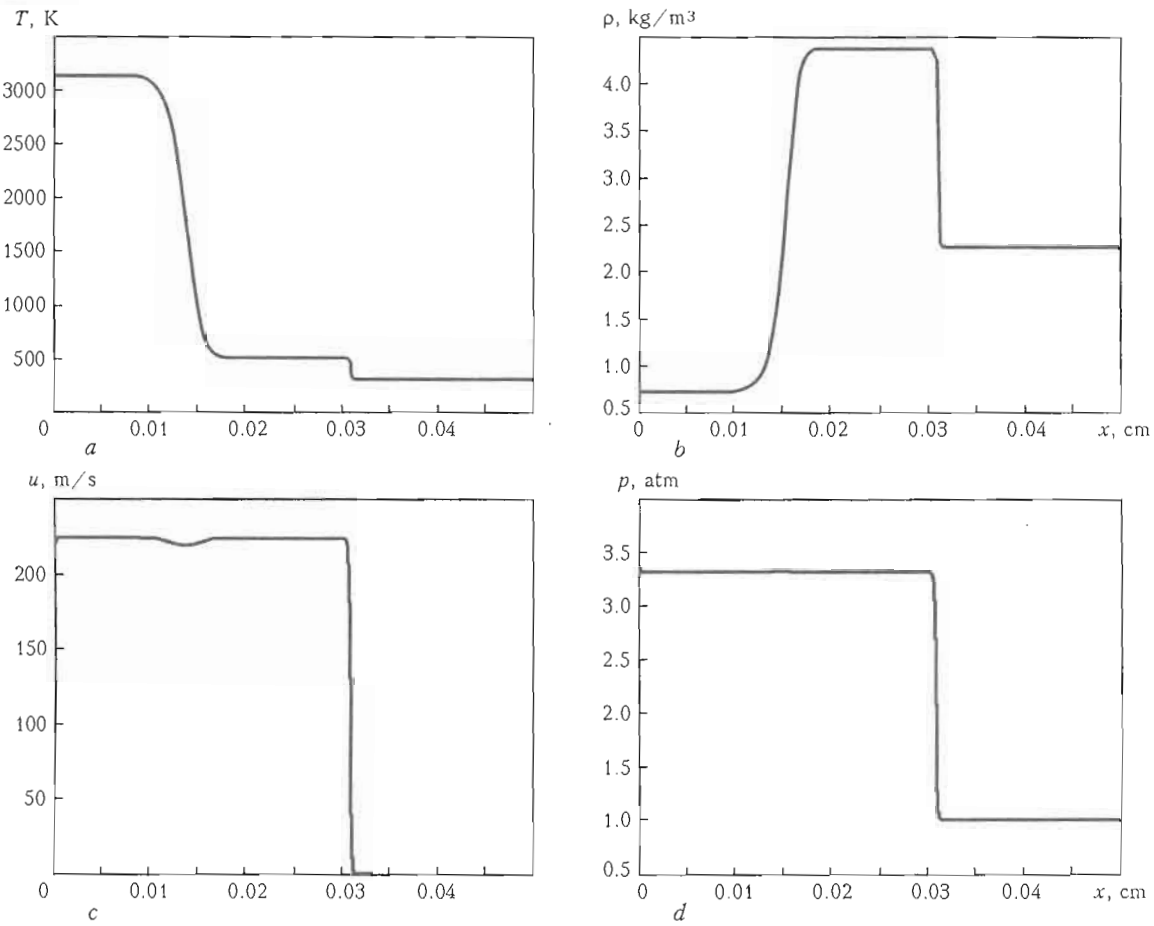


**Figure 1.** Distribution of gas-dynamic parameters along axis $x$ by the moment of time $t = 6.7 \cdot 10^{-7}$ s at $T_s = 3492$ K: $a$ — temperature; $b$ — density; $c$ — velocity; $d$ — pressure

distribution function; and ν is the collision frequency. The axis $x$ is perpendicular to the metal surface and it is directed in the line of vapor flow. Vector $\vec{\xi} = (\xi_x, \xi_y, \xi_z)$ is a velocity vector of vapor particles. If distribution function is known, macroscopic variables of the vapor are defined as follows:

$$n = \int f d\vec{\xi}, \tag{2}$$

$$nu = \int \xi_x f d\vec{\xi}, \tag{3}$$

$$\frac{3kTn}{2} = \frac{1}{2}\int M\xi^2 f d\vec{\xi}, \tag{4}$$

where $n$ is the concentration of vapor particles; $u$ is the macroscopic velocity; $T$ is the vapor temperature; $k$ is the Boltzmann constant; and $M$ is the mass of vapor atom.

Integration in formulas (2)–(4) is conducted on whole velocity space. Equilibrium distribution function has a following appearance:

$$f_M = n\left(\frac{1}{2\pi AT}\right)^{\frac{3}{2}} \exp\left(-\frac{c^2}{2AT}\right), \tag{5}$$

where $A$ is the molar gas-dynamic constant of the vapor; and $\vec{c} = (\vec{\xi} - \vec{u})^2$ is the thermal velocity. Collision frequency in the equation (1) is defined as follows: $\nu = p/\mu$; here $p = nkT$ is the pressure, and μ is the vapor viscosity. For vapor viscosity we shall accept expression which turns out as a first approximation of Chapman–Enskog method:

$$\mu = \frac{5\sqrt{\pi}}{16}\frac{M}{\pi\sigma_{\text{eff}}^2}\sqrt{kT/M}, \tag{6}$$

where $\sigma_{\text{eff}}$ is the effective size of the particle, which depends on the chosen model of interaction potential. For example, in the case hard spheres we have $\sigma_{\text{eff}} = d$, where $d$ is the diameter of a particle. For power potential of interaction $u(r) = \sigma_s/r^s$, where $r$ is the distance between centers of particles; $s$ is the extent of potential; and $\sigma_s$ is the depth of a potential well, the effective size of a particle is expressed as follows:

$$\sigma_{\text{eff}} = \left(\frac{A_2(s+1)\Gamma(4-2/s)}{2}\right)^{1/2}\left(\frac{2kT}{\sigma_s}\right)^{-1/s}. \tag{7}$$

Here $\Gamma(4 - 2/s)$ is the γ-function, and factors $A_2(s + 1)$ are calculated in [4]. Let us notice that at such choice of interaction potential vapor viscosity turns out to proportional temperature: $\mu : T^{\omega}$, where $\omega = 1/2 + 2/s$. In the limit $s \to \infty$ (hard sphere model) we obtain $\mu : \sqrt{T}$.

The equation (1) we shall solve in a dimensionless form. For this purpose we shall pass to dimensionless variables:

$$x' = x/L, \quad n' = n/n_0, \quad T' = T/T_0, \quad \xi' = \xi/c_0,$$
$$u' = u/c_0, \quad f' = f(c_0^3/n_0), \tag{8}$$

where $c_0 = \sqrt{2AT_0}$ is the thermal velocity of the particles in surrounding gas (at infinity); $L$ is the characteristic dimension of the problem; $n_0$ and $T_0$ is the concentration and temperature of vapor particles at infinity, respectively. Further strokes at dimensionless variables we shall omit.

Let us lead also standard procedure of dimension reduction. We shall pass to two new functions, which are expressed through distribution function as follows:

$$f_1 = \int f d\xi_y d\xi_z, \quad f_2 = \int (\xi_y^2 + \xi_z^2) f d\xi_y d\xi_z. \tag{9}$$

Passing to functions $f_1$ and $f_2$ also allows considering problem in spaces $(x, \xi_x)$, that essentially raises efficiency of numerical solution as in this case 3D integrals (2)–(4) become 1D. Such manner, however, demands the solution of two equations for two unknown functions, but it not strongly affects general efficiency of the method.

The equation (1) after dimension reduction and passing to dimensionless variables is written as follows:

$$\begin{aligned} \frac{\partial f_1}{\partial t} + \xi_x \frac{\partial f_1}{\partial x} &= \frac{8}{5\sqrt{\pi}} \frac{1}{\mathrm{Kn}} nT^{1-\omega}(f_1^M - f_1); \\ \frac{\partial f_2}{\partial t} + \xi_x \frac{\partial f_2}{\partial x} &= \frac{8}{5\sqrt{\pi}} \frac{1}{\mathrm{Kn}} nT^{1-\omega}(f_2^M - f_2). \end{aligned} \tag{10}$$

Equilibrium distribution functions in this case are defined as follows:

$$f_1^M = \frac{n}{\sqrt{\pi T}} \exp\left(-\frac{(\xi_x - u_x)^2}{T}\right), \quad f_2^M = T f_1^M. \tag{11}$$

The dimensionless parameter — Knudsen number, entering into the right part of the equation (10), has a form

$$\mathrm{Kn} = l_0 / L, \tag{12}$$

where $l_0 = 1/\sqrt{2} n_0 \pi \sigma_{\mathrm{eff}0}^2$ is the average free path of vapor particles in surrounding gas.

Vapor macroscopic variables are defined through required functions as follows:

$$n = \int f_1 d\xi_x, \tag{13}$$

$$nu = \int \xi_x f_1 d\xi_x, \tag{14}$$

$$T = \frac{2}{3n} \int [(\xi_x - u_x)^2 f_1 + f_2] d\xi_x. \tag{15}$$

It is necessary to note once again that integrals in formulas (13)–(15) integrated only by the variable $\xi_x$, instead of whole velocity space.

Problem for the equations (10) we shall set within interval [0, 1]. Let us assume that evaporating surface coincides with border $x = 0$, and the border $x = 1$ is in surrounding gas. On the border $x = 0$ it is necessary to define distribution function of particles leaving the sur-

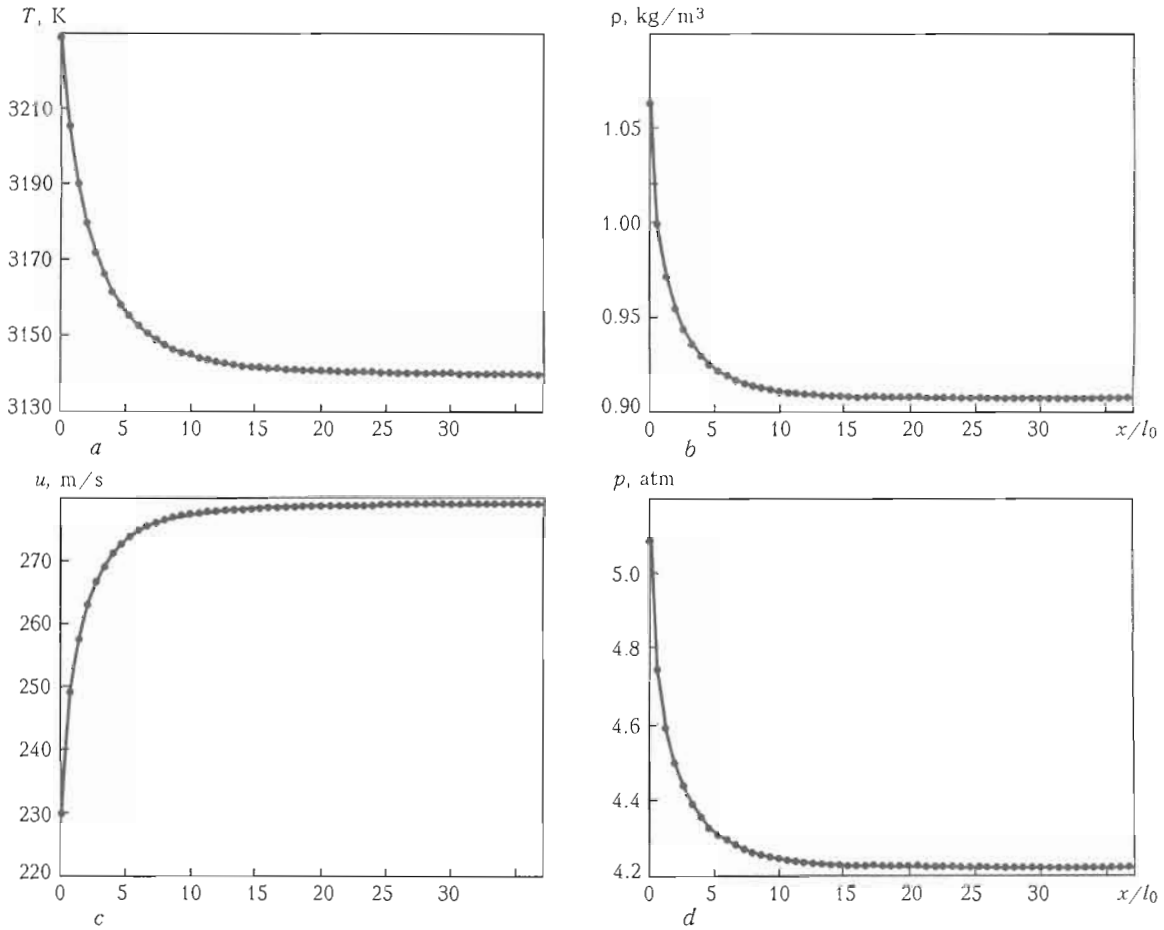


**Figure 2.** Distribution of gas-dynamic parameters inside Knudsen layer by the moment of time $t = 6.7 \cdot 10^{-7}$ s at $T_s = 3492$ K: *a* — temperature; *b* — density; *c* — velocity; *d* — pressure

face. At that, distribution function of particles falling to the surface is obtained from the solution of the problem. Let us assume that all falling particles are condensed on metal surface, and the temperature $T_s$ of the surface has the certain value and does not change in time. Distribution functions of outgoing particles on the border $x = 0$ we shall set in a following form:

$$f_1(x = 0,\ t > 0,\ \xi_x > 0) = \frac{n_s}{\sqrt{\pi T_s}} \exp\left(-\frac{\xi_x^2}{T_s}\right),$$
$$f_2(x = 0,\ t > 0,\ \xi_x > 0) = T_s \frac{n_s}{\sqrt{\pi T_s}} \exp\left(-\frac{\xi_x^2}{T_s}\right). \quad (16)$$

Here $n_s$ is the concentration of saturated vapor at temperature $T_s$. Let us assume that pressure of saturated vapor is defined by means of Clapeyron–Clausius formula

$$p_s = \exp\left\{q\left(1 - \frac{T_b}{T_s}\right)\right\}, \quad (17)$$

where $T_b$ is the metal boiling temperature, and $q = \lambda/RT_s$. Here $\lambda$ is the heat of vaporization per mole, and $R$ is the absolute gas constant. It should be noted that pressure of saturated vapor $p_s$ in the formula (17) is expressed in dimensionless units, i.e. it is divided by pressure in surrounding gas $p_0 = kn_0T_0$. Concentration of particles in saturated vapor is obtained from the state equation of ideal gas which in dimensionless variables looks like

$$n_s = p_s/T_s. \quad (18)$$

On border $x = 1$ it is necessary to define distribution function for the incoming particles. We shall accept that distribution function is equal to equilibrium function in surrounding gas:

$$f_1(x = 1,\ t > 0,\ \xi_x < 0) = \frac{1}{\sqrt{\pi}} \exp(-\xi_x^2),$$
$$f_2(x = 1,\ t > 0,\ \xi_x < 0) = f_1(x = 1,\ t > 0,\ \xi_x < 0). \quad (19)$$

As the initial condition we shall accept equilibrium distribution function

$$f_1(x,\ t = 0,\ \xi_x) = \frac{1}{\sqrt{\pi}} \exp(-\xi_x^2),$$
$$f_2(x,\ t = 0,\ \xi_x) = f_1(x,\ t = 0,\ \xi_x). \quad (20)$$

The equations (10), with initial conditions (20) and boundary conditions (16), (19), are solved numerically with the aid of the method which has been offered in work [5]. The given method is based on splitting of the equations (10) on physical processes on a small time increment. Thus the stage of free molecule transfer and the stage of the relaxation are considered separately. The basic attention at the numerical solution of the equations (10) should be turned on the validity of discrete conservation laws. For this purpose in [5] the

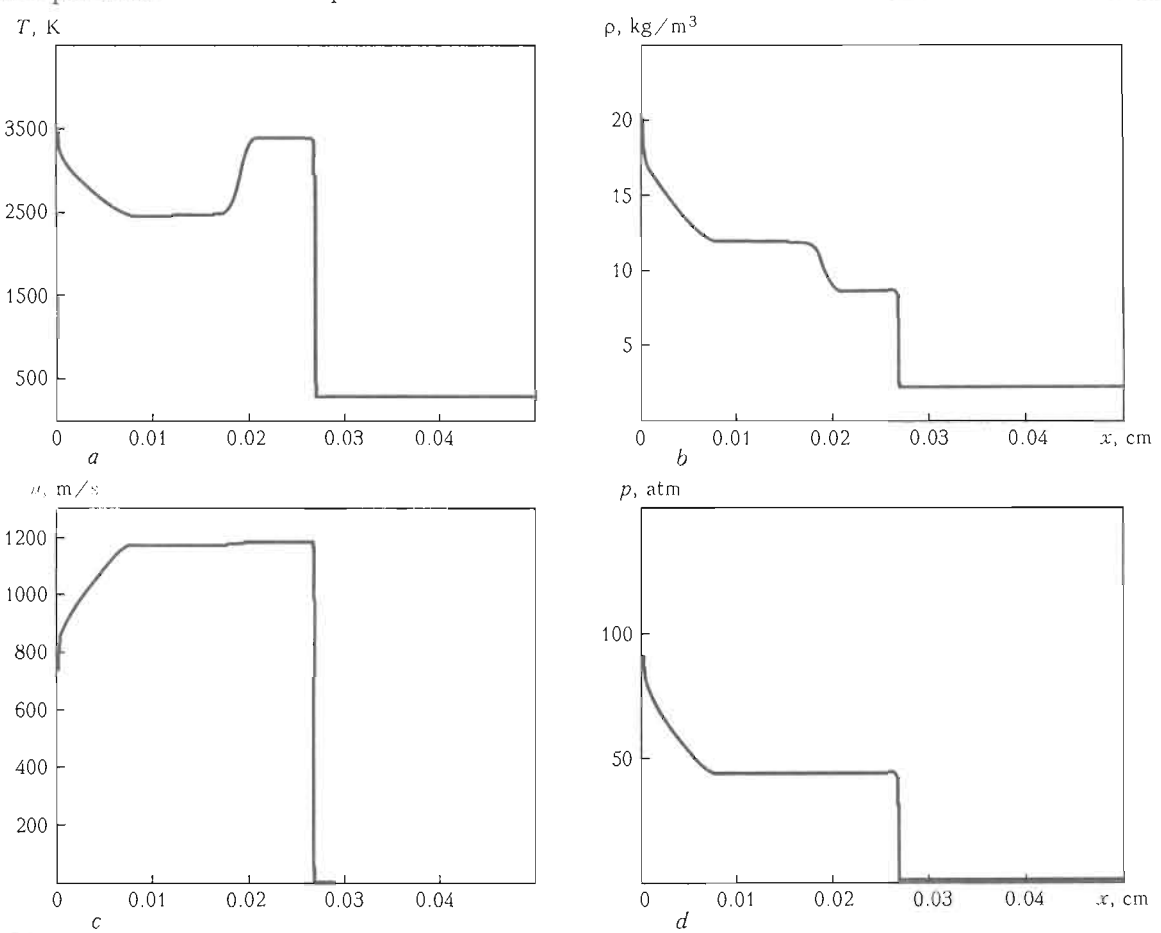


**Figure 3.** Distribution of gas-dynamic parameters along axis $x$ by the moment of time $t = 1.7 \cdot 10^{-7}$ s at $T_s = 4932$ K: *a* — temperature; *b* — density; *c* — velocity; *d* — pressure

technique of Maxwell function correction is offered on each step on time that provides strict performance of discrete conservation laws.

*Results of modeling.* Let us consider results of the numerical solution of BGK equation for iron vapor. The temperature and pressure of surrounding gas were $T_0 = 300$ K and $p_0 = 10^5$ Pa, and concentration of particles $n_0 = \rho_0 N_A/\mu_{Fe} = 2.4 \cdot 10^{25}$, where $A_{Fe} = 148.5$ J(kg·K) is the gas-dynamic constant for iron; $\mu_{Fe} = 0.056$ kg/mol is the iron mole mass; and $N_A$ is the Avogadro's number. At a given value of temperature of surrounding gas thermal velocity of particles is $c_0 = \sqrt{2A_{Fe}T_0} = 298.5$ m/s. The boiling temperature of iron was accepted equal $T_b = 3133$ K, heat of vaporization — $\lambda = 415.7$ kJ/mol. In all calculations for simplicity the hard spheres model was used. The characteristic size of iron atom $d = 0.254$ nm, thus average length of free path $l_0 \approx 1.4 \cdot 10^{-5}$ cm. The characteristic dimension of a problem was accepted equal $L = 1$ cm, then $\mathrm{Kn} \approx 1.5 \cdot 10^{-5}$.

Let us consider in the beginning a flow pattern which appear at rather small overheat of metal surface above boiling temperature. We shall result, for example, dimensional results of calculations for iron at $T_s = 3492$ K. In Figure 1 distributions of temperature, density, velocity and pressure along axis $x$ are presented by the moment of time $t = 6.7 \cdot 10^{-7}$ s.

As follows from the Figure, at a small overheat of a surface above boiling temperature the flow structure with a shock wave and contact discontinuity is established which is characteristic for a subsonic regime of vaporization. In the received solution these areas are not break surface, and have the certain structure. As the length of free path is small enough in comparison with the characteristic dimension of a problem these areas can be considered as a break surface. By virtue of the chosen scale Figure 1 does not display distribution of gas-dynamic parameters inside Knudsen layer which is located directly at an evaporating surface. Therefore in Figure 2 distribution of temperature, density, velocity and pressure is separately shown inside Knudsen layer by the same moment of time. In addition the distance from a surface of metal is specified after dividing by average length of free path. The data presented in this Figure testify that thickness of Knudsen layer in a considered case makes approximately 20–30 lengths of free path.

Let us consider now results of the solution of the kinetic equation at a significant overheat above boiling temperature. In Figure 3 distributions of temperature, density, velocity and pressure along axis $x$ are presented by the moment of time $t = 1.7 \cdot 10^{-7}$ s at $T_s = 4932$ K, and in Figure 4 distributions of gas-dynamic parameters inside Knudsen layer are shown under the same conditions.

The results of calculations, presented in Figure 3, show that at a significant overheat of a surface above boiling temperature the supersonic regime of evaporation is realized. In the given Figure the shock wave, which extends on surrounding gas, a rarefaction wave

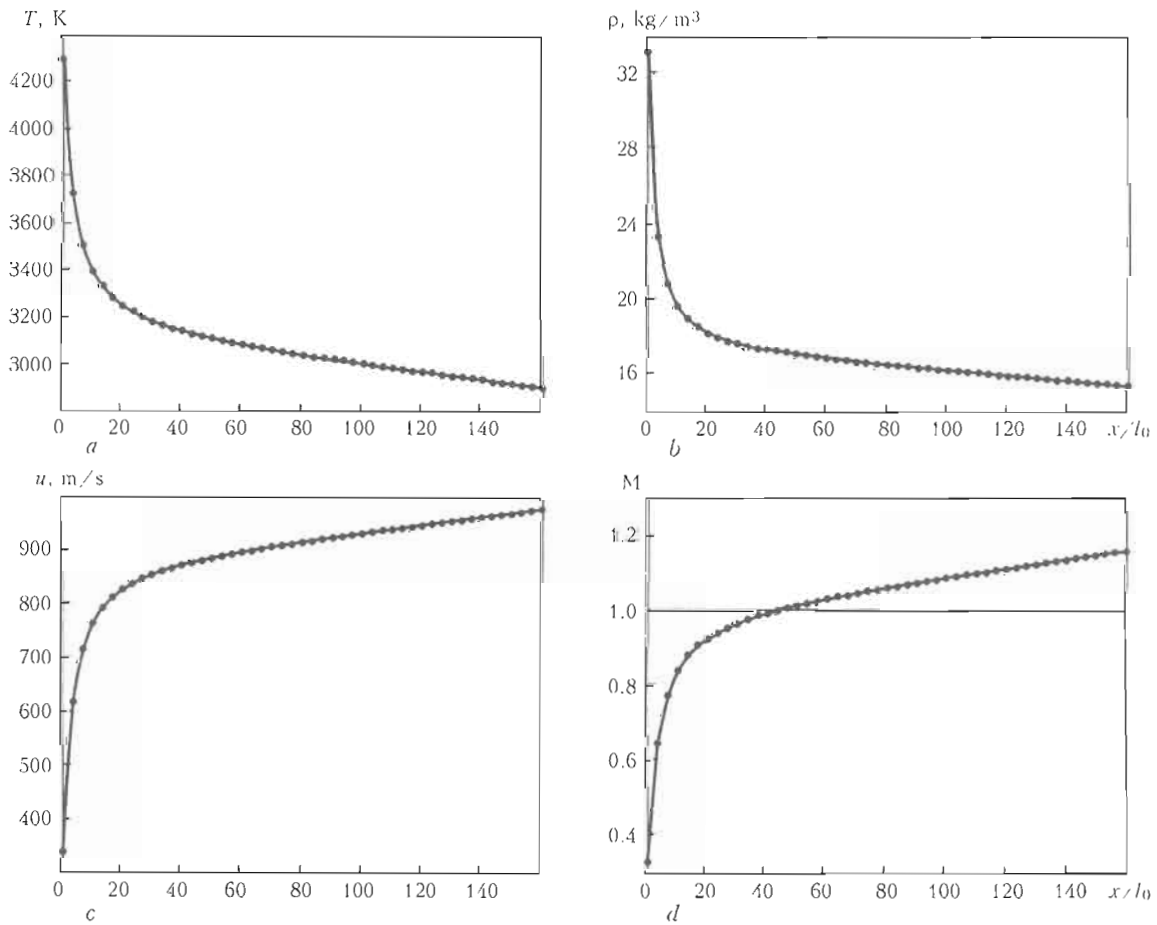


Figure 4. Distribution of gas-dynamic parameters inside Knudsen layer by the moment of time $t = 1.7 \cdot 10^{-7}$ s at $T_s = 4932$ K: *a* — temperature; *b* — density; *c* — velocity; *d* — Mach number

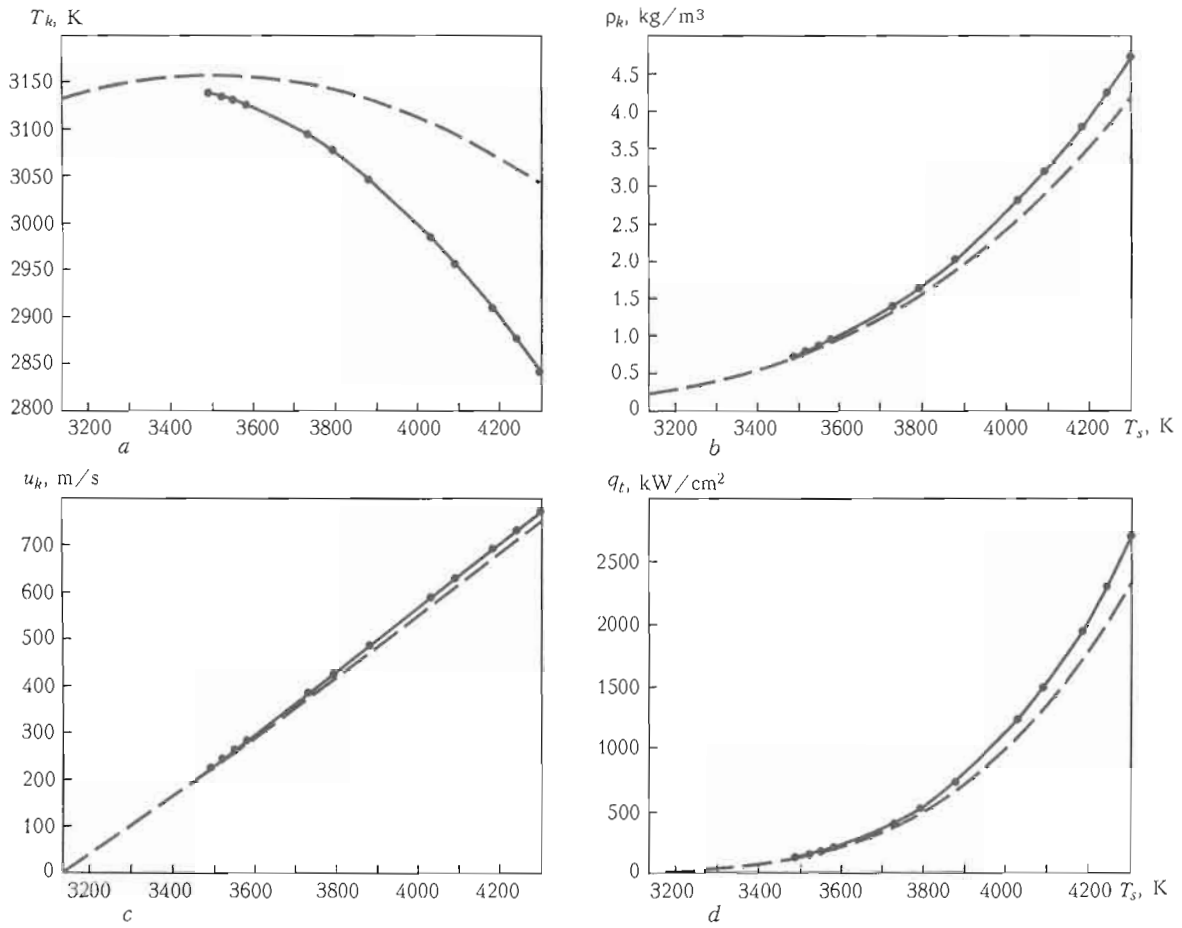


**Figure 5.** Comparison of results of calculation using Knight's model (dashed) and on the basis of kinetic equation (solid curves)

near to the metal surface and area of contact discontinuity are well visible. The data, presented in Figure 4, show that if the supersonic regime of evaporation is realized, then there is a sound point in a stream, i.e. a point in which Mach number equals one. This point also defines border of Knudsen layer, which is followed by rarefaction wave.

It is interesting to compare results of calculations, obtained by means of known Knudsen layer models, with results received by the solution of the kinetic equation. One of the most known models is the Knight's one [2]. In Figure 5 dependences of temperature $T_k$ density $\rho_k$, velocity $u_k$ and thermal loss on evaporation $q_t$ on the border of Knudsen layer on surface temperature in a subsonic regime, calculated on Knight's model and received by the solution of the kinetic equation, are shown. From this Figure follows that Knight's model gives enough greater error at definition of temperature on the border of Knudsen layer. Also there is some error in definition of density on the border of Knudsen layer. The least relative error is shown at definition of velocity, and the greatest (up to 13 %) — at definition of thermal loss.

In supersonic regime velocity on the border of Knudsen layer is equal to local speed of sound, i.e. Mach number equals one. From Knight's model it is received following values for gas-dynamic parameters on the border of Knudsen layer:

$$K_k = 0.669T_s, \quad \rho_k = 0.308\rho_s, \quad u_k = \sqrt{\gamma A_{Fe} T_k}.$$

The solution of the kinetic equation gives

$$T_k = 0.632T_s, \quad \rho_k = 0.368\rho_s.$$

In this case the relative error in definition of temperature makes 6 %, and the relative error in definition of density is 16 %. In summary it is necessary to list also values of parameters on the border of Knudsen layer, received in Anisimov's models [1]: $T_k = 0.6T_s$, $\rho_k = 0.4\rho_s$; $T_k = 0.610T_s$, $\rho_k = 0.381\rho_s$; and $T_k = 0.650T_s$, $\rho_k = 0.312\rho_s$. Here the error in definition of temperature makes 3–5 %, and in definition of density — from 4 up to 9 %.

***Acknowledgments.*** *This work was supported by the National Academy of Sciences of Ukraine and the Russian Foundation for Basic Research.*

1. Anisimov, S.I., Imas, Ya.A., Romanov, G.S. et al. (1970) *Action of high power radiation on metals.* Moscow: Nauka.
2. Knight, Ch.J. (1979) Theoretical modelling of rapid surface vaporization with back pressure. *AIAA J.*, 17(5), 519–523.
3. Bhatnagar, P.L., Gross, E.P., Krook, M. (1954) A model of collision processes in gases. *Physical Rev.*, 94, 511–525.
4. Chapman, C., Kauling, G. (1960) *Mathematical theory of inhomogeneous gases.* Moscow: AN SSSR.
5. Larina, I.N., Rykov, V.A. (2003) Numerical solution of Boltzmann equation by means of symmetric splitting method. *Comp. Mathematics and Math. Physics*, 43(4), 601–613.

# ANALYZING FORMATION OF CAPILLARY IN DEEP PENETRATION LASER WELDING

SEYEDALI ETEZAD, ILNAZ VAHDATINIA and A.A. NIKITIN
Laser Technology and Materials Science Department of the NTUU «Kyiv Polytechnic Institute», Kyiv, Ukraine

Principles of the capillary formation, results of analysis of the existent models and main factors influencing on capillary formation, influence of ultrasonic oscillation on formation and stabilization of the capillary in laser welding with differing polarization, as well as the efficiency of the deep penetration laser welding, are described in this work.

A gel is a solid, jelly-like material that can have properties ranging from soft and weak to hard and tough. Gels are defined as a substantially dilute cross linked system, which exhibits no flow in the steady-state [1]. By weight, gels are mostly liquid, yet they behave like solids due to a 3D cross linked network within the liquid. It is the cross links within the fluid that give a gel its structure (hardness) and contribute to stickiness (tack).

A solid 3D network spans the volume of a liquid medium. This internal network structure may result from physical or chemical bonds, as well as crystallites or other junctions that remain intact within the extending fluid. Virtually any fluid can be used as an extender including water (hydrogels), oil, and air (aerogel). Both by weight and volume, gels are mostly liquid in composition and thus exhibit densities similar to those of their constituent liquids. Jell-O is a common example of a hydrogel and has approximately the density of water.

Cationic polymers are the positively charged polymers. Their positive charges prevent the formation of coiled polymers. This allows them to contribute more to viscosity in their stretched state, because the stretched-out polymer takes up more space than a coiled polymer and this resists the flow of solvent molecules around it. Cationic polymers are the main functional component of hair gel, because the positive charged polymers also bind the negatively charged amino acids on the surface of the keratin molecules in the hair. More complicated polymer formulas exist, e.g. a copolymer of vinylpyrrolidone, methacrylamide, and hydrogel N-vinylimidazole.

There are three types of gels, namely: hydro-, organo- and xerogels. Hydrogel (also called Aquagel) is a network of polymer chains that are water-insoluble, sometimes found as a colloidal gel in which water is the dispersion medium. Hydrogels are highly absorbent (they can contain over 99 % of water) natural or synthetic polymers. Hydrogels also possess a degree of flexibility very similar to natural tissue, due to their significant water content.

Common uses for hydrogels include:

- currently used as scaffolds in tissue engineering. In this case hydrogels may contain human cells in order to repair tissue;
- environmentally sensitive hydrogels, which have the ability to sense changes of pH, temperature, or the concentration of metabolite and release their load as result of such a change;
- as sustained-release delivery systems;
- provide absorption, desloughing and debriding capacities of necrotics and fibrotic tissue;
- hydrogels that are responsive to specific molecules, such as glucose or antigens can be used as biosensors as well as in DDS;
- used in disposable diapers where they «capture» urine, or in sanitary napkins;
- contact lenses (silicone hydrogels, polyacrylamides);
- medical electrodes using hydrogels composed of cross linked polymers (polyethylene oxide, polyAMPS and polyvinylpyrrolidone);
- water gel explosives.

Other, less common, uses include granules for holding soil moisture in arid areas, dressings for healing of burn or other hard-to-heal wounds, reservoirs in topical drug delivery, particularly ionic drugs delivered by iontophoresis (see ion exchange resin).

Common ingredients are e.g. polyvinyl alcohol, sodium polyacrylate, acrylate polymers and copolymers with an abundance of hydrophilic groups.

Natural hydrogel materials are being investigated for tissue engineering, these materials include agarose, methylcellulose, hyaluronan, and other naturally derived polymers.

Many gels display thixotropy — they become fluid when agitated, but re-solidify when resting. In general, gels are apparently solid, jelly-like materials. By replacing the liquid with gas it is possible to prepare aerogels, materials with exceptional properties including very low density, high specific surface areas, and excellent thermal insulation properties.

Sound-induced gelation is described in 2005 in an organopalladium compound that in solution transforms from a transparent liquid to an opaque gel upon application of a short burst (seconds) of ultrasound. Heating to above the gelation temperature $T_{gel}$ takes the gel back to the solution. The compound is a dinuclear palladium complex made from palladium acetate and a N, N'-Bis-salicylidene diamine. Both compounds react to form an anti conformer (gelling) and a syn

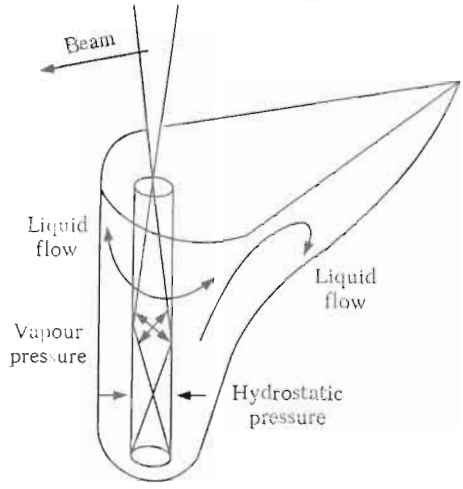


**Figure 1.** Principle of laser beam keyhole welding

conformer (non-gelling) which are separated by column chromatography. In the solution phase the dimer molecules are bent and self-locked by aromatic stacking interactions whereas in the gel phase the conformation is planar with interlocked aggregates. The anti conformer has planar chirality and both enantiomers were separated by chiral column chromatography. The (−) anti conformer has a specific rotation of −375° but is unable to gelate by itself. In the gel phase the dimer molecules form stacks of alternating (+) and (−) components. This process starts at the onset of the sonication and proceeds even without further sonication.

The power density available from an industrial laser beam spans many orders of magnitude, attaining $10^6$ W/mm in a high quality focused beam. However, such a high power density is difficult to control, and keyhole welding is normally carried out with a power density on the order of $10^4$ W·mm$^{-2}$. The surface of the material vaporizes at the point of interaction. The recoil force of vaporization from the liquid surface causes a surface depression, which develops into a deeply penetrating vapor cavity by multiple internal reflection of the beam (Figure 1). The diameter of the keyhole is approximately equal to the beam diameter.

Energy is absorbed by the material through two mechanisms, which determine the overall energy transfer efficiency. Inverse bremsstrahlung absorption (transfer of energy from photons to electrons) takes place in the partially ionized plasma formed in and above the keyhole, and it is the dominant mechanism at low welding speed. At high speeds Fresnel absorption by multiple reflections at the walk of the keyhole dominates, and it is dependent on the polarization of the beam. Plasma (ionized vapor) and plume (vapor-

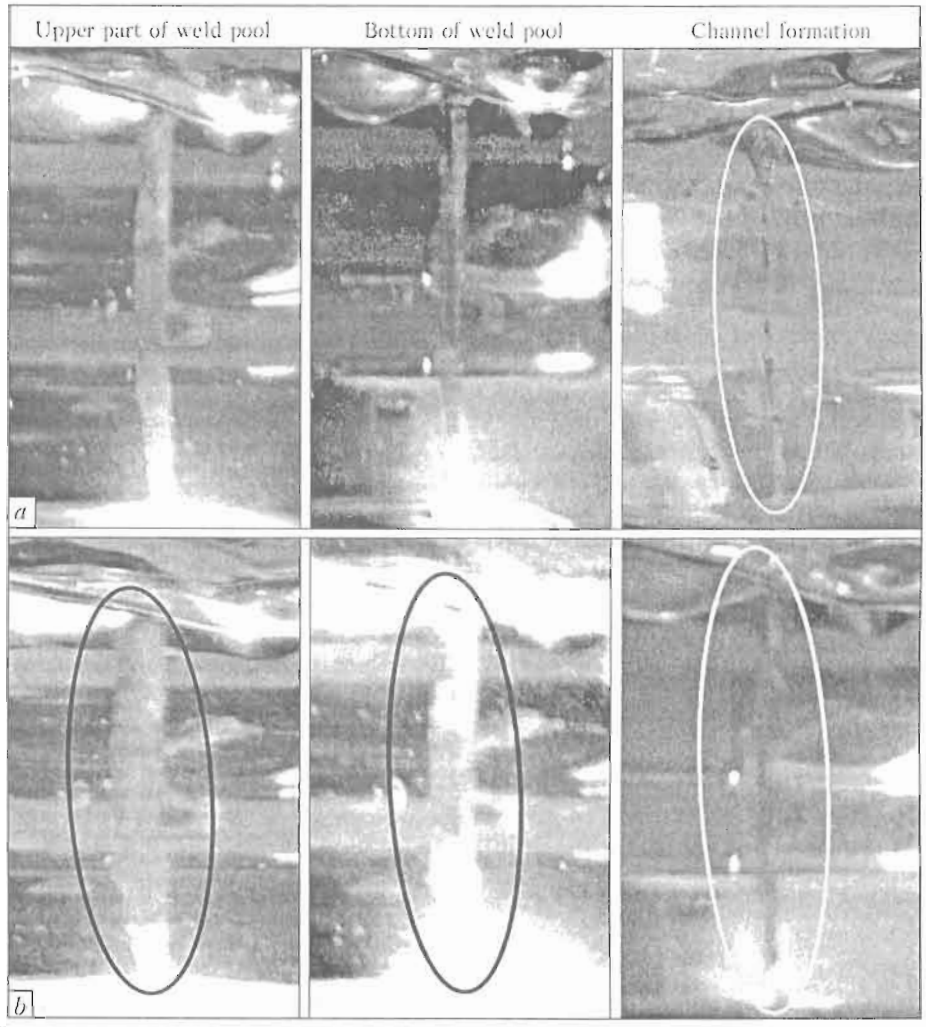


**Figure 2.** Hydrogel workpieces welded using $CO_2$-laser at pulse pumped power 0.5 (*a*) and 1.0 (*b*) kW and $\tau$ = 0.5 s

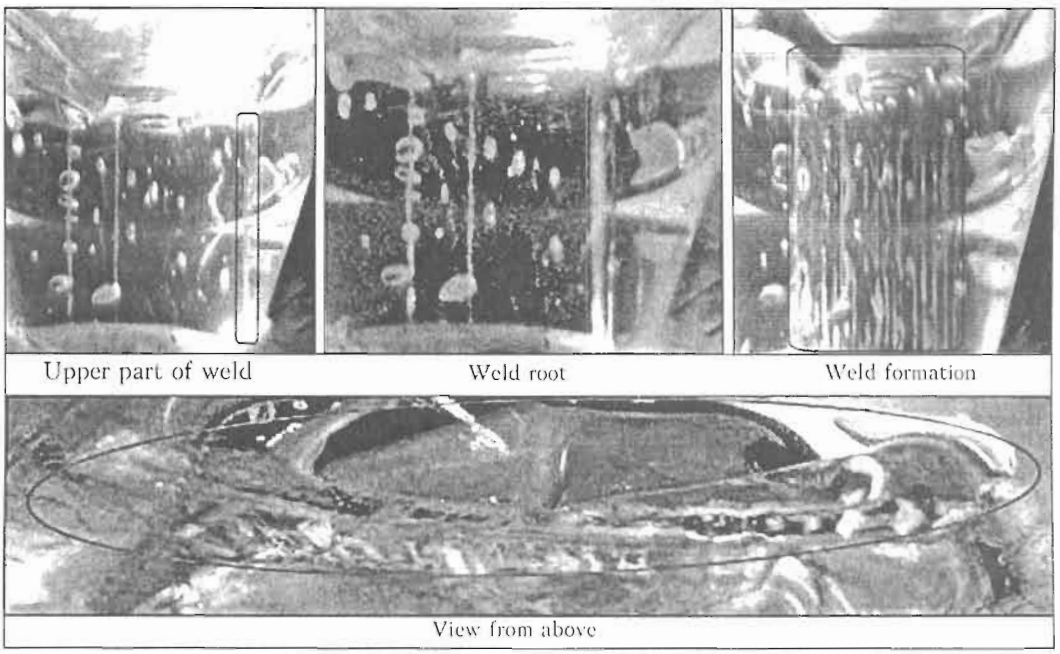


**Figure 3.** Hydrogel workpieces welded using $CO_2$-laser at $P$ = 1 kW and $v_w$ = 100 m/min

ized material) facilitate energy transfer from the beam to the material, but they also defocus the laser beam, reducing its power density.

The vapor cavity is surrounded by molten material. The cavity is maintained through equilibrium between opening forces arising from material ablation and plasma formation, and forces caused by the surface tension and hydrostatic pressure of the molten pool, which act to close it. As the beam and material move relative to one another, material is progressively melted at the leading edge of the molten pool and flows around the deep penetration cavity to the rear of the pool where it solidifies in a characteristic chevron pattern. The requirement to maintain this balance leads to practical minimum and maximum traverse rates for keyhole welding — excessive speed causes the keyhole to collapse, whereas insufficient speed results in a wide weld bead that sags. The shape and size of the keyhole fluctuate during welding. The molten pool temperature is considerably higher than that in conventional arc welding. Heat is conducted into the surrounding material to produce a narrow HAZ. When the laser beam is turned off, several processes occur, namely: the plasma inside the keyhole is extinguished; vaporization pressure decays; and the keyhole collapses through the effects of surface tension and gravity.

Keyhole-welded joint exhibit two distinct regions: fusion zone, and HAZ. Within the HAZ sub-regions can be identified, extent of which depends on the material composition and the peak temperature attained during welding. Each region has a specific composition, microstructure and set of properties.

In the fusion zone, material is melted and solidified rapidly. Grains grow epitaxially with the adjacent HAZ grains in a columnar morphology. Equiaxed grains may also be formed in the centre of the weld bead. The grain morphology depends on the welding speed: a high speed results in abrupt changes in grain orientation, causing parallel elongated grains to form along the weld centerline that are susceptible to solidification cracking. The weld bead microstructure and properties are essentially those of rapidly cooled cast material. Depending on the nature of the alloy and the composition of the weld metal, it might be possible to regain the properties of the base material through postweld heat treatment. The partially melted zone is defined as the region in which a peak temperature between the liquidus and solidus was attained during welding. Localized melting occurs, accompanied by segregation on grain boundaries. A microstructure is produced that is unable to withstand the compression stresses generated when the weld metal solidifies, rendering it susceptible to solidification cracking.

Figures 2 and 3 illustrate experimental examples.

## CONCLUSIONS

1. In modeling the shape of channel for deep penetration laser welding, a natural material was developed for the X-ray photography and for a close calculation of the mathematical model.

2. The material model was based on hydrogels, that provides formation of deep penetration channel in a transparent material.

3. The technological laser Latus provides formation of the deep penetration channels with different depth and width, with pulse radiation and with a continuous generation of radiation length of the weld and surface roughness.

1. Ion, J.C. (2005) *Laser processing of engineering materials*, 396–340.

# SUPPRESSING THE NEGATIVE EFFECT OF PLASMA IN DEEP PENETRATION LASER WELDING

SEYEDALI ETEZAD, ILNAZ VAHDATINIA and A.A. NIKITIN
Laser Technology and Materials Science Department of the NTUU «Kyiv Polytechnic Institute», Kyiv, Ukraine

Study on suppressing the negative effect of plasma on the welded joint quality by accelerating voltage between the electrodes was carried out. A detailed analysis of plasma formation identifies advantages and disadvantages of method for eliminate the negative influence of plasma. Some particular experimental results of plasma interaction with electric field in the working zone (between lens and workpiece) are discussed.

The feature of welding using powerful concentrated source of energy known as «dagger» melting, which is characterized by considerable depth at a small width of the joint. Since the beginning of channel formation, plasma appears above the workpiece surface, which consists of products of evaporation and releases particles of condensed vapor.

Under certain conditions, the plasma reduces the intensity of laser beam radiation because of the interaction between the beam and plasma in the near-surface plasma and the plasma cavity. Known methods for declining the negative effect of plasma are reducing pressure (vacuum), or applying additional stream of gas flowing directly to the zone of molten metal. The shortcomings of these methods consist in the facts that the first one needs to build a vacuum chamber for welding, and in the second one increasing the gas pressure by applying additional stream of gas will increase production costs.

In the research, the behavior of plasma [1] during the laser welding of metals with different values of laser power, welding speed, thickness of metal to be welded and the cost of shielding gas were studied. Results of study suggested use of short-focal length lenses, increasing speed of welding, flow rate of shielding gas or blowing of plasma torch by special stream of additional gas which reduces the energy parameters of plasma to help effectively clarified plasma and the dagger melting

In laser-arc welding the general effect of co-operation is too high. In the interaction zone between arc and laser, electrical power is supplied to the zone, when the arc is located on the laser heating area. Thus the electrical energy is effectively ionized material into the depth of melting channel.

The method of laser welding with deep penetration melting channel is offered, where the DC electric field between the electrodes (the lens body and metal being welded) creates a voltage in the zone of the plasma torch, that has a negative affection on the laser radiation passage. The mechanism of reducing the negative effect of plasma on the weld quality is because of the interaction between positively and negatively charged particles of the plasma, and condensed, dispersed, electrolyte particles with the electric field.

Electrical particles get movements depending on the voltage level of electric field in the cloud of neutral plasma torch. For welding steel 10 mm thicker it is necessary to raise the intensity of laser radiation, which leads to an increase in concentration of electrons in the plasma, its distribution in the direction towards the beam and increase in temperature. It causes an increase in absorption of laser radiation in plasma and an increase in the beam angle due to the refraction. At the same time, the temperature of the plasma above the cavity at a distance of 10 mm arrives to $(11–15)\cdot10^3$ K. The reflection or transparency rates depend on the thickness of torch. Electron density $n_e$ is distributed at the height of the plasma in the peripheral zones, and their maximum value is $3\cdot10^{16}$ cm$^{-3}$ [2].

Temperature of the plasma in the axial welding zones arrives approximately to $14\cdot10^3$ K, and to $7.5\cdot10^3$ K in the peripheral zone, such temperature is observed in the distance of about 10 mm from a welding cavity. In plasma there always are such electrons and ions, which under the influence of the electric field power gain velocity of about $6\cdot10^6$ m/s with the accelerating voltage $U$ ~ 100 V. The region, which joins to the cathode and anode, is an interval on which the current is passed. Such control over the conditions of the plasma front towards the laser beam using adjustable voltage DC power supply enables to move the plasma front.

Thus, an appropriate selection of electric field can decrease the influence of plasma on efficiency of melting metal during welding. The DC source makes it possible to change the polarity of electrodes connection, which in turn changes the direction of current. At the anode, ionization is almost absent and there is no positive ions, that is why electrons, formed in the cavity of weld pool, attracted to the anode, sharply increased speed of their movement and, arriving to anode, stopped and neutralized. While stopping all electrons, provided acquire kinetic energy because of anode voltage drop. The sharp decrease in the number of electrons in the cavity axis, as well as in peripheral areas, leads to transparency of plasma in the cavity channel. At the same time decreasing density in the

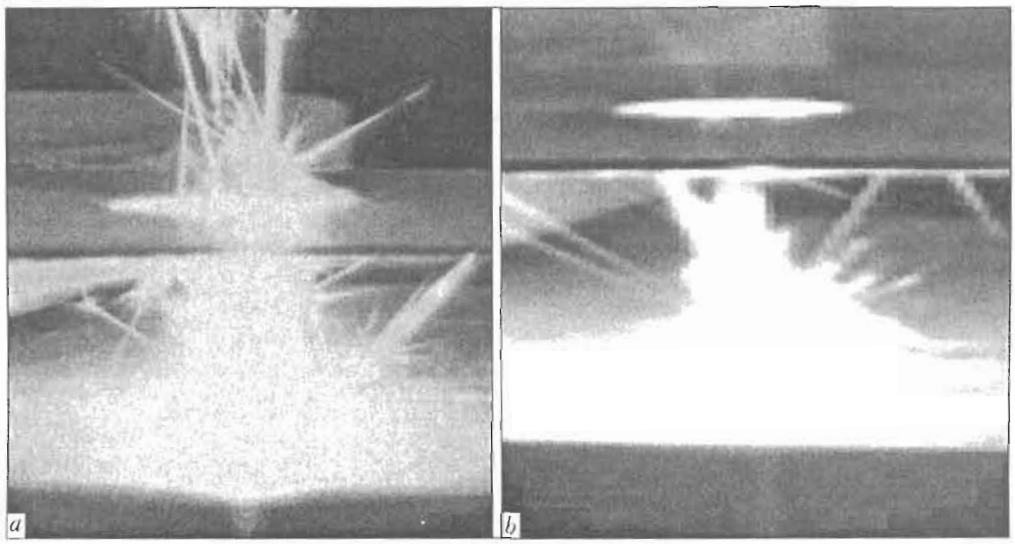

**Figure 1.** Test results obtained without (*a*) and with (*b*) electric field of 200 V

plasma cavity results in focusing of rays on the axis of cavity.

Reducing terms of distribution of plasma front in the direction of laser radiation, using an electric field of a direct current, provides reduction the energy values in the surface plasma and the plasma cavity, and contributes to the effective plasma transparency and dagger form of melting.

Study on the effect of electrical voltage field on the plasma torch was carried out on an experimental setup, Figures 1 and 2 test results obtained are illustrated.

## CONCLUSIONS

1. In laser welding in shielding gases, two types of plasma, namely surface plasma and plasma cavity, are formed.

2. In the near-surface plasma, refraction of laser radiation occurs when running subsonic radiation waves and photodetonation waves.

3. Reducing energy character in surface plasma promotes effective plasma transparency and plasma dagger melting.

4. While thickness of metal to be welded increases, it is necessary to increase the power of laser radiation and voltage magnitude of electric field.

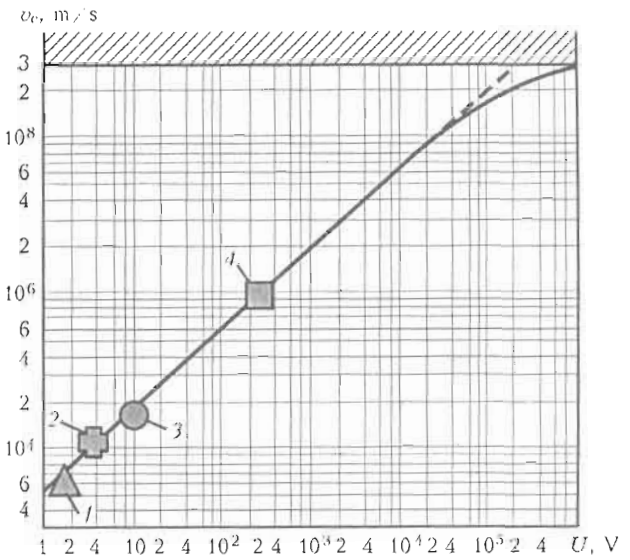


**Figure 2.** Velocity of electrons in the plasma torch before and after action of electric field in different modes: *1* — photo burning; *2* — subsonic radiation waves; *3* — photodetonation waves; *4* — treatment with tension electrical technical field of 220 V

1. Grezev, A.N. (2005) Plasma formation in laser welding with deep penetration. In: *Transact. of IPLIT of RAS on Modern Laser-Information and Laser Technologies*. Ed. by V.Ya. Panchenko, V.S. Golubev. Moscow: Interkontakt Nauka, 228, 235.

2. Grigoriants, A.G., Moryashchev, S.F., From, V.A. (1980) Effect of gas atmosphere chemistry on effective penetration in laser welding. *Izvestiya Vuzov. Mashinostroenie*, 5, 109–112.

# LASER METHOD FOR GENERATION OF MICRO- AND NANO-PARTICLES AND THEIR SELECTION IN GAS FLOW

C. SIPAVICIUS[1], K. MAZEIKA[1], P. VAITIEKUNAS[2] and J. PADGURSKAS[3]
[1]Institute of Physics, Vilnius, Lithuania
[2]Vilnius Gediminas Technical University, Vilnius, Lithuania
[3]Lithuanian University of Agriculture, Kaunas, Lithuania

Laser cutting is a relatively simple and easily controlled method for material processing and is applied here for the generation of micro- and nanoparticles which can later be separated according their size in the flow of technological gas by using a filter system. The generation of particles is discussed in the article when a steel strip of thickness of 0.2–0.6 mm is cut by pulsed Nd:YAG laser. The evaluation of changes in the chemical composition and size of the generated particles collected in the filter system is accomplished. Gas flow in the tube of smooth surface of the diameter of 30 mm is modeled when the distance between the generation and collection sites is 0.5, 1.0 and 3.0 m. The analysis of Moessbauer spectra is presented which show full or partial oxidation of particles being collected in different cascades of filters.

Micro- and nanoparticles of magnetic materials are used to produce magnetorheological and ferrofluids, as well as other suspensions. There are many methods to produce nanoparticles. The application of laser which can be applied for processing material (cutting, boring), to form 3D structures and for ablation is one of such methods. It was shown that the structure and chemical composition of materials depend on conditions of processing and laser beam parameters [1].

Although to cut or to destroy material by laser is an easy way to generate the particles but such a process is not well studied and definitely controlled. The generated particles are of different size ranging from hundreds of microns to nanometers. Therefore to separate nanosized particles, the filter system is required. When an inert gas flow is used it is possible to obtain the particles of same composition as the bulk material. In the air or oxygen flow the particles are fully or partially oxidized. The particles obtained on the base of iron magnetically interact and may be used to produce magnetorheological or ferrofluids depending on their size. In our study the laser cutting of steel was used for generation of micro- and nanoparticles which were separated according to their size in the cascades of filters.

**Experimental methods.** Optimal laser cutting regime of the strips of stainless steel 7C27Mo2 (SANDVIK) and steel 45 of thickness of 0.2–0.6 mm was used to generate the particles. The LIT-100M laser was applied. The Nd:YAG laser of about 300 W power operates in pulsed regime. The duration of pulse, frequency of which is (150±3) Hz, is (2.0±0.6) ms. For the manipulation of laser beam and its transmitting to cutting zone, the principle of flying zone is applied [2]. The cutting scheme is presented in Figure 1. In the experiments the average power of 100–150 W was used. Average cutting velocity was 100 cm/min. The air flow was directed to cutting zone by the conical nozzle, diameter of opening of which is $d$ = 0.8–1.2 mm. The pressure of gas before the nozzle was 0.35–0.60 MPa.

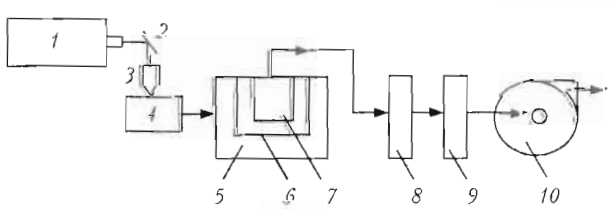


**Figure 1.** Block scheme of equipment applied for laser cutting and selection of particles: *1* – laser; *2* – mirror; *3* – objective; *4* – chamber; *5* – cyclone equipment; *6* – buffer filter (first cascade); *7* – synthetic filter (second cascade); *8* – AFA filter (third cascade); *9* – super fine synthetic filter (fourth cascade); *10* – pump

Moessbauer spectra were measured in the transmission mode at room temperature using $^{57}$Co(Rh) source. To find relative contributions of different iron compounds ($\alpha$-Fe(Cr), $Fe_3O_4$) or superparamagnetic particles, corresponding subspectra were fitted to the experimental spectra.

**Results and discussion.** Selection of particles in the process of laser cutting of thin (0.2–0.6 mm) steel strip of is also shown in Figure 1. The laser beam melts the surface of steel. The liquid metal from cutting slit is removed by effective gas flow formed by the nozzle. When optimal cutting regime is chosen, the melt is almost fully removed from the cutting slit [3]. It is found that up to 40 % of particles deposit in the cutting chamber, and the large (>10 μm) particles deposit first. The smaller and lighter particles fly further and reach the cyclone chamber. The whirl in the cyclone and the buffer filter keep 20 % of particles. In second cascade the air flow is filtered using synthetic filter, which keep the particles of the size of 0.5–0.8 μm. The particles smaller than 0.3 μm are kept by synthetic AFA filter in third cascade. The last fourth cascade consists of synthetic membrane filter. This cascade kept about 10 % of generated particles, the large part of which can be of nanometer size.

The dynamic of gas flow is essential for laser cutting. Therefore, the characteristics (velocity, pressure) of gas flow in the opening of nozzle, between the nozzle and the surface of destroyed material, and on the other side of slit were studied [4]. The optimal

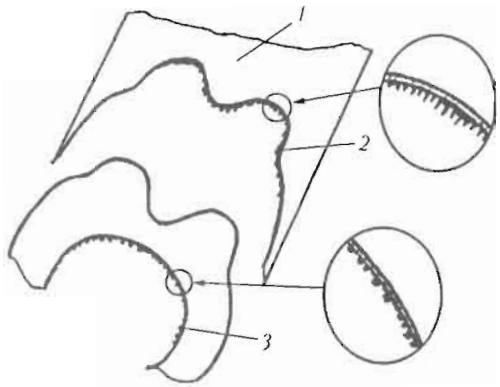


**Figure 2.** Scheme of erosion products deposited on the lower edge of the cut: *1* — stainless steel strip; *2* — icicle-like erosion products with prevailing superparamagnetic and magnetic FeCr phase in their composition; *3* — bubble-shape erosion products with prevailing magnetic $Fe_3O_4$ and $(FeCr)_3O_4$ phases

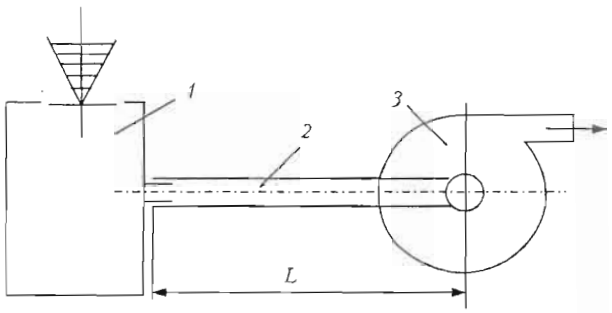


**Figure 3.** Scheme applied for simulations of characteristics of gas flow: *1* — chamber; *2* — tube; *3* — pump; *L* — length of tube

cutting regime is achieved when only minimal amount of erosion products remains on the cutting edge (Figure 2). The optimal regime is obtained at the gas pressure of 3.5–6.0 bar and sufficient power of laser beam. The erosion products were studied. It was found that at larger distances the particles are smaller and more oxidized [5].

In this study the air flow in the tube of diameter of 30 mm is studied when the distance from cutting place and the particle collection place was 0.5, 1.0 and 3.0 m. The scheme used for simulation is shown in Figure 3. The results of simulation in the case of 3.0 m length tube when the inlet velocity was 80 m/s is presented in Figure 4. The finite volume method was used for numerical solving of 2D differential equations which can be in the common form **[6]**:

$$\frac{\partial}{\partial t}(c\Phi) + \text{div}\,(c\mathbf{V}\Phi - \Gamma_\Phi \,\text{grad}\,\Phi) = S_\Phi,$$

where $t$ is the time, s; $\Phi = 1$ is the dependent variable; **V** is the velocity vector, m/s; $\Gamma$ is the variable $\Phi$ exchange coefficient; and $S_\Phi$ is the source term for variable $\Phi$.

Moessbauer studies showed (Figure 5) changes in composition of material collected in different filter cascades. In the first cascade, the material usually contains large amount of initial material (Fe, Fe(Cr)). As in the following cascades the degree of oxidation increases, material is mainly composed of magnetite. In the Moessbauer spectra of material collected in the fourth cascade last, the superparamagnetic contribution of nanosized particles (<10 nm) is evident.

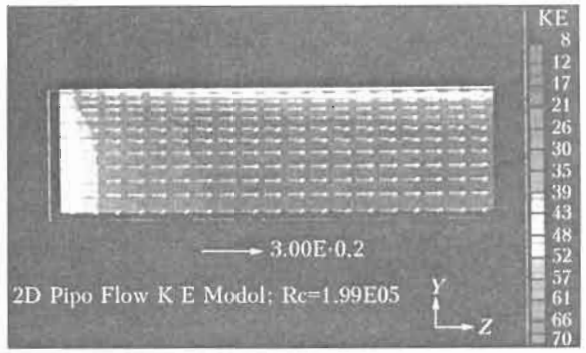


**Figure 4.** Velocity vectors and contours of the kinetic energy of turbulence in the tube inlet at tube length of 3 m, diameter of 0.03 m and section length of 0–0.5 m, inlet velocity of 80 m/s and velocity vectors scale of 300 m/s

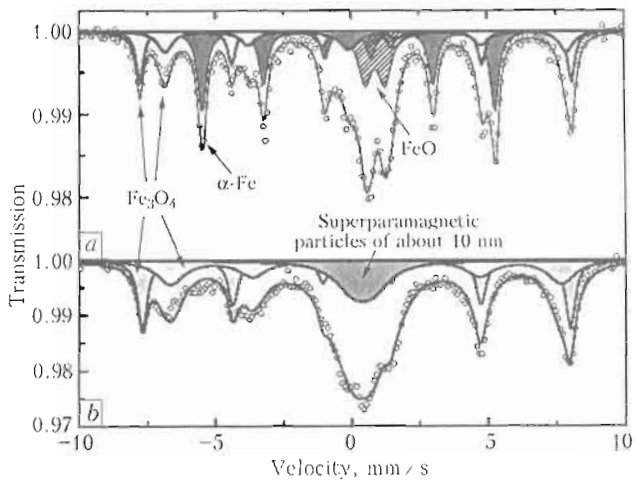


**Figure 5.** Moessbauer spectra of material generated by laser cutting and collected in the first (*a*) and fourth (*b*) cascade

## CONCLUSION

The generation of micro- and nanoparticles using laser cutting of steel strips 0.2–0.6 mm thick and the separation of particles according their size was studied. At optimal cutting conditions (laser power, gas pressure before the nozzle), the cutting quality is good when a small amount of fully oxidised erosion products on the edge of cutting slit is obtained. The study showed that the cascade filter system can be used to separate the particles up to nanometers dimensions, and the simulation of gas flow can be used for obtaining optimal conditions to collect generated particles of required dimensions.

1. Amulevichius, A., Daugvila, A., Davidonis, R. et al. (1998) Chemical compositions of nanostructured erosion products produced upon laser cutting of steel. *Physics of Metals and Metallography*, 85(1), 84–89.
2. Sipavicius, C. (2000) Universal laser machine: Investigation and application. *Aviation*, 5, 45–51.
3. Golubev, V.S. (2004) *Melt removal mechanisms at the gas-assisted laser cutting of materials:* E-print 3. Shatura: RAN.
4. Sipavichius, Ch., Amulevichius, A., Mazheika, K. (2009) Optimization of the quality of laser cutting and power consumption. In: *Proc. of ICONO/LAT Conf.* (Minsk, Belarus, May 28–June 1, 2007) (to be publ.).
5. Amulevichius, A., Daugvila, A., Davidonis, R. et al. (1998) Determination of optimal regime of laser cutting by composition of erosion products. In: *Proc. of SPIE*, 3688, 196–200.
6. Sipavichius, Ch., Shlezhas, R., Vaitekunas, P. (1998) Investigation of gas stream outflow from conical nozzles in process of laser cutting. *Ibid.*, 144–151.

# DEVELOPMENT OF INDUSTRIAL EQUIPMENT FOR LASER HYBRID WELDING OF PIPE STEELS

G. TURICHIN[1], I. TZIBULSKY[1], A. KUZNETSOV[1], O. GRININ[1], Ya. PEVZNER[1] and A. LOPOTA[2]
[1]Institute of Laser and Welding Technology, St. Petersburg, Russian Federation
[2]Laser Technology Center, St. Petersburg, Russian Federation

The article devoted to description of design of automatic laser-arc installation for hybrid welding of thick metal parts. Division of the equipment on to subsystems and their interaction are discussed as well as technological usage of the developed machine.

Idea to use together laser radiation and electric arc for welding and other processing of metals, so that both of heat sources influence a product within the limits of one heating zone, was born in the end of 1970s [1–4]. There were offered some ways of welding, cutting, drillings and treatment of a surface, at which a laser beam is directed onto a processable target, and simultaneously an arc between the electrode and the target is excited in the zone of thermal influence of laser radiation. Until recently powerful $CO_2$-lasers were applied as a laser source, they generated radiation with wavelength of 10.6 μm. Interaction of radiation of this wavelength with metals is accompanied by beginning of the optical discharge in the affected zone that influences essentially the focused beam parameters and part of the absorbed energy in the target and plasma in the interaction zone. Interaction of the 1.06 μm wavelength laser radiation with the target is essentially different. However, powerful laser plants with such wavelength had poor radiation quality and small reliability. Only recently technological solid-state lasers with continuous radiation power of 10–30 kW were developed, they possess high beam quality and high reliability. Such lasers are ytterbium fiber lasers. Solid-state lasers compete directly with earlier developed and well proved high power $CO_2$-lasers.

Now in Russia there are problems of modernization and the further development of key industries such as aircraft building, shipbuilding, and pipeline transport.

The main disadvantages of laser welding are high requirements on assembling plate edges for welding and impossibility of obtaining of demanded mechanical properties of welds and heat-affected zone. The specified disadvantages are eliminated by means of combined laser-arc influence on metal.

Advantages of laser-arc welding in comparison with laser welding are as follows:

- greater tolerance in relation to accuracy of assembling;
- opportunity of filling of cutting for one pass;
- higher efficiency;
- maintenance of steel weldability due to additional alloying by means of an electrode wire.

Results of the works stated in the report are executed within the frames of the project carried out with the purpose of development of a pre-production model of the laser-arc technological complex (LATC) and technology of welding plate providing getting strength properties of the welded zone as for the basic metal.

*Basic technical features of the LATC.* Source of laser radiation is the powerful fiber laser providing melting of steel plates 12 mm thick with an arc source by one pass with a speed of up to 3 m/min; laser source power is not less than 15 kW; beam diameter in focus is 0.3 mm; welding current is not less than 500 A; diameter of the electrode wire is in range of 1–2 mm.

The functional scheme of the complex and its overview are shown in Figures 1 and 2 accordingly.

*Fiber laser LS-15* (Figure 3) is manufactured by SPA IRE-POLUS on the basis of the ytterbium fiber laser with fiber cable completed with chiller Riedel PC250 *2* (see Figure 2).

*Arc equipment complex* includes serial power supply, wire-drive unit and welding torches. In the LATC there are applied VDU-506dk and PDGO-511 manufactured by ITS.

*Laser-arc module* (working tool) *4* (see Figure 2) is intended for work in technological complexes for hybrid laser-arc welding metals of high thickness. It consists of manipulator *14*, laser welding head *13*, arc welding torch *15*, sensor *18* of the welded joint monitoring subsystem, and sensor *19* of the weld monitoring subsystem. Gas shielding of the weld is provided.

Control and stabilization of position of the hybrid laser-arc module relative to the joint is fulfilled by drives system. It operates the executing devices of the manipulator *14*, such as keep of position of the focus point of the laser head relative to surfaces being welded (vertical moving) and to the joint (cross moving).

Acting devices are made based on linear moving modules (actuators) of ISEL, namely LES3 *20* (vertical moving) and LES5 *21* (cross moving), in which

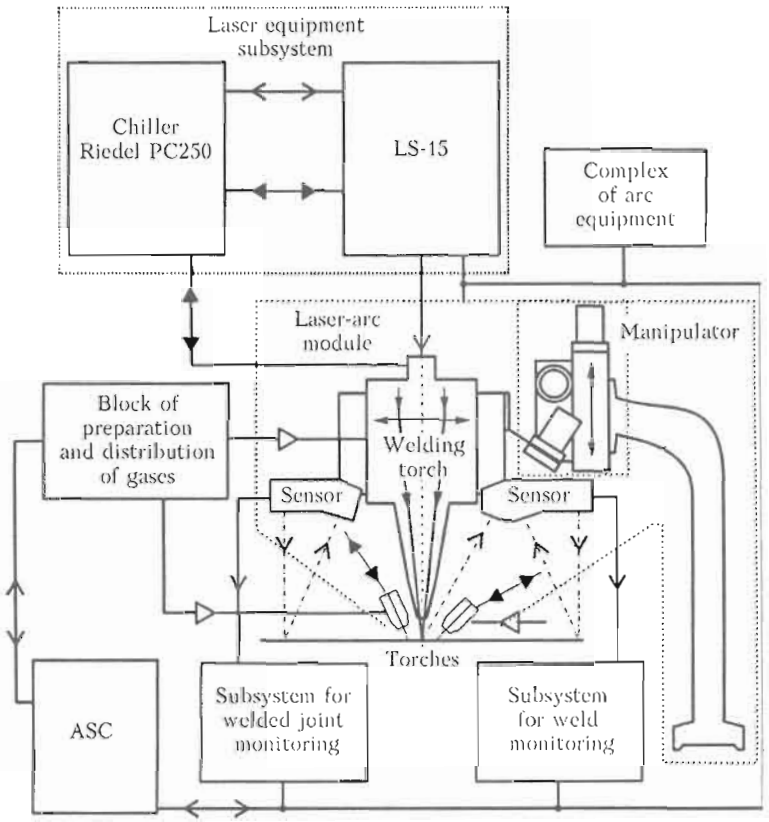


**Figure 1.** LATC functional scheme

step motors M160 *22* are used as sources of movement, line bearings are used as guide ways, and ball-screw pairs are used as movement transfer devices. Accuracy of keep of the focus point position of the laser head in relative to welded surfaces in the vertical direction is ±0.2 mm, and to the joint in the cross-section direction is ±0.5 mm

The Precitec laser welding head *13* incorporates a scanning device to mix the melt in the weld pool. The arc welding torch *15* provides preliminary heating of edges, filling of the gap, feeding of filler material into the welding zone. The torch is set as controlling position relative the focus point of laser radiation along the axis. A model of the hybrid welding head is shown in Figure 4.

Sensors of the welded joint monitoring subsystem *4* (see Figure 2) and the weld monitoring subsystem *5* are the triangulation laser sensors.

*Block of preparation and distribution of gases* provides cleaning and feeding of working and shielding gases with demanded parameters into the laser welding head *13* and arc torch *15*. The block consists of fine *1* and hyperfine *2* cleaning filters; pressure *3* and gas consumption *5* controllers; pressure indicator sensors; pneumatic throttle valves *6*; electromagnetic pneumatic valves *7*; mixers *8*; control module *9*; power suppliers *10* and *11* (Figure 5).

The gas feed system is assembled into five gas lines (channels), namely: 1st channel – for feed of cleaning compressed gas into the air shutter of the laser welding head *13* (see Figure 2) (500 l/min); 2nd channel – of $CO_2$ through the mixer for forming the working gas mixture for the arc torch *15* (1–30 × × 2 l/min); 3rd and 4th channels – of argon through the mixer for forming the working gas mixture for the arc torch *15* (1–30 l/min); 5th channel – of argon into protective nozzle of the laser welding head *13* (1–30 l/min).

In developing, the block there is applied pneumatic equipment of FESTO and flow regulators of the Russian developer and manufacturer ELTOCHPRIBOR. Fine cleaning filters are used in the block, that provides a hysteresis of the chosen pressure regulators of not more than 0.02 MPa and regulation error of the gas flow for the used regulators PPG-12 of not more than 3 %. It provides stability of the flow and composition of the gas mixtures going into the laser welding head and arc torches, and it is not worse than 10 %.

*Welded joint monitoring system, welds monitoring system and automatic control system.* The control system of the laser-arc complex is realized as a hardware-software complex (HSC). This is a distributed computing operating system, which manages all components of the welding complex and consists of the welded joint monitoring subsystem, welds monitoring subsystem and ACS.

The HSC carries out:

- reading of a joint profile of sheets being welded accurate of not worse than 0,5 mm;
- control of the joint geometrical characteristics;
- tracking coordinates of the joint at welding speed of up to 6 m/min with the following parameters:

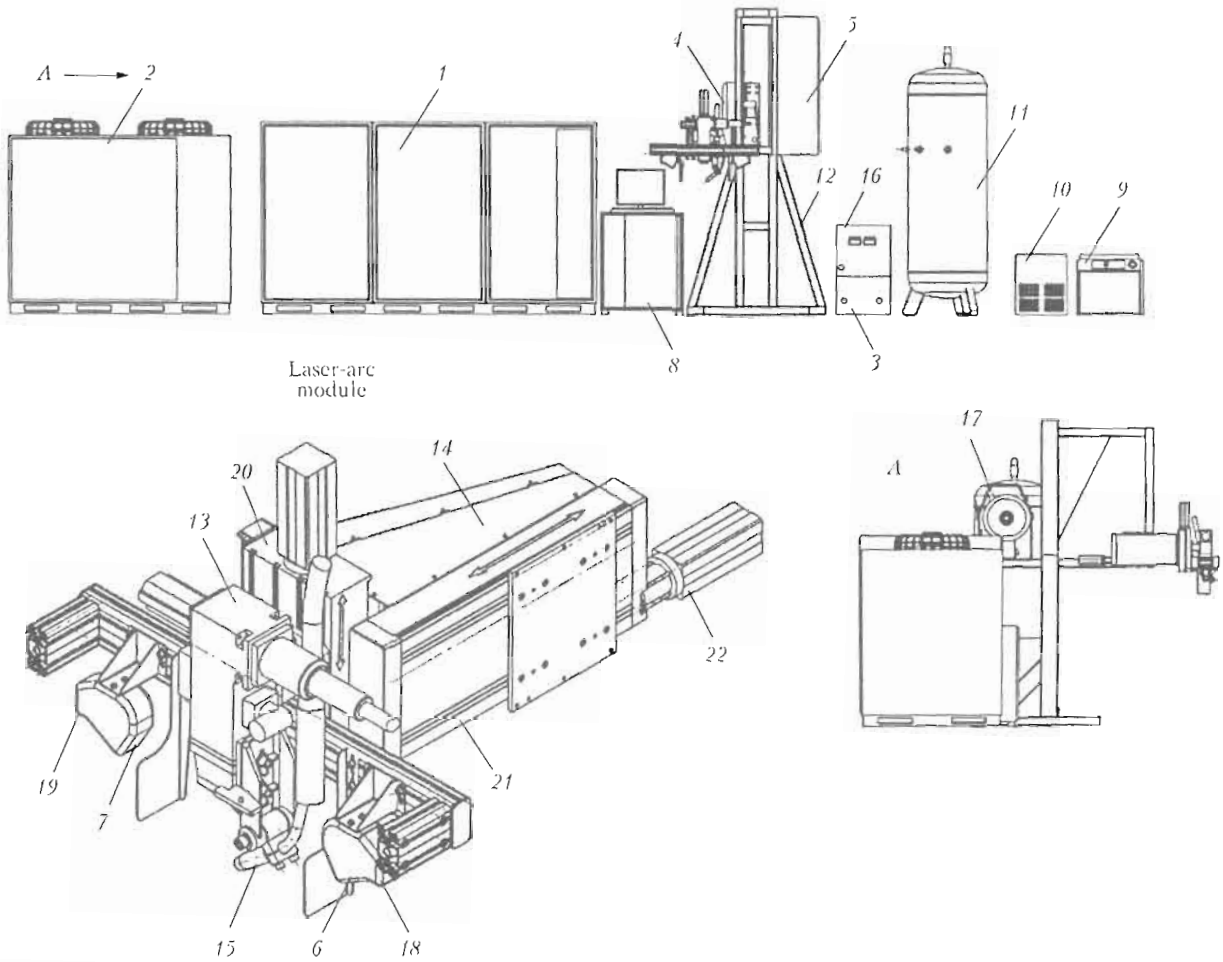


Figure 2. Overview of the LATC: *1* – fiber laser LS-15; *3* – complex of arc equipment; *4* – laser-arc module (working tool); *5* – block of preparation and distribution of gases; *6* – subsystem for welded joint monitoring; *7* – subsystem for weld monitoring; *8* – automatic control system (ACS); *9* – compressor plant with refrigerator drier *10* and receiver *11*; *12* – technological post; for the rest designations see the text

±0.5 mm in a cross-section direction to the joint, and ±0.2 mm in a vertical direction;

• positioning of the welding head above the welded joint;

• control of the laser radiation source on all parameters given by the manufacturer of the laser equipment;

• control of the arc source;

• control of shielding gases feed;

• control of the welding process parameters and their documenting;

• measurement of the welding head parameters and protection against invalid modes;

• quality control of the welds by using the necessary sensors.

According to solved problems the HSC consists of several subsystems: control of the laser; control of the arc equipment; control of the gas equipment; welding head positioning; reading of the metal joint ge-

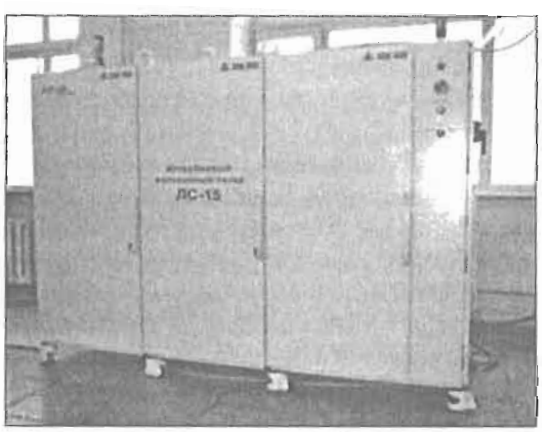

Figure 3. Fiber laser of 15 kW power

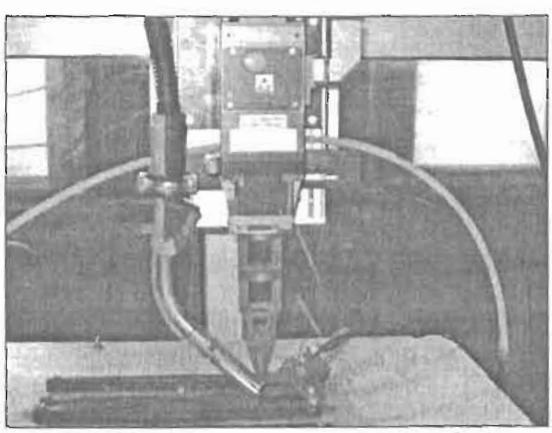

Figure 4. Hybrid welding head

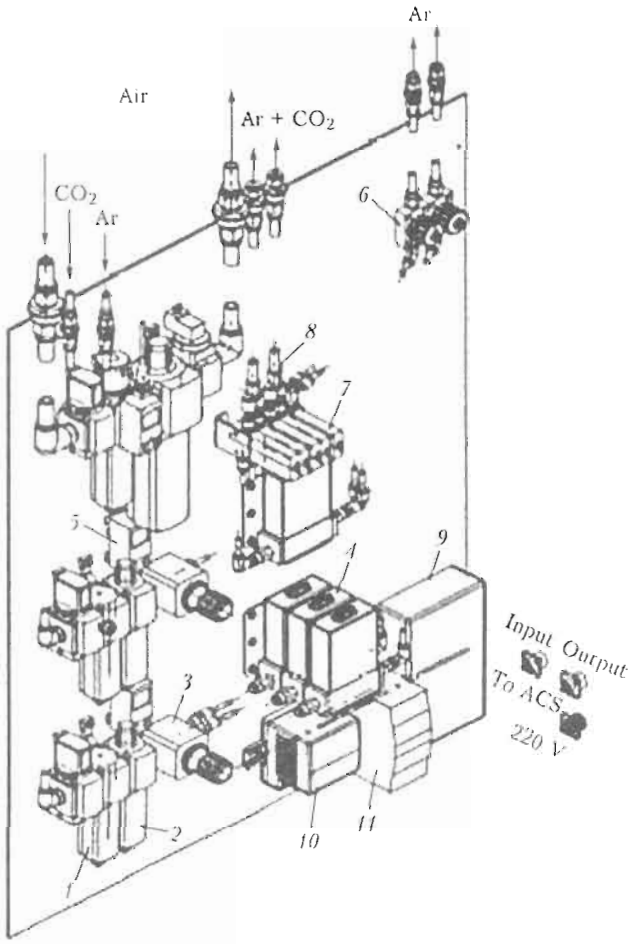


Figure 5. Block of preparation and distribution of gases (for designations see the text)

ometry; control of parameters and protection of the laser welding head; module of the central controller; operating computer.

An industrial computer is used as operating computer. It is placed in 19 inch post together with other HSC components. It contains the modern dual core processor providing demanded calculation speed in real time mode. To communicate with other modules of the complex a card of CAN interface is placed into the computer.

Now experimental research of melting ability of the LATC prototype are carried out. It is shown that

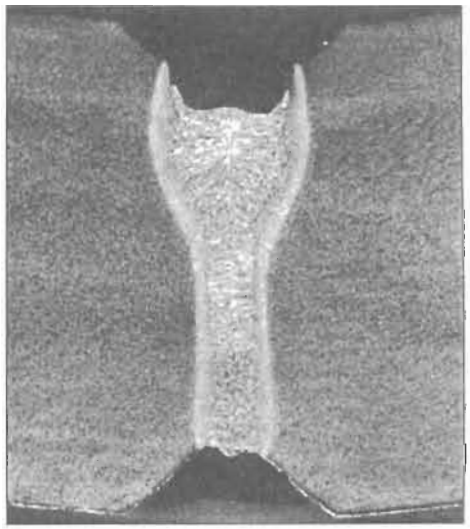

Figure 6. Weld macrosection

LATC is capable to solve problems in welding of high thickness steels. Transverse section of the weld with penetration depth of 15 mm on pipe steel made by means of the developed device is shown in Figure 6.

## CONCLUSION

During work with the project the technology and laser-arc complex are developed for welding of the high thickness metals. There was shown an opportunity of welding steels up to 15 mm thick with welding speed of not less than 2 m/min, and up to 12 mm thick with welding speed of not less than 3 m/min. Now there is a work on producing a LATC pre-production model.

1. Steen, W.M. *Methods and apparatus for cutting, welding, drilling and surface treating.* Pat. 1547172 Great Britain. Int. Cl. B23K 26/00, 9/00. Publ. 06.06.79.
2. Steen, W.M. *Improvements in methods and apparatus for cutting, welding and surface treating.* Pat. 1600796 (add to patent 1547172) Great Britain. Int. Cl. B23K 26/00, 9/00. Publ. 21.10.81.
3. Steen, W.M. *Methods and apparatus for cutting and welding.* Pat. 4167662 USA. Int. Cl. B23K 9/00. Publ. 11.09.79.
4. Steen, W.M. *Verfahren und Vorrichtung zur Bearbeitung von Werkstucken mittels eines Laserstrahls.* Pat. 2813642 Germany. Int. Cl. B23K 26/00. Publ. 04.10.79.

# LASER HYBRID WELDING OF PIPE STEELS — MODELING AND TECHNOLOGY

G. TURICHIN[1], I. TZIBULSKY[1], E. VALDAYTSEVA[1] and A. LOPOTA[2]
[1]Institute of Laser and Welding Technology, St. Petersburg, Russian Federation
[2]Laser Technology Center, St. Petersburg, Russian Federation

The article devoted to usage of mathematical modeling for development of industrial technology of pipe steel welding. On the base of quasi-stationary and dynamic models of weld pool in laser-MAG welding the range of mode parameters was determine for one-pass welding of pipe steels up to 15 mm thick. Results of welding trials and mechanical tests approve the results of simulation. The technology of welding with arbitrary gap and influence of edge preparation are also discussed as well as an influence of beam scanning and welding zone shielding.

Idea to use together laser radiation and electric arc for welding of metals, so that both of heat sources influence a product within the limits of one heating zone, was born in the end of 1970s [1]. Until recently powerful $CO_2$-lasers were applied, they generated radiation with wavelength of 10.6 μm. Interaction of radiation of this wavelength with metals is accompanied by beginning of the optical discharge in the influence zone that effects essentially the focused beam parameters and part of the absorbed energy in the target and plasma in the interaction zone. Interaction of laser radiation of wavelength 1.06 μm with the target is essentially different. However, powerful lasers with such wavelength had poor radiation quality and small reliability. Only recently technological ytterbium fiber lasers with continuous radiation power of up to 30 kW were developed, they possess high beam quality and high reliability.

Now in Russia there are problems of modernization and the further development of pipeline transport. The problems in this way can be formulated as follows:

- necessity of increase of working pressure inside a pipe to increase its capacity;
- construction of pipeline systems in areas where repair is complex, expensive or completely impossible;
- necessity of order of the ecological safety norms which excludes pollution of territories and water areas.

The solution of the listed problems is application of big diameter pipes with the increased wall thickness made from new materials with raised strength properties. Production of such pipes demands new technologies of welding. Until now the problem of the automatic welding of thick-walled structures (up to 35 mm) with demanded quality and high efficiency is not solved up to the end. Available ways of welding have disadvantages because of which welding of pipes does not give demanded weld quality and productivity.

Arc welding does not provide demanded mechanical properties of welded joints on the new high strength steels. Application of electron beam welding is associated with use of vacuum chambers that extremely complicates its application. The main disadvantages of laser welding in relative to welding of pipes are high requirements on assembly of edges for welding and impossibility of getting of demanded mechanical properties of welds and heat-affected zone. The specified defects are eliminated by means of joint laser-arc influence on metal.

The laser-arc process in comparison with laser welding allows providing greater tolerance in relation to accuracy of assembly, possibility of filling of cutting for one pass, higher efficiency, weldability of special pipe steels due to additional alloying by means of an electrode wire.

The analysis of results of the fulfilled research of laser-arc welding process enables to define a number of problems which decision is necessary to develop reliable technology of welding of great thickness metals. In particular, it is necessary to eliminate the sharp increase of the weld width in the top part of its cross section, unwanted direction of crystals growth, presence of hardening structures in deep penetration zone, presence of set of gas pores, and unsatisfactory values of impact toughness of the axial zone, especially at negative test temperatures.

Results of preliminary experiments on laser and hybrid welding of pipe steels have shown that demanded parameters on impact toughness cannot be reached without additional alloying of metal of the cast zone of a weld. During this work alloying was carried out due to additional metal-particle wire melted by electric arc. To alloy metal of the bottom part of the cavity the way of control of the melt flow hydrodynamics in the weld pool by laser beam scanning was used.

Simulation of process of hybrid laser-arc welding by means of computer program LaserCAD developed at ILIST of St. Petersburg State Technical University has allowed predicting the weld shape depending on the set parameters of energy sources and material. An example of simulation of hybrid welding of steel AISI 1330 is shown in Figure 1. There are shown also calculation of cross-section of the melting and heat-affected zones, and the calculated thermal cycles combined with continuous cooling transformation dia-

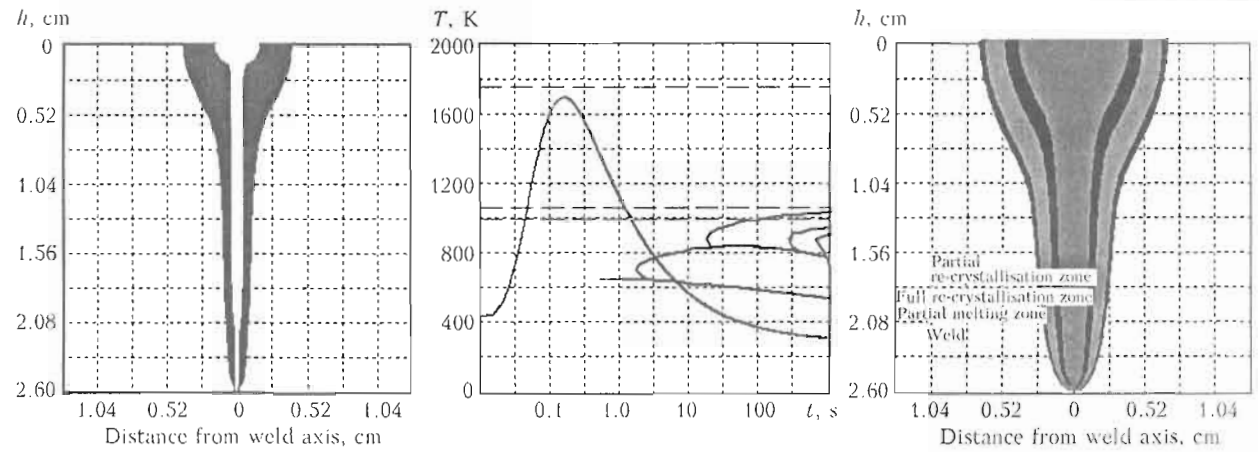


**Figure 1.** Results of mathematical simulation of laser and hybrid welding of steel AISI 1330 at (10 + 4) kW

gram allowing phase-structure combination of metal to be estimated.

The given model allows estimating demanded parameters of heating sources, predicting phase-structure of metal combination after welding and thereby lowering number of experiments.

Processes of hybrid laser-arc welding with deep penetration just as related processes of laser welding are often accompanied by occurrence of porosity and formation of root peaks in welds [2]. According to modern conceptions about the physical nature of laser welding processes the reason of it is propagation of self-oscillations of the cavity and weld pool in welding with deep penetration [3] that proves by numerous experimental results [4–6].

Comparative research of liquid metal movement on the weld pool surface and process of the root peaks formation confirm correspondence between peak formation and spillage of molten metal from the weld pool. The same results have been obtained later at X-ray shooting [7]. The analysis of self-oscillatory processes at influence of the concentrated energy sources on substance is based usually on the linear theory of stability [8, 9] in view of joint development of thermal, hydro- and gas dynamic disturbances, relaxation processes and shielding of the target surfaces by evaporation products. Attempts to consider real geometry of the cavity surface in laser welding were earlier undertaken by authors of [10, 11], but direct use of the obtained results for a case of hybrid welding is not obviously possible.

It is necessary to note that the linear analysis of stability allows defining only borders of area of the stable welding modes, but it is unsuitable for the analysis of the case of the developed oscillation of the big amplitude. For these purposes the description of time dynamics of the cavity radius based on a reduction of the problem to one ordinary differential equation, similar resulted in [12], is more convenient. Authors of this work consider pressure balance upon the cavity surface as motive power of the process and use axial symmetry of the model problem to reduce the equations of hydrodynamics to one ordinary differential equation, but the given model predicts only oscillation damping. Research of the nature of self-oscillations in laser welding proceed in recent years [13]. To understand in detail the nature of the dynamic processes in the weld pool in welding with deep penetration, it is necessary to have dynamic model of the welding process based on a physically adequate picture of the process of laser welding with deep penetration. Use of such model in monitoring and control systems demands a possibility of work in real time mode. These requirements do not allow creating dynamic model of laser welding on the basis of direct solutions of all interconnected physical problems as it has been made for stationary model [14–16]. The most reasonable way of development of dynamic model is use of variational principles and a formalism of Lagrange mechanics that allows the model to system of the ordinary differential equations to be reduced.

The dynamical model of laser welding process described in [17] has been improved to take into account the arc influence and then has been used in the frame of present work for simulation of temporary behavior of molten pool in hybrid welding.

*Experimental research of technological process of laser-arc welding*. In experiments there were used the hybrid laser-arc technological complexes developed in ILIST of St.-Petersburg State Technical University. Ytterbium fiber lasers LS-5 with maximum power 5kW and LS-15 with maximum power 15 kW were used as laser radiation sources. Radiation was transported on a fiber cable to the Precitec optical welding head YW50 with built in scannator, with focal distance 350 mm and focal beam diameter 0.4 mm.

The plant is completed by the ITS arc power supply VDU-506DK, licensed for welding of pipelines. It provides demanded values of the inclination of the external characteristic in MIG/MAG mode. In the range of welding currents of 300–400 A and voltage of 29–30 V there can be reached effective heat capacity of the arc source 6500–9000 W. A semiautomatic device PDGO-511 was used for feeding filler material, it is a part of the arc module set. The hybrid laser-arc complex is shown in Figure 2.

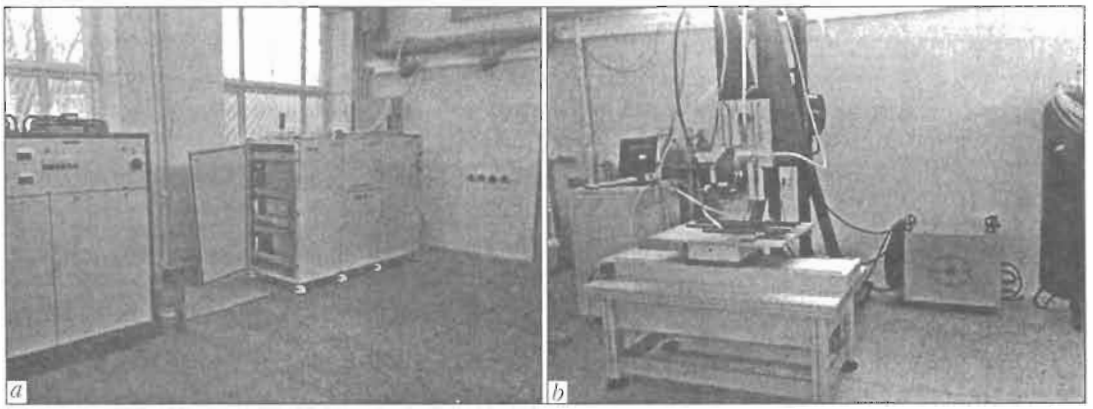

**Figure 2.** Installation for hybrid laser-arc welding: *a* — fiber laser LS-15; *b* — two-coordinate product manipulator, hybrid head with the manipulator, arc source, feed device, and control unit

During experiments the flat samples 8, 10, 12 and 24 mm thick from steels St3, 25G2S, 10G2FBU and 12Kh18N9T were melted and butt-welded. Welding was carried out by rectilinear butt welds in downhand spatial position. Argon, carbon dioxide and their mixtures were used for shielding weld pool and weld metal. Distance from a coaxial shielding gas jet nozzle to sheet was 8 mm. Non-coaxial protection of the weld pool was used additionally.

Quality of all welded joints was estimated visually on their appearance and basing metallographic research of cross-sections. The penetration depth and other weld geometry parameters were determined.

*Results of experiments.* Tests of the experimental complex have shown its high technological opportunities. At joint using the laser of up to 5 kW and the arc module with consumable electrode, the penetration in the butt joints was get for steel of not less than 8 mm thick with filling of the gap 0.5 mm and more at high weld density (Table).

In the fulfilled experiments, the volume of the melted filler metal was about 30 % from total amount of the weld pool metal.

At joint using the laser of up to 15 kW and the arc module with melted electrode, the butt joint penetration was get for steel up to 18 mm thick and filling the gap of 1 mm and more at high weld density (Figure 3).

By means of the experiments, influence of welding speed, arc energy and filler material on the welding process has been established and accordingly their influence on the weld formation under conditions of laser-arc welding process. Nevertheless, theoretical research and calculations have been carried out to physically interpret the observable phenomena in detail.

Welding modes

| Mode number | Laser radiation power, W | Welding speed, mm/s | Welding current, A | Arc voltage, V | Wire feed rate, mm/s | Weld area, $mm^2$ | Penetration depth, mm | Root gap, mm | Quantity of built-up metal, % |
|---|---|---|---|---|---|---|---|---|---|
| 3 | 4500 | 20 | 0 | 0 | 0 | 7.80 | 6.65 | 0 | 0 |
| 4 | 4500 | 14 | 0 | 0 | 0 | 11.28 | 7 | 0 | 0 |
| 7 | 4500 | 15 | 80 | 22 | 68.33 | 13.95 | 7.05 | 0.50 | 29.5 |
| 8 | 4500 | 8.5 | 80 | 19 | 68.33 | 23.40 | 8 | 0.75 | 31.1 |

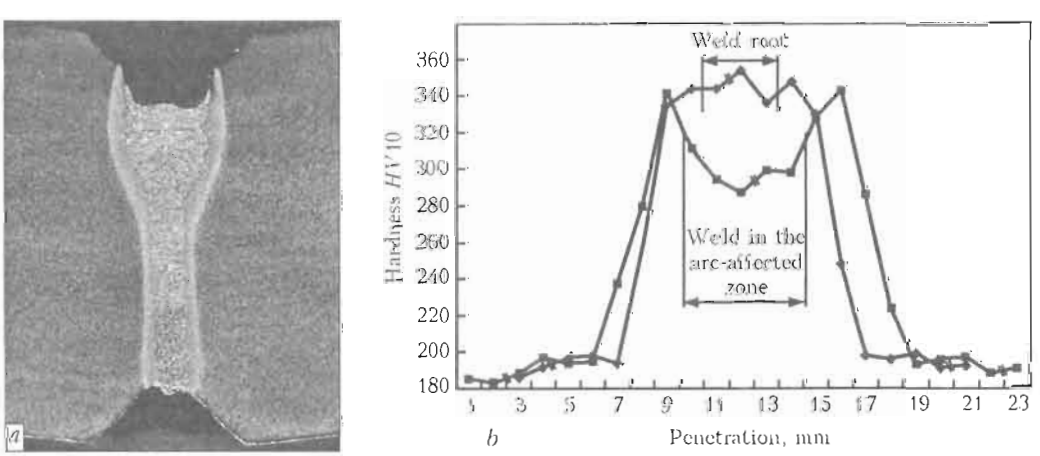


**Figure 3.** Formation of joint in hybrid welding of big diameter pipes (*a*) and weld metal hardness versus penetration at distance 0.5 mm (*b*)

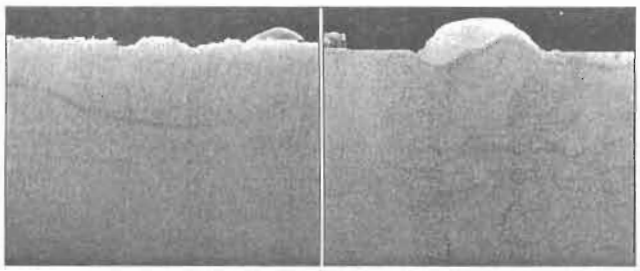

Figure 4. Formation of weld without (*a*) and with (*b*) humping

*Research of dynamic behavior of the weld pool in hybrid welding.* Technological experiments on welding low-carbon and stainless steels, fulfilled by means of the hybrid laser-arc complex described above, have shown that in some cases formation of the weld is accompanied by formation of increased quasi-periodic wave instability on its top and bottom surfaces (humping effect). Thus, various combinations of the welding mode parameters providing identical penetration depth are characterized by different degree of the weld formation stability (Figure 4).

There were fulfilled experiments on measurement of dynamic behavior of the discharge interval brightness to determine time characteristics of dynamic processes in the hybrid discharge zone above the target surface and on identification of their connection with dynamic processes in the weld pool. To except influence of the heated sample surface there were used optical collimators, limiting the size of the investigated zone so that the surface was outside field of view of the optical system. Band optical filters were used to except influence of the reflected laser radiation. Experiments have shown that dynamic brightness behavior (Figure 5) characterized by presence of low-frequency oscillations which spectral characteristics coincide with a spectrum of the melt oscillations in the weld pool, and the peaks of brightness corresponding to luminescence of drops of electrode metal transferred through the discharge interval.

To analyze the reasons of humping effect in hybrid welding and to choose ways of its elimination, it is most expedient to simulate mathematically the process on basis of the physically adequate model, allowing analyzing connection between various physical phenomena responsible for development of the weld pool instabilities. To determine initial conditions at

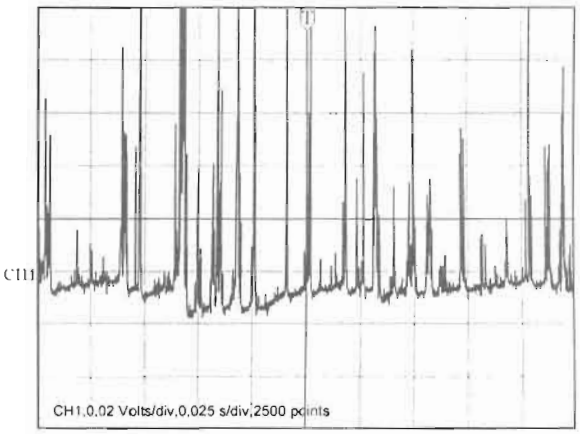


Figure 5. Oscillogram of dynamic behavior of the plasma plume brightness

simulating dynamic behavior of the weld pool in laser-arc welding, there has been used a quasi-stationary model of this process with LaserCAD.

To verify model in welding by the fiber laser a series of experiments on welding of low-carbon steel was fulfilled at various welding modes. Examples of the experiment results are shown in Figure 6. Comparison of calculation and experimental results has confirmed applicability of the model and the high accuracy of calculations.

The dynamic model of hybrid welding process based on the Lagrange mechanics was used to simulate dynamic processes in the weld pool in hybrid laser-arc welding.

The developed mathematical formalism has been built in the CAE system LaserCAD that allows using it for the dynamic analysis of occurrence of porosity and spiking (Figure 7).

Technological experiments on melting samples of stainless steel confirm unstable character of formation both for top and bottom weld surfaces predicted by the theory (Figure 8). This character is described by formation of quasi-periodic melt waves on these surfaces.

In addition, there are results of simulation of time behavior of the penetration depth and the area of the cavity cross-section (Figure 9).

Thus, it is possible to conclude that the dynamic model of the weld formation process in hybrid laser-arc welding is effective way of the analysis of non-

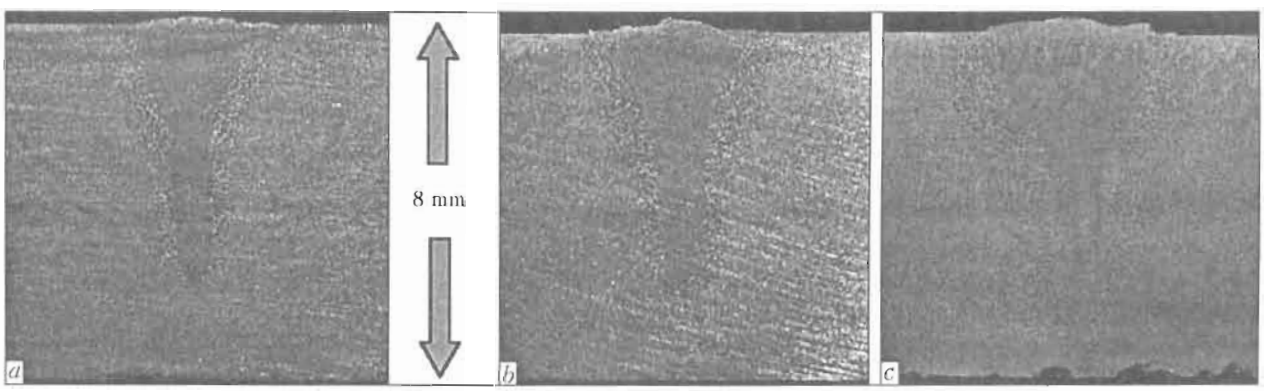


Figure 6. Samples sections welded at welding speed 30 (*a*), 25 (*b*) and 15 (*c*) mm/s at laser radiation power of 4.5 kW for verification of the calculation model

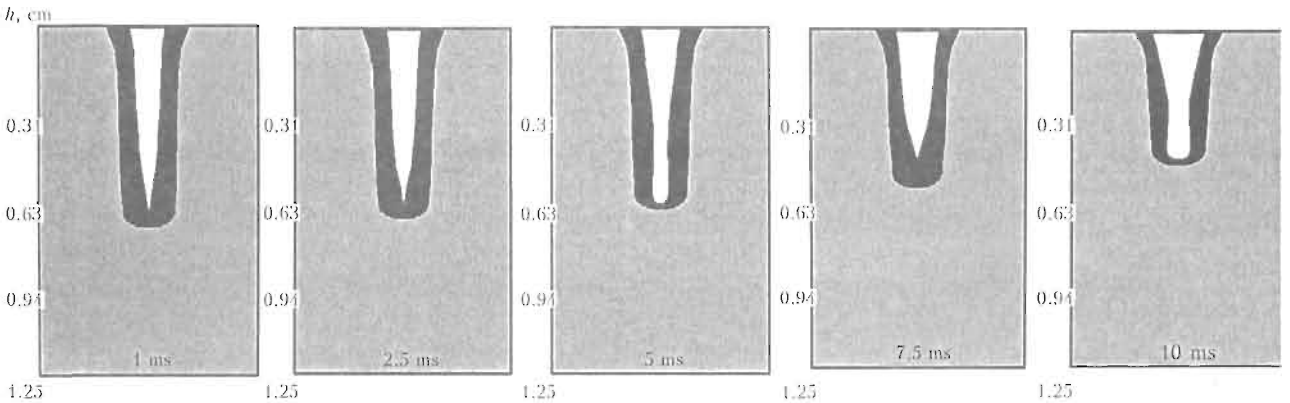


**Figure 7.** Simulation of dynamic behavior of the weld pool in hybrid laser-arc welding for steel 10, laser radiation power 4.5 kW, welding speed 12 mm/s, beam focal radius 0.2 mm, focal distance 30 cm and arc power 2.5 kW

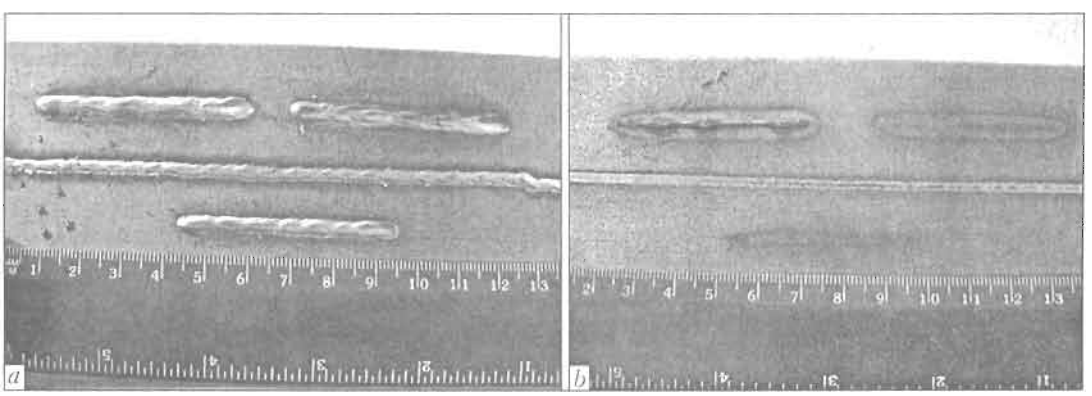


**Figure 8.** Formation of top (*a*) and bottom (*b*) surfaces of a weld

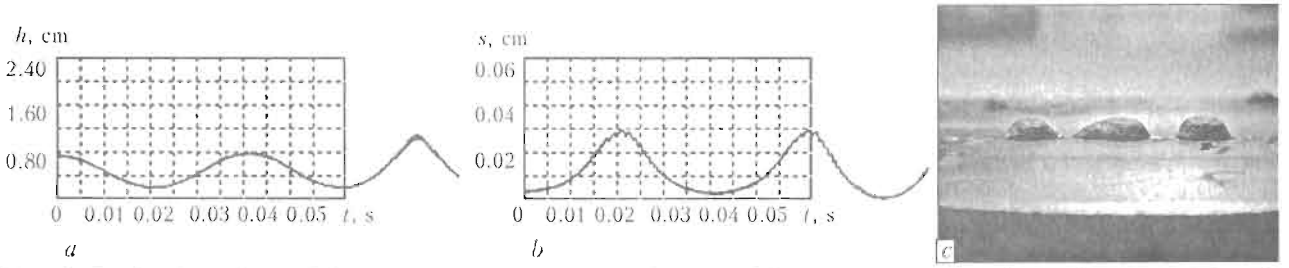


**Figure 9.** Results of simulation of the penetration depth oscillation (*a*), areas of the cavity cross-section (*b*) and formation of the weld bottom surface (*c*)

stationary processes and can be reasonably applied to selection of stable technological modes. Results of simulation and experimental research show that stability of the weld formation is determined, basically, by values of the laser beam focal radius and the shape of laser radiation intensity distribution. At the same time, increase of the welding speed up to the values exceeding 1 m/min leads to increase in the weld formation stability. Also, increase of the arc current and electrode wire feed rate stabilize the process.

## CONCLUSION

Laser-arc welding is a complex multi-parameter process. It is described not only by the laser welding parameters (wavelength, power and quality of laser radiation, sizes and position of the focused beam) and arc welding ones (current, voltage and length of the arc, electrode extension, wire feed rate) but also by specific parameters, which are typical for laser and arc joint influence, for example, position of the laser beam relative to the arc spot on the target surface. Besides the composition of gas shielding atmosphere, chemistry of filler material, preparation of edges to be welded is important.

During this work there were been carried out research of influence of some parameters on geometry of the penetration zone. It is established that in the examined ranges of parameters it is probable to obtain penetration zones providing small specific energy contribution and sufficient for monolithic weld formation. Thus the heat-affected zone, which can be a source of origin of such defects as cracks, is narrow enough and does not exceed 1.0–1.5 mm at weld sample thickness of 8 mm.

There was shown possibility of formation of single-pass weld at which the filler material penetrated into all melt depth. The factor promoting penetration of the filler material into the weld root can be scanning

of laser beam inside the weld pool. To reveal optimum scanning frequencies during the work there were investigated peak-frequency characteristics of plasma plume oscillations flowing from the zone of interaction of the beam and material being welded. There was shown presence of typical oscillation frequencies in a range of tens, hundreds and thousand hertz, which coincide with frequencies of moving of the liquid phase inside the weld pool and ones of the interaction zone of the laser beam on a forward wall of the cavity. The possibility of the weld metal formation due to filler material in combination with possibility to control part of the base metal in this process due to scanning provides its demanded mechanical properties.

To prevent pores formation and gas dissolution (nitrogen, oxygen) in liquid metal, reduce metal splashing and finally provide quality of the welded joint, it is necessary to operate the welding process in the shielding gases. It is rational to use argon or mixtures of argon with small additives of carbonic-acid gas (5–10 %) as shielding atmosphere.


1. Steen, W.M. *Methods and apparatus for cutting, welding, drilling and surface treating.* Pat. 1547172 Great Britain. Int. Cl. B23K 26/00, 9/00. Publ. 06.06.79.
2. Matsunawa, A., Mizutani, M., Katayama, S. et al. (2003) Porosity formation mechanism and its prevention in laser welding. *Welding Int.*, 17(**6**), 431–437.
3. Lopota, V., Turichin, G., Tzibulsky, I. et al. (1999) Theoretical description of the dynamic phenomena in laser welding with deep penetration. In: *Proc. of SPIE*, **3688**, 98–107.
4. Forsman, T., Powell, J., Magnusson, C. (2001) Process instability in laser welding of aluminum alloys at the boundary of complete penetration. *J. Laser Appl.*, 13(**5**), 193–198.
5. Bashenko, V.V., Mitkevich, E.A., Lopota, V.A. (1983) Peculiarities of heat and mass transfer in welding using high energy density power sources. In: *Proc. of 3rd Int. Coll. on EBW* (Lion, 1983), 61–70.
6. Lopota, V.A., Smirnov, V.S. (1989) Structure of a material and its parameters in the beam action zone in laser welding with deep penetration. *Fizika i Khimiya Obrab. Materialov*, **2**, 104–115.
7. Matsunawa, A., Kim, J.-D., Seto, N. et al. (1998) Dynamics of keyhole and molten pool in laser welding. *J. Laser Appl.*, 10(**6**), 247–254.
8. Zuev, I.V., Selischev, S.V., Skobelkin, V.I. (1980) Self-oscillations under action of high density energy source on materials. *Fizika i Khimiya Obrab. Materialov*, **6**, 3–7.
9. Uglov, A.A., Selishchev, S.V. (1987) *Self-oscillatory processes at influence of the concentrated streams of energy.* Moscow: Nauka.
10. Mirzoev, F.H. (1994) Evaporation and capillary instability in deep keyhole. *Kvant. Elektronika*, 21(**2**), 147–150.
11. Turichin, G.A. (1996) Hydrodynamic aspects of the cavity stability at beam kinds of welding. *Fizika i Khimiya Obrab. Materialov*, **4**, 74–81.
12. Semak, V.V., Hopkins, J.A., McCay, M.H. et al. (1995) Melt pool dynamics during laser welding. *J. Phys. D: Appl. Phys.*, **28**, 2443–2450.
13. Lee, J.Y., Ko, S.H., Farson, D.F. et al. (2002) Mechanism of keyhole formation and stability in stationary laser welding. *Ibid.*, **35**, 1570–1576.
14. Kaplan, A. (1994) A model of deep penetration laser welding based on calculation of the keyhole profile. *Idid.*, **27**, 1805–1814.
15. Beyer, E., Dahmen, M., Fuerst, B. et al. (1995) Tool for efficient laser processing. In: *Proc. of 14th ICALEO Int. Congress on Application of Lasers* (San Diego, USA), 1035–1039.
16. Schulz, B., Fuerst, S., Kaierly, G. et al. (1996) Powerful features for LBW including theoretical aspects. In: *Proc. of ICALEO* (Detroit, USA), 1–9.
17. Turichin, G., Valdaitseva, E., Pozdeeva, E. et al. (2008) Theoretical investigation of dynamic behavior of molten pool in laser and hybrid welding with deep penetration. *The Paton Welding J.*, **7**, 11–15.

# RUSSIAN-GERMAN CENTER OF LASER TECHNOLOGIES — GOALS AND PROSPECTS

A.T. ZELNICHENKO
E.O. Paton Electric Welding Institute, NASU, Kyiv, Ukraine

Advantages of laser welding over the arc one, such as avoidance of straightening and trimming, high precision (precondition of easy fit-up and automation), high, productivity etc., considering a sheer fall in prices and rise in power of fiber lasers, increased interest of the welding community in new capabilities of the laser technologies. This is confirmed by a growing number of workshops, conferences and symposia dedicated to this subject, which are held in Ukraine and Russia [1–4], as well as by opening of the Russian-German Laser Center.

On August 3, the opening of Russian-German Center of Laser Technologies, founded on the base of Institute of Laser and Welding Technologies (ILWT) of Faculty of Technology and Research of Materials took place at St.-Petersburg State Polytechnic University (SPSPU). The purpose of founding the Center is the search for ways of effective application of laser technologies in industry and research works. The furnishing of the Centre with the most advanced equipment allows its direct participation in realization of definite projects in aerospace branches, shipbuilding, metallurgy, in chemical, oil-gas-production industries and other sectors of industry.

At the opening ceremony of the Center Prof. M.P. Fyodorov, Corr. Member of RAS, rector of SPSPU; Prof. Karl-Dieter Grueske, rector of Erlangen-Nurnberg University; Prof. V.A. Lopota, Corr. Member of RAS, President of RSC «Energiya»; Prof. Michael Schmidt, director of Bavarian Laser Center; Prof. G.A. Turichin, director of Russian-German Center of Laser Technologies of SPSPU, took part.

In the presentations the honorary guests and official persons outlined mainly the role of the Center in scientific-educational and industrial cooperation between Russia and Germany.

Prof. Fyodorov, after receiving the symbolic key for the newly opened Center from the hands of Prof. Schmidt, said: «This key is going to open the new pages of our cooperation and never to close them».

Prof. Grueske said: «It was a pleasure for us to work on founding this Center together with Russian colleagues. This project united the efforts of Ministry of Science and Education of Germany and a number of German companies-producers of laser equipment. I foresee a great potential of cooperation between our universities to be developed».

Prof. Lopota said: «The equipment, presented today, is a result of almost 30-year work of Russian and German scientists. The technological processes which could be realized on its basis can provide success of one of the main problems of machine building, i.e. making the structures lighter. Before us now there are real technologies capable to make revolution in machine building, create systems providing the vital activity of a man».

Holger Junge from the Ministry of Science and Education of Germany, expressed the following: «We have been cooperated already over 20 years. Russia has strong science, Germany has strong machine building, and we can achieve a lot by common efforts. The main purpose of this Center is teaching of students. The future technologists, designers can use the equipment for teaching and practicing. This Center will be

Speech of Prof. V.A. Lopota, Corr. Member of RAS, President of RSC «Energiya»

Prof. G.A. Turichin, Director of Russian-German Center of Laser Technologies of SPSPU, making a tour around the Center

Demonstration of robotic system of remote-control laser welding ROFIN SWS

the demonstration site for medium and small enterprises as well. Besides, the Center will be able to earn».

Prof. Turichin, Director of the Center, said: «This Center is visible embodiment of dream of a big group of people working on the performance of the project on founding the Center. It is equipped with the most updated laser technological complexes covering as to its possibilities almost all spheres of application of laser technologies in machine building. Together with ILWT, the SPSPU forms the largest structure in Europe in the field of machine building laser technologies. The Center will not only provide teaching of students, performance of research works and developments, and orders of industrial enterprises, but also will serve as «the crystallization center» for innovation of companies working in the field of laser and related technologies».

After the opening ceremony Prof. Turichin made technical excursion for honorary guests, representatives of science and industry and journalists. The equipment of the Center allows realization of the following technologies:

- ERLASER® HARD+CLAD – the robotic laser powder cladding and thermal strengthening;
- JENOPTIK VOTAN C-BIM – the laser 3D cutting of non-metallic materials and thin metals;
- ROFIN SWS – the robotic remote-control laser welding of metallic materials;
- ROFIN StarWeld 500 – the laser pulsed microwelding and deep engraving;
- ROFIN StarShape 300C – the laser perforation, holes drilling, marking of non-metallic materials;
- ARNOLD – the laser welding and cutting of 3D metallic billets including thick-walled and large-size ones;
- LIMO-LASER WORKSTATION – the laser welding of plastics.

The flexibility of the presented equipment and high level of its automation allows quick resetting of technological complexes and change of technologies being used, thus processing the wide range of materials and workpieces.

In the same day the Agreement was signed on the cooperation between SPSPU and High School of Advanced Optic Technologies of Erlangen-Nurnberg University. In accordance with the Agreement the universities will conduct research works on the trends of mutual interest. The Agreement implies the students and post graduate students exchange; realization of common research projects; participation of professors, engineers and students in conferences, seminars and trainings which will be held in both universities; organization of different mutual events.

Laser thermal strengthening of press-form (Erlaser Hard+Clad)

On August 4, the excursion to ILWT of SPSPU took place headed by G.A. Turichin who outlined the following trends in ILWT activity:

- investigation of processes of interaction of laser radiation with substance;
- technological investigations and developments in the field of laser and electron beam technologies;
- development of hybrid technologies and laser-arc welding and cladding;
- construction of mathematical models of laser, electron beam, laser-arc and light-laser welding.

ILWT is equipped with two unique continuous ytterbium fiber lasers of the capacity of 5 and 15 kW of the company IPG (IRE-Polus Group). The output beams divergence of these lasers is much lower than that of other lasers having the same range of capacity allowing the use of long-focal focusing optics with a large working range. I.A. Tsybulsky, Deputy Director on Production, noted that considering simplicity of supply of laser radiation to the object the main fields of application of fiber lasers can be 3D cutting, remote-control welding, pipe welding, body welding, cladding and other related technologies of material treatment.


1. (2003) *Proc. of Int. Con. on Laser Technologies in Welding and Materials Processing* (Katsiveli, Ukraine, May 19–23, 2003). Kiev: PWI.
2. (2005) *Proc. of 2nd Int. Conf. on Laser Technologies in Welding and Materials Processing* (Katsiveli, Ukraine, May 23–27, 2005). Kiev: PWI.
3. (2006) *Proc. of 5th Int. Conf. in Beam Technologies and Application of Lasers*. St. Petersburg, SPbGPU.
4. (2007) *Proc. of 3rd Int. Conf. on Laser Technologies in Welding and Materials Processing* (Katsiveli, Ukraine, 29 May–1 June, 2007). Kiev: PWI.

# Name Index